City Research Online

City St George's, University of London

Citation: Penny, P. H. G. (1978). The application of liquid powered fluidics to the sorting of aggregates. (Unpublished Doctoral thesis, City, University of London)

This is the accepted version of the paper.

This version of the publication may differ from the final published version. To cite this item please consult the publisher's version.

Permanent repository link: https://openaccess.city.ac.uk/id/eprint/37689/

Copyright and Reuse: Copyright and Moral Rights remain with the author(s) and/or copyright holders. Copies of full items can be used for personal research or study, educational, or not-for-profit purposes without prior permission or charge, unless otherwise indicated, provided that the authors, title and full bibliographic details are credited, a hyperlink and/or URL is given for the original metadata page and the content is not changed in any way. For full details of reuse please refer to City Research Online policy.

City Research Online: http://openaccess.city.ac.uk/ publications@citystgeorges.ac.uk

678

THE APPLICATION OF LIQUID POWERED FLUIDICS TO THE SORTING OF AGGREGATES

by

Peter Henry Gordon PENNY

Submitted for the degree of

DOCTOR OF PHILOSOPHY

THE CITY UNIVERSITY

LONDON

Department of Mechanical Engineering

August 1978

ABSTRACT

The sorting of aggregate materials into acceptable and unacceptable groups is a common requirement in the food processing and mining industries. These industries commonly process large volumes of these aggregates and the application of high speed switched fluid jets has proved attractive. Rapidly escalating costs and complexity have been experienced with the deflection of large, heavy bodies. This work has been concerned with this area of application.

The fundamental requirements of a sorting machine have been considered and, having postulated that liquid jets may alleviate many of the problems connected with the sorting of large and heavy bodies, the methods of liquid jet control have been reviewed.

The dynamic movement of a body whilst under the influence of a liquid jet has been examined both mathematically and experimentally and the investigation concluded that under certain conditions liquid jets were suitable for the deflection of large and heavy bodies.

After reviewing a number of pertinent literature sources on swirling flow a new axial vortex fluid element was designed and built for the purpose of sorting aggregates. The device was examined under steady state conditions both experimentally and theoretically and a number of interesting features were highlighted; regions of fluid stagnation, flow separation, air core formation and control flow

instability. A number of transient response experiments were performed and whilst not meeting the original requirement in every respect the vortex element was shown to be fast and capable of improvement.

The final conclusion was that a liquid jet sorting machine using the proposed axial vortex device could, with some minor modifications, meet the original requirement for sorting large, heavy aggregates.

ACKNOWLEDGEMENTS

Hindsight, almost invariably, colours one's judgement, nevertheless I wish to acknowledge a debt to three distinct groups of people.

To those institutions and people who have supported my work as part of their general policy. To [redacted] (Head of the Mechanical Engineering Department), the Senate of The City University and the Science Research Council.

Secondly, to those past and present research workers who through their own efforts have assisted those that have followed.

Lastly, to those people who have become intimately involved with this particular work. To my supervisor, Dr. R.S.Neve, for his unflagging assistance through all aspects of this work. To [redacted] of The City University computer unit for his patient help. To [redacted] and the technicians of the Mechanical Engineering Department (in particular [redacted], and finally to my long suffering family.

PRINCIPAL NOMENCLATURE

A - area, (unless specified otherwise)

a - acceleration, (unless specified otherwise)

C - capacitance

c - constant

C_{dc} - control flow discharge coefficient

C_f - friction coefficient

C_v - velocity coefficient

D - differential operator

d - diameter; differential increment

E - voltage

F - force

f - friction factor (Ch.3); frequency (Ch.4)

$\dot{G}$ - linear momentum flux

g - gravitational acceleration (Ch.1);
bilateral admittance (Ch.4)

H - change in fluid 'head'

$\dot{H}$ - angular momentum flux

h - body drop height (Ch.2); vortex chamber depth (Ch.3)

h_1, h_2, h_3 - metric coefficients in the coordinate directions x_1, x_2, x_3

I_G - moment of inertia about mass centre

K - constant

k - curvature

L - inductance (Ch.4); unbroken jet length (App.1)

l - control nozzle depth

M - molecular weight (Ch.1); moment (Ch.3)

M_G - moment about mass centre

m - mass (Ch.1); stream surface curves (Ch.3)

$\dot{m}$ - mass flow rate

N - a function

n - number of moles (Ch.1); curves orthogonal to stream surface (Ch.3)

n_o, n_i - outer and inner values of an 'n' curve respectively

P - power

P_{CR} - control pressure ratio

p - pressure (a suffix 1 to 7 specifies an expt. measurement station)

Q - volumetric flow rate

R - radius (Ch.3); radius of curvature (App.6)

Re - Reynolds number

R_o, R_i - outer and inner values of the radius at a specific station respectively

r - radius

s - Laplace operator (unless specified otherwise)

$St.$ - Strouhal number

t - time (unless specified otherwise)

u - stream velocity (Ch.3); unilateral admittance (Ch.4)

u_∞ - velocity outside the boundary layer

V - volume

v - velocity (if unspecified, the mass centre for a rigid body, the stream velocity for a fluid)

We - Weber number

ω_n - resonant 'radiancy'

x - horizontal displacement (unless specified otherwise)

x_1, x_2, x_3 - general orthogonal coordinates (App.7)

y - vertical displacement (unless specified otherwise)

z - axial coordinate of cylindrical coordinate system

Greek symbols

α - tangent of velocity ratio at nozzle orifice (Ch.3); gain constant (Ch.4) (unless specified otherwise)

β - liquid sheet semi-angle; gain constant (Ch.4)

Γ - fluid circulation

Δ - a change

δ - boundary layer thickness; a small change (unless specified otherwise)

θ - deflection angle (Ch.2); coordinate axis of symmetry (unless specified otherwise)

λ - inlet velocity ratio; meridional stream surface angle, from axis of symmetry

μ - fluid dynamic viscosity

ν - fluid kinematic viscosity

ρ - fluid density

σ - surface tension (water/air); stress (with appropriate suffices)

τ - shear stress (Ch.3); time constant (Ch.4); liquid sheet thickness (App.6)

ϕ - flow distribution function (unless specified otherwise)

ψ - stream function

Superscript:

$\hat{}$ - maximum value

Subscripts:

x,y,z - coordinate directions

r,θ,z - cylindrical coordinate directions

$1,2,3$ - general orthogonal coordinate directions, the distances between coordinate increments being represented by θ, m, n respectively

m,n - refers to the 'm' or 'n' characteristic curves which are also the x_2 or x_3 coordinates

J - refers to the liquid jet

p - refers to the particle (or body)

s - refers to the stream flow supply

c - refers to the control flow

o,e - refers to the exit point (unless specified otherwise)

ANN - refers to the annulus

i - refers to an inlet condition

w - refers to the wall

T - 'total' conditions

CONTENTS

LIST OF TABLES

Chapter 2

LIST OF FIGURES

Page number

Chapter 3

LIST OF PHOTOGRAPHIC PLATES

1. INTRODUCTION

1.1 An Introduction to Sorting Machines

Loose aggregate materials are sorted in a large number of industries, particularly the mining, chemical and food processing industries; either defective items are removed or mixed components separated. Until comparatively recently the standard method of removing defective material was by visual examination and hand sorting, (Moder and Oswalt, 1959). With the development of electrical and optical instruments capable of measuring and comparing internal or external characteristics of the aggregate, automatic machine sorting has become feasible.

The sorting operation requires that the material be fed into a position for examination, that some identifiable characteristic difference between acceptable and defective material be observed, that a signal be initiated and a mechanism operated for the physical removal of the item examined.

A number of firms manufacture ranges of sorting machines which can sort materials ranging in size from small plant seeds to rocks the size of a cricket ball; only a small particle size range is catered for on any one machine. The examining technique usually used is that of electronic colour sorting, as described by Schaub (1965), based on either mono-chromatic selection, (tone discrimination), or bi-chromatic selection,(colour discrimination).

Figure 1-1 shows the schematic layout of a typical sorting machine. The aggregate mixture to be sorted is held in a hopper which is usually vibrated to feed material at a uniform rate either directly into, or on to an endless belt and then dropped into the

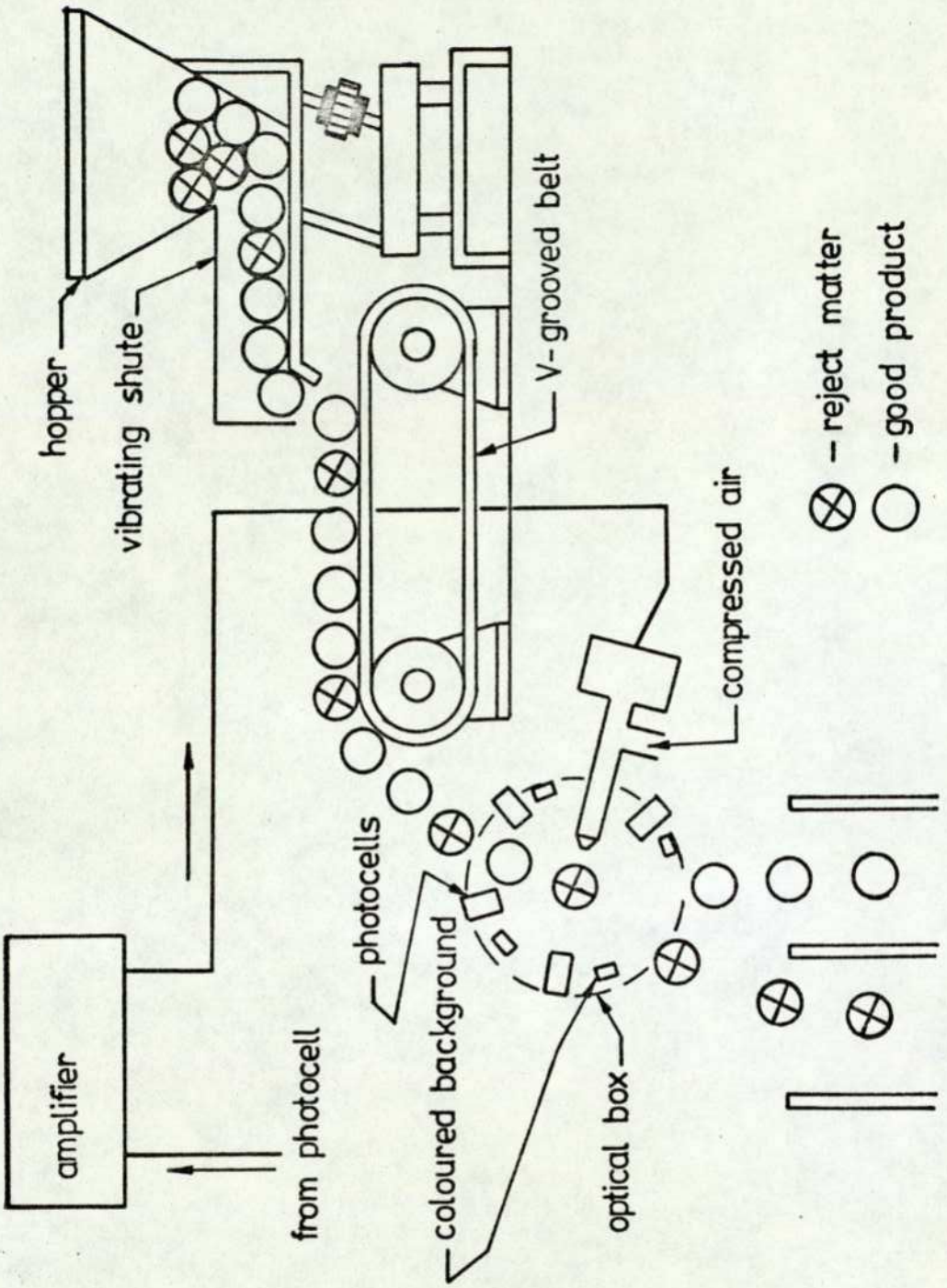

Sorting machine scheme.

Figure 1-1

photocell viewing chamber. A characteristic missmatch between the body being examined and a reference background results in an electrical signal being passed from the viewing photocells into an amplifier. The amplified electrical signal then activates either electrostatic deflection plates, in the case of sorting small plant seeds, or (as in Figure 1-1) an electro-pneumatic valve or valves to produce an air jet, or jets, for the larger bodies. The impact of the air jet, or jets, on the body eventually results in the required horizontal deflection of the body and its entry into the appropriate container. Sometimes up to six air jets are required to produce the necessary deflection forces. Obviously either acceptable or reject material could be deflected, although usually, for reasons of power consumption economy, the smallest proportion of the component being sorted is chosen for deflection.

1-2 Preliminary Design Considerations for Sorting Machines

Examination of Figure 1-1 indicates that since the machine elements operate in series, the rate of sorting of the entire system will be determined by the slowest element. A consequence of a feed rate greater than the response rate of the deflecting device is the lack of selectivity with which items can be ejected and the resulting loss of acceptable material. The electrical amplifiers and viewing apparatus usually have a far quicker transient response than the two mechanical elements of the sorting machine, (the feed system and the deflecting device), and the electrical elements will not be considered further in this work.

Consider a number of items falling from a hopper under the influence of gravity; their horizontal and vertical velocities, respectively Vx and Vy, are approximately zero on leaving the hopper. If now a photo-cell viewing chamber is placed a distance 'y' below the hopper exit then, ignoring retarding forces such as aerodynamic drag, the velocity of any body entering the viewing chamber is $(2g_c y)^{\frac{1}{2}}$. Therefore the time available for examination of the body increases with increasing particle size and decreases with an increase in the distance 'y'; it will also be obvious that the decreasing viewing time will not affect the feed rate of the material. If the deflection time is defined as the time required to obtain a specified horizontal displacement whether immersed in the liquid jet or in free fall below the jet then the maximum deflection time that can be tolerated by the system for it to remain selective is the reciprocal of the material feed rate. A deflection time greater than this may result in the loss of acceptable material, whereas a quicker response than this focusses attention on the now inadequate feed rate mechanism.

A further point to be considered is the time during which the jet impacts on the body, since this determines the time during which momentum transfer between the jet and the body occurs. Neglecting, for the moment, details of the jet forces on the body, it would appear that the best position for the deflecting device is close to the hopper exit, bearing in mind that the viewing chamber must precede the deflecting device. It will be shown in Chapter 2 that the apparent solution of placing the deflecting device close to the hopper exit will not

invariably give the optimum value for material sorting rate or the most efficient use of the jet power.

The present state of sorting machine development is that the machines for the smaller bodies, such as rice grains, have switching devices that can operate at frequencies greater than the present feeding mechanisms. This is not true for machines deflecting the larger bodies, which can have up to six air jets to obtain the required deflection forces, and the deflection device consumes a considerable quantity of power. The current viewing times as given by Chadda (1972), vary from one milli-second for the smaller bodies such as rice grains, to twenty or thirty milli-seconds for the larger ones, approximately the size of a cricket ball. These figures would indicate that a deflection device for the larger bodies should be capable of switching at a rate of approximately thirty-five Hertz. The author has seen no theoretical or experimental work carried out on the mechanics of a body's movement whilst under the action of a jet. Chadda (1972) investigated the forces exerted on spherical bodies whilst held stationary and partially immersed in a supersonic air jet. Chadda's work, in connection with body deflection, was primarily concerned with the variation of the body's horizontal deflecting force with respect to its position within the jet. The objective of the work was towards increasing the horizontal deflection forces and no reference was made to the dynamics of the situation, in other words the time dependence of the changing deflecting force. As a result of Chadda's work a number of shortcomings with high power air jets became evident.

(i) Their momentum flux was rapidly diffused as a result of surrounding air entrainment thus giving a large jet cross section. This made them rather inefficient and indiscriminate for body deflection purposes.

(ii) High power air jets, especially when supersonic, were unpleasantly noisy; at times on the threshold of pain.

(iii) High power air jets consume considerable quantities of power. The efficiency of the power used in deflecting the smaller bodies is usually not very important, since the power used is fairly small; however for the larger bodies power consumption efficiency can become a major consideration. In this case a high switching rate would not be sought at the expense of a disproportionate increase in power consumption.

It was thought that the relatively large deflection forces required by the larger bodies could be obtained effectively by using a fluidically controlled water jet. It was also thought that the use of liquid jets would confer the advantages of:

(i) A high jet momentum flux for a given orifice and jet velocity; thus leading to a quieter and more efficient jet.

(ii) A low degree of jet spreading, thus giving a very selective deflection device.

It was recognised almost immediately that there were two major areas of concern. One was the considerable difference in behaviour between air and liquid jets; whether the jets were surrounded by gas or submerged. It was decided that there should be a preliminary survey into the behaviour of liquid jets to ensure that any proposed fluid device would operate in a satisfactory manner.

The second area of concern was that of the liquid jet/body dynamic interaction. At one time, because of the very different jet momentum flux profile of a liquid jet compared to an air jet, it was considered that some bodies may not enter the liquid jet sufficiently to utilise the high jet momentum flux available. This point had not, to my knowledge, been considered before when the jet/body interaction process had been analysed.

A third point, but not sufficient to cause concern, was that the body must tolerate the presence of the water jet.

1-3 An Introduction to Liquid Jet Behaviour

There are a number of differences between air and liquid jets, whether they flow into surroundings of the same fluid or not. The parameters thought to be of the greatest significance in this investigation were, to some extent, interrelated. The power consumed in producing the jet was of importance and the density of the liquid used and hence inertial effects, would influence this. Also certain accelerations imposed on the liquid could result in cavitation (where gas solubility and surface tension effects would become apparent). Surface tension effects would also manifest themselves during the passage of the liquid jet through gas surroundings and the combined effects of surface tension, gas solubility and entrainment contribute to the influence of any boundary geometry.

1-3-1 Power Consumption

Considering simple incompressible fluid flow from an orifice, the power consumption of the device is given by:

$$P = \Delta p.Q \quad , \quad \text{and} \quad P = \rho A \bar{v}^3 / 2 C_v^2 \quad ,$$

where

$$\bar{v} = C_v \sqrt{2 \Delta p / \rho}$$

If a certain jet momentum flux is required for body deflection and the jet momentum flux is given by:-

$$\dot{G} = \rho A \bar{v}^2 \quad ,$$

then for two different fluids under identical nozzle flow conditions:

$$\rho_1 \bar{v}_1^2 = \rho_2 \bar{v}_2^2$$

$$\frac{P_2}{P_1} = \frac{\bar{v}_2}{\bar{v}_1} = \sqrt{\frac{\rho_1}{\rho_2}}$$

The density ratio for water compared with air (at NTP) is approximately 800 therefore:

$$\frac{P_{WATER}}{P_{AIR}} \triangleq \frac{1}{28}$$

This large power advantage would not be entirely realised because the Reynolds numbers of the jets would be different and therefore so would the discharge coefficients; also compressibility effects with the larger air jet devices are significant. However, it was expected that a considerable power advantage could be obtained by operating with water jets.

Kelley and Boothe (1968) used a term called the Reynolds Coefficient to show that only moderately higher pressures would be required to produce water jets of a given Reynolds number than would be required for air. They also showed that the power consumption for any given supply pressure was considerably less for liquids than for air, but mention that fluid amplifiers usually operate at given Reynolds numbers.

1-3-2 Surface Tension Effects

When a coherent liquid jet issues from a circular orifice into air, a rather complex series of events occurs, which results in the break-up of the jet. There appears to be a general consensus of opinion (Levich, 1962; Grant and Middleman, 1966; Vitman, 1969) that at least two types of jet break-up occur.

At low jet velocities, where the dynamic action of the air can be neglected, the surface energy of the cylindrical jet, (resulting from a circular orifice), is not a minimum; therefore an energy gradient exists to break the jet into droplets. Small capillary wave disturbances occur on the jet surface, the severity of which depend upon the liquid turbulence, nozzle roughness and vibration, air movement and jet velocity profile, and result in a varicose oscillation of the jet. Some of those waves will be damped by the liquid viscosity but certain waves will be unstable and grow in amplitude until the cylindrical jet breaks into drops.

At high jet velocities, relative to the surrounding air, the dynamic effect of the air is considerable. The result is that the jet breaks up into a large number of droplets with a total surface area considerably in excess of the original jet surface. This is due to the aero-dynamic effect of the surrounding air leading to a large number of unstable surface waves. The short waves grow in amplitude and separate small droplets from the liquid jet surface. The longer waves, also unstable, result in a sinusoidal oscillation of the entire jet and eventually break the jet into large drops.

Some research workers have reported periodic oscillations of the jet when the nozzle is other than a circular cross section. Levich (1962) has pointed out that with an elliptical cross section the jet semi-axes interchange in a periodic manner; however, Taylor (1960) mentions that only one interchange of the axes is usual. Pai (1954) mentions the experimental work of other researchers where orifices of elliptical, triangular, rectangular and other polygonal cross sections all resulted in a periodic structure to the unbroken jet. A decision, which will be examined more closely in the next section, was made to use an orifice of circular cross section.

It was important in this investigation to know whether the liquid jet would break up within the fluidic device or before impacting upon the body being deflected. If the jet broke up within the fluidic device it was anticipated that considerable difficulty would be experienced in controlling the switching of the device. If the jet broke up before impacting upon the body then an analysis similar to that of Abramovitch (1963) would be required, since the velocity and density profiles of the jet, and hence the momentum flux profile, would be required. An approximate theory was used to choose an orifice size and existing formulae were then used to check that the jet remained unbroken throughout the field of interest, (Penny, 1973). Specimen calculations for the jet break-up length are given in Appendix 1; the formulae used are those of Levich (1962), Grant (1965) and Vitman (1969). These theories indicate that for the jet velocity range expected to be used in this investigation, the unbroken jet length should vary between 0.25 m. to 2.07 m.

The large variations in the predicted jet break-up length given in Appendix 1 are typical of the published research work on this phenomenon and may be due to the lack of research work on the larger liquid jets and the number of parameters thought to influence the jet's behaviour.

The survey papers Putnam 'et al' (1957) and Miesse (1955) are worth consultation should further information on this subject be required, also Garmendia (1975) who included the effects of an electrostatic field and a co-flowing air stream.

1-3-3 Gas Solubility Effects

Liquid jets, even when operating submerged, cannot sustain a pressure lower than the local vapour pressure and retain a single phase flow regime. If pressures lower than the local vapour pressure, (a function of a number of parameters the most significant of which is temperature), are reached then voids would occur within the liquid and, providing the bubbles do not collapse, a two phase flow regime would exist downstream of the cavitation point. Taft (1967), in an early paper on hydraulic fluidics, mentions the problem of air coming "-- out of solution --" at points of low pressure and the resulting difficulties in removing trapped air. The introduction of two phase flow into a device which has been designed for a single phase fluid flow is usually accompanied by a significant fall in the operating efficiency. For this reason cavitation is usually avoided if at all possible and several criteria have been used in the past to predict the onset of cavitation. The best known of these is probably the Thoma cavitation factor, which was originally applied to turbines, and the next most common being

the cavitation number, although Pearce and Lichtarowicz (1971) used a slightly different factor termed a 'K' factor.

For liquids an additional problem to the phenomenon of cavitation, where the liquid cannot sustain the tensile stress imposed upon it, is that of gas diffusion to and from the liquid. A number of papers have been published on the diffusion of various gases into cylindrical jets, however only laminar flow jets are considered. Scriven and Pigford (1959) obtained a two dimensional solution to the diffusion equations which also took into account, by means of a boundary layer analogy, the effect of shear stress relaxation on the laminar jet velocity profile as it left the orifice. Figure 1-2 reproduces one of Scriven and Pigford's graphs showing the absorption rate of carbon dioxide into water. It can be seen that, apart from very close to the orifice, the absorption rate appears to be directly proportional to the square root of the exposed jet length; also increasing the jet velocity increases the absorption rate. From Figure 1-3, assuming no evaporation occurs, it can be seen that the volumetric flow rate of carbon dioxide passing station (2) can be given by:

$$\left[Q_{co_2}\right]_2 = \left[\frac{\dot{m}_{co_2}}{\rho_{co_2}}\right]_2 = M\left[\frac{\dot{n}_{co_2}}{\rho_{co_2}}\right]_2 \quad , \text{ since } \quad n = \frac{m}{M}$$

Therefore the rate of change of volumetric flow rate with axial distance is:

$$\frac{d(Q_{co_2})}{dx} = M\left[\frac{1}{\rho_{co_2}} \cdot \frac{d(\dot{n}_{co_2})}{dx} - \frac{\dot{n}_{co_2}}{\rho_{co_2}} \cdot \frac{d(\rho_{co_2})}{dx}\right]$$

In order to approximate the diffusion rate of carbon dioxide gas into the liquid jet, density changes will be neglected. From the graph in Figure 1-2 then:

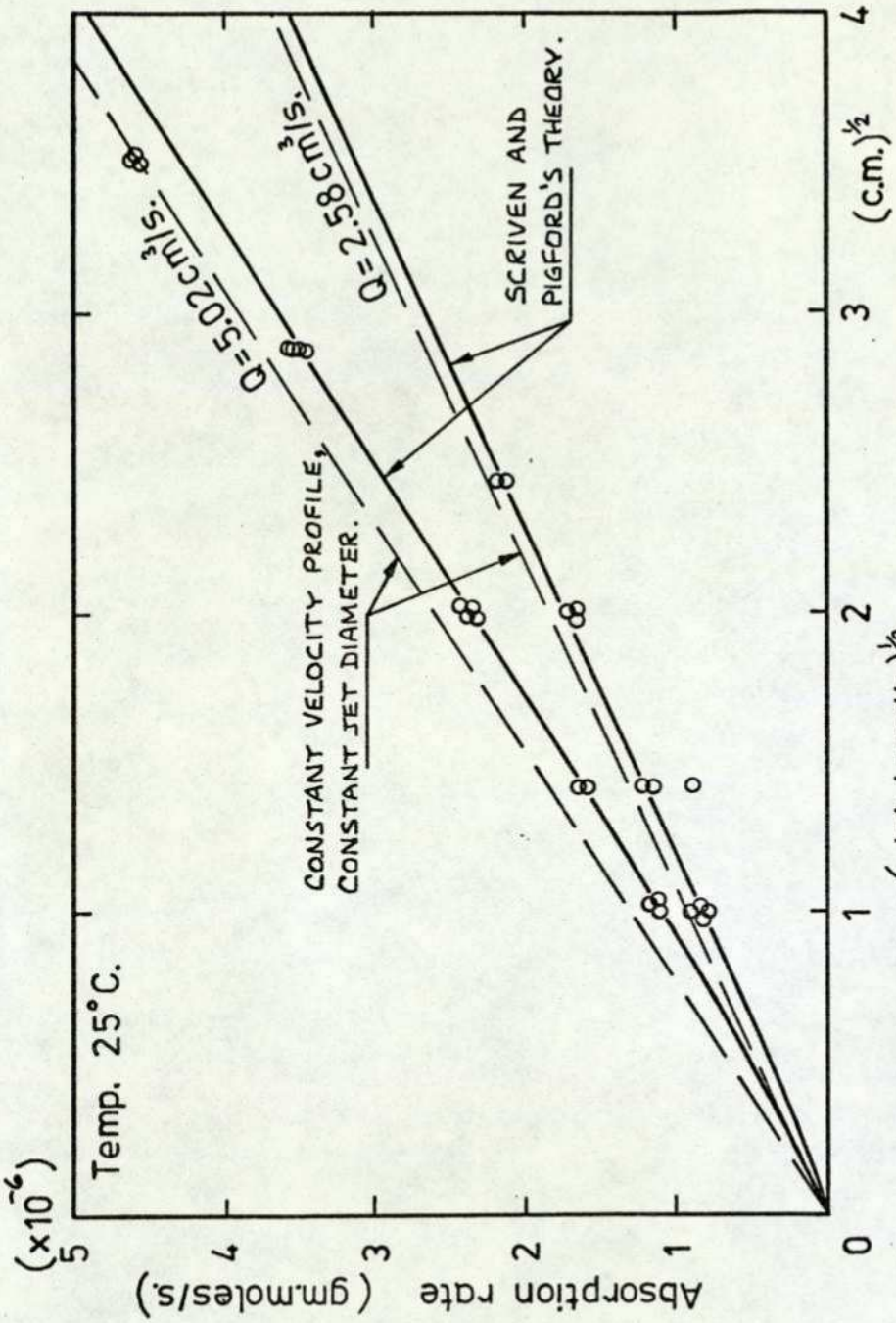

Absorption of carbon dioxide into a water jet (Scriven & Pigford (1959)).

Figure 1-2

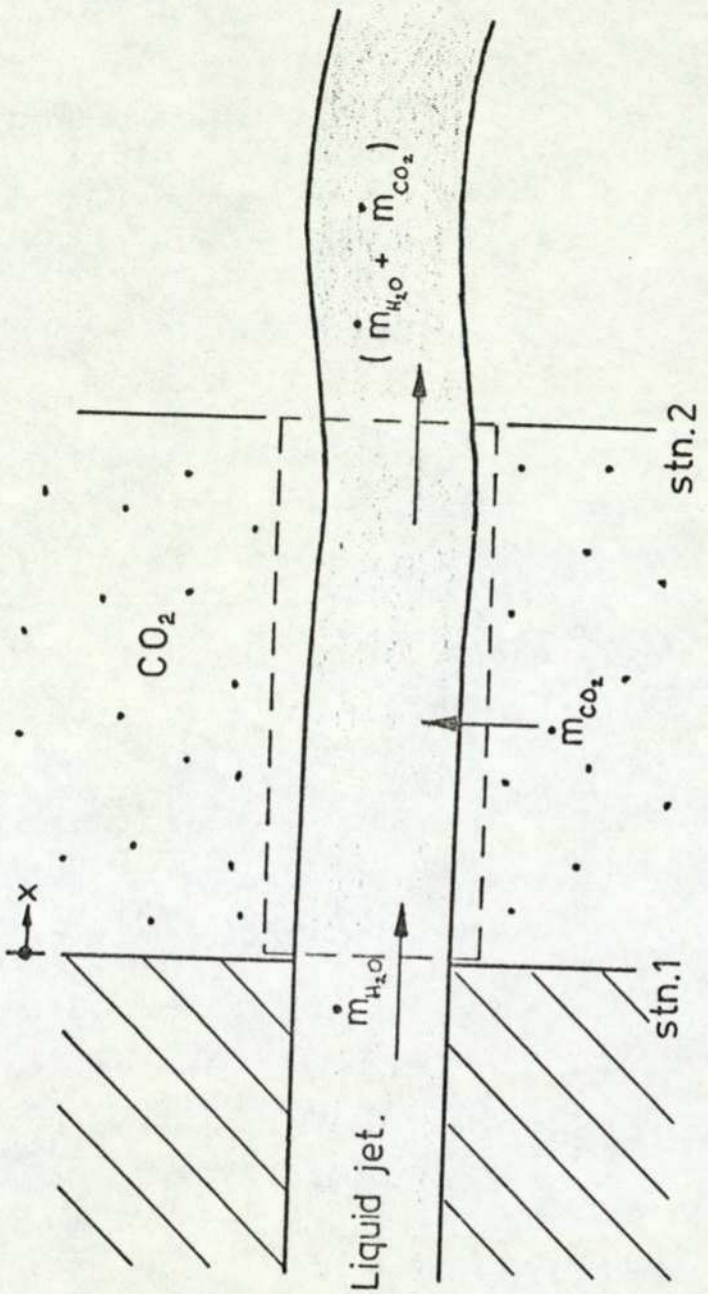

Liquid jet

Figure 1-3

$$\dot{n}_{CO_2} \triangleq c x^{\frac{1}{2}} \quad , \quad \text{and therefore}$$

$$Q_{CO_2} = \frac{M}{\rho_{CO_2}} \int_{x=0}^{x} \frac{c}{2x^{\frac{1}{2}}} . dx$$

$$= \frac{M c x^{\frac{1}{2}}}{\rho_{CO_2}}$$

Let x = 50 m.m., (likely to be the maximum permissible bubble length of a wall attachment amplifier), then from Scriven and Pigford's data:

$$Q_{CO_2} = \frac{44.01 \times 2.5 \times 10^{-9} \times 0.224}{1.78 \times 0.224} = 61.8 \text{ m.m.}^3/\text{s.}$$

It is, perhaps, worth noting that the volume of diffused carbon dioxide gas is approximately 1.2% of the liquid jet's volumetric flow rate. If a constant diffusivity and jet velocity are assumed then the volumetric diffusion rate is approximately 0.038% for every nozzle diameter downstream. This can be compared with a quoted mass entrainment rate of almost 33% for air jets (Briffa and Dombrowski, 1966). This extremely small volume of diffused gas would indicate that with practicable switching chamber volumes and reasonable switching times, gas diffusion would be insufficient to develop the required pressure difference across the jet for a wall attachment type of device to operate with a liquid jet and gas surroundings.

It should also be noted that the diffusion rates obtained were maximised by carefully removing all the dissolved gas from the water. A paper by Duda and Vrentas (1968) showed that other gases commonly found in air had similar diffusivities.

A number of authors have mentioned the inhibiting effects of the jet velocity profile and various surface active agents on diffusion rates and also the increased diffusivities due to fluid turbulence and surface waves (Scriven and Pigford, 1958, 1959; Raimondi and Toor, 1959; Duda and Vrentas, 1968). However, even an increase by orders of magnitude would leave doubt as to whether this was sufficient to obtain wall attachment and no reference was found which would be specific on this point.

1-4 Liquid Powered Fluerics

Fluerics, the control of a fluid stream without the intervention of moving mechanical parts, is generally accepted as having been introduced explicitly by the Harry Diamond Laboratories in the United States of America during 1959. There have been a number of ingenious derivatives, but most of these have been developed from four basic flueric devices. These are:

(a) Jet deflection proportional (momentum effect) devices

(b) Wall attachment or pressure controlled devices

(c) Vortex devices

(d) Turbulence devices

The typical characteristics of these basic devices have been given by Neve (1965) and from Neve's report it was apparent that the turbulence devices, being designed for low pressure operation, would be unsuitable.

A considerable number of research papers, taking fluerics as their subject, have been published over the last sixteen years but since this investigation is concerned only with the rather restricted subject of liquid jet fluerics, an exhaustive review of all flueric research will not be attempted. For those interested in a broader background to the general subject of fluidics, a book by Foster and Parker (1970) is recommended, together with the British Hydromechanics Research Association's series of Cranfield Fluidics Conference proceedings.

Much of the research work in fluerics has been devoted to air powered devices, thus all the phenomena reported result from single phase fluid flow. Liquid powered fluerics generally borrows heavily on the large volume of published work on air devices, and the liquid devices have then been modified to overcome any difficulties that have arisen due to the differences in fluid behaviour.

Considering liquid fluerics generally, Kelley and Boothe (1968) and Skoog (1972) defined a Reynolds coefficient to show that both air and water jets would reach a given Reynolds number at similar pressures, (water requiring a slightly higher pressure), whereas other common liquids require much higher pressures. Also they both noted that the response of the amplifier was directly dependent upon the jet transport time and that for a given Reynolds number, the liquid amplifier would have a slower response. Again both papers showed that for a given Reynolds number, more power was consumed by the liquid amplifiers; however it has been shown earlier in this investigation, (Section 1-2) that if a given momentum flux is required then a liquid powered device

should consume less power (this, of course, assumes that the device will operate at the resulting Reynolds number).

1-4-1 Jet Deflection Proportional (momentum) Devices

Skoog (1972) in his work on a proportional liquid flueric amplifier used the jet velocity profile of Simson (1966). After studying a number of papers where this velocity profile was used, (Simson, 1966; Foster, 1970; Brown, 1964), it would appear that Skoog's application must entail submerged flow. In this case the interaction of a surrounding gas would be avoided; however cavitation, as mentioned in the previous section and by Taft (1967), would not. Skoog does indeed mention cavitation problems. A point mentioned by Kelley and Boothe (1968) and expanded upon by Ozgu and Stenning (1971) is that the response of the element may be degraded due to the inertia of the liquid in the amplifier output legs and vents.

Skoog also showed, for submerged jet flows, the variation of the inviscid core length with nozzle aspect ratio. This may explain the proportional amplifier results of Kelley and Boothe and their use of a 'stretched' Reynolds number to obtain a consistent comparison.

Both Waters (1969) and Cousins (1970) investigated the proportional control of a water jet by air jets. Waters used a liquid jet Reynolds number of less than 2,000. He found rather inhomogeneous mixing occurred and that the velocity profile was not Gaussian. Cousins used a turbulent main jet with a Reynolds number of approximately 20,000. He noted high velocity gradients at the jet/air interface, leading to considerable mixing at the

fluid interface and also high density gradients at this point. However he also mentioned excessive turbulence, unstable two phase flow and vortex formation.

A paper by Taylor (1960) on the impact of cylindrical liquid jets in air indicated that the subject was relatively unexplored. Taylor used jets of equal diameter and velocity and, by varying the angle of impact, obtained liquid sheets of various shapes. It was thought that the poor power gain obtained with a fluidic device using the impact of equal jets would be unacceptable and, although it was not thought to be impossible to manufacture a jet impact device using unequal jets, it was decided not to pursue this subject.

1-4-2 Wall Attachment or Pressure Controlled Devices

Rechten (1967) investigated flow stability within a bistable element using a water table. He noted good flow stability and pressure recovery with latching vortices and a cusped splitter. Both Rechten and Ozgu and Stenning (1971) mentioned the earlier work of Sarpkaya (1965) on the influence of a latching vortex on the steady and transient behaviour of a bistable fluid amplifier.

A further water operated bistable wall attachment device was studied by Peichev (1972). Again the central splitter had a cusp formed within it and mention is made of the important flow stabilising effect of a vortex.

Fisher and Thomson (1968) developed a low pressure high flow rate wall attachment device for use as a diverter valve. They found that gravitational body forces were significant when the device was operated in either the vertical or horizontal

plane and this resulted in spillover into the passive output leg. Lowering the main jet aspect ratio to 1.0 reduced this effect. Also a pointed splitter gave an unstable vortex on the 'outside' edge of the jet, this vortex being of an air-water mixture, since the passive leg of the device was air filled. The device was stabilised by using a cusped splitter, (with the resulting vortex), and the device then gave good wall attachment and low spillover.

Ryoichi (1968) also used a liquid powered wall attachment device. He listed the difficulties of operating a liquid jet into air as: a long switching time or no response to an input signal; a low degree of jet wall attachment and spillover into the passive output port. His solution was to fill the interaction region of the device with liquid by means of an auxiliary jet mounted in the splitter nose and directed into the main jet. The flow rate of the auxiliary jet had to be large enough to fill the interaction region without spilling down the passive output leg or causing oscillation by restricting the output of the main jet. Ryoichi required a switching time of less than 100 ms., which he achieved. He also noted the presence of a 'latching' vortex on the 'outside' edge of the jet.

Skoog (1972) mentions the work of Foster (1970) on an oil powered bistable fluid amplifier. Turbulent flow was maintained at low Reynolds numbers by introducing sharp edges at the main nozzle orifice. Foster obtained the transition from laminar to turbulent flow at a Reynolds number below 300, (based on hydraulic mean depth). Foster mentions the deleterious influence of the amplifier walls and splitter on Bahrton's (1970) original amplifier design and these features were removed.

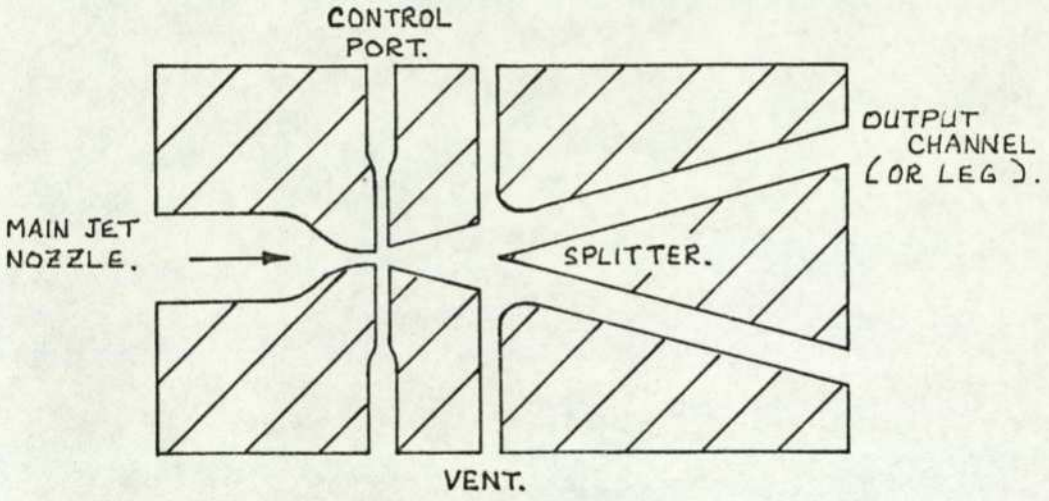

(a) Typical wall attachment amplifier.

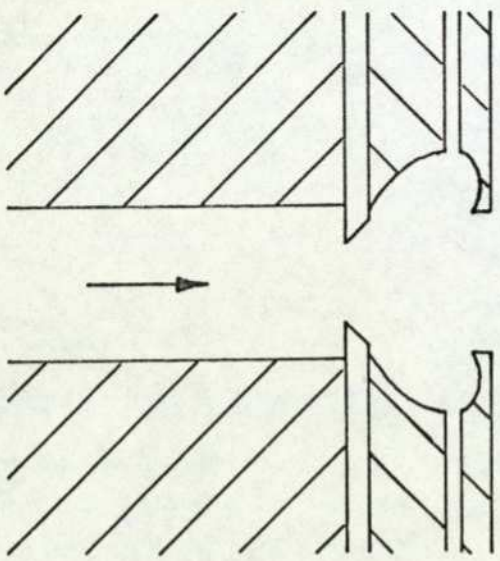

(b) Amplifier type used by Foster(1970).

Figure 1 – 4

The amplifier as tested by Foster with submerged oil flows is shown in Figure 1-4 (b).

Bahrton (1970), using the same type of device as Foster, specifically mentioned its operation with a liquid power jet and gas surroundings. Under these conditions he stated that:- "the downstream edges of the chambers prevent air passing into the low pressure region when the control port is closed."

Woods (1972) introduced a rather more unusual device although not, unfortunately, operating a liquid jet into air surroundings. A liquid jet entrained liquid from an upper pair of vents and 'dumped' any excess liquid in a lower pair. The jet was deflected by a pneumatic pressure difference across the jet above the upper liquid vents. The liquid gas surface tension prevented any measurable flow of air into the liquid, within certain pressure limitations.

An unusual diverter valve was described by Ohta (1973). Two small liquid sub-flows were provided, through suitable restrictors, from the same source as the main liquid jet. With no air control signal the flow was submerged and attached to the output walls. When an air control flow signal was made into one of the sub-flow channels this was carried into the low pressure region adjacent to the main jet. The small shear forces existing between the air and liquid resulted in the liquid jet separating from that wall. The pressures used were comparatively low and downstream of the control signal the flow was naturally two phase; however, the device appeared to operate well up to a switching frequency of 25 Hz.

1-4-3 Vortex Devices

Most vortex devices differ from other devices not only in type but in that the impedance of the outlet orifice is very much higher than either the control or the main jet orifice impedances. This usually ensures that the control and main jet flows mix in a contained volume since the outlet impedance dominates the device.

There are two types of vortex device, the conventional radial type as investigated by a large number of authors, (Duff, Foster and Mitchell, 1965; Neve, 1965, 1971; Syred, Royle and Tippetts, 1968; Bichara and Orner, 1969; among others) and the axial vortex type (Al-Shamma 'et al', 1972; McCloy and Stevenson, 1972; Rimmer, 1975). Unfortunately the relative switching speed of a radial vortex device is slow and appears to be directly related to the time taken to fill the vortex chambers (Neve, 1965, 1971). Taplin and Seleno (1970) set their vortex device switching time constant equal to the chamber filling time and Otsap (1968) stated that it increased with the chamber volume.

The axial device investigated by Al-Shamma (1972) had a large central body inserted in the vortex chamber. It was thought that this reduction in the chamber fluid volume could significantly improve the transient response of the amplifier.

This device was chosen for development into a sorting machine deflection device. The reasons for its selection are given more fully in the conclusions to this chapter (Section 1-5) and a review of vortex flow literature prior to the design and testing of the device is given in Chapter 3, Section 3-1.

1-5 Summary - Introduction

A number of points have been decided as a result of the preceding sections.

First it was decided to investigate the dynamics of a body dropping into a liquid jet. To the best of the author's knowledge this has never been attempted before. The investigation was to be conducted by means of a theoretical model and supported by experimental results. With regard to body deflection, the parameters thought to be of the greatest significance were:-

(a) The sorting rate (the reciprocal of the ejection time).

(b) The displaced distance of the body

(c) The size and mass range of the bodies sorted.

As a result of the investigation into the dynamic interaction between a body and a liquid jet it would be decided whether liquid jet deflection was suitable for sorting aggregate materials of the required sizes.

From the brief review given of liquid flueric literature it was noted that cavitation, trapped air and two phase flow resulted in unstable fluid flow and inefficient operation. Also liquid powered devices had a lower transient response due to longer transport or chamber filling times. Further, that successful liquid powered devices often maintained the control jet/main jet mixing region filled with liquid, kept main jet aspect ratios close to unity and used vortices to generate the large pressures necessary to stabilise and control the liquid flow.

It was decided that the most suitable deflection device would be a new axial vortex device. This device would be free from cavitation and two phase flow in the mixing region, generate the required control forces and (due to the presence of a central body within the vortex chamber) have a reasonable transient response.

Following the investigation into a body's movement under the action of a liquid jet, a review of the pertinent literature on swirling liquid flow and the subsequent development of a vortex deflection device is given in Chapter 3.

2. THE DEFLECTION OF A BODY BY A LIQUID JET.

2-1 The Forces Exerted Upon a Body by a Liquid Jet

When an unbroken cylindrical liquid jet strikes a flat plate it is transformed into a sheet which flows radially outwards over the plate from a region of impact whose dimensions are of the order of the cross section of the jet. In the impact region pressure is built up which deflects the streamlines from the direction of the jet to lines in the impact plane which spread out radially. The stream velocity varies in passing through the impact region but, if the fluid is inviscid, it will regain its original value on leaving the region. Taylor (1966) mentions that for this physical situation frictional effects at the solid surface are in most cases relatively unimportant.

For a two-dimensional inviscid jet striking a flat inclined plate it can be shown that by conserving the jet momentum parallel to the plate the jet divides such that a fraction of the volume Q_1 is directed back up the plate while the remainder Q_2 flows forward along the plate. Q_1 and Q_2 are given by:

$$Q_1 = Q_J \sin^2(\theta/2) \qquad -(2\text{-}1)$$

$$Q_2 = Q_J \cos^2(\theta/2) \qquad -(2\text{-}2)$$

The forces on the plate, in the x and y coordinate directions, due to the change in the jet direction are given by:

$$F_x = \rho Q_J v_J \sin^2\theta = \dot{G}_J \sin^2\theta \qquad -(2\text{-}3)$$

$$F_Y = -\rho Q_J v_J \sin\theta\cos\theta = -\dot{G}_J \sin\theta\cos\theta \qquad -(2\text{-}4)$$

Taylor (1966) calculated the pressure distribution in the impact region for the two-dimensional jet and for the three-dimensional case defined a function $F(\theta, \phi)$ that determined the thickness of the radially outflowing sheet, (see Figure 2-1). Taylor did not determine the function $F(\theta, \phi)$ analytically but, in another paper on the oblique impact of two cylindrical jets (Taylor, 1960), this function was measured for three values of θ. Graphs of the function $F(\theta, \phi)$ are shown in Figure 2-2 and it can be seen that the radial distribution of fluid is strongly dependent on θ, particularly at low values of the jet collision angle. The distribution of the jet over a flat plate will not affect the resultant forces F_x and F_Y but, over any other shaped body the distribution of the jet is important in determining the resultant forces exerted on the body.

Taylor (1966) also raised the point that if a jet is issuing downwards at an angle θ on to a flat horizontal plate and the plate is moving upwards with a velocity u, then the velocity of the jet approaching the impact region is $(v_J + u.\mathrm{cosec}\,\theta)$. Therefore pressures greater than the stagnation pressure of the jet are possible when the surface of impact is moving relative to the jet, as is the case with a body falling through a jet.

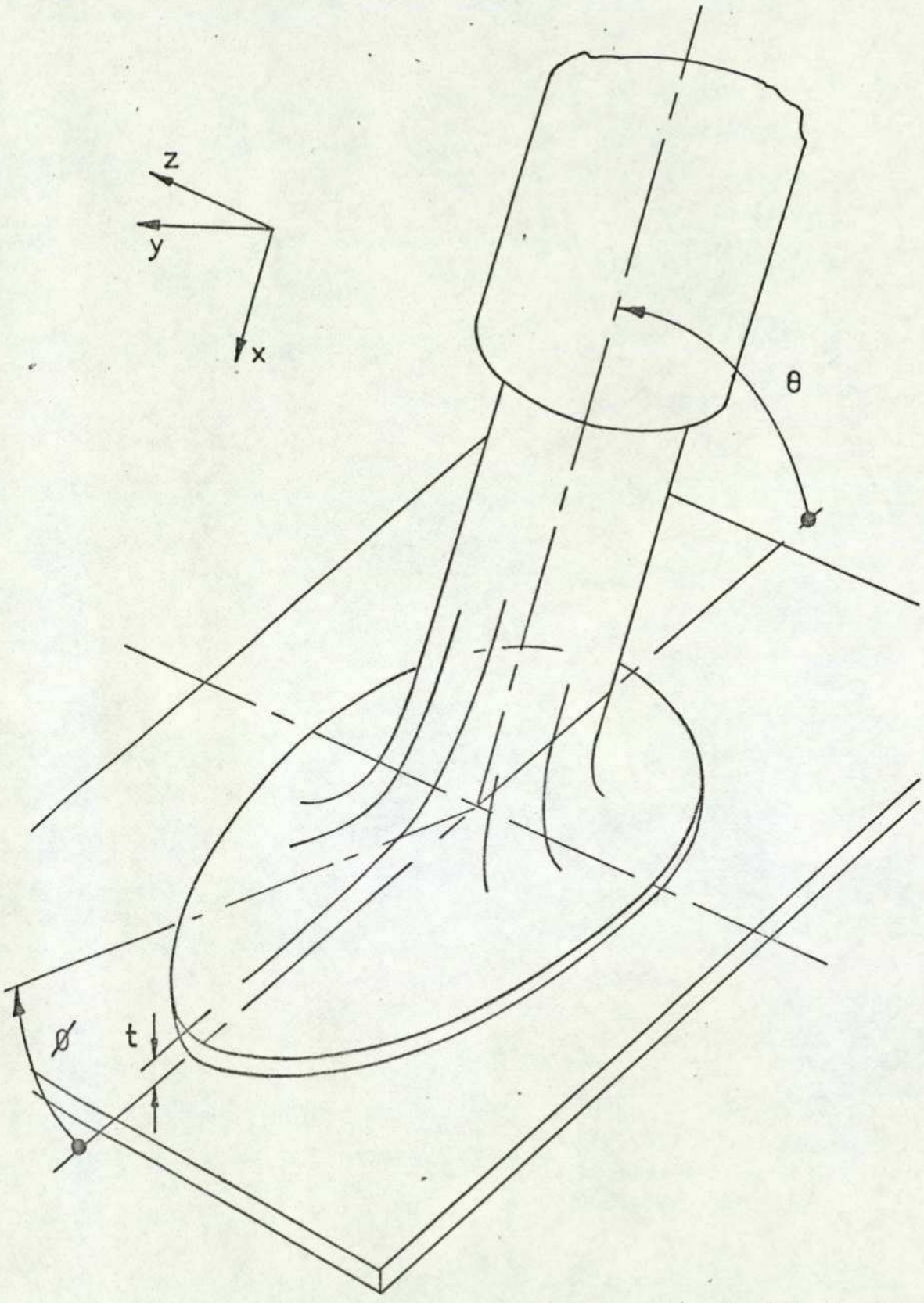

The impact region of an inclined cylindrical liquid jet on a flat plate.

Figure 2-1

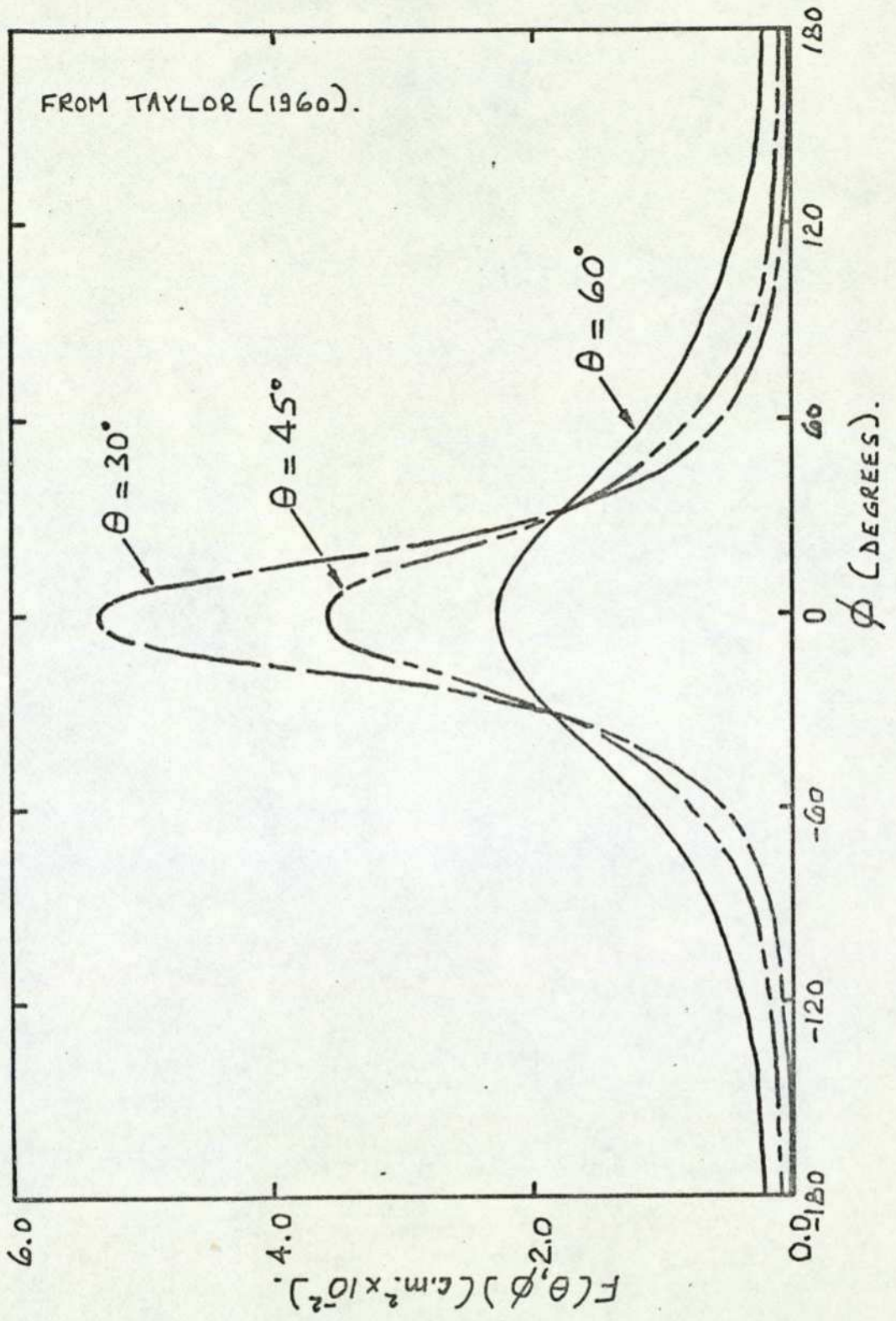

Flow distribution function

Figure 2-2

2-2 The Two-Dimensional Movement of an Arbitrary Shaped Body

A quasi-static method of analysis will be used throughout this section on body movement. The forces exerted upon the body by the jet in the horizontal (x) and vertical (y) directions were calculated and then used to solve the Newtonian equations of motion for the body.

For a body of arbitrary geometric shape the equations of motion to be solved at any instant are:

$$a_Y = \frac{F_Y}{m_P} + g \qquad \text{—(2-5)}$$

$$a_X = \frac{F_X}{m_P} \qquad \text{—(2-6)}$$

$$\ddot{\theta}_P = \frac{M_G}{I_G} \qquad \text{—(2-7)}$$

Integrating the vertical cartesian coordinate equation of motion gives:

$$\int_{V_{Y1}}^{V_{Y2}} V_Y \, dV_Y = \frac{V_{Y2}^2 - V_{Y1}^2}{2} = \int_{y_1}^{y_2} a_Y \, dy \qquad \text{—(2-8)}$$

Substituting from equation (2-5) into equation (2-8) gives:

$$V_{Y2} = \left[2 \int_{y_1}^{y_2} \left(\frac{F_Y}{m_p} + g \right) dy + V_{Y1}^2 \right]^{1/2} \qquad \text{—(2-9)}$$

Providing the initial velocity V_{Y1} is known and the function F_Y against y is known then the integration in equation (2-9) can be performed analytically or numerically and the velocity and acceleration of the body at any point 'y' determined.

To proceed further with the analysis, the variable time must be introduced. This is possible analytically only if the forces on the particle are known against time; failing this a function must be assumed. The time interval could then be obtained by using an iteration procedure to solve equation (2-10), since the function F_Y and the value of the integral would now both be known.

$$\int_{V_{Y1}}^{V_{Y2}} dV_Y = \int_{t_1}^{t_2} a_Y dt = V_{Y2} - V_{Y1} = \int_{t_1}^{t_2} \left(\frac{F_Y}{m_p} + g \right) dt \qquad \text{—(2-10)}$$

Therefore once the time intervals corresponding to the increments in 'y' are known the velocities and displacements in the 'x' direction could be calculated from equations (2-11), (2-12).

$$\int_{V_{X1}}^{V_{X2}} dV_X = V_{X2} - V_{X1} = \int_{t_1}^{t_2} a_X dt \qquad \text{—(2-11)}$$

$$\int_{x_1}^{x_2} dx = x_2 - x_1 = \int_{t_1}^{t_2} v_x \, dt \qquad \text{—(2-12)}$$

Both these equations could be integrated analytically or numerically since F_x would be known against 'y' and hence against time.

The moment equation could be solved in a similar manner to the 'x' component equation of motion. Hence the equations of motions for the body could be solved at any instant of time as the body passed through the jet and the motion traced.

It should be noted that when solving equation (2-10) to obtain the time interval corresponding to the change in V_Y, if there were no change in V_Y (a_Y therefore equals zero), then no time interval could be calculated. Also, if the vertical forces retarding the body's progress through the jet were of a sufficient magnitude then the vertical velocity would reach zero. In this case the force F_Y may exceed the magnitude of the gravitational force, but in a negative sense, and the body would start to rise back out of the jet. Since the forces exerted upon the body are a function of the relative velocity between the jet and the body then, as the body accelerated in the horizontal direction (x) the relative

velocity would fall. In theory, therefore, the body would pass through the jet if immersed for a sufficiently long time.

A cylindrical body was chosen for further analysis since it was thought to be a reasonable approximation to a practical situation whilst allowing a two-dimensional analysis.

2-3 A Two-Dimensional Analysis of the Movement of a Cylindrical Body

2-3-1 General Quasi-Static Theory

Consider a circular cylindrical body passing through a horizontal liquid jet of circular cross section, as is shown in Figure 2-3 (a). Depending upon the body's position relative to the jet part or all of the jet's momentum flux will be incident on the body and the jet will be disrupted and deflected through some unspecified angle. For the purpose of a mathematical model the following assumptions were made:

(1) The diameter of the body was greater than the diameter of the liquid jet.

(11) Jet momentum forces only were calculated and therefore since the body was cylindrical and circular there was no moment and hence no rotation of the body about its mass centre.

(111) When the body intercepted only part of the jet's cross section then the momentum flux incident on the body was that corresponding to the intercepted portion of the jet's cross section. The interaction between the deflected intercepted portion of the jet and the remainder of the jet was neglected.

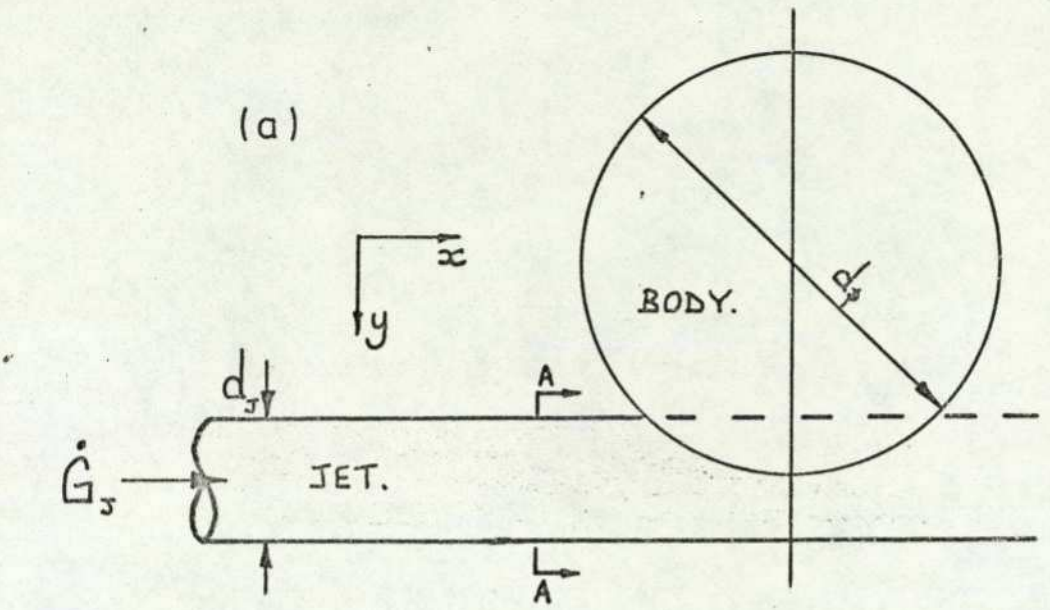

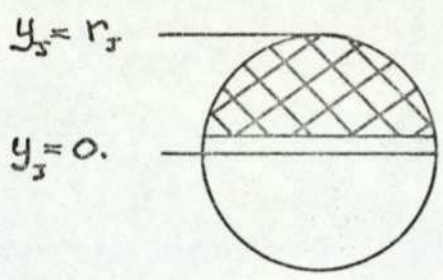

(b)

SECTION A-A.

CROSS-HATCHED AREA IS THE PROPORTION OF THE JET'S CROSS-SECTIONAL AREA INTERCEPTED BY THE BODY.

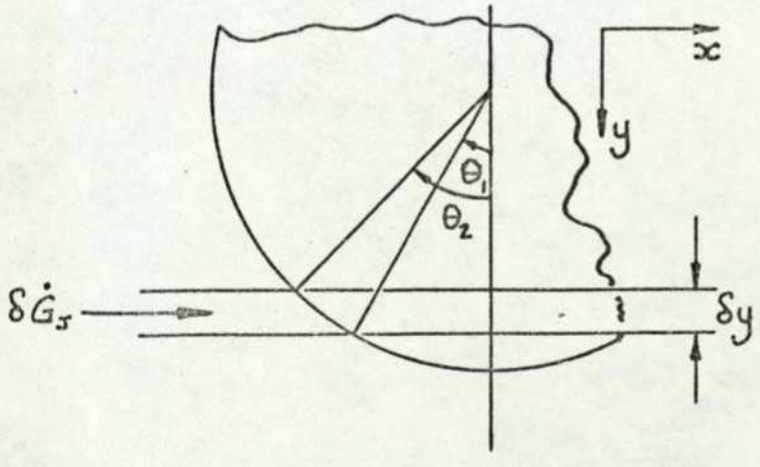

(c)

Jet/body configuration

Figure 2-3

An incremental vertical movement of the body was chosen, 'δy' (also referred to as the step size) and the perpendicular cross section of the jet corresponding to the step was calculated; see Figure 2-3 (b) where:

$$\delta A_{1-2} = \iint_R f(x,y)\,dR = 2\int_{y_{J1}}^{y_{J2}} \left(r_J^2 - y_J^2\right)^{1/2} dy_J \qquad \text{—(2-13)}$$

Substituting $y_J = r_J \sin\theta$ it can be shown that:

$$\delta A_{1-2} = 2r_J^2 \int_{\theta_1}^{\theta_2} \cos^2\theta\, d\theta$$

Which after integrating and a little manipulation becomes:

$$\delta A_{1-2} = 2r_J^2 \left[\frac{\sin\theta\left(1-\sin^2\theta\right)^{1/2}}{2} + \frac{\theta}{2} \right]_{\theta_1}^{\theta_2}$$

$$= r_J^2 \left[\frac{y_J}{r_J}\left(1 - \left(\frac{y_J}{r_J}\right)^2\right)^{1/2} + \sin\left(\frac{y_J}{r_J}\right) \right]_{y_{J1}}^{y_{J2}} \qquad \text{—(2-14)}$$

Having calculated the jet's incremental cross sectional area then the incremental momentum flux incident on the corresponding area of body could be calculated.

Considering now the cylindrical body; the body angles corresponding to the step 'δy' were calculated and an average angle obtained through which that portion of the jet was considered to be deflected, (see Figure 2-3 (c)). As the body passed through the jet, the jet's cross section was progressively intercepted by the body. From the average angles calculated for each incremental step a weighted jet angle was finally obtained, through which it was assumed the fraction of the jet

incident on the body was deflected. The jet angle was defined as:

$$\theta = \theta_M = \sum_1^n (\delta A . \theta_{AV.}) / \sum_1^n (\delta A) \qquad \text{—(2-15)}$$

where $\theta_{AV.} = \theta_1 + (\theta_2 - \theta_1)/2$

This definition of the jet deflection angle weights the angle to the jet's centre line, where the maximum jet area is exposed for an incremental step 'δy'; the area being proportional to the jet momentum flux. Having obtained the angle through which the jet was assumed to be deflected then the forces exerted on the body were given by:

$$F_x = \dot{G}_J \sin^2\theta \qquad \text{—(2-3)}$$

$$F_Y = -\dot{G}_J \sin\theta \cos\theta \qquad \text{—(2-4)}$$

The force profiles are shown in Figure 2-4.

For a cylindrical body considering momentum forces only then no moment exists about the body axis.

Since the forces exerted on the body by the jet could now be obtained at any given position in the jet then, referring to the theory given in section 2-3, equation (2-9) could be solved analytically for a cylindrical body. The functions F_Y and hence a_Y against time were not known and it was assumed that they could be represented by truncated Taylor series. This was thought to be reasonable providing the second and higher order derivatives were small and that the resulting time interval was small. The integration of

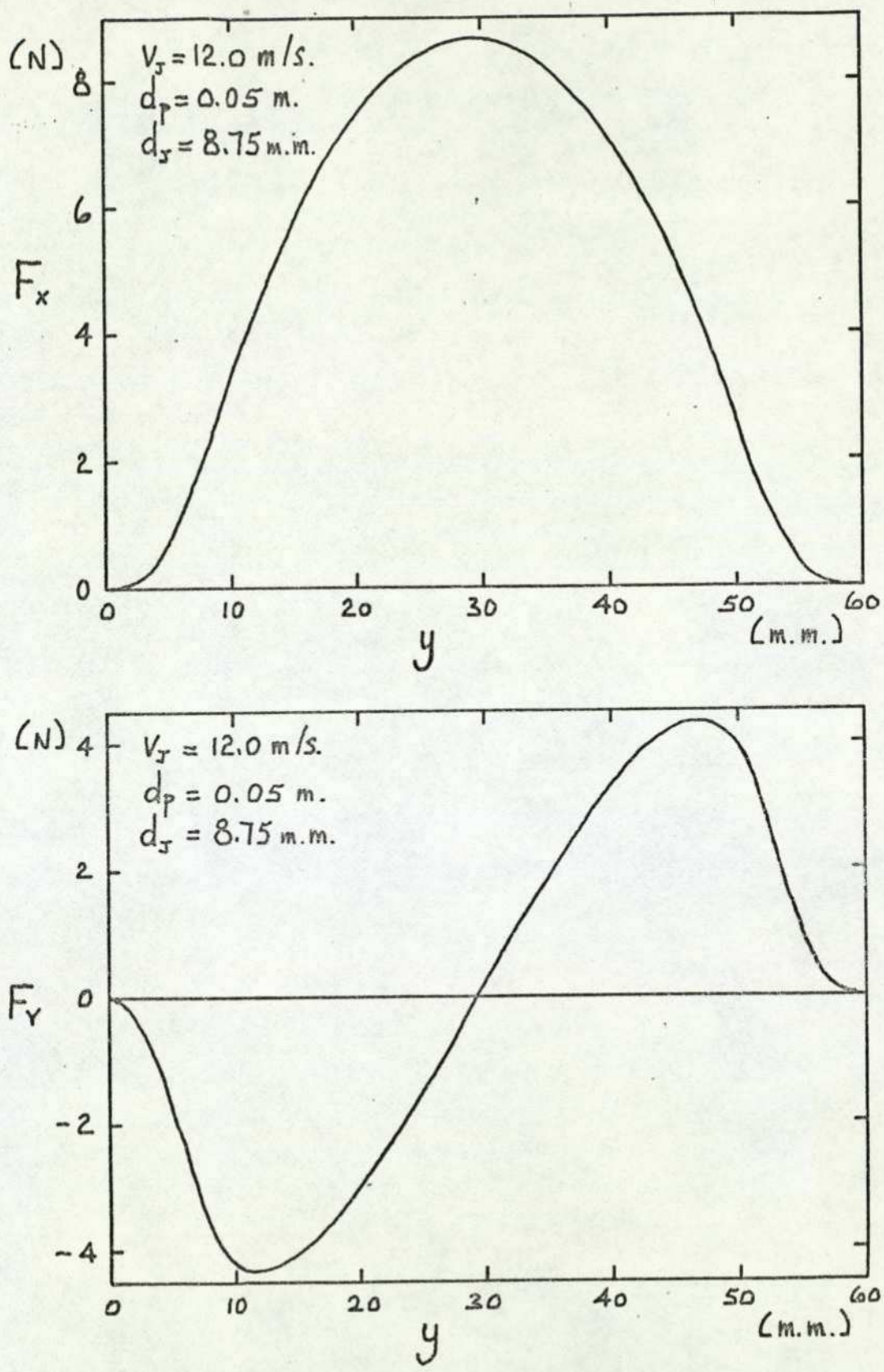

Cylindrical body force profiles.

Figure 2-4

equation (2-10) became an application of the prismoidal rule and hence:

$$(t_2 - t_1) = 2(v_{Y2} - v_{Y1})/(a_{Y2} - a_{Y1})$$

Having obtained the time intervals corresponding to the step increments 'δy' through the jet then equations (2-11) and (2-12) could be solved numerically to obtain the body's horizontal velocity and displacement.

A computer program was written to solve the equations of motion for a number of cylindrical body sizes and masses and for various jet velocities. For the numerical integration of equations (2-11) and (2-12) any of the proprietary computer subroutines could have been used that can integrate tabulated data spaced at unequal intervals. It was, however, recognised that errors would have been introduced from the assumed function introduced for a_Y against time and that a sophisticated integration procedure could only minimise further errors and not eliminate errors inherent within the analysis. For this investigation the prismoidal rule was thought to be adequate for the integration of equations (2-11) and (2-12) except where the time interval for an incremental step 'δy' became relatively large; this was checked by examining the computer program print-out. Account was also taken within the program of the reduction of jet momentum flux incident on the body due to the body's increasing horizontal velocity.

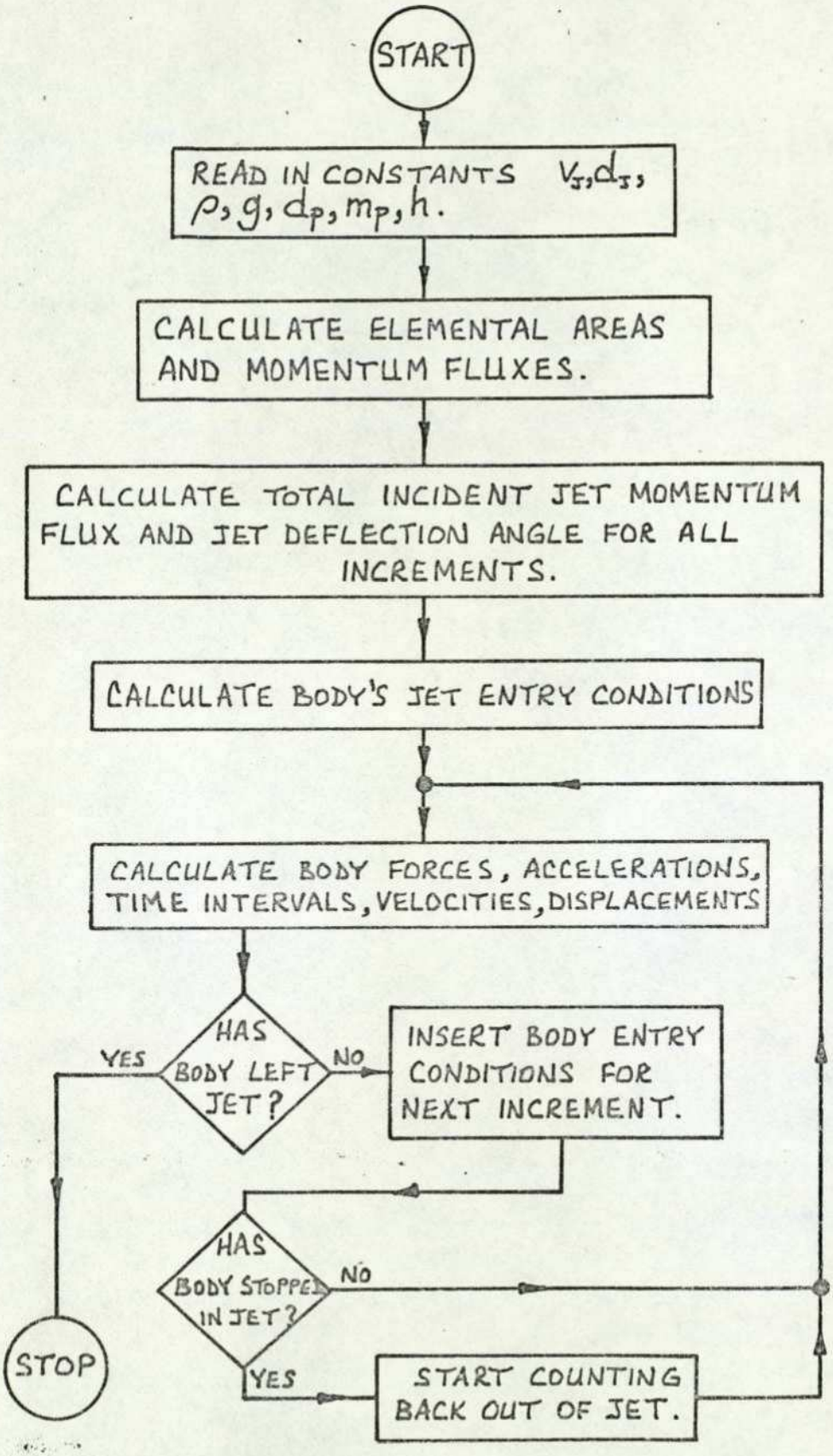

Computer algorithm for body movement.

Figure 2-5

The flowchart for the computer program used is shown in Figure 2-5 and graphs showing the theoretical curves and comparing them with experimental results are given in section (2-5).

2-3-2 The Minimum Jet Entry Velocity required for a Cylindrical Body to Pass Directly Through a Liquid Jet

It can be shown that there is a minimum downward velocity which the body must attain before entering the jet if it is to pass directly through it. The analysis assumes that the incident jet momentum flux is a constant. Substituting for F_Y from equation (2-4) into equation (2-5) then:

$$a_Y = -\frac{\dot{G}_y}{m_p} \sin\theta \cos\theta + g \qquad \text{—(2-16)}$$

Consideration of equation (2-16) indicates that if the incident momentum flux was of sufficient magnitude then a_Y would become negative; also if the deceleration was of sufficient magnitude and over a sufficient period of time then the body velocity would reach zero. If this occurred before the body was approximately half way through the jet then the body would not pass through the jet. From equation (2-9) $V_Y = 0$ when:

$$V_{Y1}^2 = -2 \int_{y_1}^{y_2} \left(\frac{F_Y}{m_p} + g \right) dy \qquad \text{—(2-17)}$$

The integral is shown in a schematic form in figure 2-6 as the cross-hatched area. The figure is only schematic since 'δy'

does not equal $\delta\theta$ but follows the relationship $dy = r_p \sin\theta d\theta$

If the cross-hatched area exceeds $(V_{Y1}^2/2)$ then the body will not pass directly through the jet. A minimum jet entry velocity was defined such that:

$$V_{Y1(MIN.)}^2 = -2\int_{y_1}^{y_2}\left(-\frac{\dot{G}_J}{m_p}\sin\theta\cos\theta + g\right)dy \qquad \text{—(2-18)}$$

Transforming the variables, then:

$$dy = r_p\sin\theta\, d\theta \quad ; \quad \cos\theta = 1 - y/r_p$$

$$V_{Y1(MIN.)}^2 = 2\int_{\theta=0}^{\theta}\left[\frac{\dot{G}_J r_p}{m_p}\sin^2\theta\cos\theta - g r_p\sin\theta\right]d\theta \qquad \text{—(2-19)}$$

$$= \left[\left(\frac{2\dot{G}_J r_p}{3m_p}\right)\sin^3\theta - 2gr_p(1-\cos\theta)\right]_{\theta=0}^{\theta_*} \qquad \text{—(2-20)}$$

To obtain the upper integration limit θ_* the case will be taken where the body just reaches zero velocity. At this point:

$$a_Y = 0 \qquad \text{and} \qquad -\frac{F_Y}{m_p} = g$$

Therefore $\sin\theta_*\cos\theta_* = \dfrac{gm_p}{\dot{G}_J}$ and since

$$\sin\theta_* \cos\theta_* = \frac{1}{2}\sin 2\theta_* \qquad \text{then}$$

$$\theta_* = \frac{1}{2}\left[\sin^{-1}\left(\frac{2gm_P}{\dot{G}_J}\right)\right] \qquad \text{—(2-21)}$$

There are two solutions to equation (2-21) for $0 \leq \theta \leq \pi/2$ and the upper integration limit is the larger of these, see Figure 2-6. The signifance of $\dot{G} < 2gm_P$ is that the acceleration curve no longer crosses the axis $a_Y = 0$ and therefore the body accelerates continuously through the jet.

Substituting from equation (2-21) into (2-20) and using the trigonometrical identities:

$$\sin^2\theta + \cos^2\theta = 1 \quad ; \quad \cos\theta = \left[\frac{1}{2}(1+\cos 2\theta)\right]^{1/2}$$

$$\sin\theta = \left[\frac{1}{2}(1-\cos 2\theta)\right]^{1/2}$$

Then, if care is taken when obtaining the square roots that the higher value of θ_* is inserted:

$$V^2_{Y1(MIN)} = K_1\left[\frac{1}{2}\left[1+\left(1-K_3^2\right)^{1/2}\right]\right]^{3/2} - K_2\left[1+\left[\frac{1}{2}\left(1+\left(1-K_3^2\right)^{1/2}\right)\right]^{1/2}\right]$$

where $K_1 = \frac{2\dot{G}_J r_P}{3m_P}$; $K_2 = 2gr_P$; $K_3 = \frac{2gm_P}{\dot{G}_J}$

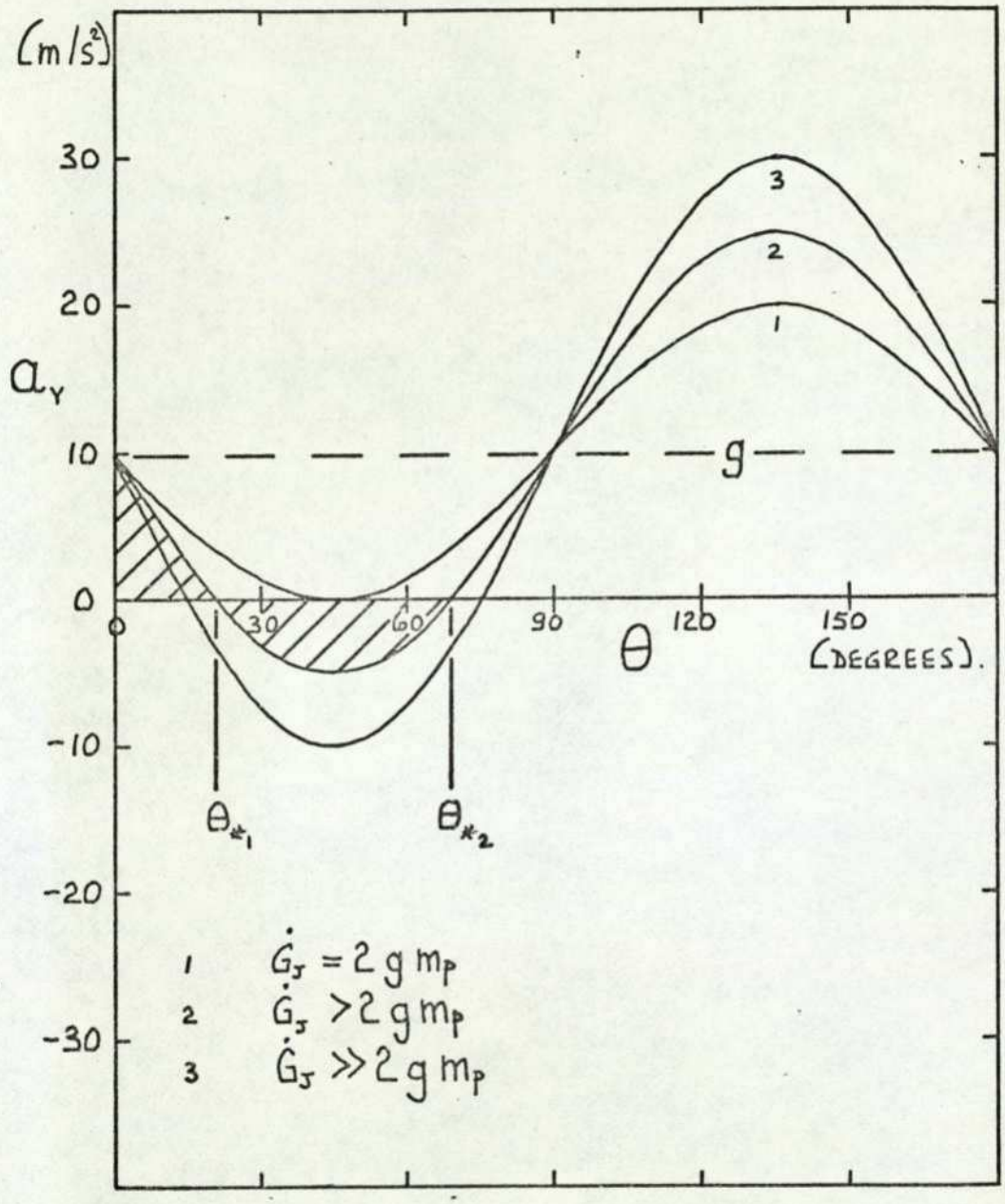

Body vertical acceleration against jet penetration.

Figure 2-6

Correct to four places of decimals the expression for the minimum jet entry velocity becomes:

$$V_{YI(MIN)} = \sqrt{\left[0.2357\left(\frac{\dot{G}_J r_P}{m_P}\right)\left[1+\left[1-\left(\frac{2gm_P}{\dot{G}_J}\right)^2\right]^{\frac{1}{2}}\right]^{\frac{3}{2}} - 2gr_P\right.}$$

$$\left.\left[1 - 0.7071\left[1 - \left[1 - \left(\frac{2gm_P}{\dot{G}_J}\right)^2\right]^{\frac{1}{2}}\right]\right]\right] \qquad \text{—(2-22)}$$

As has been mentioned previously, it is not physically possible to have the square root of a negative quantity since under these conditions the body accelerates continuously through the jet. It should also be noted that the analysis is for a limiting case where the body advances as far as is possible without going through the jet. At jet velocities higher than the limiting value or for a body entry velocity less than the minimum then the body should stop advancing through the jet before the point θ_{*2} and it should be driven back out of the jet since the acceleration will be negative.

Providing that in practice the jet entry velocity of the body exceeds the theoretical minimum jet entry velocity then the body should pass directly through the jet. This is ensured because the body's increasing horizontal velocity has been ignored in the analysis as has the fact that in practice the entire jet momentum flux is not incident on the body as it enters the jet and therefore the real incident momentum flux on the body is less than that assumed in the analysis.

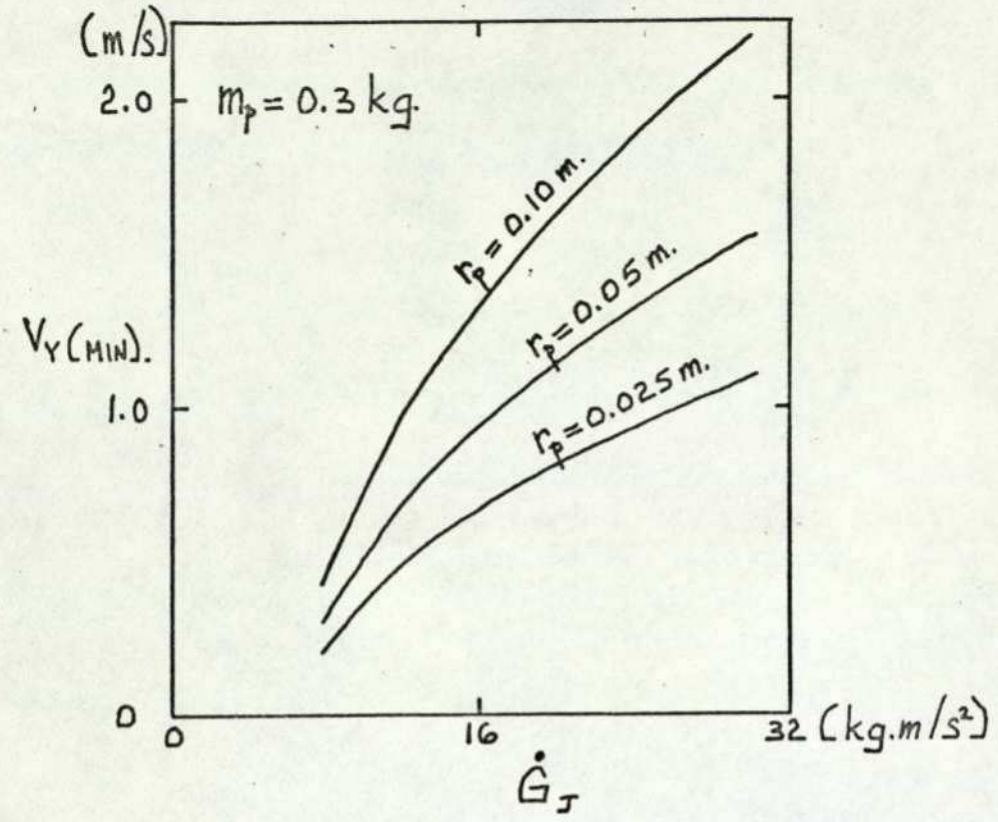

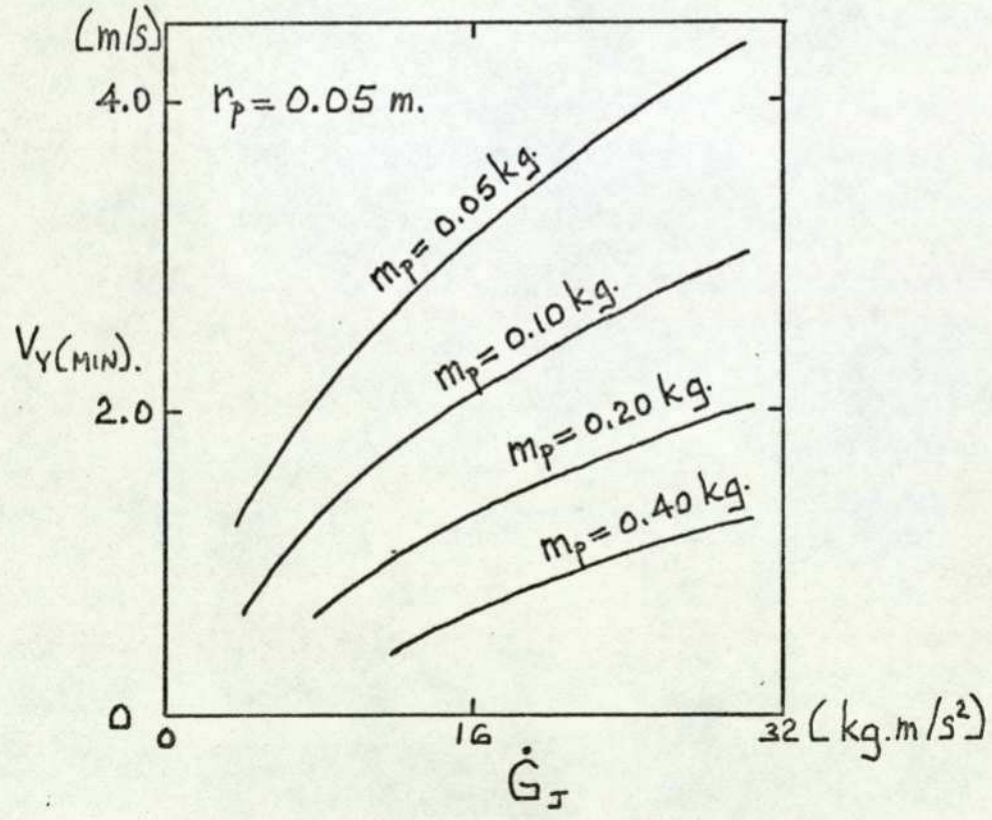

Minimum jet entry velocity

Figure 2-7

Figure 2-7 shows the variation of the minimum jet entry velocity with changes in the three parameters. A discussion of the analysis and a comparison with experimental results is given in section (2-5).

2-4 Cylindrical Body Deflection Experiments

2-4-1 Experimental Precautions, Preliminary Tests and Error Estimates

The theoretical configuration was a horizontal liquid jet of constant circular cross-section impacting on cylindrical bodies of known size and mass. The liquid properties are given in Appendix 2. The water temperature was monitored using a thermometer and maintained at approximately a constant temperature. To ensure that the experimental liquid jet closely approached the theoretical ideal aluminium honeycomb was inserted into the supply pipe to eliminate residual swirling flow in the pipe and a convergent nozzle, as shown in Figure 2-8 was used to minimise the effects of boundary layer growth on the jet velocity profile. The jet velocity was measured with a hypodermic total head tube, the pressure being sensed by a pressure transducer and the resulting electrical signal displayed on an oscilloscope. An experiment was performed to calibrate the pressure transducer's electrical signal in terms of the liquid jet's velocity; the results of this experiment are given in Appendix 3.

The hypodermic probe was used to traverse the jet in both the vertical and horizontal planes; a flat topped constant velocity profile was obtained.

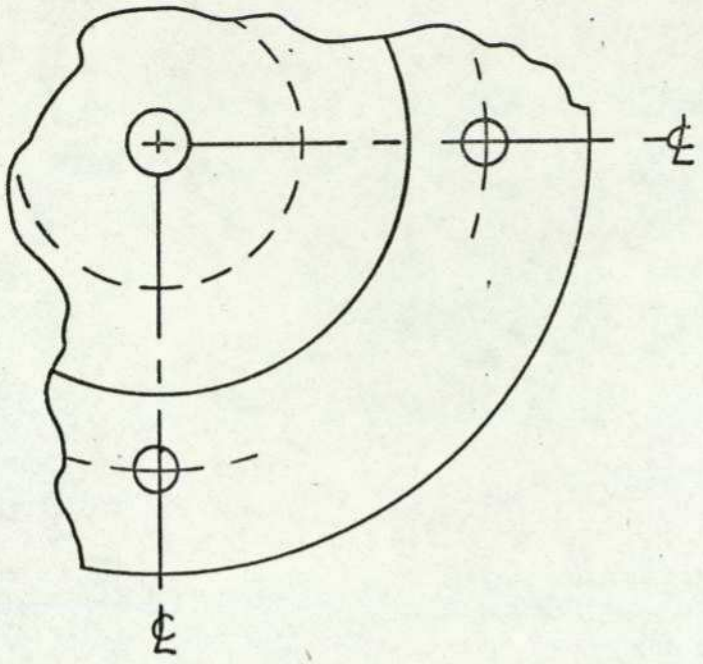

MERIDIAN PLANE SECTION.

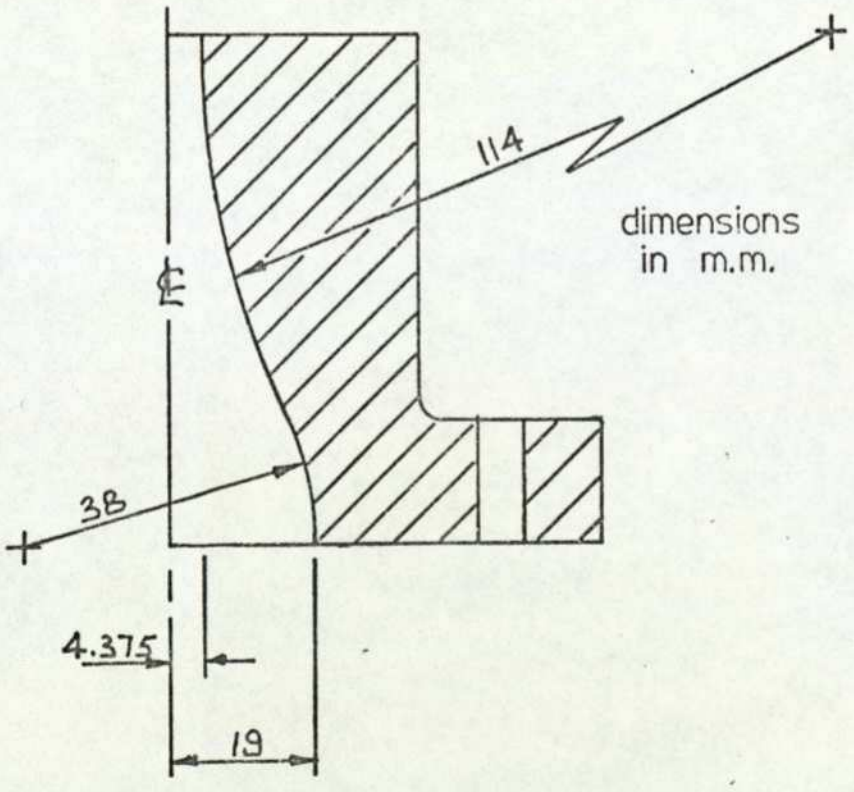

Convergent nozzle.

Figure 2-8

The effect of neglecting the gravitational body forces acting on the jet resulted in the introduction of three errors. Examination of Figure 2-9 (b) shows that the angle of impact of the jet would be $(\theta + \alpha)$ not θ ; the body would drop an increased distance before touching the jet, the increase being labelled 'e' in Figure 2-9 (a); the length of the body's path through the jet would be $d_J \operatorname{cosec} \alpha$ not d_J . These errors would be a maximum with the combination of the lowest jet velocity, furthest distance from the jet orifice and smallest cylindrical body. The maximum errors were calculated to be:

$$\alpha_{MAX.} < 2.0^{\circ}$$

$$V_{Y\,(ENT.\ ERROR)} < 2.5\,\%$$

and for this investigation were neglected.

2-4-2 Cylindrical Body Deflection Experiments

The jet nozzle was adjusted so that the liquid jet issued horizontally between two vertical 'Perspex' plates, one containing a 4 c m. reference grid. The hypodermic total head tube was inserted into the jet and a flow control valve adjusted to give the desired jet velocity; the probe was then removed from the jet. Three cylindrical bodies of a known size and mass were held a known distance downstream from the jet orifice and a known distance above the jet. As the bodies were dropped one by one into the jet their movement was photographed with a high speed camera. Timing marks were placed

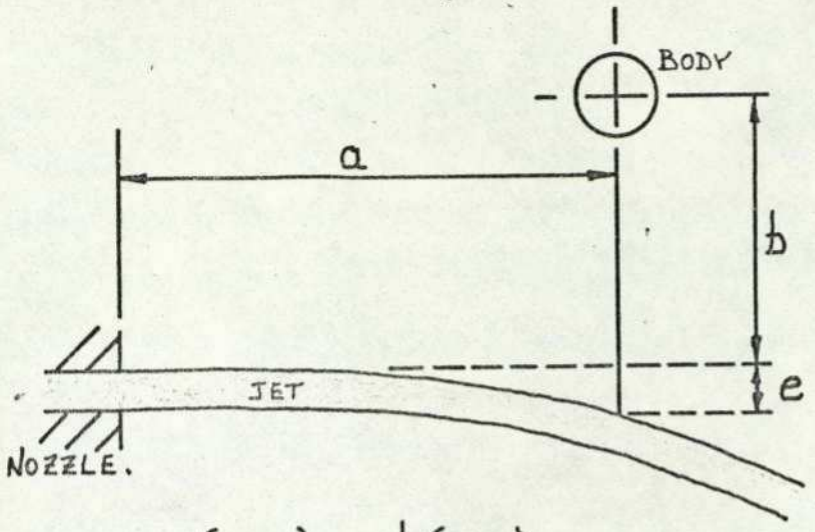

a (c.m.)	b (c.m.)
11.9	14.0
19.9	22.0
27.9	

(a)

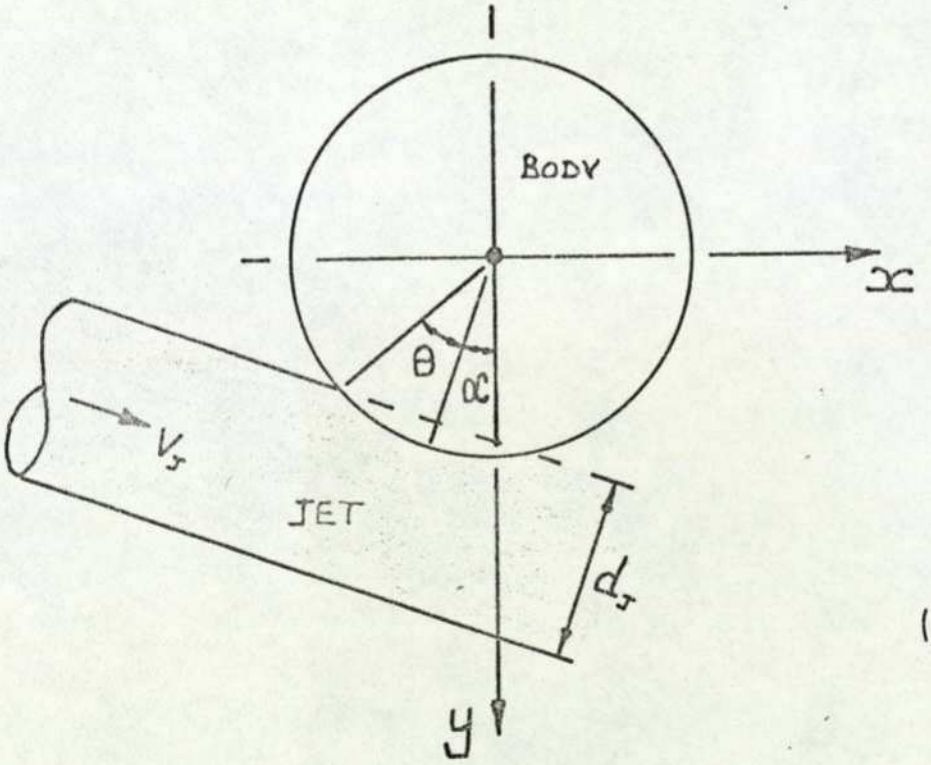

(b)

Jet/body configuration

Figure 2-9

directly on to the film every 10 m s. The film was developed and projected on to a wall where measurements were made of the vertical and horizontal displacements of the body's mass centre. Angular rotation of the body, as indicated by a white radial line, was also noted.

A series of tests was performed to compare the benefits of projection magnification against film definition. The optimum magnification was found to be approximately 1.5:1 and this was used for all the experiments.

Details of the proprietary equipment used are given in Appendix 4 and an illustration of the experimental configuration is shown in Figure 2-10.

2-4-3 The Results of the Cylindrical Body Deflection Experiments

The horizontal and vertical deflections of the mass centre together with the angular displacement of the body were tabulated against time, the data being taken from the projected frames of film. The displacements were adjusted to give a zero displacement at the time the cylindrical body touched the jet; at this instant the time was also defined as zero. The source data and measurement tolerances are given in Appendix 5.

Three terms previously mentioned as being of importance in the deflection of a body were: (a) deflection time, (b) deflected distance, (c) the time of impact of the jet on the body. The deflection time, as has been mentioned in Chapter 1, is probably the most important term since it determines the sorting capacity of the deflection machine element, (ignoring

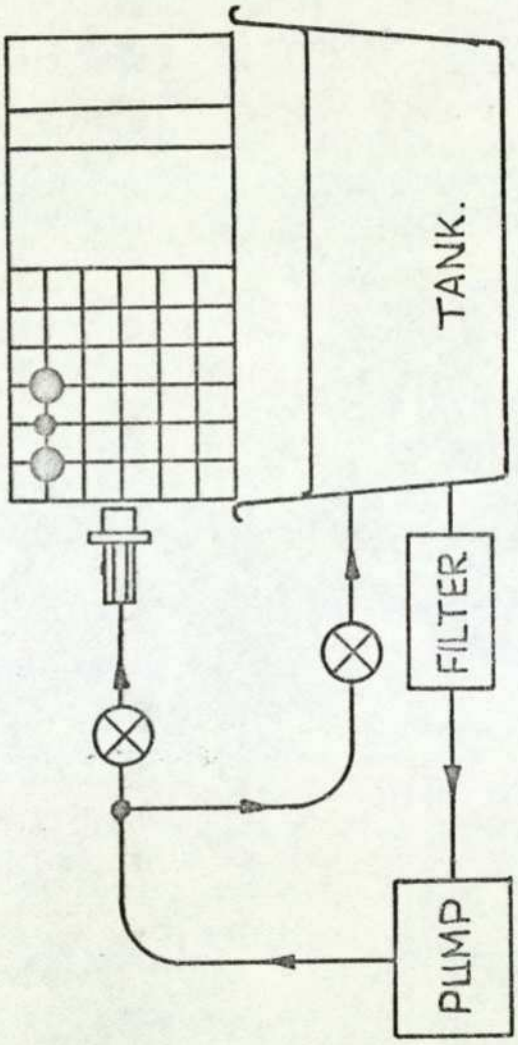

Scheme of body deflection experimental equipment.

Figure 2-10.

for the moment the transient response of the element). The deflection time, however, is a function not only of jet velocity, jet cross-sectional area, body size and mass but also upon the required horizontal deflection. Therefore before a deflection time can be determined, a deflection distance must be defined. The deflection distance chosen was necessarily arbitrary and in this work it was defined as $(d_p/2)$ since this would be the minimum distance a body would have to move to tip from an accept bin into a reject bin.

Graphs of the vertical and horizontal deflections of the body for both theory and experiment are given in the next section and the consequences of some of the definitions are discussed; also, the effects of the body rotation before and during the jet impact are discussed.

2-5 Discussion of the Cylindrical Body Results

2-5-1 A Comparison between Theoretical and Experimental Body Displacements

The theory given in section 2-3-1 will predict a body's position, velocity, acceleration, time elapsed and the forces exerted upon it. Figures 2-11 to 2-18 show the detailed movements of a number of cylindrical bodies as they pass through a cylindrical liquid jet.

The effect of jet velocity

The solid lines in Figure 2-11 and 2-12 show the predicted movement for a cylindrical body in liquid jets of various velocities. If no jet lay in the body's path the vertical (y) graph would show an upward parabolic curve,

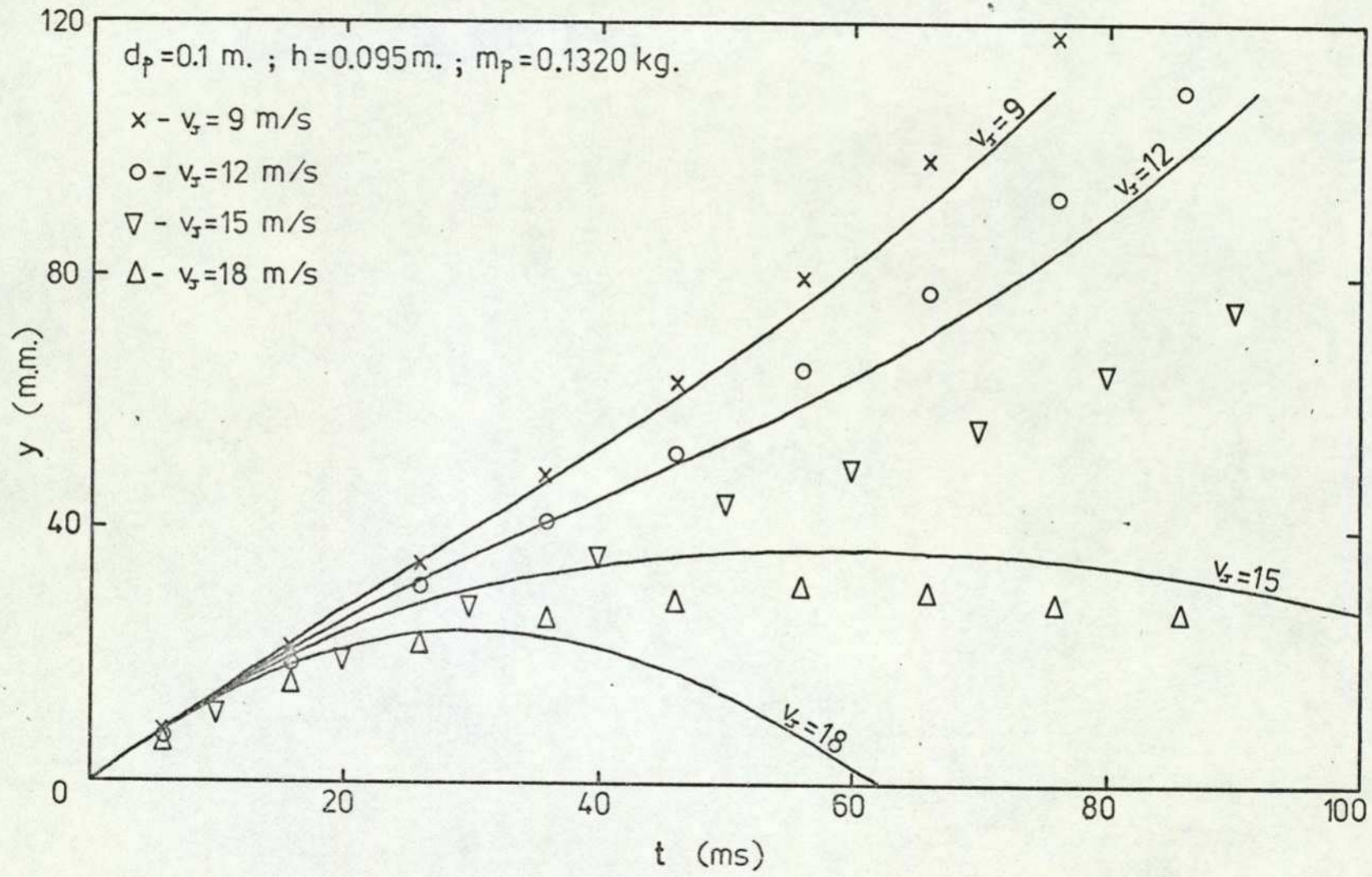

Vertical movement of body

Figure 2-11

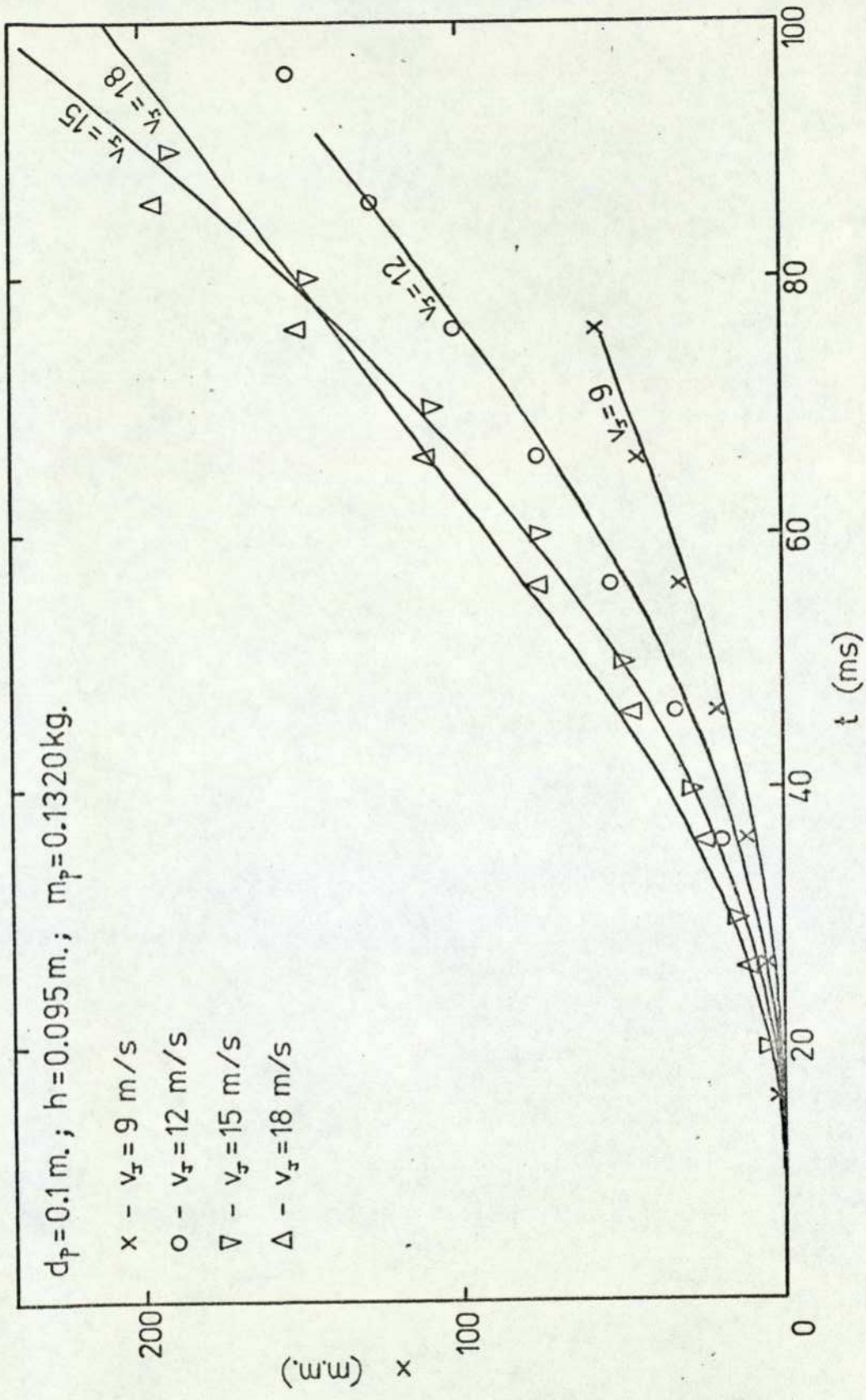

Horizontal movement of body

Figure 2-12

indicating that the body was accelerating downwards. It can be seen from Figure 2-11 that according to the theory the vertical deceleration increases with the jet velocity until the body is expelled from the top surface of the jet without passing through it. The experimental results show that the vertical deceleration experienced by the body is consistently below that predicted; however the agreement between theory and experiment is generally quite good until near the point where the body should not pass directly through the jet. It can also be seen that increasing the jet's velocity increases the time the body spends in the jet. A further point to note is that the initial penetration of the jet is lower than that predicted. This could be accounted for by a lower jet entry velocity than predicted.

The corresponding horizontal deflections are shown in Figure 2-12. The theory shows that when the body cannot penetrate the jet (when V_J = 18 m/s), the horizontal deflection forces remain small and the expected deflection is ultimately less than that expected from a lower velocity jet. The experimental results show that the body proceeded further through the jet than expected, the deflection then obtained being higher than predicted. The agreement between theory and experiment is quite good however, apart from the case where the jet momentum flux considerably exceeds $\dot{G}_*$ (that value of jet momentum flux which just prevents the body passing directly through the jet).

The effect of body mass

Figure 2-13 shows the effect of cylindrical bodies of different masses on the penetration of the liquid jet. As before (Figure 2-11) the initial experimental penetration is lower than

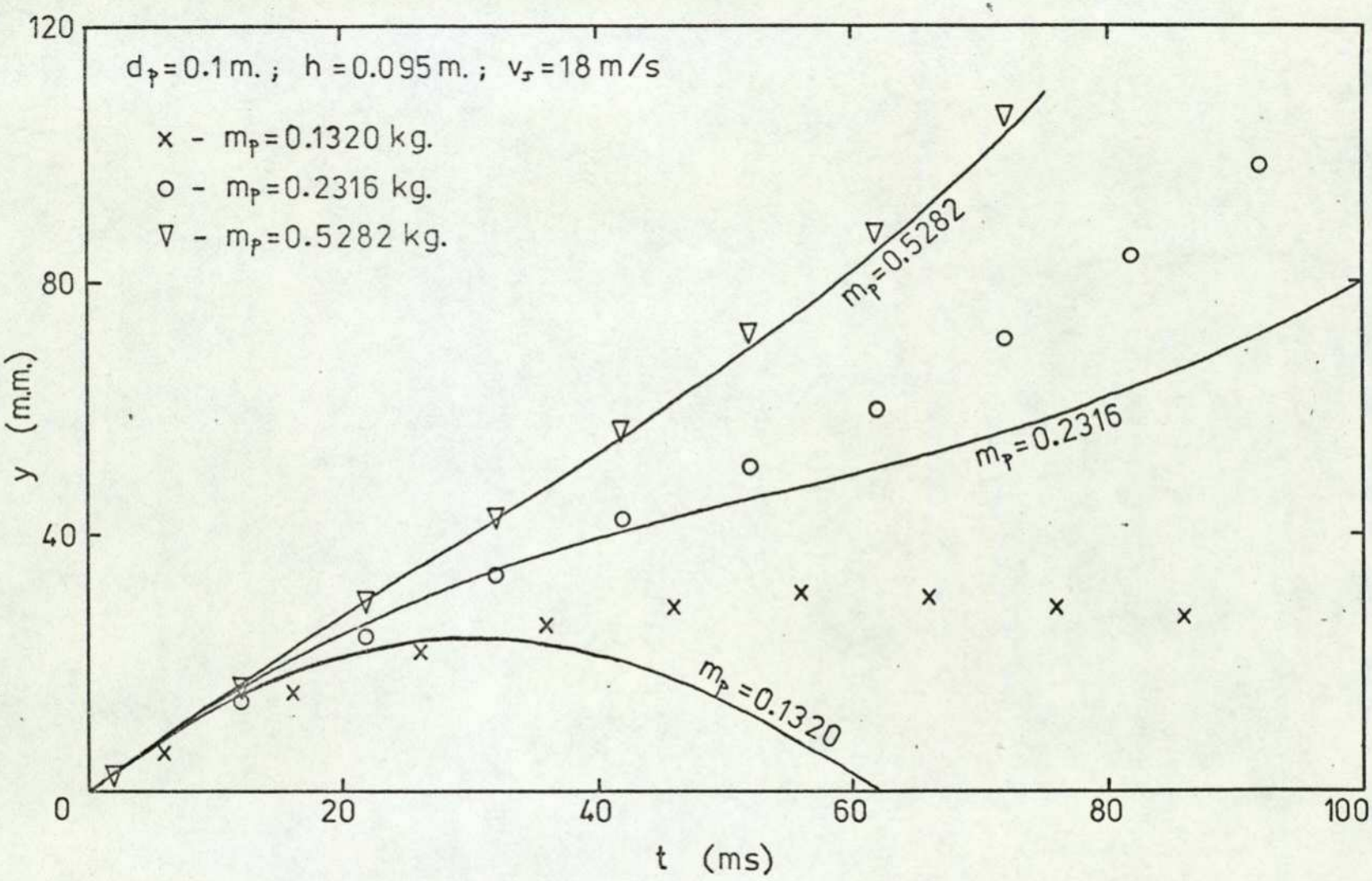

Vertical movement of body

Figure 2-13

Figure 2-14 Horizontal movement of body

that predicted by the theory. The agreement between theory and experiment on jet penetration is quite good, becoming worse as the point is reached where the body should not pass directly through the jet; the jet contact time increases with decreasing body mass. For the horizontal deflections (Figure 2-14), the comparison between theory and experiment is again quite good. The agreement remains good for the case where the theory would indicate an expulsion from the top surface of the jet and where the body actually passed through the jet. This could be due to the horizontal deflecting force profile being symmetrical about the jet centre-line, as shown in Figure 2-4, and therefore the forces exerted on the body are similar whether passing upwards or downwards from the jet centre-line.

The effect of body jet entry velocity

Figures 2-15 and 2-16 show the effects of varying a body's entry velocity into the jet (the body's jet entry velocity being a function of the drop height).

Again it can be seen that the initial jet penetration from the experiments is marginally lower than that predicted, also the agreement between theory and experiment becomes worse as the point where the body should not pass directly through the jet is reached. It should be noted that both theory and experiment indicate an increase in jet contact time with increasing jet velocity, as noted previously, and decreasing jet entry velocity (reducing the drop height). The horizontal displacements (Figure 2-16) show fairly good agreement between theory and experiment with confirmation of the expected results;

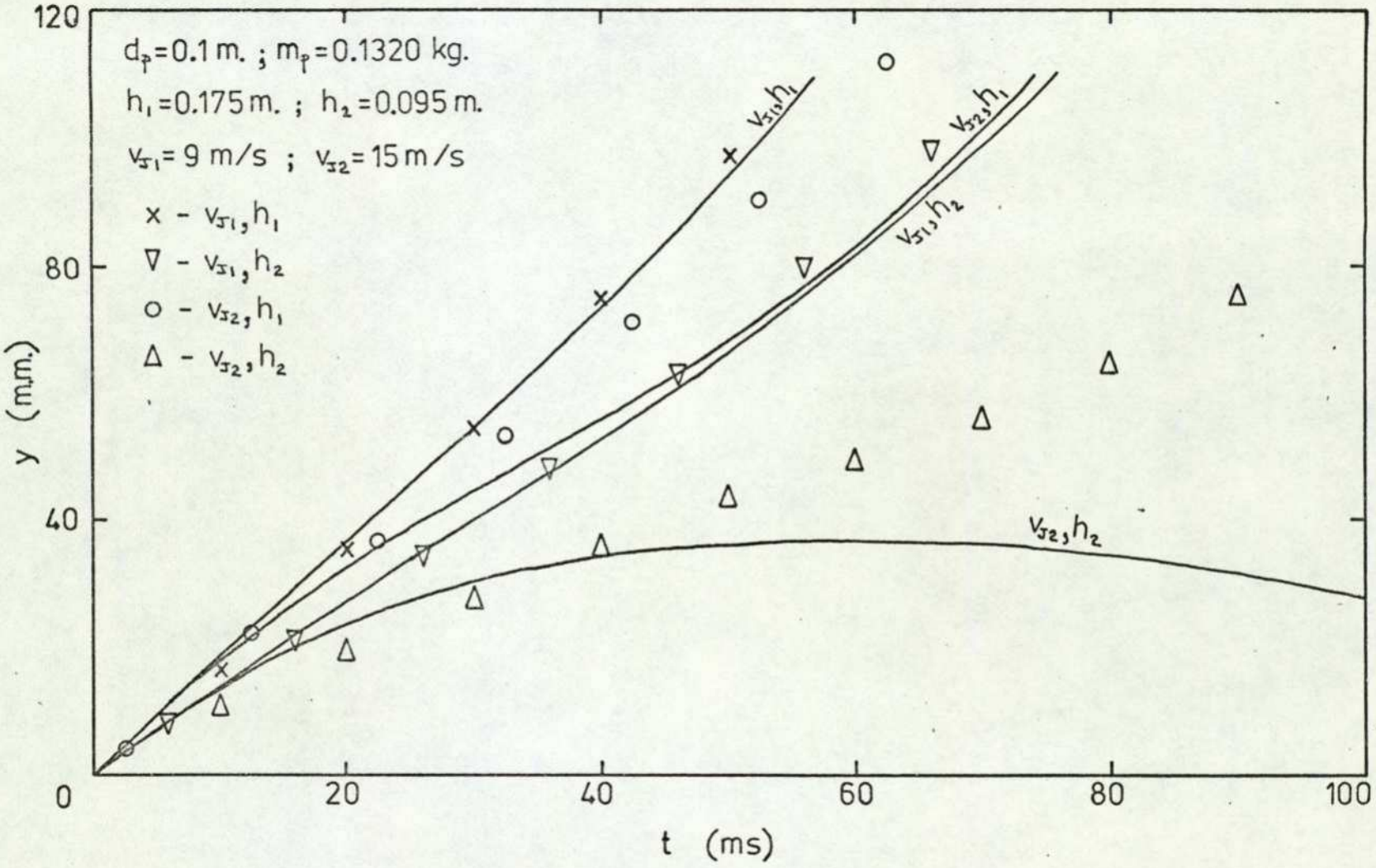

Figure 2-15 Vertical movement of body

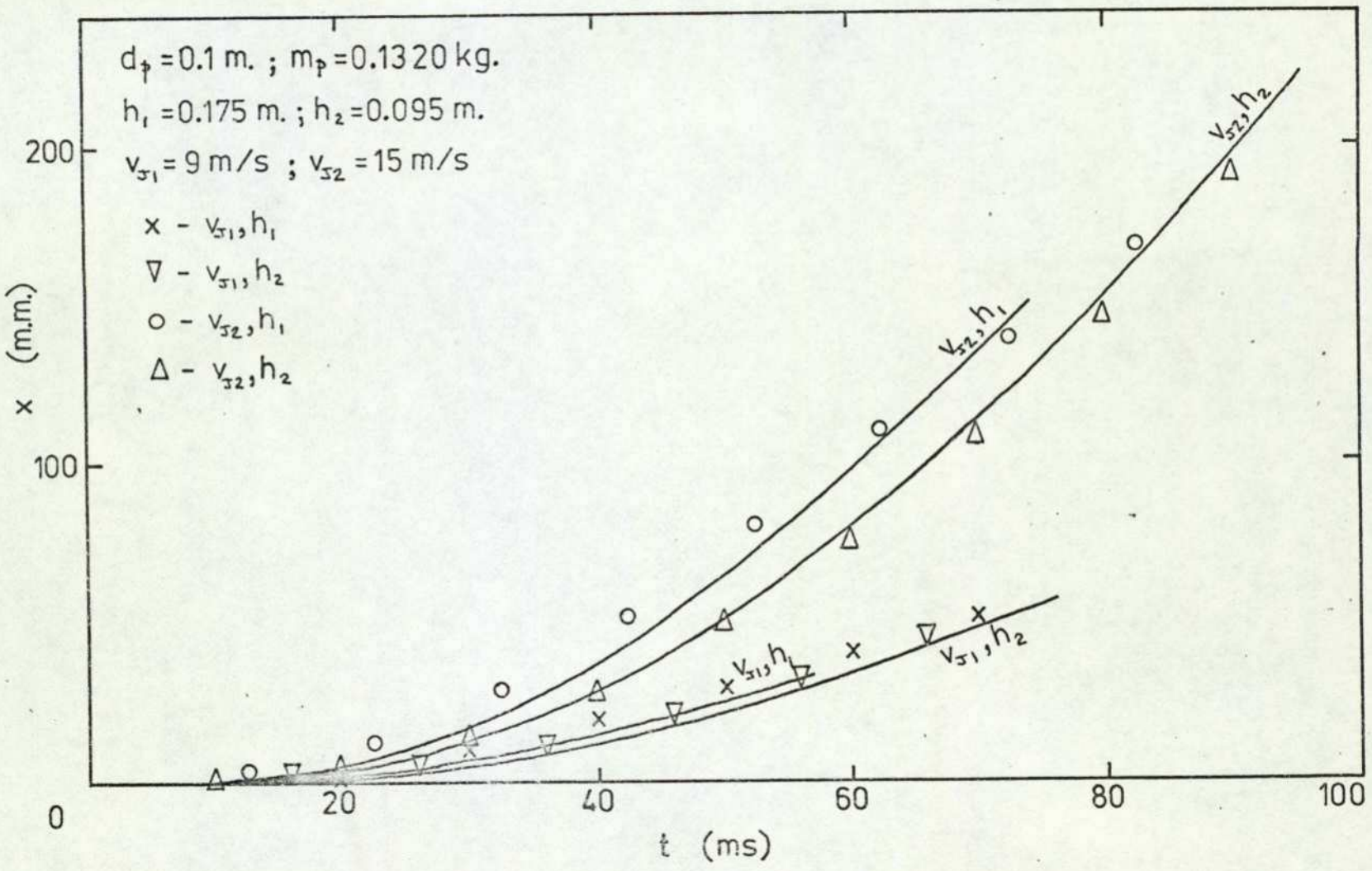

Figure 2-16 Horizontal movement of body

an increase in the horizontal deflection with an increase in jet velocity (as previously seen in Figure 2-12), for a given time an increase in deflection with an increase in jet entry velocity and, ultimately, a larger deflection through the jet with a lower jet entry velocity.

The effect of body size

Figures 2-17 and 2-18 show the results of two bodies of almost equal mass dropped almost the same distance but differing in diameter. From Figure 2-17 it can be seen that, as in the graphs Figures 2-11, 2-13, 2-15, the experimental penetration of the jet is higher than that predicted by the theory. Theory and experiment do agree, however, in that larger bodies penetrate the jet at a slower rate. The horizontal deflections shown on Figure 2-18 indicate that the smaller body is deflected a greater distance for a given time whilst it remains in the jet, however, since the larger body remains in the jet for longer its displacement eventually exceeds the smaller body's. The agreement between theory and experiment for the smaller body is not particularly good and this is a noticeable feature of the smaller bodies used in these experiments.

The Figures (2-11) to (2-18) have shown the detailed displacements of a body as it passes through a liquid jet. As previously stated, the theory will also calculate the velocities, accelerations and forces experienced by the body as it passes through the jet; however it was thought that the displacements and times to reach given displacements together with the time spent in the jet were the most important parameters for sorting machine design.

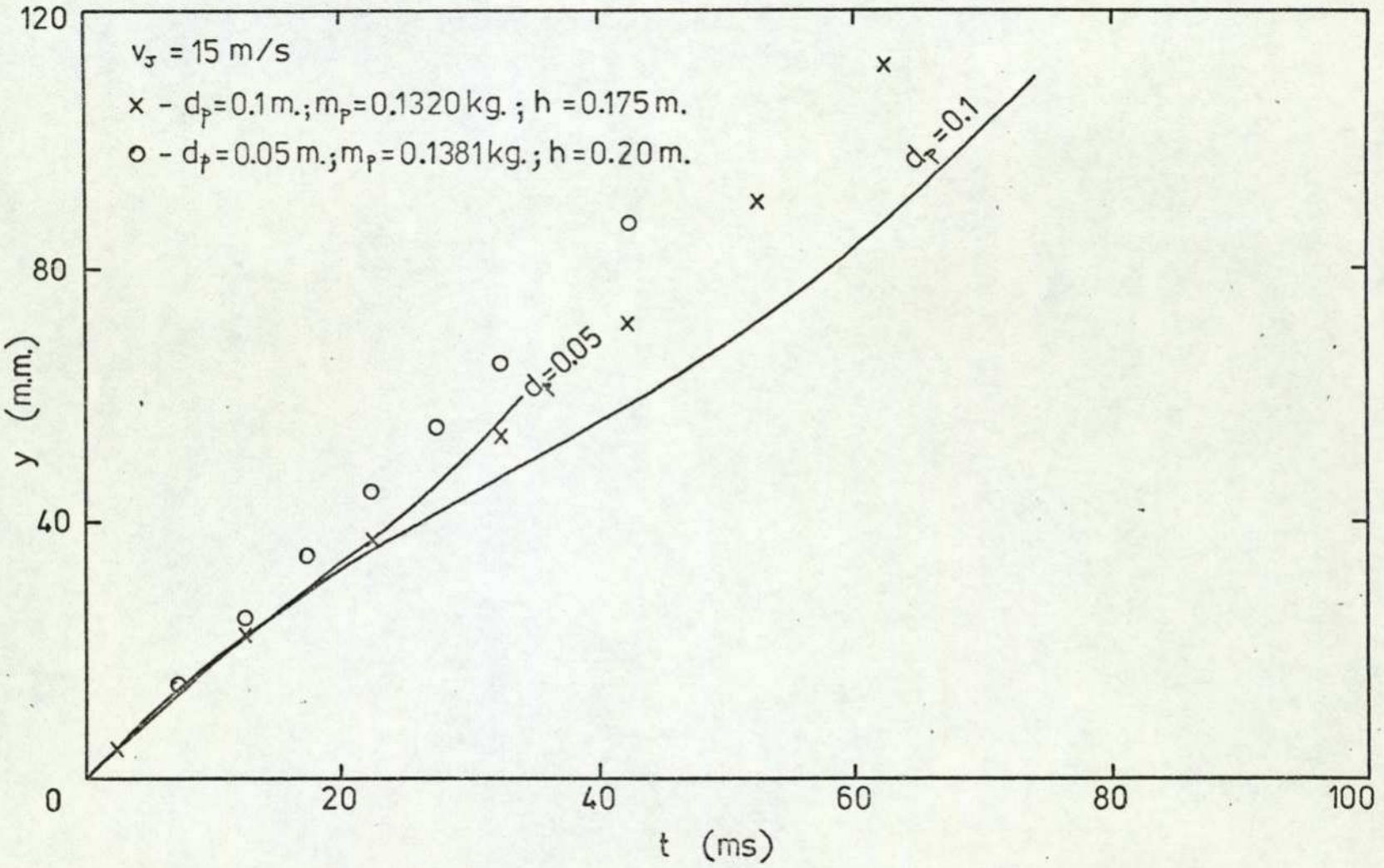

Vertical movement of body

Figure 2-17

The effect of body size on horizontal displacement

Figure 2-18

2-5-2 A Comparison between Theoretical and Experimental 'design' Parameters

The three parameters thought to be the most important for sorting machine design were:

(a) Deflection distance

(b) Deflection time

(c) The time the body spent in the jet.

Figure 2-19 (a) shows a comparison between the theoretical and experimental times taken to reach a horizontal displacement of half the body's diameter, this being the minimum deflection distance and set quite arbitrarily. Figure 2-19 (b) shows a comparison between theory and experiment for the time the body spent in the jet. Several points were thought to be worthy of note. The agreement between theory and experiment is better in Figure 2-19 (a) than Figure 2-19 (b); this is because the horizontal distances are not large (50 m.m. maximum) and the agreement remains good over small distances (see Figures 2-12, 14, 16, 18). Figure 2-19 (b) shows a more severe test of the theory since, providing the body passed through the jet, the trace is not truncated at a specified deflection but the body is followed until leaving the jet. This time is determined from the vertical deflection traces which, (as can be seen from Figures 2-11, 13, 15, 17), do not agree as well as the horizontal deflection graphs. It was noted that almost all the points lie below the line of perfect agreement, indicating that the bodies passed through the jet quicker than predicted.

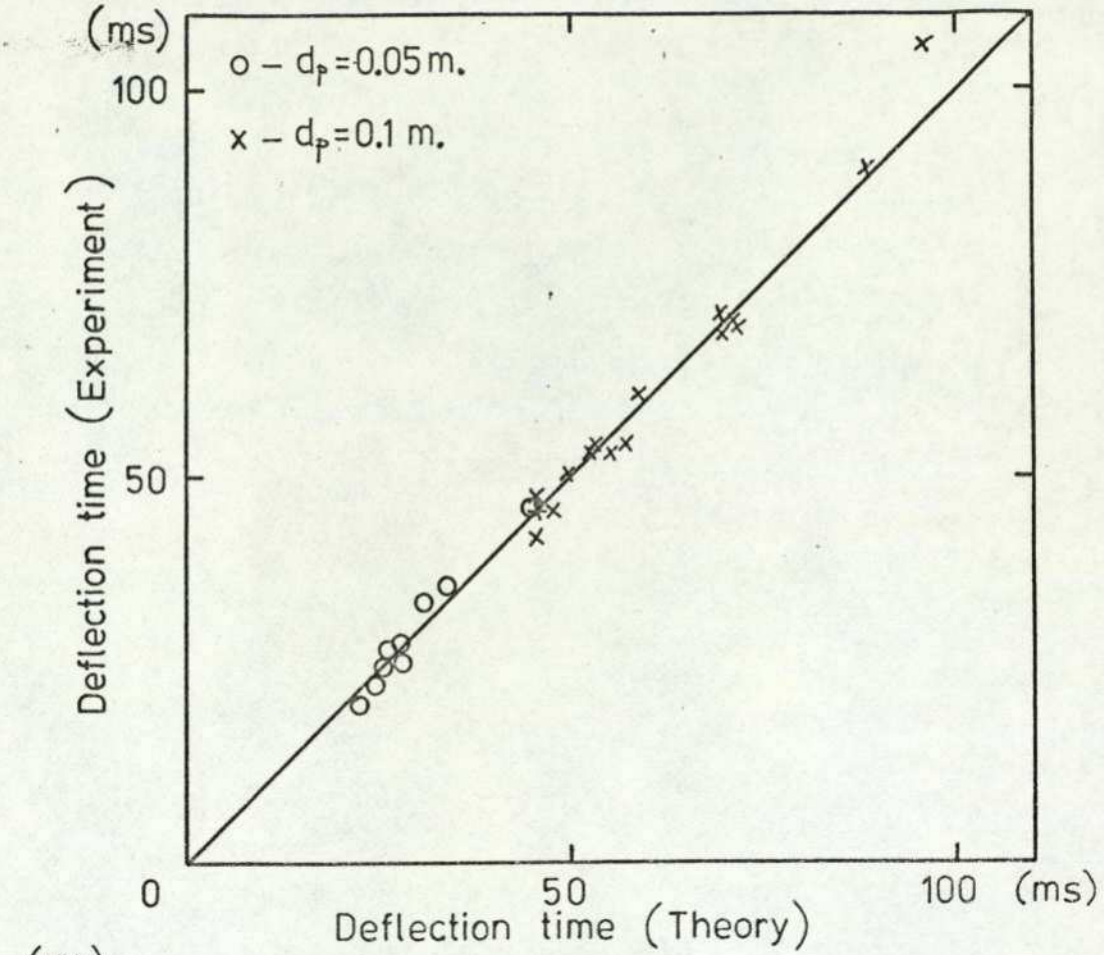
(ms)
100
50
0
o – d_p = 0.05 m.
x – d_p = 0.1 m.
Deflection time (Experiment)
50
100 (ms)
Deflection time (Theory)

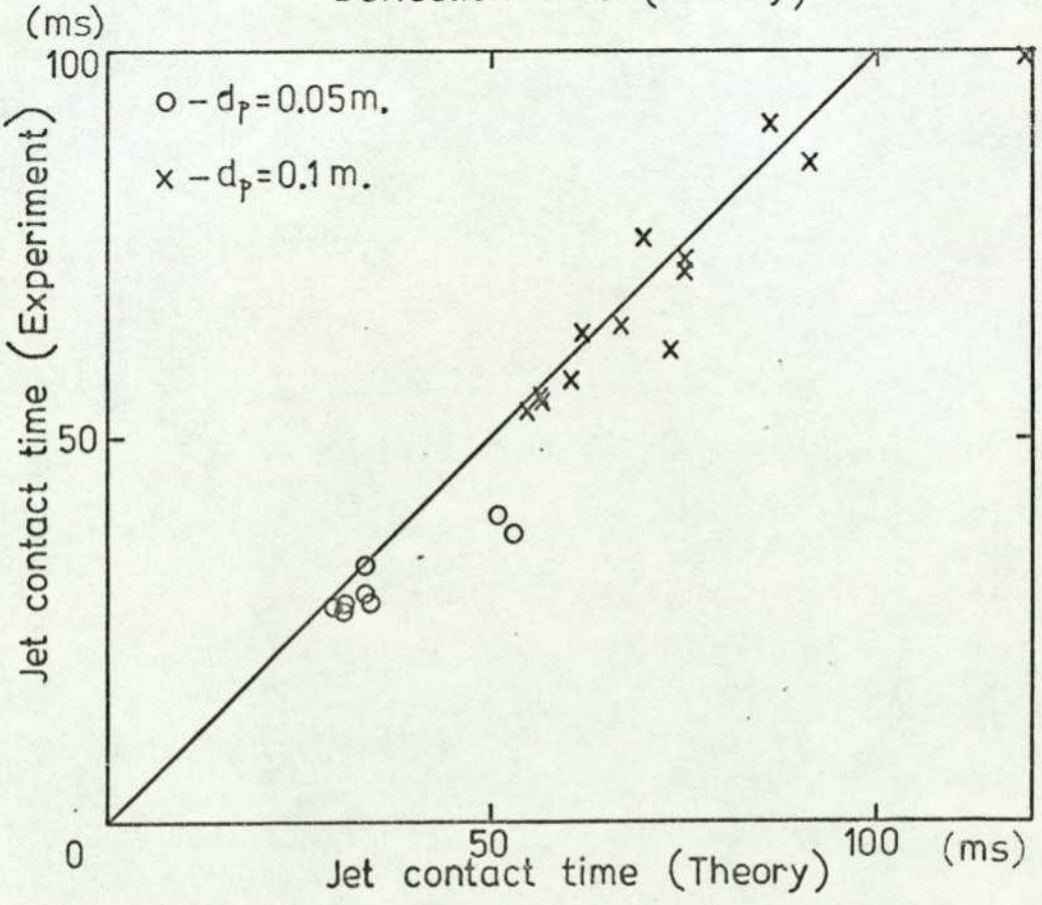
(ms)
100
50
0
o – d_p = 0.05 m.
x – d_p = 0.1 m.
Jet contact time (Experiment)
50
100 (ms)
Jet contact time (Theory)

Figure 2-19

A still more severe test of the theory is shown in Figure 2-20 where the total horizontal deflection on passing through the jet is compared. It will also, no doubt, be noted that again most of the experimental points lie below the line of perfect agreement. The severity of this test can be indicated by explaining that the errors in the calculation steps are cumulative. A very small error at the beginning of the body's entry into the jet will be carried over into the next step, thus giving an incorrect starting point for that step. Apart from the cumulative errors within the analysis small differences in the jet contact time between theory and experiment will give large differences in the deflected distance since, near the jet exit, the body may be moving at a considereble velocity. Figure 2-21 further illustrates this point; the correlation between errors in deflected distance and errors in jet contact time are clearly shown. Further, points worthy of note are that the gradient of the line is approximately two, indicating that a 10% error in time will give approximately a 20% error in deflection and that the line almost passes through the point $X_{EXP}/X_{CALC} = t_{EXP}/t_{CALC} = 1.0$

The mean and standard deviation on the basis of time ratio are respectively 0.929 and 0.089 and on the basis of deflection ratio are 0.848 and 0.189.

A further important point predicted by the theory is the deflection time against jet momentum flux. Figure 2-22 shows that the theory predicts a reduction in deflection time with an increase in jet momentum flux, however, the

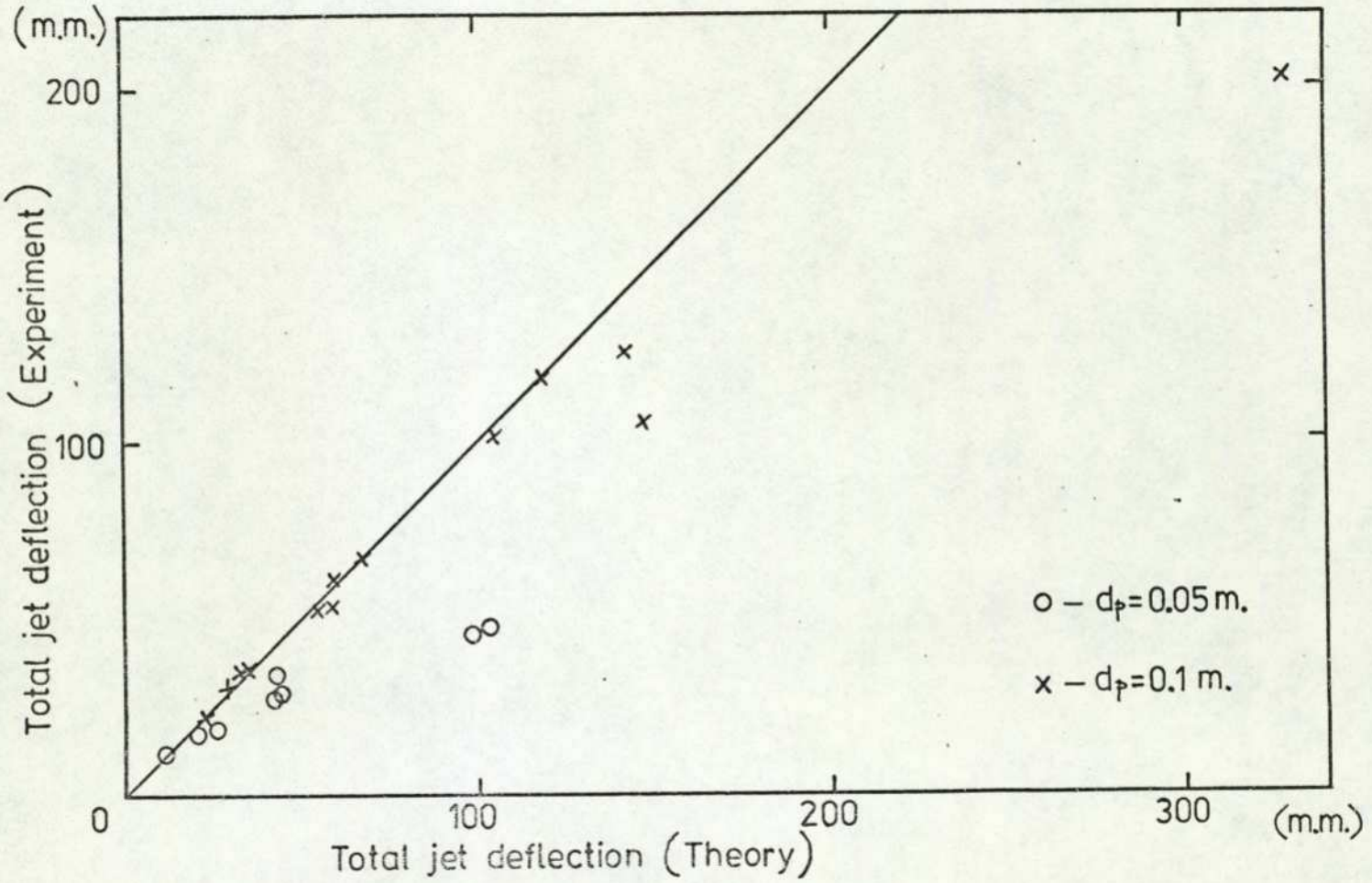
(m.m.)
200
100
0
Total jet deflection (Experiment)
100
200
300
(m.m.)
Total jet deflection (Theory)
o – d_p=0.05 m.
x – d_p=0.1 m.

Figure 2-20

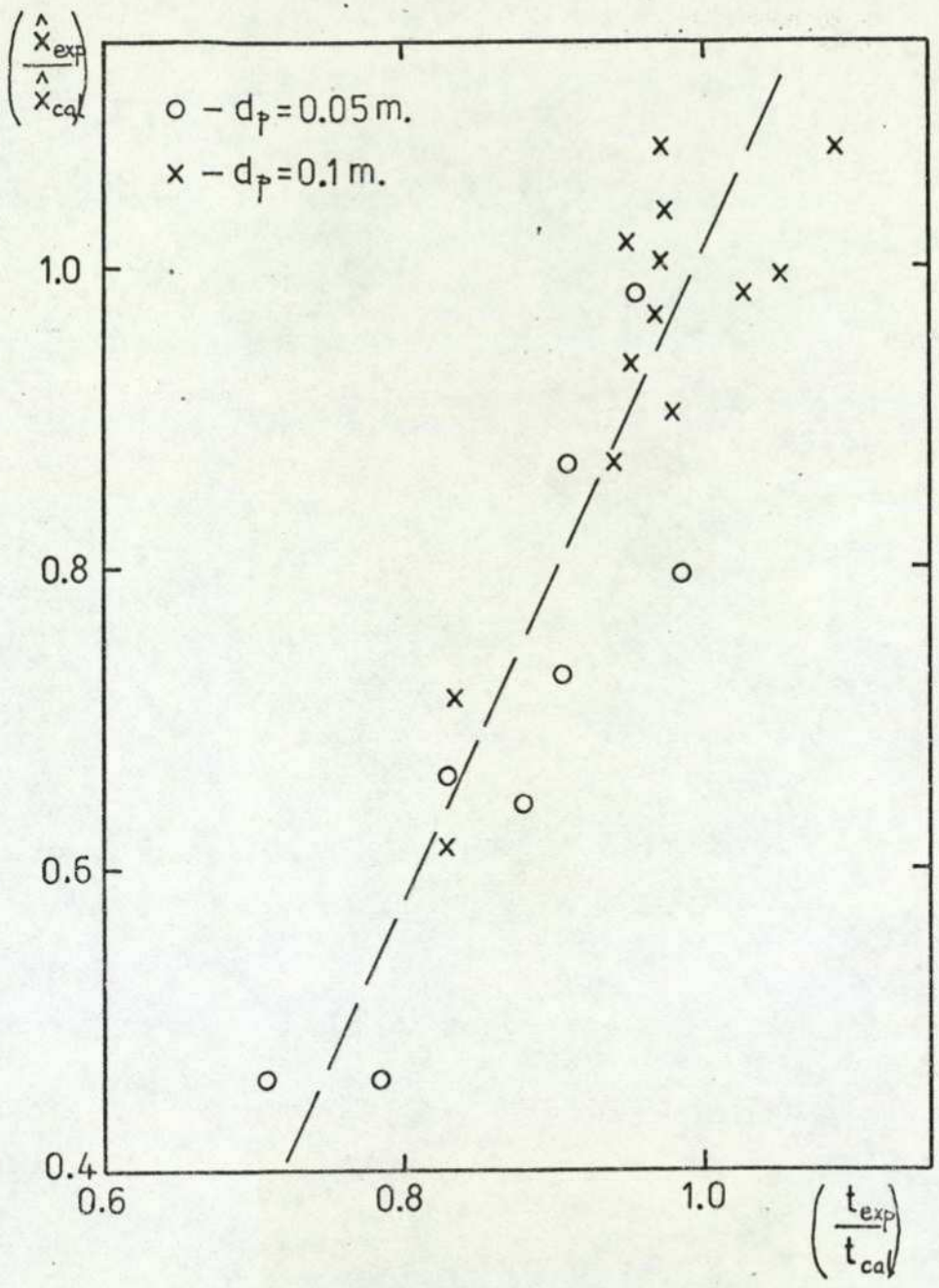

Correlation between changes in jet contact time and jet deflection.

Figure 2-21

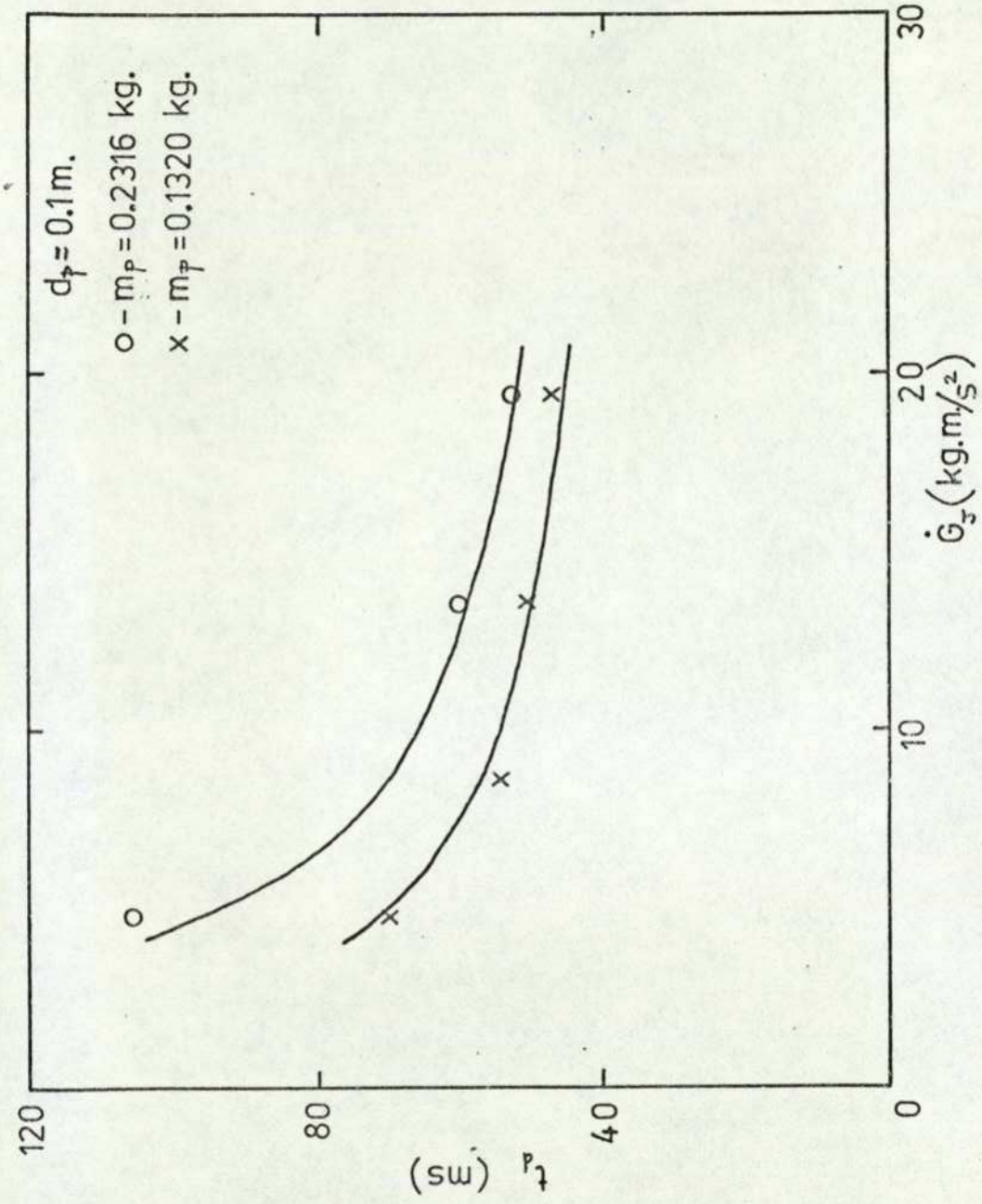

Body deflection time against jet momentum flux .

Figure 2-22

reduction in time rapidly becomes very small compared with the increase in jet momentum flux and hence the power consumed by the deflecting device. Operating a device with a jet momentum flux considerably in excess of the momentum flux which will theoretically just prevent the body passing directly through the jet will consume additional power for very little predicted reduction in deflection time. It is interesting to note from Figure 2-7 that the maximum jet momentum flux for a body to pass directly through the jet increases rapidly with body mass. It would appear from the theory that ultimately a light body could take almost as long to move through the deflection distance as one weighing considerably more. The agreement between theory and experiment is thought to be good considering that this is the initial test of the theory; no experimental coefficients have been incorporated and errors are known to exist within the analysis.

2-5-3 Observations on the Theoretical and Experimental Results

Errors inherent within the analysis

Three errors have been mentioned previously, namely the parabolic form of the liquid jet's trajectory and the consequent errors in the body's drop height and distance to pass through the jet (see Figure 2-9); these errors could be corrected if it was thought that they had a significant effect on the results.

The three dimensional nature of the liquid flow away from the jet/body impact area will introduce a further

error. The analysis is two dimensional and from Taylor's graphs, (Taylor, 1960; see Figure 2-2), it can be seen that at small angles of impact the flow away from the impact point is approximately two dimensional with very little flow on to the side guide walls; this condition is shown on Plate 6. It can also be seen from Figure 2-2 that as the angle of impact increases the quantity of fluid impinging on the side walls increases, Plates 7, 8 and 9 confirm this increase.

Also, with reference to both the general and the minimum jet entry velocity theories, there are inevitable energy losses within the impact region of the jet on the body and further losses as the liquid flows away from the impact region. The losses were expected to be due to viscous effects within the fluid and, energy losses due to evaporation at the interface between the liquid and the air. These effects could be partially accounted for by inserting into the theory a momentum flux coefficient. From this point of view it was encouraging to note that Figure 2-19 (b) and Figure 2-20 show experimental readings generally lying below the predicted level.

As far as the equation for the body's minimum jet entry velocity is concerned a momentum flux coefficient could again be used to overcome the energy losses; this would raise the value of jet momentum flux required to prevent the body passing directly through the jet. A further error with the minimum jet entry velocity theory is that the incident jet momentum flux and jet velocity is assumed to be constant, therefore the velocity is only correct at the instant the jet hits the body since the body then accelerates. However it was thought to be a useful concept

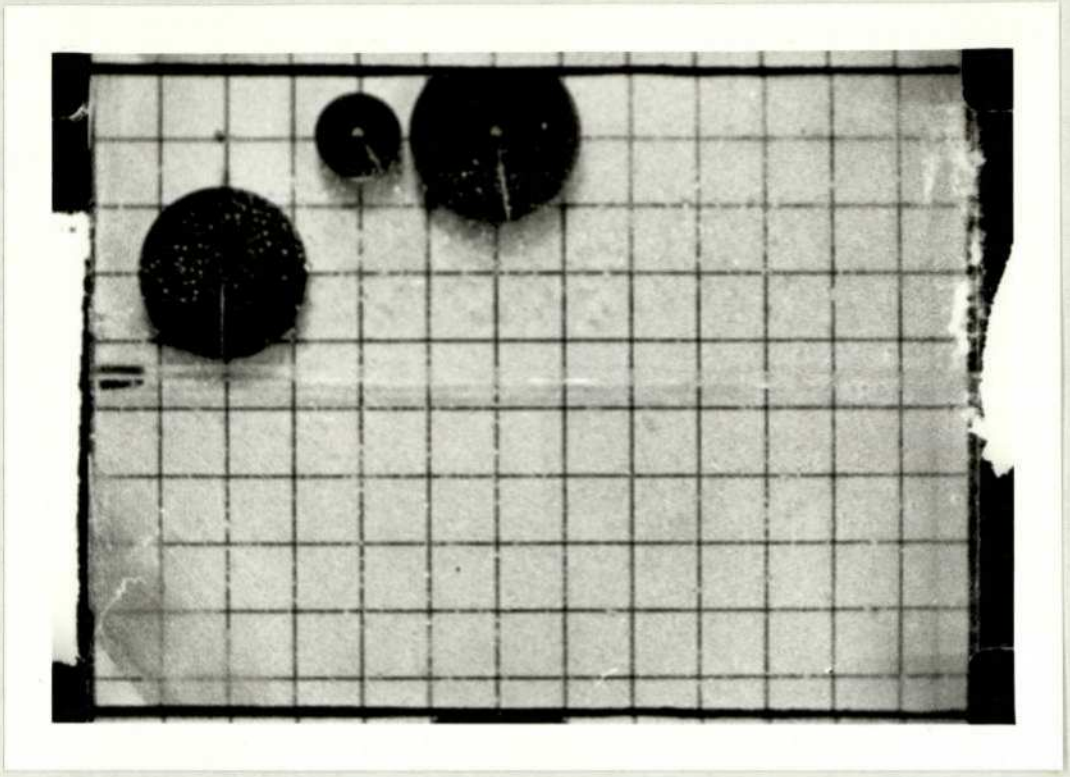

PLATE 1

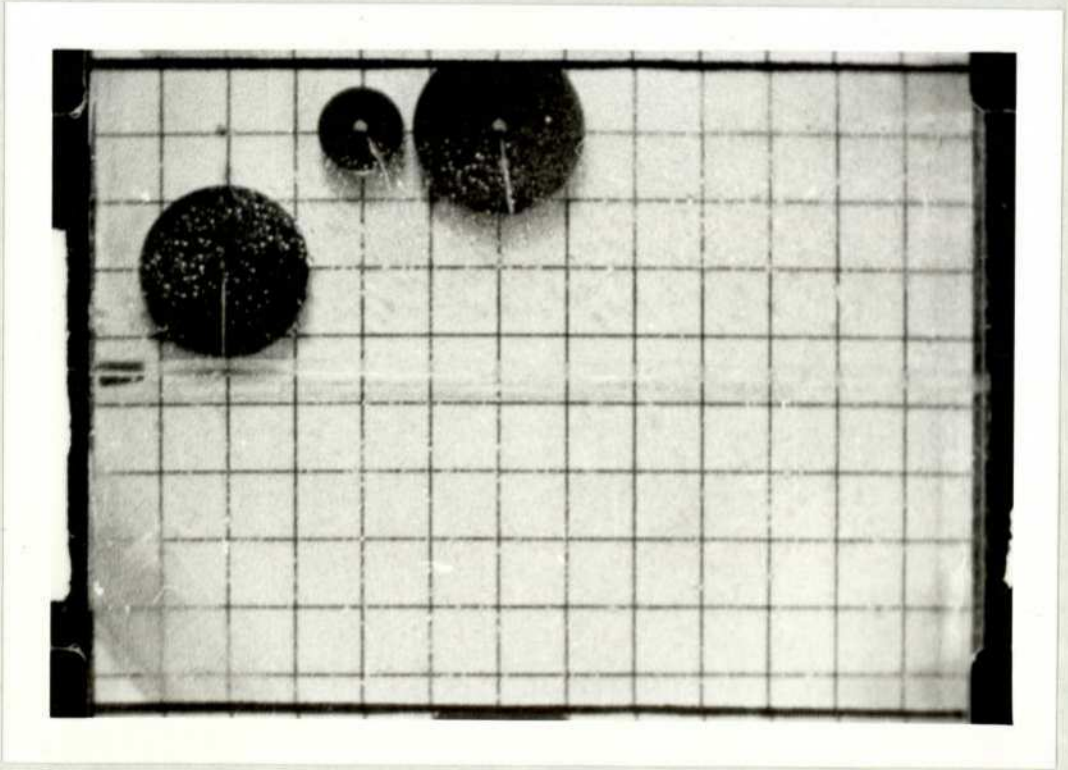

PLATE 2

Body illustrations

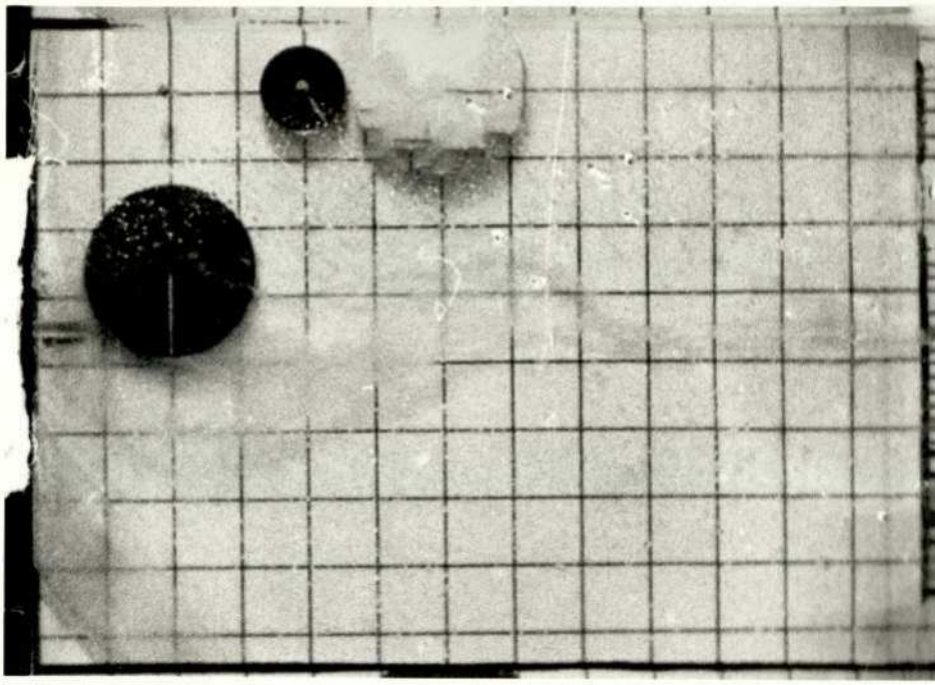

PLATE 3

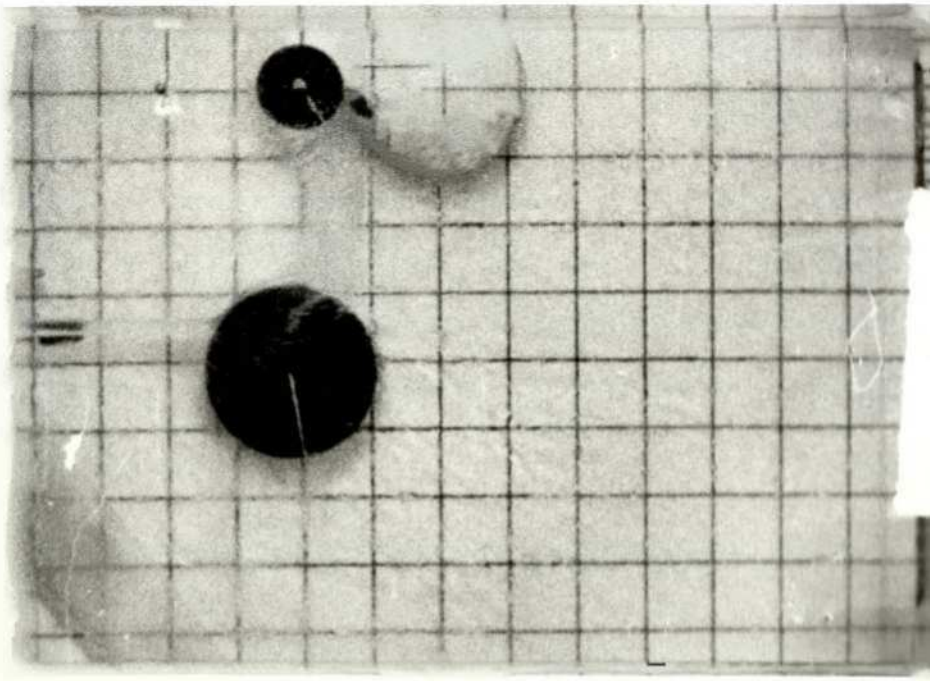

PLATE 4

Body illustrations

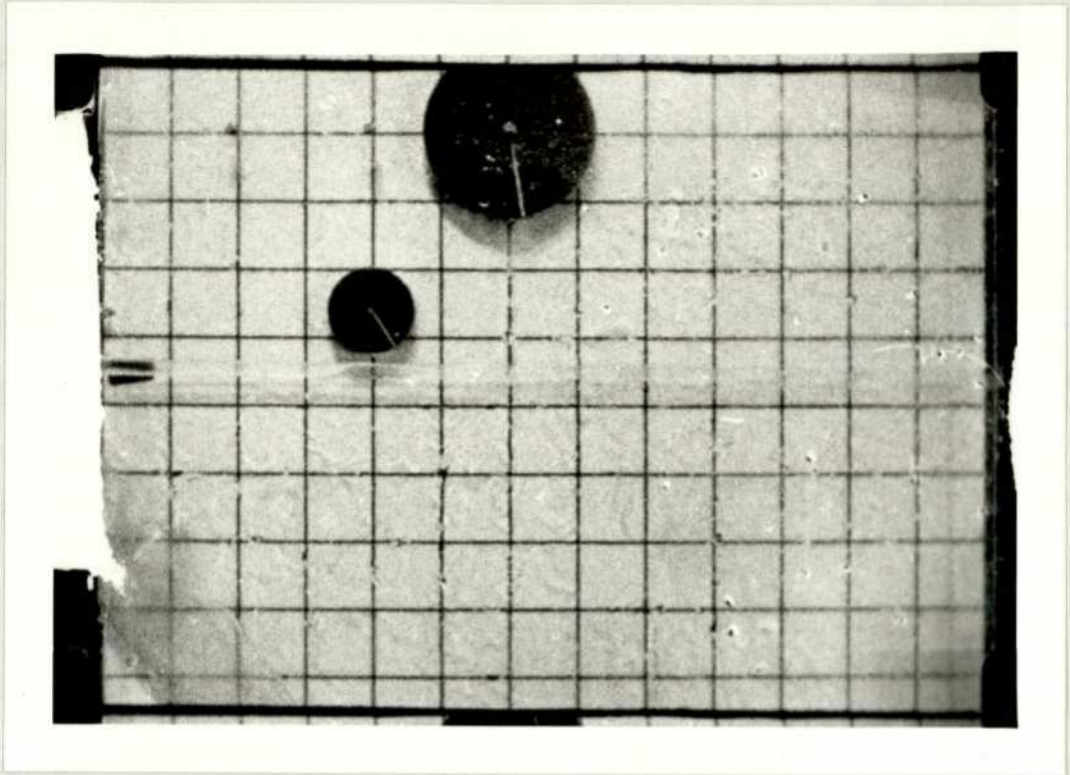

PLATE 5

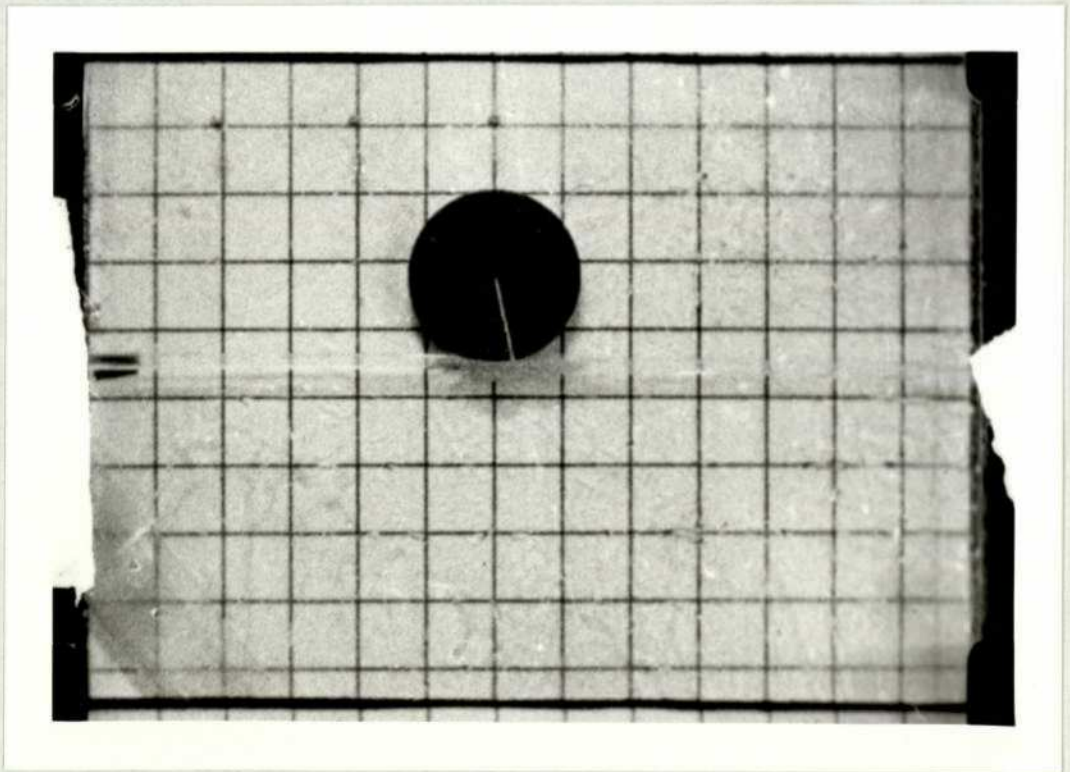

PLATE 6
Body illustrations

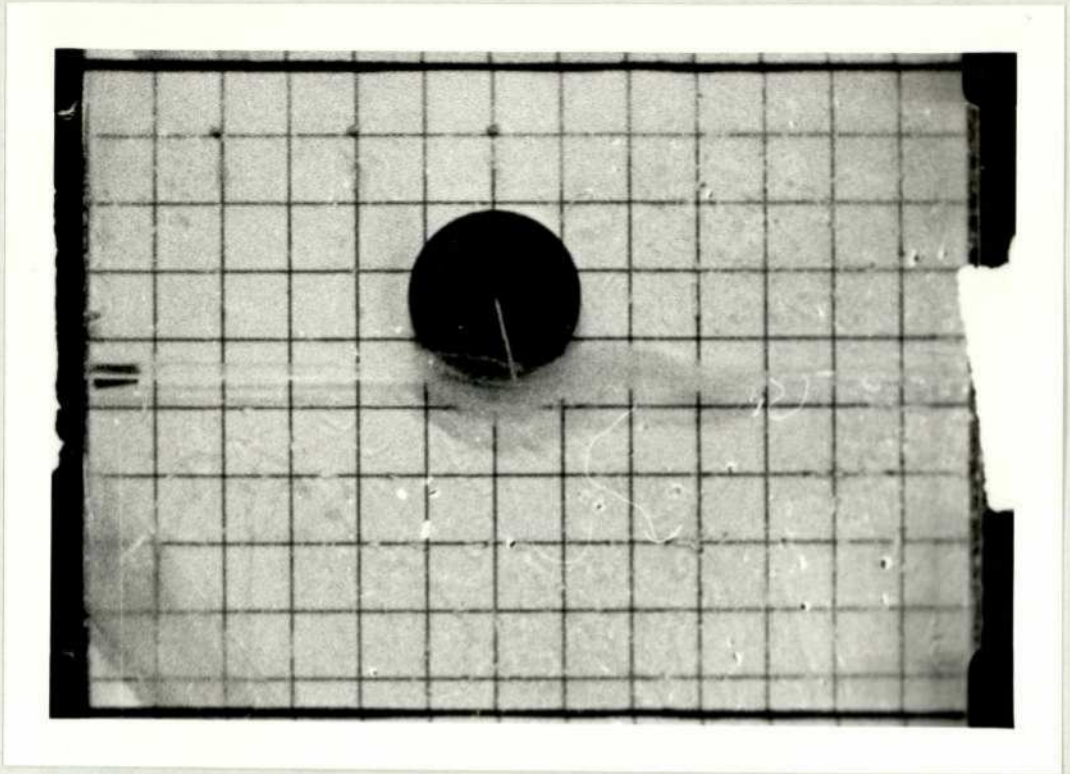

PLATE 7

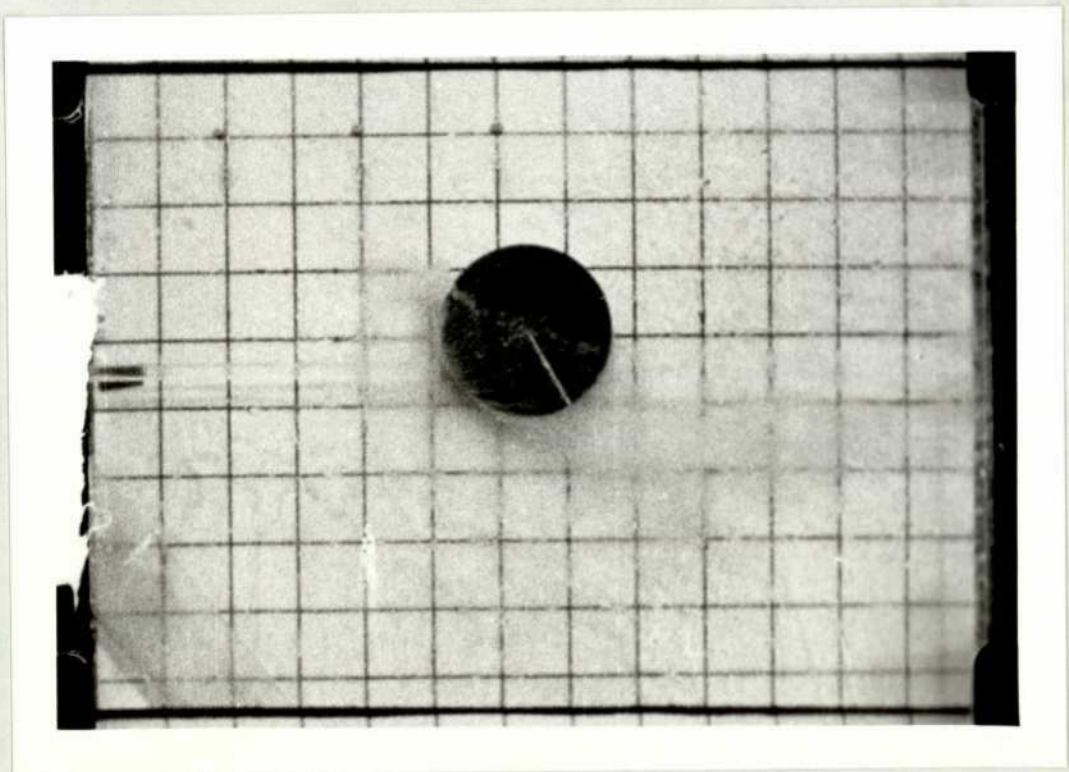

PLATE 8

Body illustrations

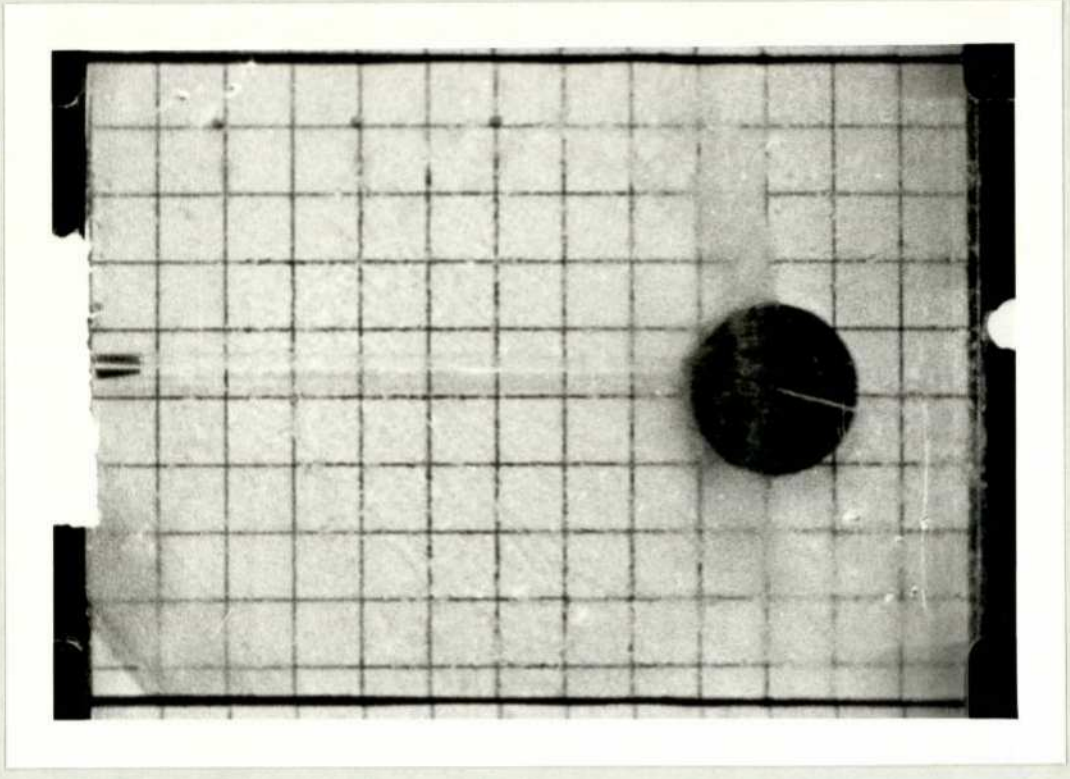

PLATE 9
Body illustration

and, providing the body's velocity was low compared with the jet's, and the diameter considerably exceeded the jet diameter, the equation was thought to be a useful guide. It was noted that the errors introduced by the constant momentum flux assumption would be increasingly significant as the body/jet diameter ratio tended to unity. In practice the body would accelerate until the incident jet momentum flux fell below the critical value and then the body would pass through the jet. Table 2-1 gives a comparison between theory and experiment.

A possible error of unknown magnitude was associated with the definition of the mean angle through which the jet was assumed to be deflected. In this initial investigation the deflected angle of the jet was weighted with the jet momentum profile; (since the velocity was constant across the jet the weighting became that of the elemental area exposed). It was noticed that on a graph of jet deflection angle against jet penetration, (see Figure 2-23), there was an inflection just before the entire jet impacted on the body. This occurred because the elemental area weighting would bias the deflection angle toward the jet centre-line if θ_{AV} were directly proportional to 'y'; however θ_{AV} was not directly proportional to 'y' and hence the increments of θ_{AV} are larger when 'y' is small. The increase in gradient after the inflection occurs when the first few large increments of θ_{AV} again result by the passing of the lower edge of the jet. If the calculated value of θ_M was higher than the true value then, ignoring other interactions, the

TABLE 2 - 1

Eligibility - All bodies with a horizontal deflection (whilst within the jet) exceeding 100 m m.

$\dot{G}$ (kg m^2/s)	dp (m)	mp (kg)	ΔxJet (m m.)	$(2gh)^{\frac{1}{2}}$ (m/s)	V_y(min) (m/s)	COMMENTS
8.64	0.10	0.1320	125	1.37	1.13	Passed through the jet
13.5	0.10	0.1320		1.37	1.56	Passed out of field of view
13.5	0.10	0.1320	105	1.85	1.56	Passed through the jet
13.5	0.10	0.2316	118	1.37	1.02	Passed through the jet
19.44	0.10	0.1320		1.37	1.98	Did not pass through jet
19.44	0.10	0.2316	202	1.37	1.37	Passed through the jet
19.44	0.10	0.2316	101	1.85	1.37	Passed through the jet
19.44	0.05	0.0581	112	1.53	2.25	Passed through the jet

Comparison between theory and experiment

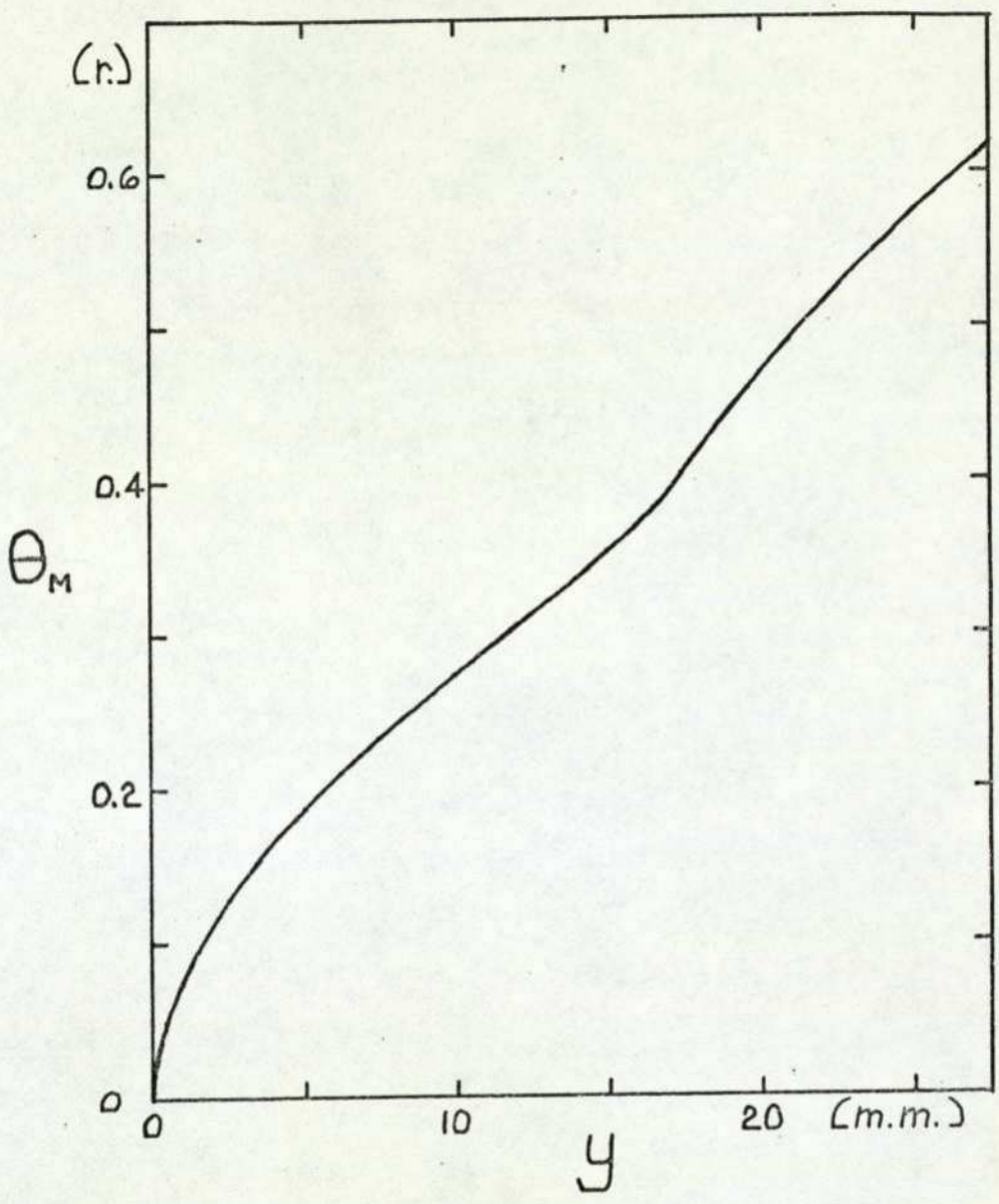

Mean jet deflection angle against jet penetration.

Figure 2-23

horizontal and vertical force magnitudes would be overestimated. In spite of these possible errors there was thought to be scope, within the same analysis framework, for an improved mathematical model; also the existing analysis was thought to be useful and indicate areas for further examination.

Experimental observations

Most previous work in this subject (Chadda, 1972) has been concerned with the forces exerted by a jet on a body held stationary in the jet; under these circumstances it is common to use a momentum flux coefficient (often termed C_D from aeronautical engineering). For the conditions prevailing in these experiments however, the value of this coefficient may vary with the relative position of the jet and body. Since, as far as the author is aware, this is the first investigation into the dynamic movement of a cylindrical body under the impact of a liquid jet, no attempt has been made to introduce any coefficient, although obviously there are energy losses within the jet impact region, and the theory has been compared against experimental results after its formulation.

The arguments given below are postulated to explain various phenomena observed during examination of the experimental high speed films. Since no other research papers were found on this subject a considerable volume of experimental work would have to be undertaken to verify, or disprove, these arguments.

The theory assumed that the bodies did not rotate as they entered the jet. In some of the experiments the body

did not fall 'cleanly' and it was rotating as it entered the liquid jet. When this occurred the agreement between theory and experiment for the time spent in passing through the jet generally became much poorer. It was noted that if the body rotated after it had entered the jet the agreement between theory and experiment was not greatly changed. A further point of interest, which would require more specific and controlled testing to prove, was that the direction of rotation appeared to have little effect on the errors in jet contact time; Figure 2-24 illustrates the deterioration of the theory with body rotation.

The theory also assumed that the cylindrical body diameter exceeded the liquid jet diameter. It was noticeable that the agreement between theory and experiment was poorer with the smaller diameter bodies, (see Figures 2-19 (b) and 2-20). With the smaller diameter bodies any disparity between theory and experiment occurring close to the jet entry would exist for a greater percentage of the body's jet contact time. Also since the discrimination of time was approximately two milliseconds, with small jet contact times and high body velocities, a discrimination error of two milliseconds would be approximately seven per cent of the total immersed time.

It can be seen from the plates 1 to 4 that the fluid impinging on the side walls flowed between the side guide walls and the body. This flow of liquid between the body and the side walls would introduce a viscous shear stress on the body which was not accounted for in the theory.

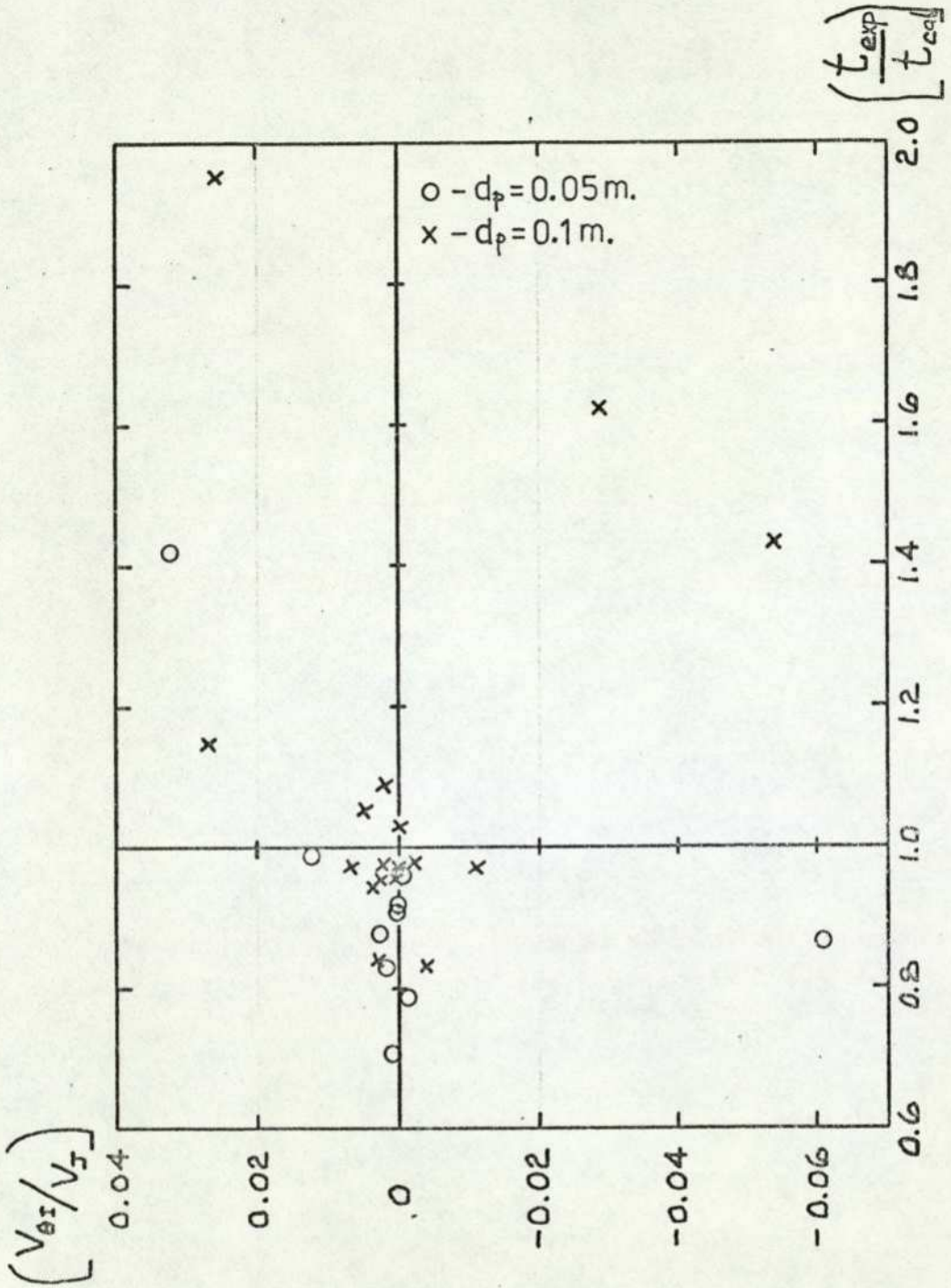

Relationship between body rotation and jet contact time.

Figure 2-24

This fluid may also act as a liquid seal between the side walls and the body thus resulting in a modified pressure distribution on the body.

A further point observed and not accounted for within the theory was that as the body approached close to the jet, the jet appeared to rise slightly to meet the body. It was thought that the liquid jet accelerated the air adjacent to it to form a moving 'sheath'; surface waves visible on the jet's surface were thought to increase this effect. The presence of the body close to the jet restricted the flow of air adjacent to the jet thus creating a low pressure region and causing the jet to rise and the body to accelerate downwards; this is illustrated in Plates 1, 2 and 5.

With the liquid jet still passing below the body and accelerating the air adjacent to it, the low pressure region could be formed as described above. As the body entered the jet Plate 7 shows the jet to be fairly strongly attached to the body, considering its high linear momentum flux. This could be due to the maintenance of the low pressure region by the liquid film seal visible on the side of the body. The low pressure region would encourage the attachment of the jet to the body and modify the trajectory of the body through the jet. This phenomenon would not occur when the body left the underside of the jet since the jet would have been disrupted and therefore the partial evacuation of the air would not occur; the body could also be moving at a considerable velocity by this time, thus further reducing

the evacuation effect. Plates 3 and 4 illustrate the different flow patterns.

2-6 Summary - Body Movement

It was considered that several important points have been made in this limited investigation. With regard to a body's movement under the action of a liquid jet it would appear that:

(a) For the body/jet sizes tested the general theory would appear to be capable of predicting the time taken to obtain a specific deflection, the total time spent within the jet, the resulting deflection and velocity of the body at the jet exit, within reasonable tolerance bounds.

(b) Any significant rotation of the body prior to entering the jet would generally appear to increase the time spent in the jet. This was not invariably the case and further work would be required on this point.

(c) The results of this investigation indicate that a continued increase in the jet momentum flux would give increasingly smaller reductions in the body deflection time.

(d) There was thought to be reasonable scope within the analysis framework to improve the theory; in particular to estimate the energy losses, improve the calculation of the mean jet deflection angle and eliminate the influence of the side guide walls.

Further experimental work should be undertaken to verify these results since no other work has been found with which to compare them.

As a result of the entire investigation it would appear that liquid jets are eminently suitable for body deflection purposes, being quiet, powerful and selective. It was decided to continue with the design of a liquid powered axial vortex device.

3. THE DESIGN AND ANALYSIS OF A SWIRLING LIQUID JET FLUERIC ELEMENT

3-1 Introduction

As a result of the review of liquid powered flueric literature given in Chapter 1 it was decided that, provided a liquid jet appeared to be suitable for body deflection, a vortex element would be the most suitable deflection device. It was also noted that the transient response of vortex devices may be improved by inserting a centre body within the vortex chamber and thus reducing the fluid volume.

Chapter 2 gave a detailed account of the investigation into cylindrical body movement under the action of a liquid jet and it was determined that a liquid jet was indeed suitable for deflecting bodies of the size and mass range expected. As a result of the successful investigation into body movement the project was advanced to the next stage, that of designing an axial vortex flueric element suitable for body deflection purposes. The jet size and velocity range were determined from the preceding chapter.

All vortex devices operate upon the same principles and the approximate configuration of the proposed device was determined by considering qualitively a number of simple physical precepts. The proposed vortex device was considered to be designed such that zero control flow resulted in a cylindrical liquid jet issuing from the orifice whereas with control flow a conical liquid sheet would result. In order to minimise the transient response time, that is the time interval between the initiation of a control flow and the 'opening' of the swirling jet into a

conical sheet downstream of the orifice, the length of the nozzle should be small and the streaming velocity high. When a control flow is introduced into the streaming flow it is transported into the body of the fluid by momentum interaction, viscosity and fluid turbulence. In order to minimise the time taken to effect this process the radial extent of the fluid should be small. Two further considerations were that a thin annular device would result in high velocity gradients and therefore large shear stresses and that if the stream velocity was accelerated throughout the nozzle then the boundary layer effects should be minimised. Finally, conservation of angular momentum indicated that a high swirl velocity at the orifice could be obtained by injecting the control flow at some radial distance from the orifice axis.

The usual configuration of an axial vortex amplifier is shown in Figure 3-1 (a) and that of a radial device in Figure 3-1 (b). Swirling flow spray nozzles differ in that they usually have only tangential fluid entry.

The output signals most commonly used from a vortex amplifier are pressure drop and flow attenuation, both of which are dependent upon the control flow. The usual measure of flow attenuation is the ratio of the output flow compared with the flow through the device with zero control flow, termed the Turn Down Ratio. The TDR is usually measured with reference to a constant pressure drop across the device, (main inlet to exit). The second variable usually recorded is the control pressure ratio; the ratio of the pressure at the control flow

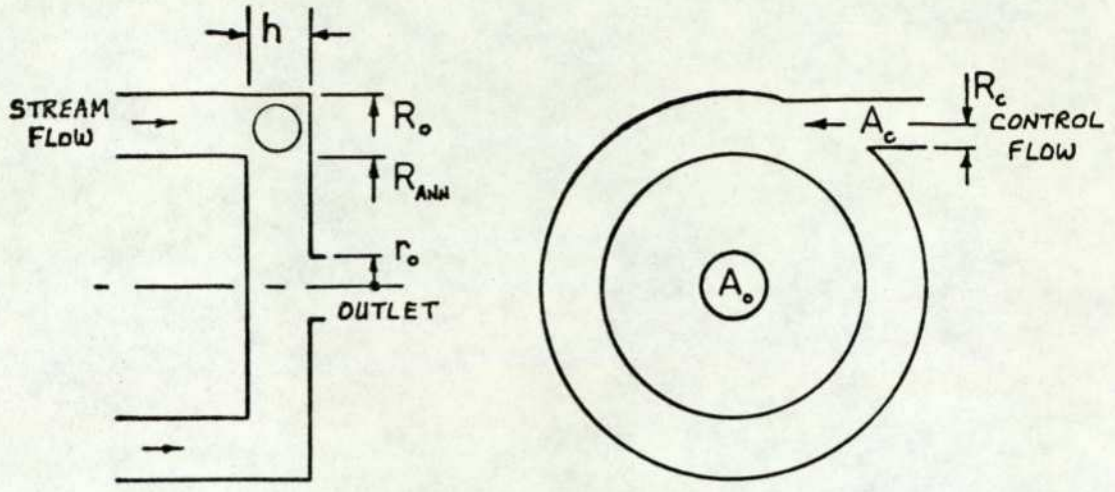

(a) Axial vortex element.

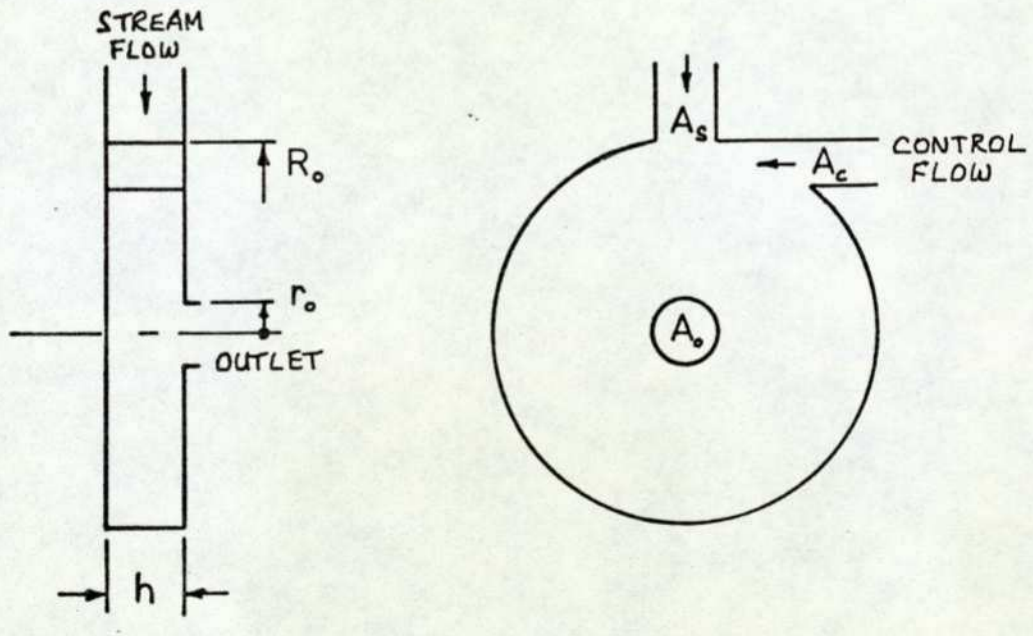

(b) Radial vortex element.

Figure 3-1

port to the pressure at the main inlet port. Pressure measurements taken as output signals require their location to be carefully defined since large pressure gradients occur within the device in both the radial and axial directions.

A literature review of swirling flow research was conducted to obtain quantitative information to assist in the detailed design of the proposed axial vortex device. The literature review considered the published works from two different aspects. The first aspect considered the literature sources on the basis of experimental evidence which would directly assist in the vortex element design. The second aspect was to assess the mathematical models used for the analysis of swirling fluid flow, since this would enable a performance prediction to be given for the proposed vortex device. Literature sources containing axial or radial vortex devices were examined as were swirling jet and spray nozzle sources.

3-2 Swirling Flow Literature Review

3-2-1 The Effects of Vortex Element Geometry

Duff, Foster and Mitchell (1965) mentioned the considerable influence the exit orifice size had on the vortex device characteristic; however, they did not give sufficient information within the paper to enable an estimate to be made of the relative impedances of the main inlet and exit orifices. Their device was a radial vortex unit, as was Neve's (1971) and both authors mentioned, and Neve illustrated, the existence of a 'complementary' vortex, (see Figure 3-2). Neve mentioned that

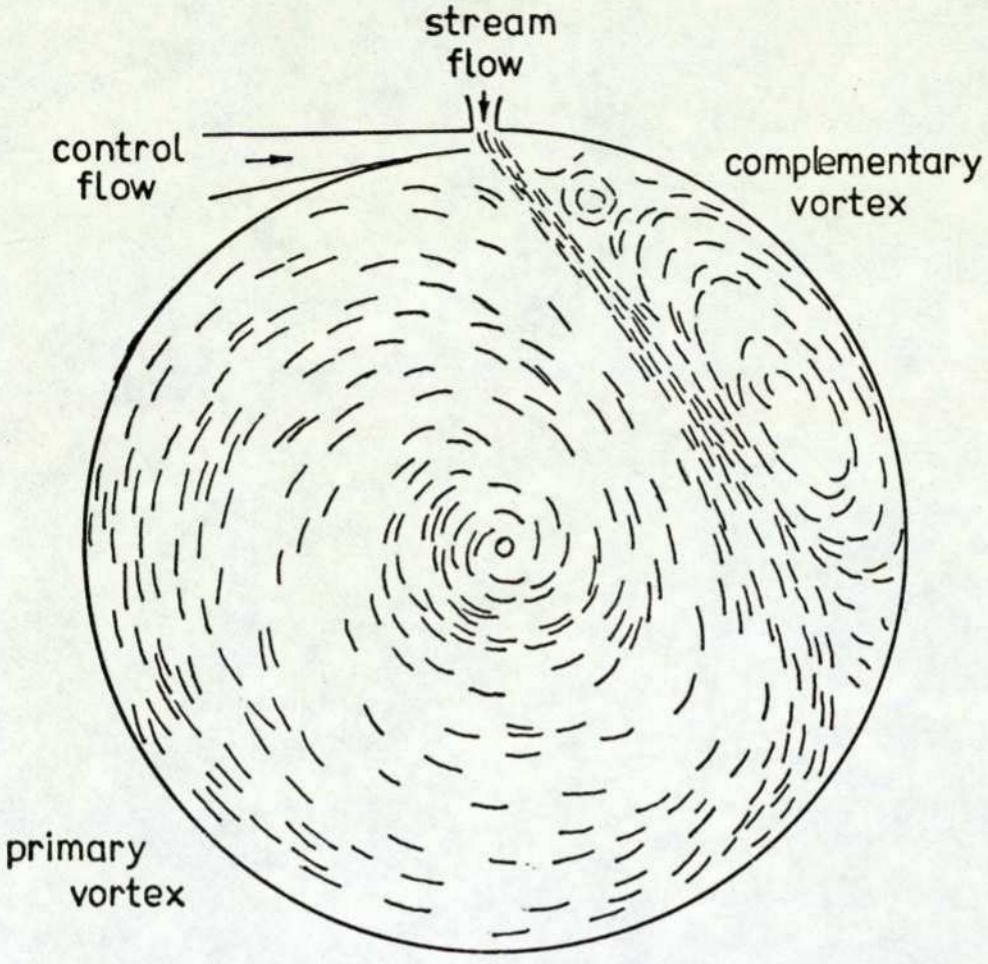

Flow Pattern in a Radial Vortex Element
(from Neve (1971)).

Figure 3 - 2

this complementary vortex became smaller with increasing control flow but did not disappear until the control flow was completely dominant. The flow pattern observed was at variance with the normally accepted mathematical model used for analysis although Duff, Foster and Mitchell modified their analysis to take this into account.

Both Wormley and Richardson (1968) and Bichara and Orner (1969) constructed computer models of radial vortex units. Skoog (1972) gave the governing parameters of Wormley and Richardson's model as:

(i) Vortex chamber exit to periphery radius ratio.

(ii) Control port to exit port area ratio.

The limitations of applicability were given as:

$$\frac{A_s}{A_o} > 3 \; ; \; 0.144 < \frac{h}{R_o} < 0.64 \; ; \; \frac{h}{r_o} > 2$$

$$3000 < R_e = \left(\frac{2\dot{m}}{\pi \mu R_o} \right)_{\dot{m}_c = 0} < 13200$$

Therefore, apparently, Wormley and Richardson found that within a broad range, chamber height, supply port area and Reynolds number had little effect upon the non-dimensional device characteristic.

In his work with oil powered vortex devices Skoog (1972) found that it was difficult to remain within the Reynolds number criterion specified by Wormley and Richardson. Even so, Skoog noted characteristic changes due to variations in the vortex chamber height.

Neve (1971) investigated both the static and transient

characteristics of vortex amplifiers, in particular characteristic changes due to 'aspect ratio', the ratio of the vortex chamber diameter to height. Depending upon the output required Neve generally recommended aspect ratios of between one and three with a small exit orifice; Skoog's device had an aspect ratio of just below three.

In a continuation of his work on radial vortex amplifiers, Wormley (1969) also took into account the effect of the end wall boundary layers. He introduced a term BLC^* (modified boundary layer coefficient) and stated that as BLC^* increased the end wall boundary layers played an increasingly dominant role on the circulation and pressure distributions across the vortex chamber. In terms of vortex amplifier parameters BLC^* depended strongly upon the non-dimensional total and control flows, the chamber radius, the control port area, inlet jet recovery factor, and the end wall friction coefficient. Therefore the parameter BLC^* included the chamber aspect ratio, the ratio of the peripheral tangential to radial velocity, an end wall friction coefficient and, weakly, a Reynolds number.

Taylor (1970) pointed out that turn down ratio was not always a good indication of vortex amplifier performance since turn down ratio could be increased by decreasing the ratio (Ac/As), however by so doing increased power consumption could result. McCloy and Stevenson (1972) performed a number of experiments on both axial and radial vortex devices using oil as the fluid medium. For comparison between devices they

defined a term 'index of performance'which related the power consumed and flow attenuation achieved. Their work on optimising the performance of the button vortex amplifier showed that:

(i) The control flow inlet was positioned at an axial distance of $(h/2)$ although the 'performance index' was fairly insensitive to this parameter.

(ii) The 'index of performance' was also fairly insensitive to aspect ratio, when greater than approximately 0.1 (for the device tested).

(iii) The parameters R_c, R_{ANN}, R_o and r_o were found to be interdependent. With (A_c/A_o) fixed at 0.25 the optimum ratio of (R_{ANN}/R_o) was approximately 0.95 for $0.25 \geq (r_o/R_o) \geq 0.10$. As (r_o/R_o) was increased above 0.25 the optimum value of (R_{ANN}/R_o) appeared to decrease.

(iv) The optimum ratio of (R_c/R_o) for their device was given as approximately 0.08 and this occurred with the relatively large value of (r_o/R_o) of 0.332.

The maximum 'index of performance' obtained with a single outlet device was about four, although this was improved slightly when a radius was put on the outlet orifice.

It was noticed that McCloy and Stevenson found that their results were most suitably presented using the same Reynolds number as Wormley and Richardson (1970) and also that the Reynolds number obtained was generally fairly low. However the Reynolds number quoted by Skoog (1972) is four times greater than that quoted by McCloy and Stevenson.

McCloy and Stevenson's experiments with a single outlet

"jet vortex valve" (i.e. a radial device) indicated that the 'index of performance' was considerably inferior in comparison to the button vortex device.

Al-Shamma (1971) also investigated the characteristics of an axial vortex device. He used a term called 'power turn down ratio' (PTDR) which was identical to McCloy and Stevenson's 'index of performance'. Al-Shamma presented a graph (see Figure 3-3) showing that the power turn down ratio reached a maximum of between 4.5 and 6 with a ratio of (R_o/r_o) of between 3 and 4.5, depending upon the area of the control ports.

It was interesting to note the fairly close agreement between Mc Cloy and Stevenson and Al-Shamma on the ratio (R_o/r_o) Also that the axial device of McCloy and Stevenson gave a higher power turn down ratio than the radial unit and that this was further improved when a radius was put on the outlet orifice; the element investigated by Al-Shamma had a radius on the outlet orifice. The significantly higher power turn down ratio obtained by Al-Shamma may be accounted for by the fact that most vortex devices have to turn the streaming flow through 90° at the exit orifice where the stream and swirl velocities are high, (a point mentioned by Royle and Hassan (1967) and Neve (1971)), whereas Al-Shamma's device does not.

There appears to be some general agreement on 'aspect ratios' of between one and four with a tendency to be on the high side. Also it was noticeable with McCloy and Stevenson's results, although mentioned by other authors, that with a small exit orifice the impedance became so high as to

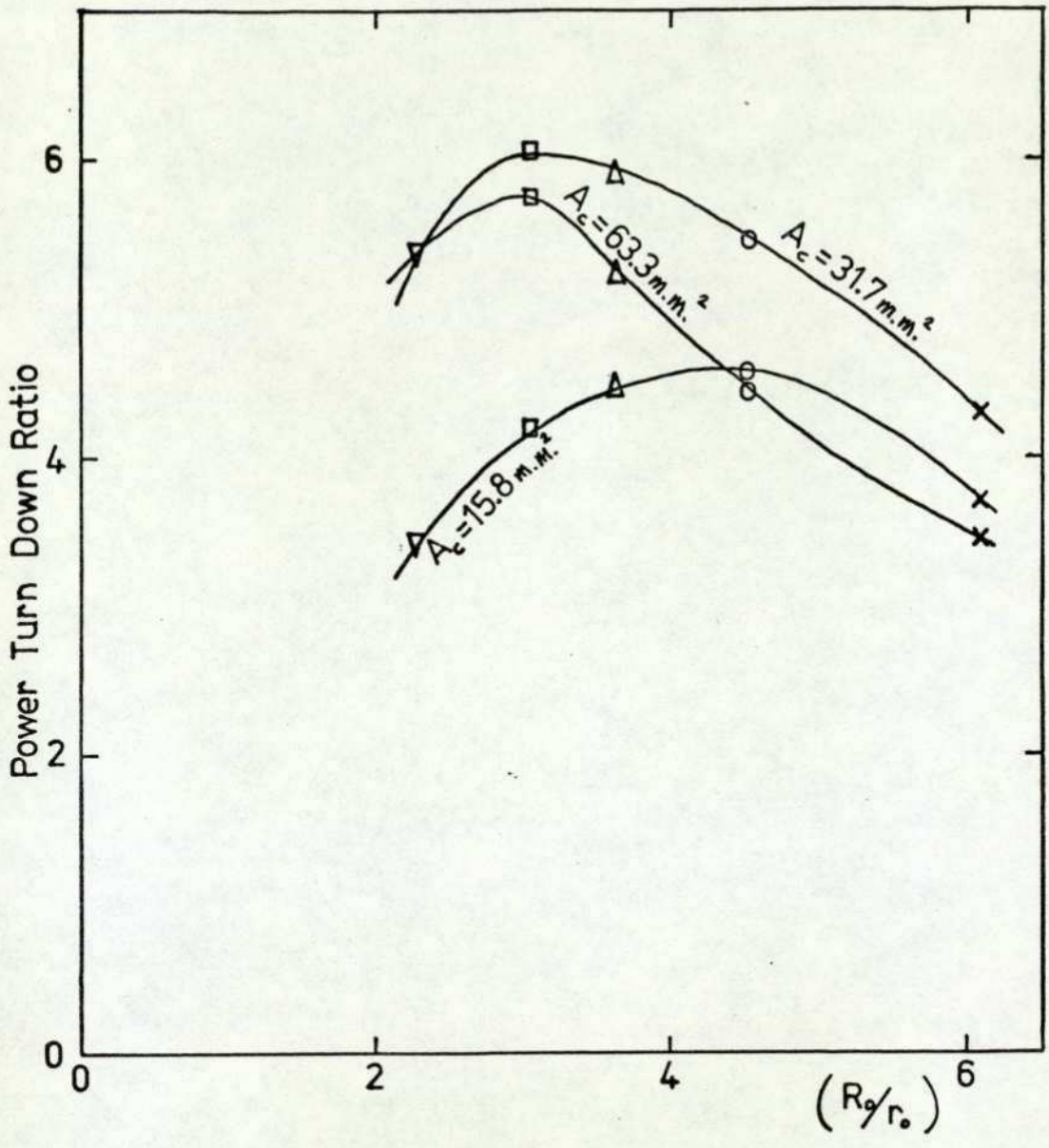

Power Turn Down Ratio against Orifice Size
(from Al-Shamma (1971))

Figure 3-3

dominate the characteristics of the device. The formation of a 'complementary' vortex was considered to be less likely in an axial vortex element especially if the control and supply flows had mixed before any radial in-flow occurred.

3-2-2 The Effects of Fluid Viscosity

In many swirling flow devices high fluid velocities have led to high shear gradients. With these high shear gradients viscosity dependent phenomena have a considerable influence on the performance of a vortex device.

Syred, Royle and Tippetts (1968) stated that vortex element design was heavily dependent upon experimental evidence because of the dominant effect of boundary layers. Certainly a number of authors have mentioned the considerable influence the boundary layer has on flow near the exit orifice, (Taylor, 1948, 1949; Binnie and Harris, 1949; Wormley, 1969; Boucher, Asquith and Royle, 1973). Royle and Hassan (1967) and Wormley (1969) state that with radial vortex units much of the radial inflow throughout the device may occur through the boundary layers. Taylor (1949) predicted that the entire output from a swirl nozzle could be through the boundary layer, although Cooke (1952) questioned one of Taylor's assumptions and calculated a much smaller boundary layer. Rosenzweig, Lewellen and Ross (1964) studied the effect of end wall boundary layers on the circulation and mass flow distributions. They pointed out that boundary layer mass ejection has been shown to occur at geometric discontinuities such as circular steps or the sharp edge of an outlet orifice. If this is suppressed such that much

of the boundary layer flow returns to the stream flow then the circulation distribution may be almost constant over a considerable proportion of the chamber radius. Changes have been made to the geometry of radial vortex units in an attempt to suppress the effects of boundary layer flows. Syred, Royle and Tippetts (1968) tried a double exit orifice, concave chamber walls and the addition of diffusers to the outlets, all with some success.

Skoog (1972) noted that with fluids of relatively high viscosity the turn down ratio was markedly reduced and it became impossible to obtain a supply cut-off. He attributed these effects to viscosity but did not specify whether it was due to boundary layer effects or shear stress effects distributed throughout the body of the fluid.

Some authors have attempted to predict the effects of viscosity by applying a mathematical shear stress model to the entire fluid volume. The shear stress models are examined in detail in section 3-2-5; however, it was noticeable that almost invariably the tangential shear stress was assumed to be dominant and this resulted in the decay of angular momentum flux with downstream distance. In diffuser flows the plane cross section is increasing with downstream distance and the shear gradients decreasing. Conservation of angular momentum flux may not be unreasonable (Wirasinghe, 1975); however So (1967) states that he obtained poor agreement between predicted and experimental vortex decay. A further problem with the decelerating fluid velocities found in pipe and diffuser flows

is the phenomenon of vortex breakdown; this is much less likely to occur within a swirl nozzle with increasing stream and swirl velocities. Nevertheless the nozzle exit orifice is a region associated with flow instability under certain conditions and this is considered in the next section.

3-2-3 Flow Instability

In a concise paper on vortex flow controllers Boucher, Asquith and Royle (1973) stated that: "A limitation of high performance vortex amplifiers arises in low swirl conditions, when instability in the form of oscillation is encountered. This instability is associated with the outlet region and is a consequence of the vortex breakdown phenomenon." They also mentioned that flow instability was likely at intermediate swirl levels where an air core irregularly reached the narrowest nozzle section; stability was restored when the swirl level was raised sufficiently to establish an air core permanently. These observations agree closely with those described by Binnie, Hookings and Kamel (1957). Boucher, Asquith and Royle also mention that the stable operation of a vortex amplifier is dependent upon its outlet geometry. Large outlet devices and those with a central body tend to be stable because a reverse flow core can be established without unstable throttling.

Syred, Royle and Tippetts (1968) mention the troublesome effects of large amplitude low frequency noise on vortex element design. They confirmed that flow instability or 'noise' was

associated with the vortex core issuing into a free atmosphere, with consequent reversed flow and entrainment. Either the addition of a diffuser to the chamber outlet or the axial insertion of a small diameter rod into the outlet stabilised the flow considerably. Neve's (1971) experiments appear to confirm these conclusions. Neve stated: "- - - the audible noise, caused undoubtedly by the problems involved in turning a solid body vortex core through 90° to exhaust normal to the vortex amplifier plane, is beyond normal human tolerance - - -". Royle and Hassan (1967) also mentioned that radial inflow may be highly stable and that any noise from the radial vortex element may be associated with the axial outlet.

McCloy and Stevenson (1972) noted that the button vortex valve's characteristics were more linear and stable than those of the radial vortex element. They also mention that this could be due to the relatively large values of $\left(r_o/R_o \right)$ used in their experiments.

Most references have dealt with flow instability near the outlet orifice and this is certainly the most sensitive area of a vortex element; however, under certain geometric conditions, other unstable flow conditions can occur. At geometric discontinuities or regions of high stream curvature flow separation, aeration or cavitation can occur within the vortex element. Using the definitions of Pearce and Lichtarowicz (1971) aeration could occur at pressures corresponding to the saturation pressure of the gas dissolved

in the liquid and dissolved air would then come out of solution. Cavitation inception would occur when the local static pressure fell below the vapour pressure. There could be a considerable difference between the two pressures and therefore what would apparently be an early onset of cavitation could be, in fact, aeration. A deterioration in performance would usually be noticed and some authors have attributed poor performance to cavitation (Al-Shamma, 1971; Skoog, 1972).

Shinn and Boothe (1964), in a paper explaining some of the problems of connecting fluidic elements into circuits, warn of the problems of instability. They showed that where regions of the source impedance exhibit a negative gradient and are crossed by the load characteristics then flow instability could occur. Al-Shamma (1971) in his work on an axial vortex amplifier showed that the control flow equation could exhibit bistable values and that these characteristics could exist in a practical amplifier.

It appeared from the foregoing references that an axial vortex unit should be more stable and have a higher power turn down ratio than a radial unit. The outlet should be relatively large and care taken to ensure that neither the stream curvature nor the fluid velocities should be excessive. Care should also be taken to ensure that the control flow instability mentioned by Al-Shamma (1971) will not have a detrimental effect on the operation of the proposed device.

3-2-4 Swirling Liquid Jets in Air

A number of authors have attempted to predict the included angle of the liquid sheet or spray after leaving the orifice in terms of the fluid conditions within the orifice. Invariably the references quoted in this section come from investigations into the swirl nozzles commonly used for the injection or atomisation of combustible fuels. The swirl velocities are high and a stable well established air core is assumed to exist under all operating conditions. There is no mention in any of the references to flow instability with low swirl velocities, although in a swirling flow nozzle these would not normally be sought.

Novikov (1948), using inviscid theory, gave the included angle of the liquid sheet in terms of the tangential and axial component velocities at the orifice and in terms of the relative sizes of the outlet orifice and the air core. If the included angle was 2β then:

$$\tan\beta = \left(V_\theta / V_z\right)_{ORIFICE} = \frac{1-a}{(a/2)^{1/2}}$$

where $$a = 1 - \frac{r^2_{air\ core}}{r_o^2}$$

Taylor (1948) also used inviscid theory and obtained the following expression for the liquid cone semi-angle:

$$\cos\beta = \bar{V}_z / V \quad , \text{ where}$$

$\bar{V}_z$ was the axial velocity of the liquid after leaving

the orifice and V was the total velocity due to the total pressure head. In using the axial velocity after leaving the orifice Taylor attempted to account for the conversion of pressure energy stored between the air core and the orifice boundary into additional kinetic energy of the fluid sheet. This region considered by Taylor is one of the most difficult because of the boundary and hence pressure discontinuities associated with the nozzle orifice plane.

Harvey and Hermandorfer (1943) and Wolfsohn (1970) performed similar analyses. Their theory allowed for the fact that the liquid sheet surface was perpendicular to the orifice plane in the immediate vicinity of the nozzle orifice and that therefore the included angle of the sheet varied from zero to a constant cone angle some distance downstream of the orifice. From the equations given by these authors a constant cone angle could be obtained only with constant velocity ratios.

An analysis was made of the effect of surface tension on swirling liquid sheets. The work was relegated to an appendix (Appendix 6) since it was found that for the velocities used in this investigation there was no appreciable curvature of the liquid sheet due to surface forces. Also, the initial conditions requiring specification were those most difficult to obtain (initial velocities, divergent angle and sheet thickness). Nevertheless the theory does show that for given conditions there are velocities where the liquid sheet curvature is not negligible and that the fluid sheet can form

a closed water bell. The theory also predicts the maximum extent of the conical liquid sheet before break-up. These low jet velocities will not be encountered during this investigation.

From the research papers examined it can be seen that the low and moderate swirl conditions, (before the jet centre has opened to form an air core and during the establishment of a stable air core), are not specifically catered for. The correlation between theory and experiment will be examined.

3-2-5 Analyses of Swirling Fluid Flow

Swirling flow devices have generally been analysed from two different viewpoints. The first approach considers the mechanics of the fluid flow, whilst the second considers the device in terms of its transfer function. Obviously the results should be identical but it is probably worth stating that the view generally taken in this report is in terms of the mechanics of the fluid flow.

Almost all the analyses of the mechanics of swirling flows in pipes, swirl nozzles and other vortex chambers have been performed using either cylindrical or spherical coordinate systems. The major difference between authors, in the continuing research on swirling flow analyses, lies in the form and number of the shear stresses modelled. Three general types of shear stress model have been used and invariably tangential shear stresses have been included. The shear stress models have been based on:

(i) The Newtonian shear stress law based on fluid velocity gradients

(ii) Shear stress laws adapted from boundary layer theory for turbulent flow over flat plates.

(iii) Shear stress laws adapted from the Moody friction factor equation.

A number of authors have sought to solve the Navier-Stokes equations (see Appendix 7) with the Newtonian shear stress terms. Royle and Hassan (1967), in their mathematical investigation into the behaviour of a vortex sink, modelled a tangential shear stress according to the formula:

$$\tau_\theta = \mu \left(\partial v / \partial r - v / r \right)$$

They noted that the tangential velocity tended to a forced vortex at low radial Reynolds numbers and a free vortex at higher radial Reynolds numbers. Of particular interest was their comment that the radial inflow appeared to be highly stable and that instability may be due to the axial outlet. Rosenzweig, Lewellen and Ross (1964) rewrote the Navier-Stokes equations in terms of the circulation and stream functions, but then referred to other work (Lewellen, 1962, 1964) to justify a two dimensional solution. Both Binnie and Harris (1948) and Taylor (1949) used spherical coordinates and obtained boundary layer momentum integral expressions from the Navier-Stokes equations. Each author assumed a different velocity component was negligible and integrated the resulting equations to obtain the boundary layer parameters. Wormley (1969), in his work on the boundary layers in vortex chambers,

specifically excluded the mixing and outlet regions. Wormley also used a momentum integral analysis and made the same assumption as Binnie and Harris (1948) and Taylor (1949), in that he assumed all velocity components to have the same boundary layer thickness. Cooke (1952) pointed out that this assumption is unlikely to be true.

The shear stress equations used by Wormley were derived from those used for turbulent flow over flat plates. Wormley gave them in non-dimensional terms as:

$$\bar{\tau}_{tw} = \frac{c_f \lambda \Gamma v_f}{(1-x)(\bar{\delta} v_f)^{1/4}} \quad ; \quad \bar{\tau}_{rw} = \frac{c_f U v_f}{(\bar{\delta} v_f)^{1/4}} \quad ,$$

where the non-dimensional core velocity and friction factor were:

$$v_f = \sqrt{u^2 + \frac{\Gamma^2 \lambda^2}{(1-x)^2}} \quad ; \quad c_f = \frac{f}{\left(\frac{\rho h u_o}{2\mu}\right)^{1/4}}$$

Two other authors who have used shear stress models derived from flat plate theory are Duff, Foster and Mitchell (1965) and Bichara and Orner (1969). The analysis by Duff, Foster and Mitchell was interesting in that it calculated the shear stresses on a discrete fluid element before continuing to the next element. The radial shear stress terms were calculated from:

$\tau = A_\tau \, du/dy$, where the eddy viscosity was taken as: $A_\tau = \mu(1 + 15 v_m)$ and v_m the mean velocity over the element. The end wall shear stresses were calculated according to:

$$\tau = 0.0225 \rho u_\infty^2 \left(\frac{\nu}{u_\infty \delta} \right)^{1/4}$$

The shear stresses and velocity changes over the element were calculated using an iterative procedure. The inclusion of the shear stresses resulted in a considerable improvement over their inviscid model; however, an infinite static pressure drop still occurred at the nozzle exit orifice.

Bichara and Orner (1969) divided the vortex chamber into three sections; an inlet mixing region, the main body of fluid and an exit region. In the inlet region the cylindrical wall shear stress was represented by:

$$\tau_{\theta i} = \rho V_{\theta i}^2 f_1 \Big/ \left[\frac{V_{\theta i} \delta_i \rho}{\mu} \right]^{1/4}$$

where, $$\delta_i = r_i \Big/ \left[\frac{V_{\theta i} r_i \rho}{\mu} \right]^{1/5}$$

Bichara and Orner's shear stress model compares favourably with those of Duff, Foster and Mitchell and Wormley. The angular momentum loss attributed to the mixing of the stream and tangential flows and in overcoming the tangential wall shear stress was depicted using a 'jet recovery factor', see Figure 3-4. In the main body of fluid Bichara and Orner used a simple friction factor equation to represent the end wall shear stresses, thus:

$$\tau \Big|_{z=+h/2} = f_2 \rho V_\theta^2$$

This simple mathematical model was also used by Nissan and Bresan (1961) and Youssef (1966) in their investigations into

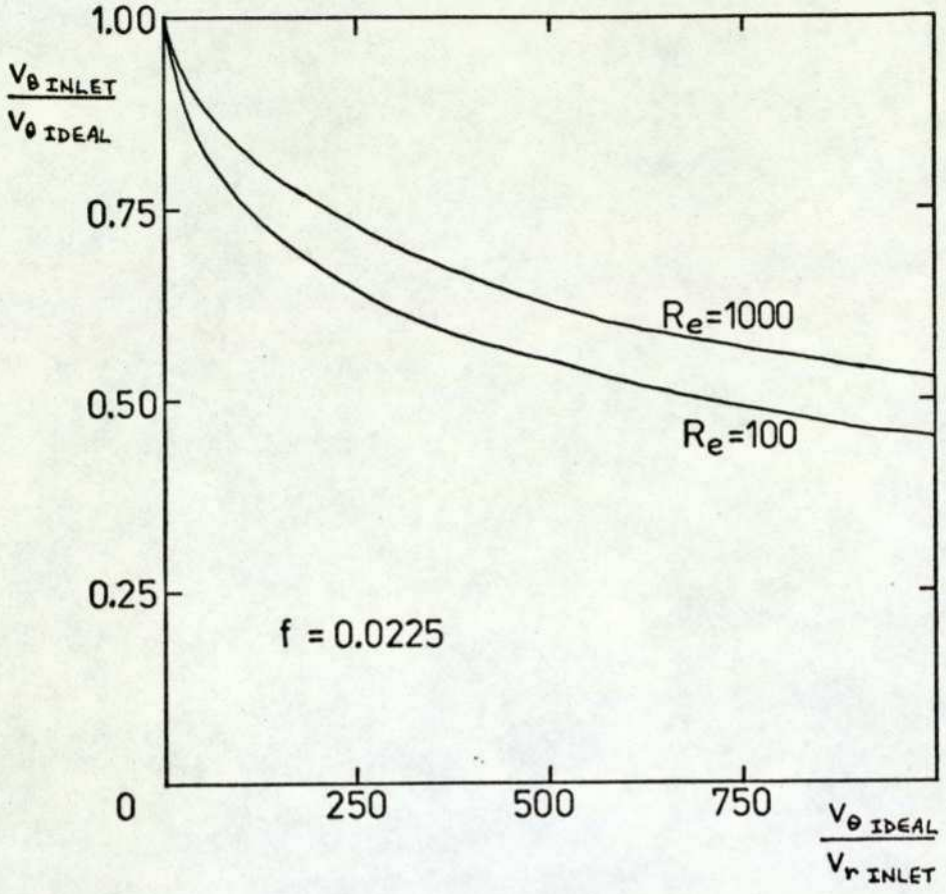

(from Bichara & Orner (1969); author's definitions used for 'f' and 'R_e')

Jet Recovery Factor .

Figure 3-4

swirling flow in pipes, and by Al-Shamma (1971) in his work on an axial vortex device.

The Moody friction factor equation was originally applied to streaming flow in cylindrical pipes and the friction factor used in the equation was a function of the Reynolds number, amongst other parameters. With swirling flow a number of Reynolds numbers have been defined but there appears to be no generally accepted form for Reynolds number evaluation; high shear gradients can occur with either high swirl velocities and low stream velocities, or low swirl velocities and high stream velocities. Whereas the shear stress model of Bichara and Orner used the tangential velocity, that of Youssef used the true fluid velocity at the pipe radius, thus:

$$\tau = \frac{\rho}{2} C_f V_o^2 \quad , \text{ where} \quad V_o = \sqrt{\left[V_\theta^2\right]_{R_o} + \left[V_z^2\right]_{R_o}}$$

Nissan and Bresan initially based their friction factor upon a Reynolds number calculated from a mean axial velocity. Experimental agreement was poor and it was found that a Reynolds number based on the average tangential velocity and a pipe diameter ratio gave better agreement.

King, Rothfus and Kermode (1969) performed work similar to that of Nissan and Bresan but presented their vortex decay graph in terms of a weighted tangential velocity. If the tangential velocity profiles are assumed to be similar then the decay of the average tangential velocity would be directly proportional to the decay of angular momentum flux. Figure 3-5 illustrates the decay of angular momentum flux,

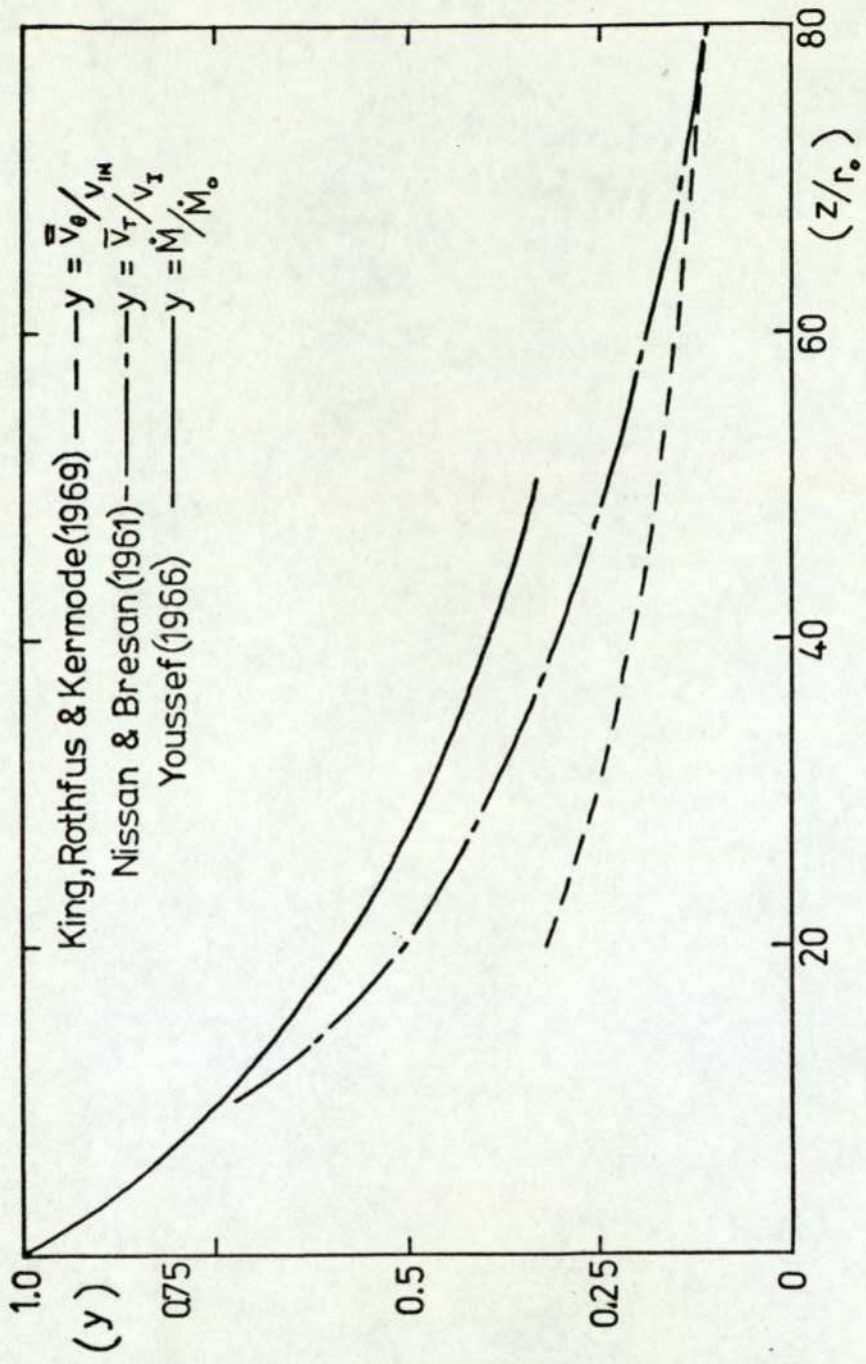

Decay of Swirling Flow in Pipes
(various listed authors)

Figure 3 - 5

or some specified tangential velocity, with downstream distance for the three studies on swirling pipe flow (Nissan and Bresan (1961); Youssef (1966); King, Rothfus and Kermode (1969)). The similarity of the vortex decay curves was thought to be encouraging; however, it was noted that neither in the papers mentioned nor in others examined was an example found of vortex decay within a swirl nozzle with an increasing tangential velocity.

A further point, which caused some concern, was that the proposed axial vortex device would, like Al-Shamma's, have relatively large regions where the curvature of the boundary would mean that neither cylindrical nor spherical coordinate systems would fit the device geometry.

3-3 The Design and Testing of an Axial Vortex Flueric Element

3-3-1 Axial Vortex Element Design

Using the references quoted in the previous section as a guide, an axial vortex flueric element was designed and is shown in Plate 10 and Figure 3-6. The dimensions compare favourably with the axial vortex elements of Al-Shamma (1971) and, in a number of respects, McCloy and Stevenson (1972).

	McCloy and Stevenson (1972)	Al-Shamma (1971)	Test Device
(A_c/A_o)	0.250	0.888 0.222	0.955
(R_{ANN}/R_o)	0.950	0.737	0.643
(r_o/R_o)	0.250	0.329	0.286

(geometry No·1 shown)

Geometry	R_1	R_2	R_3	R_4
No·1	18	22	10	6
No·2	6	10	22	18

Section A-A

(dimensions in m.m.)

Figure 3 - 6

Axial Vortex Element Geometry.

Vortex amplifier

PLATE 10

The stream and control flow inlet areas were larger than those used by most authors. It was anticipated that, unlike most vortex devices, the minimum control flow would be used to 'open' the jet into the required conical liquid sheet. Control flows of the magnitude of the supply cut off value were not expected to be used. The stream velocity was expected to remain fairly close to its zero control flow value. Since a considerable volume of fluid was to be passed through the device the shear gradients were reduced by increasing the annular inlet area and the required control pressure reduced by having a large control port area.

Because of the decisive influence of the nozzle geometry, particularly near the nozzle exit, a special centre body was designed. It was unlike any device known at that time and it was intended that this centre body would suppress any tendency for flow separation in the stream and swirling flow conditions, also that it would improve the flow stability, in the swirling flow condition, near the orifice plane.

In order to compare the effect of the nozzle geometry two configurations were used in the ensuing experiments; Figure 3-6 shows the two configurations. A number of static pressure tappings were added to the nozzle to provide information on the changes in fluid flow conditions with changes in streaming and swirling flows. Figure 3-7 shows the location of the pressure tapping points. It should be noted that the element exhausted into air at the orifice plane and that for all the ensuing experimental investigations the jet catcher,

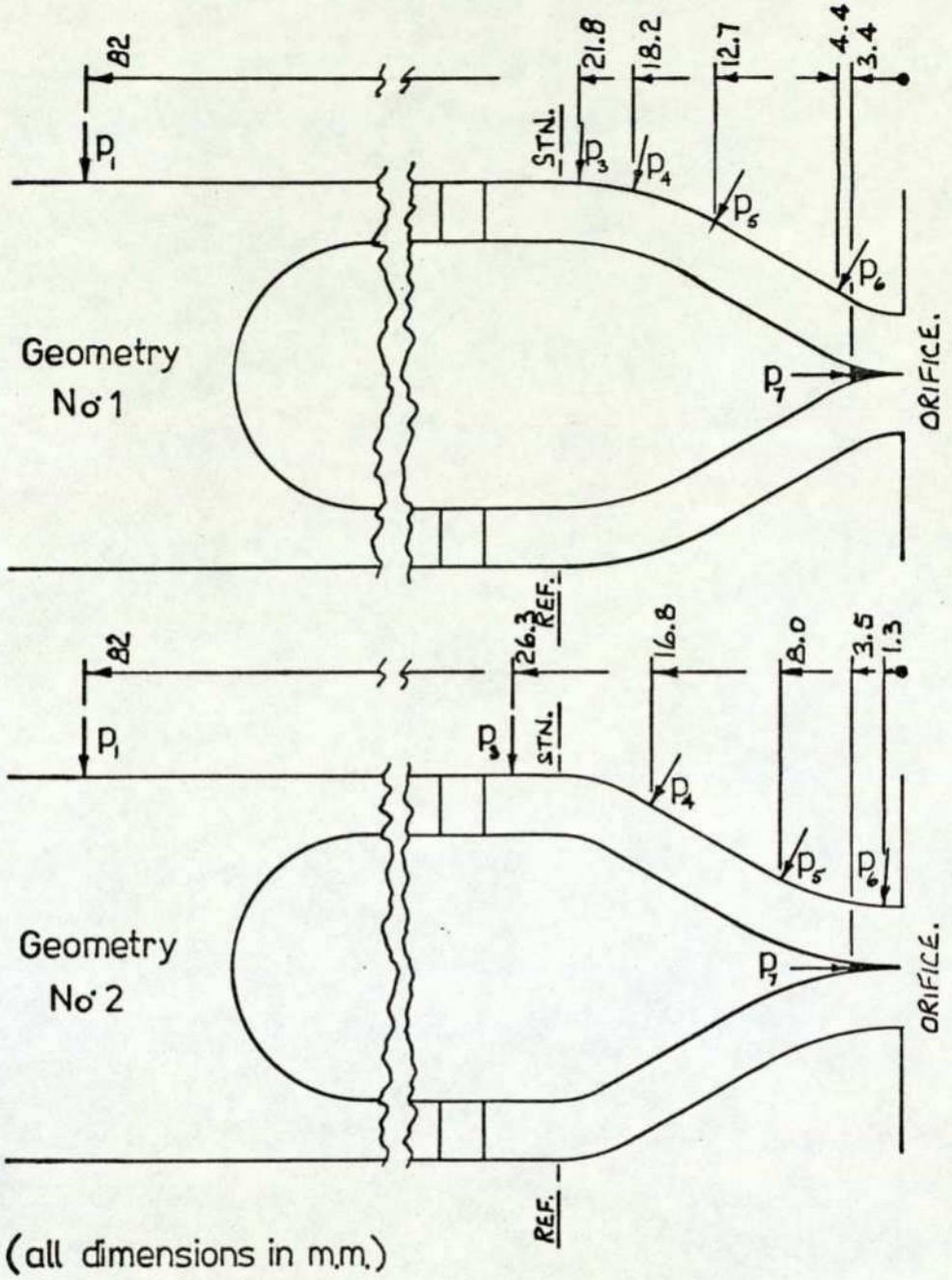

Location of Pressure Tapping Points .

Figure 3 - 7

used to collect the swirling conical sheet when the device was in the switched condition, was removed.

3-3-2 Experimental Procedure

A schematic diagram of the experimental apparatus is shown in Figure 3-8. All flow measurement was made using two Rotameters, the calibration of which is given in Appendix 8. The water temperature was monitored using a thermometer and maintained at approximately constant temperature. All static pressure measurements were made using mercury manometers.

With the first nozzle configuration and zero control flow the stream flow was varied and the static pressure readings and flow rates noted.

With zero stream flow and varying control flow the static pressure readings and flow rates were again noted. Apart from the static pressure readings within the nozzle this enabled the control flow characteristic to be examined.

At certain selected stream flow rates and with no control flow, (so that a continuous cylindrical liquid jet issued from the orifice), the velocity profile close to the nozzle orifice plane was obtained. The velocity head of the jet was measured using the hypodermic total head tube used in the body deflection experiments. The electrical output from the pressure transducer mounted on the total head tube was measured with a digital voltmeter since the voltage changes were thought to be small. (See Appendix 3 for the voltmeter calibration).

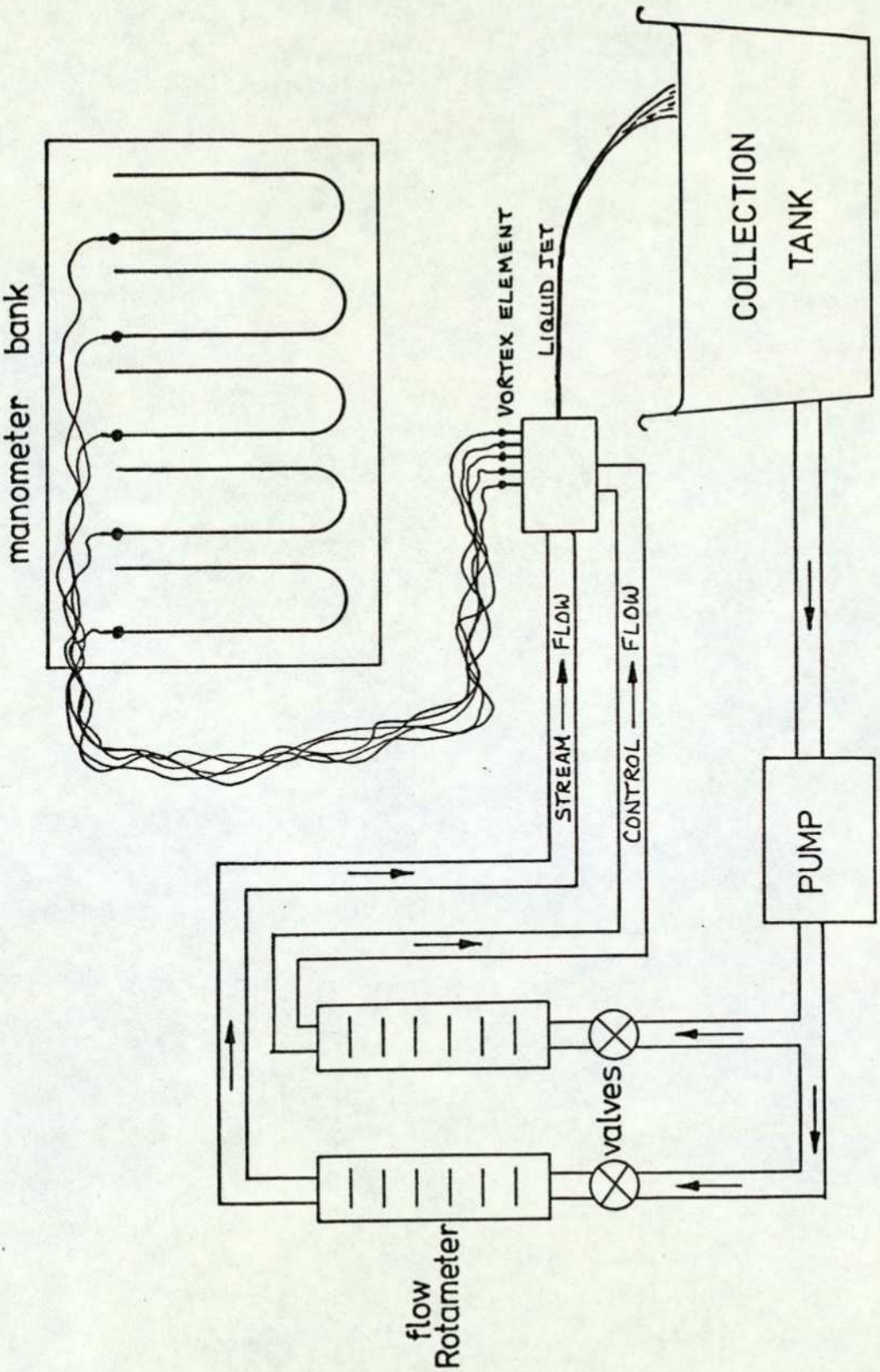

Scheme of vortex element experimental equipment.

Figure 3 - 8

A number of tests were performed to obtain the characteristic of the vortex element. This entailed holding the inlet pressure constant and gradually increasing the swirling flow content from zero until the streaming flow was entirely cut off. At each value of the stream and control flow the manometer readings and flow rates were noted and a photograph taken of the jet to obtain the angle of divergence.

The entire series of experiments were repeated for the second nozzle geometry. The device characteristics are shown in Figures 3-9 and 3-10 and the cone angle results in Figures 3-11 and 3-12. The raw data is given in Appendix 9.

In addition an attempt was made to obtain the ratio between the stream and swirl velocities at the orifice. A very fine black thread was introduced into the fluid stream from the static pressure tapping close to the nozzle orifice. The thread was photographed with various stream and swirl velocities.

A number of experiments were also performed to investigate the transient response of the vortex element. The transient response of the device is the subject of Chapter 4.

3-3-3 Experimental Error Estimates

The errors in the various measurements and measurement systems were assessed.

The errors in the Rotameter flow rates were very small and the repeatability was very good. The reading error in the manometer scales was estimated to be within 0.5 m.m.Hg.

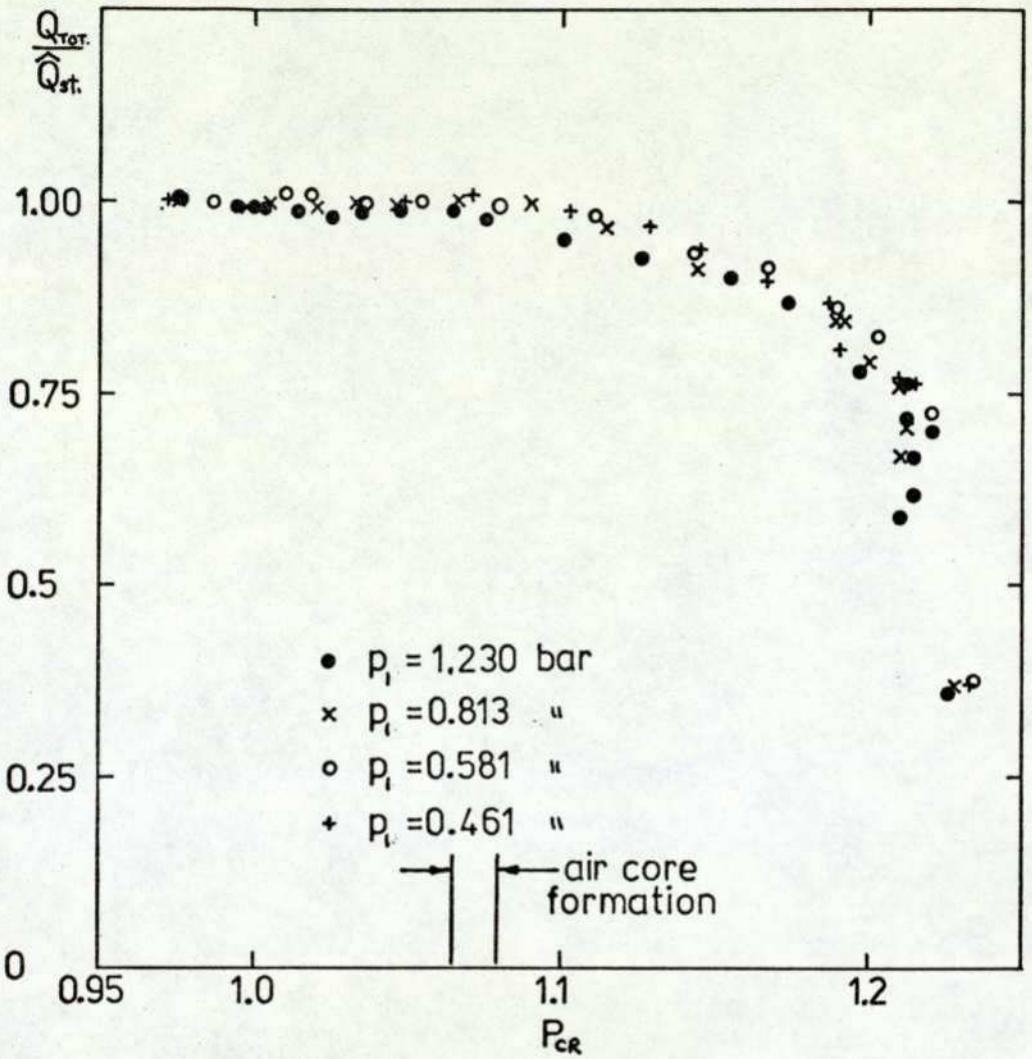

Vortex device characteristic - geometry No 1

Figure 3-9

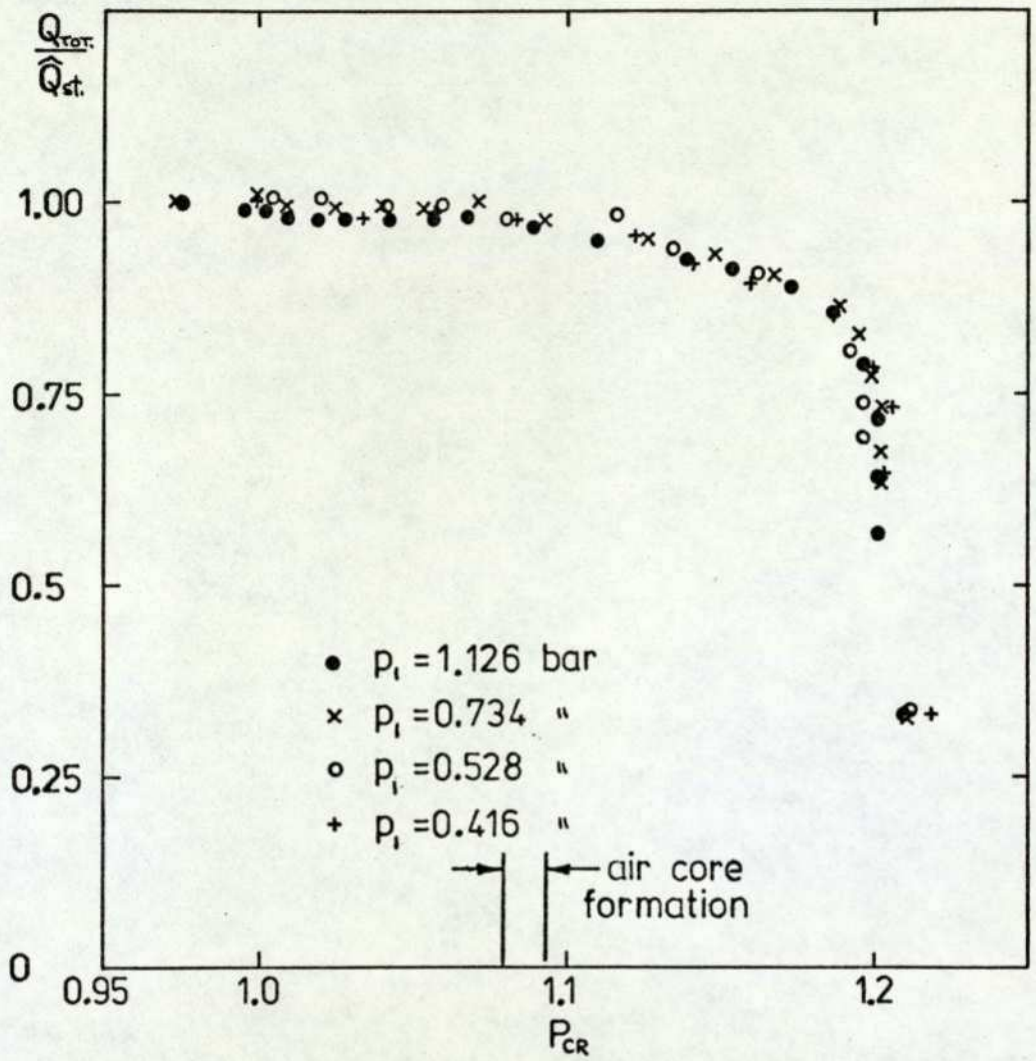

Vortex device characteristic - geometry No 2

Figure 3-10

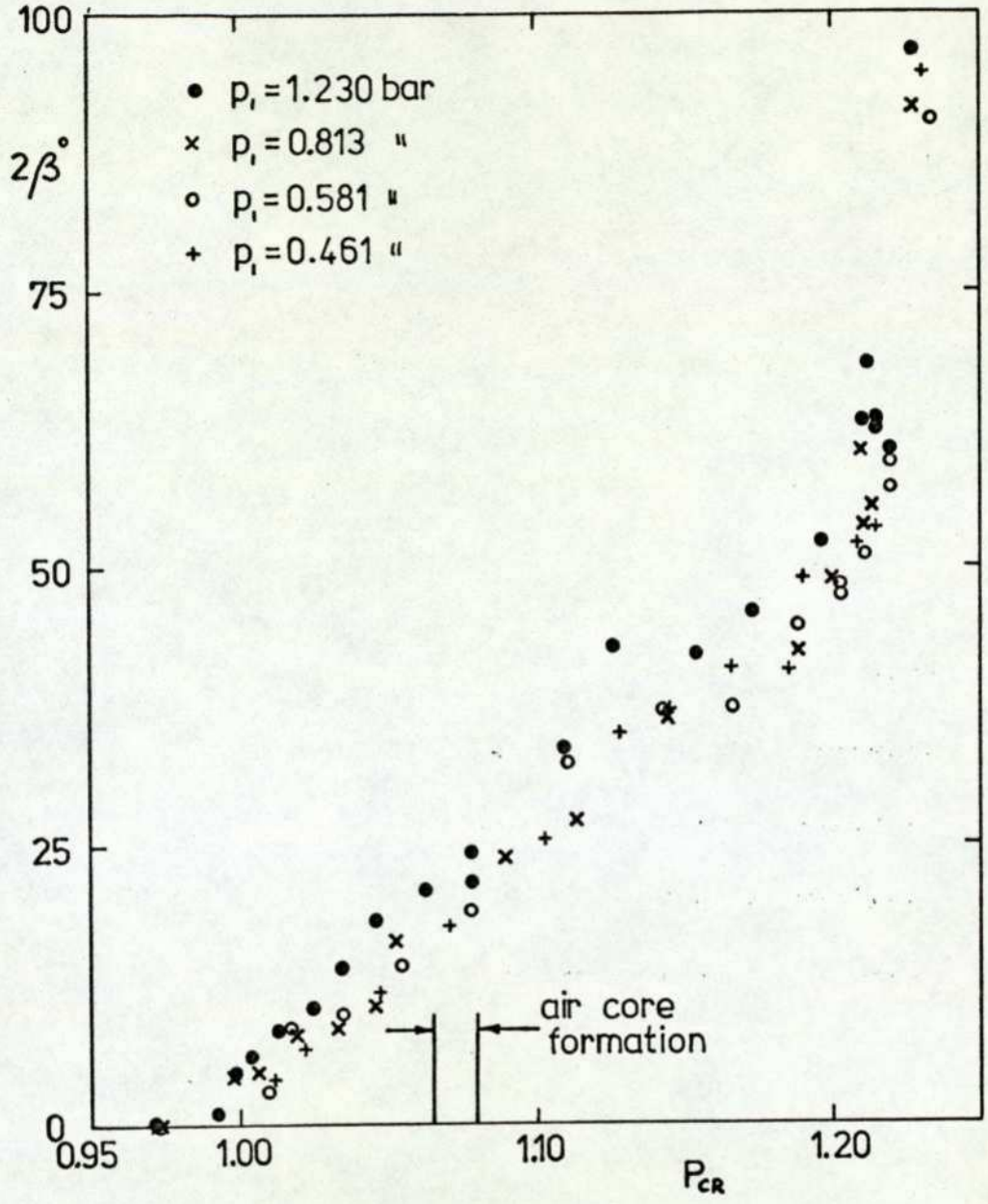

Included jet angle - geometry No'1

Figure 3-11

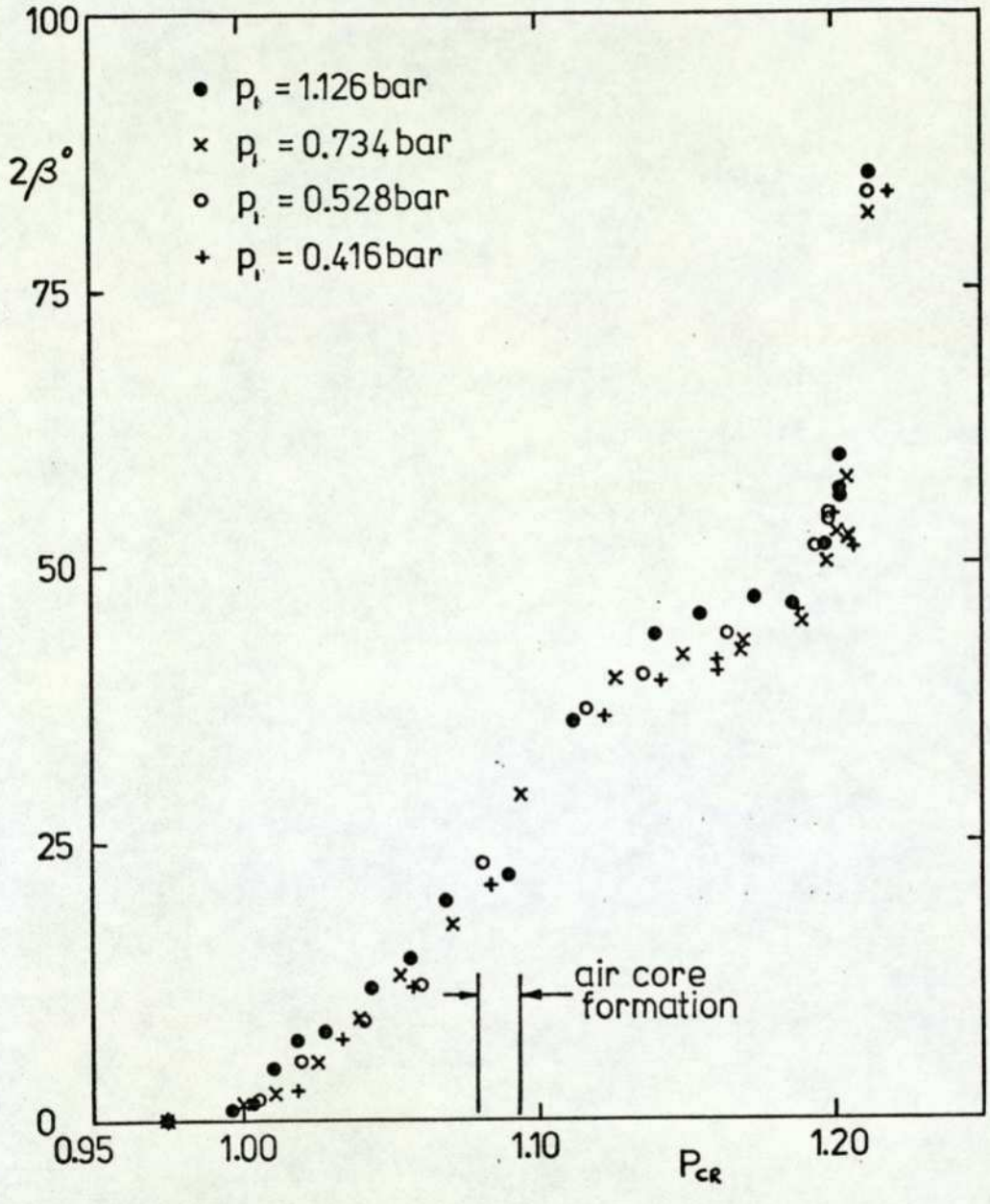

Included jet angle - geometry No 2

Figure 3-12

The errors in measuring the spray cone angle and the velocity ratio thread angle from the photographs was estimated to be less than 0.5 degrees for each measurement. Thus the tolerance on the velocity ratio angle was 0.5 degrees and for the included jet cone angle was 1.0 degree. Further errors were introduced due to the fact that the photographic print was a two-dimensional representation of a three-dimensional figure. The errors are illustrated in Figure 3-13. The errors in the liquid sheet cone angles were calculated to be very small; however the velocity ratios obtained from the thread angle photographs were more doubtful. In angular terms the photographic errors were estimated to be less than 10%.

The tolerance on the measured axial position of the static pressure tappings was approximately 0.3 m.m. Also the pressure tapping down the centre body axis meant that the ideal design geometry was not realised and that the centre body terminated within the nozzle rather than at the orifice plane. It was unfortunate that the geometry of this important region of the nozzle was affected but information on the pressure changes in this region was thought to be of considerable benefit. It was realised that due to the orientation of the pressure tapping within the centre body the true static pressure could not be measured. To measure the true static pressure the tapping should enter normal to the fluid stream surfaces. The centre body tapping was inclined at almost 180° to the fluid stream flow and therefore the pressure measured was expected to be less than the true

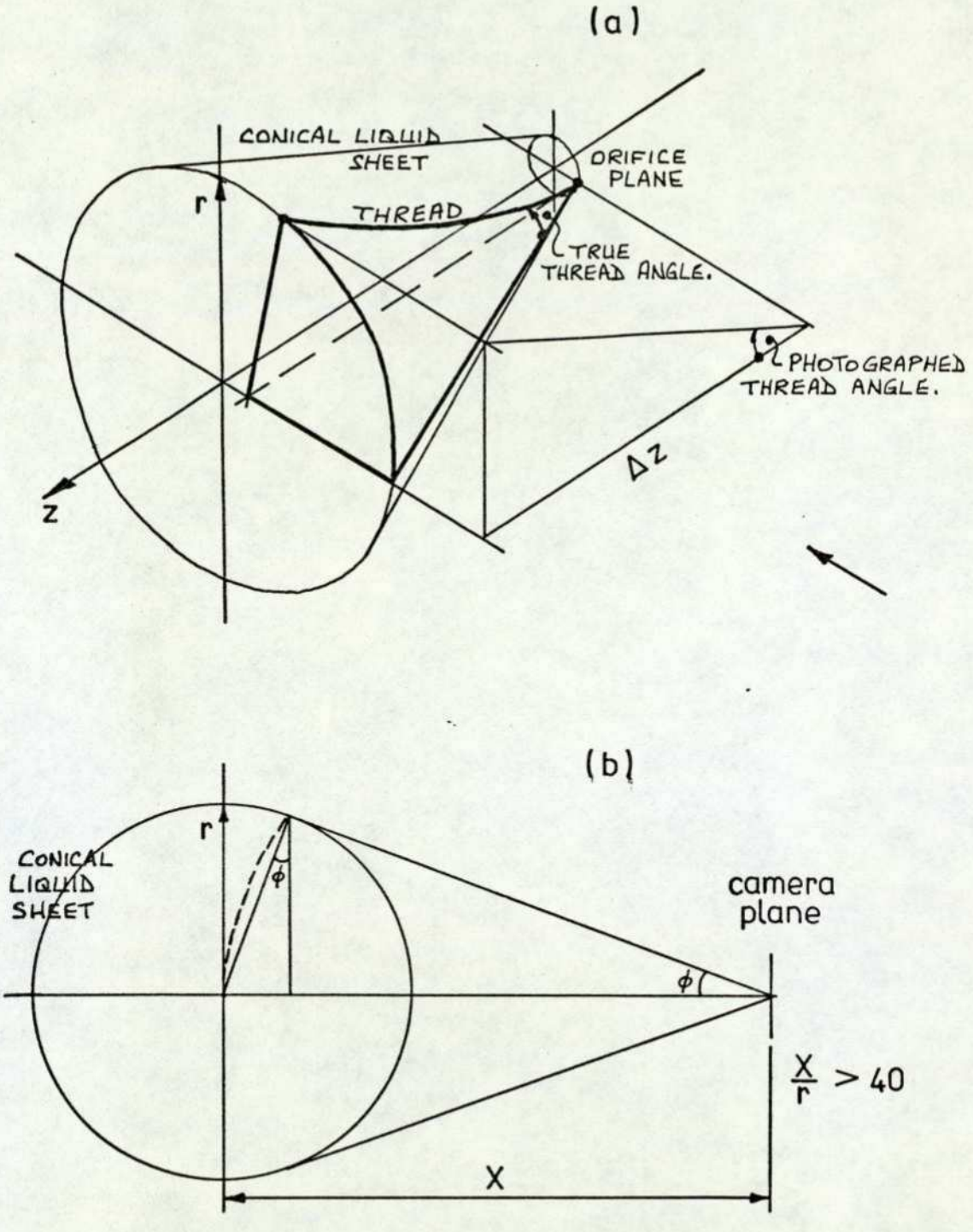

Photographic measurement errors.

Figure 3-13

static pressure. The reduction of the measured pressure below the true static pressure would depend upon the stream velocity and therefore provided the flow rate remained close to the original value then it was thought that the changes in the measured pressure should correspond to the changes in the real static pressure. It can be seen from the experimental readings for swirling flow within the nozzle that the flow rate was indeed very nearly constant for a considerable proportion of the vortex device characteristic. An air core was well established before the point was reached where the flow through the device was rapidly attenuated.

3-4 Axial Vortex Element Analysis

3-4-1 Introduction

Examination of the proposed vortex element geometry (see Figures 3-6 and 3-7) showed that at some point within the nozzle every velocity component had a significant value. Also, due to the curvature of the flow path, regions of high and low pressure could occur within the nozzle. These regions could result in aeration or flow separation. To predict the occurrence of these regions required at least a two dimensional solution of the fluid flow equations. As has been mentioned in the previous sections in this chapter, the region close to the nozzle outlet was considered critical to the performance of the device and it was thought desirable to extend any analysis into the outlet region. In an effort to satisfy the analysis requirements it was decided to use a stream surface

system of coordinates and to attempt to model a tangential shear stress (which was thought to be the predominant shear term).

A few authors have used stream surface or streamline coordinate systems. Johnston (1960) performed an interesting analysis and a very thorough review was given by Neve (1971); however, the necessary metric coefficients were missing and therefore his equations could not be used directly. Vavra (1960) performed an inviscid analysis with compressible flow and the inviscid analysis presented in this investigation is based on his work.

The element analysis was divided into a number of sections:

(a) The control flow characteristic was examined for signs of instability, as mentioned by Shinn and Boothe (1964) and Al-Shamma (1971).

(b) The mixing region was analysed using a simple model and a loss coefficient inserted based on the work of Bichara and Orner (1969).

(c) At the end of the mixing region a reference station was defined and a two dimensional solution of the fluid equations made until the orifice plane was reached. Irrotational and rotational fluid streams were analysed and later a tangential wall shear stress was incorporated into the theory. This analysis enabled the static pressure and orthogonal velocity components to be predicted at any point within the nozzle.

(d) The cone angle of the swirling liquid sheet

was also calculated.

3-4-2 Control Flow Stability

Consider the control flow from the control flow annulus into the main nozzle annulus. The control flow would be given by the orifice equation:

$$Q_c = C_{dc} A_c \sqrt{\frac{2}{\rho}(p_c - p_{ANN})} \qquad -(3\text{-}1)$$

Using Bernoulli's equation in the same manner as Al-Shamma (1971), then at the annulus entrance:

$$Q_s = A_s v_s = Q_{ANN} = A_{ANN} v_{ANN}$$

$$p_r = p_s + \frac{1}{2}\rho v_s^2 = p_{ANN} + \frac{1}{2}\rho v_{ANN}^2$$

Therefore:

$$Q_c^2 = (C_{dc} A_c)^2 \left[\frac{2}{\rho}(p_c - p_s) + Q_s^2 \left(\frac{1}{A_{ANN}^2} - \frac{1}{A_s^2}\right)\right] \qquad -(3\text{-}2)$$

Equation (3-2) shows that there are two components comprising the control flow, a linear pressure term and a non-linear term dependent upon the supply flow and the ratio $\left(A_{ANN}/A_s\right)$. In order to minimise any non-linear effect due to the supply flow it was decided to use a fairly large annular area and not to try and maximise the venturi effect of the centre body. In spite of this the device did not meet the recommended parameter values given by Al-Shamma.

	Al-Shamma (1971)	Test device
(A_{ANN}/A_o)	> 10	5.5
P_{CR}	> 2	1.234

Of the parameters included in equation (3-2) all the areas and the fluid density were known. The vortex element was assembled and with zero supply flow the control flow against pressure difference across the control orifices characteristic obtained. From this experimental data the coefficient of discharge Cdc was obtained (Cdc = 0.7596). Figure 3-14 shows a graph of the data contained in Appendix 9. The flow equation was then written as:

$$Q_c^2 = K_1(p_c - p_s) + K_2 Q_s^2$$

where $K_1 = 2.658 \times 10^{-12}$; $K_2 = 0.0127$

When stream flow was permitted the vortex element characteristic appeared to show very little bistability and any that did exist was close to the supply flow cut-off point. It was thought that if the characteristic inflexion mentioned by Al-Shamma was very tight then it would be difficult to discern. In order to display any instability more clearly it was decided to display the control flow components separately. A high flow rate was chosen to maximise the contribution made by the supply flow and thus any instability; the results are shown in Figure 3-15. The control flow characteristics for both device configurations (Geometry No.1 and Geometry No.2) are shown in Figures 3-16

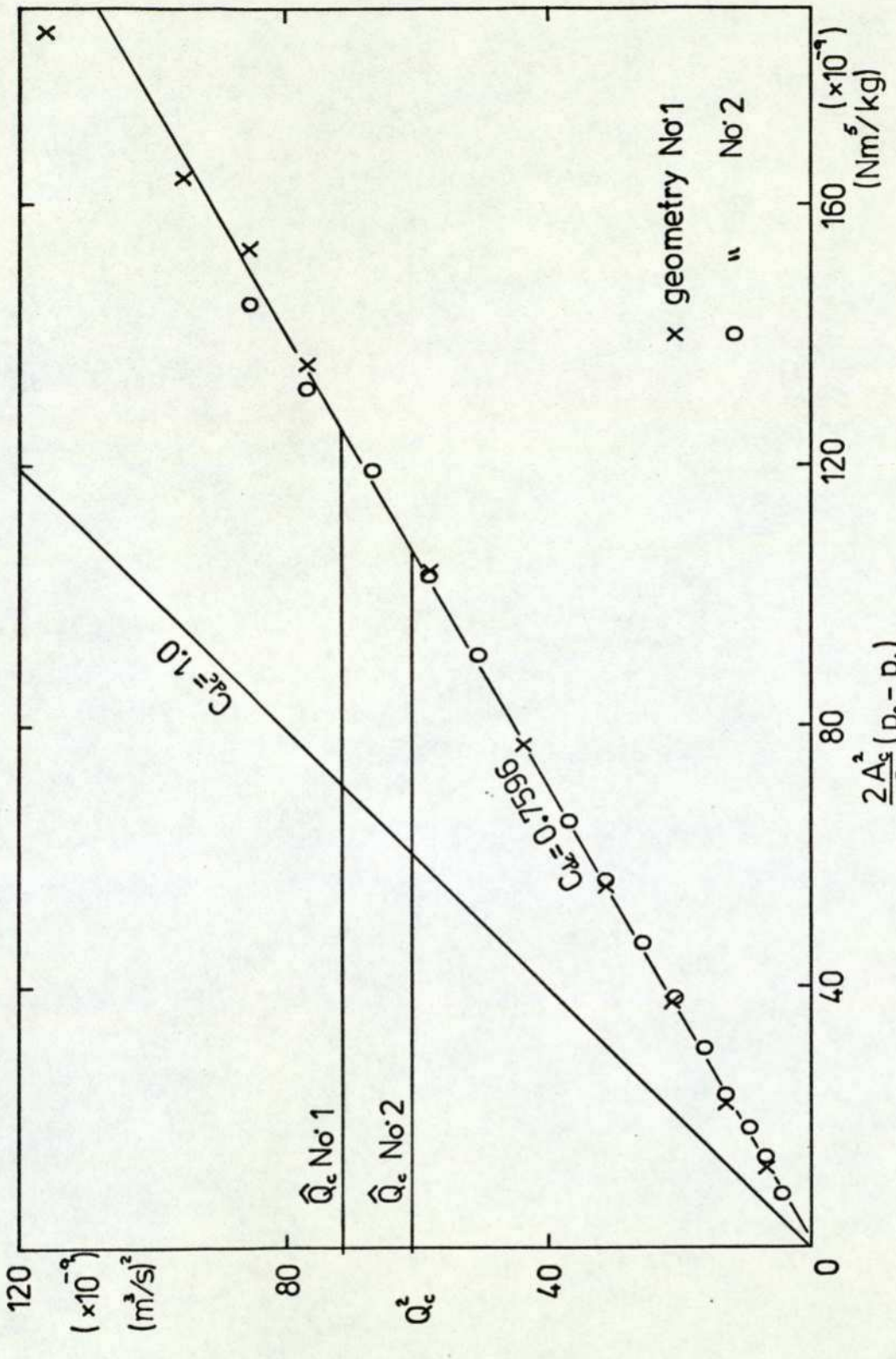

Control flow coefficient of discharge.

Figure 3 - 14

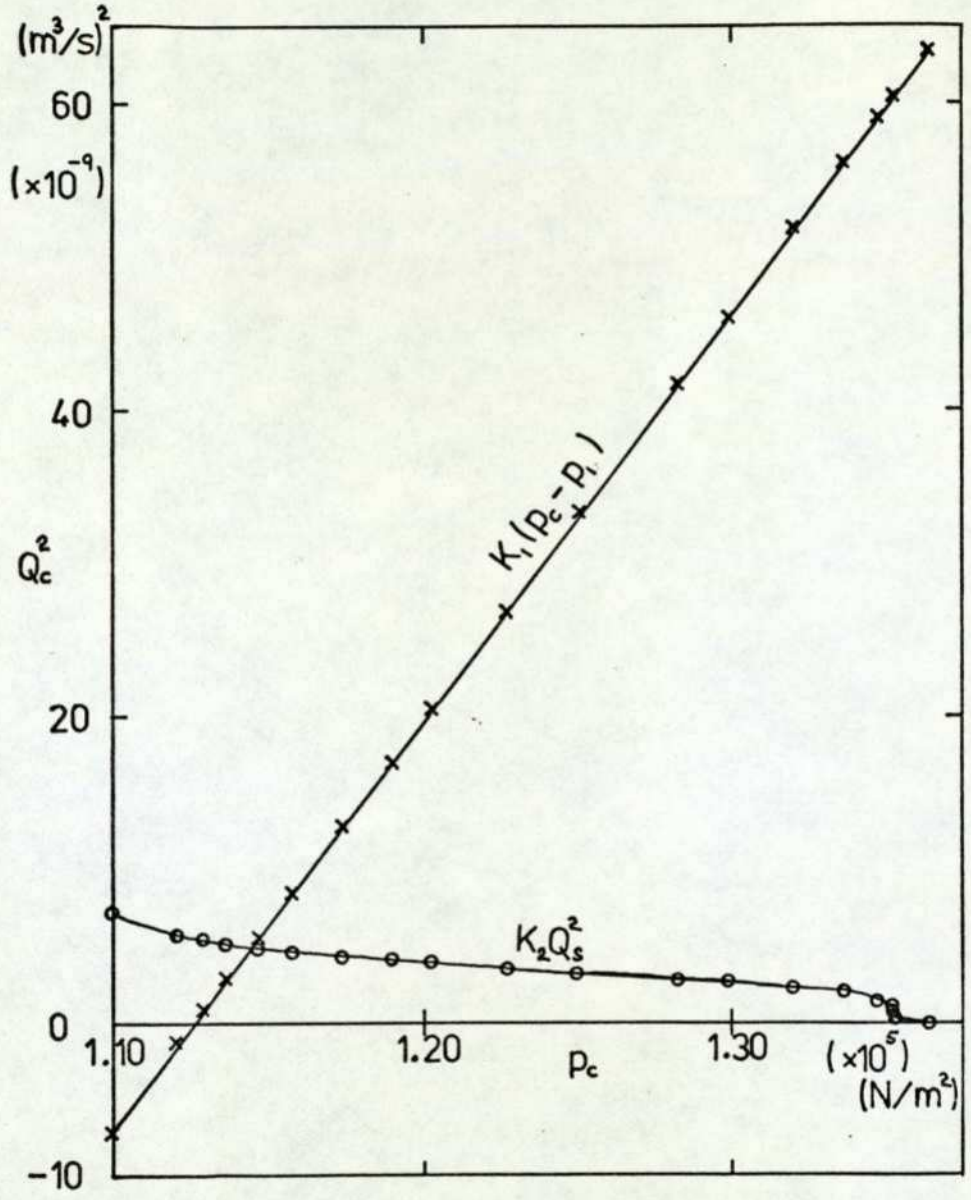

Components of control flow.

Figure 3-15

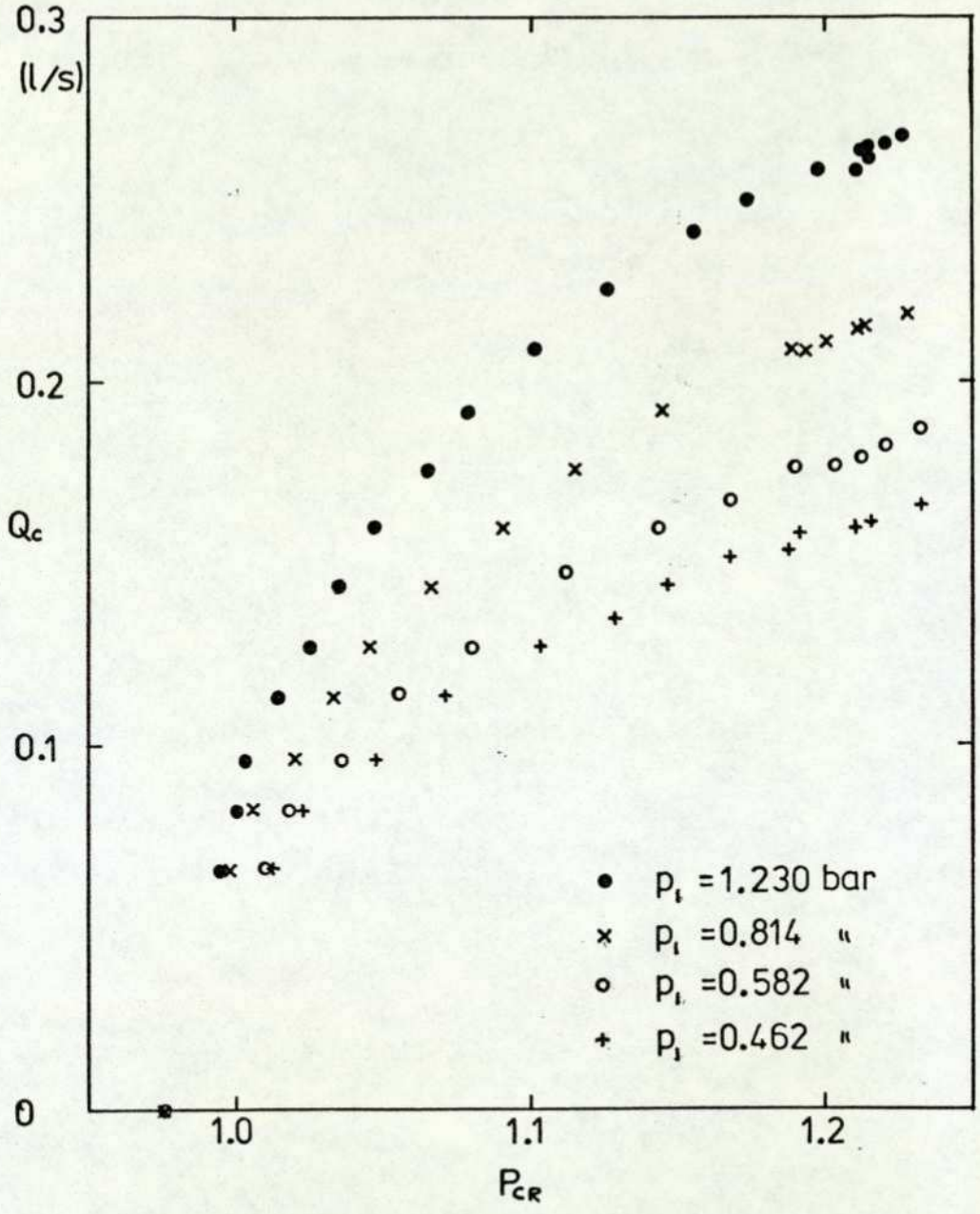

Control flow against control pressure ratio, geometry No° 1

Figure 3 - 16

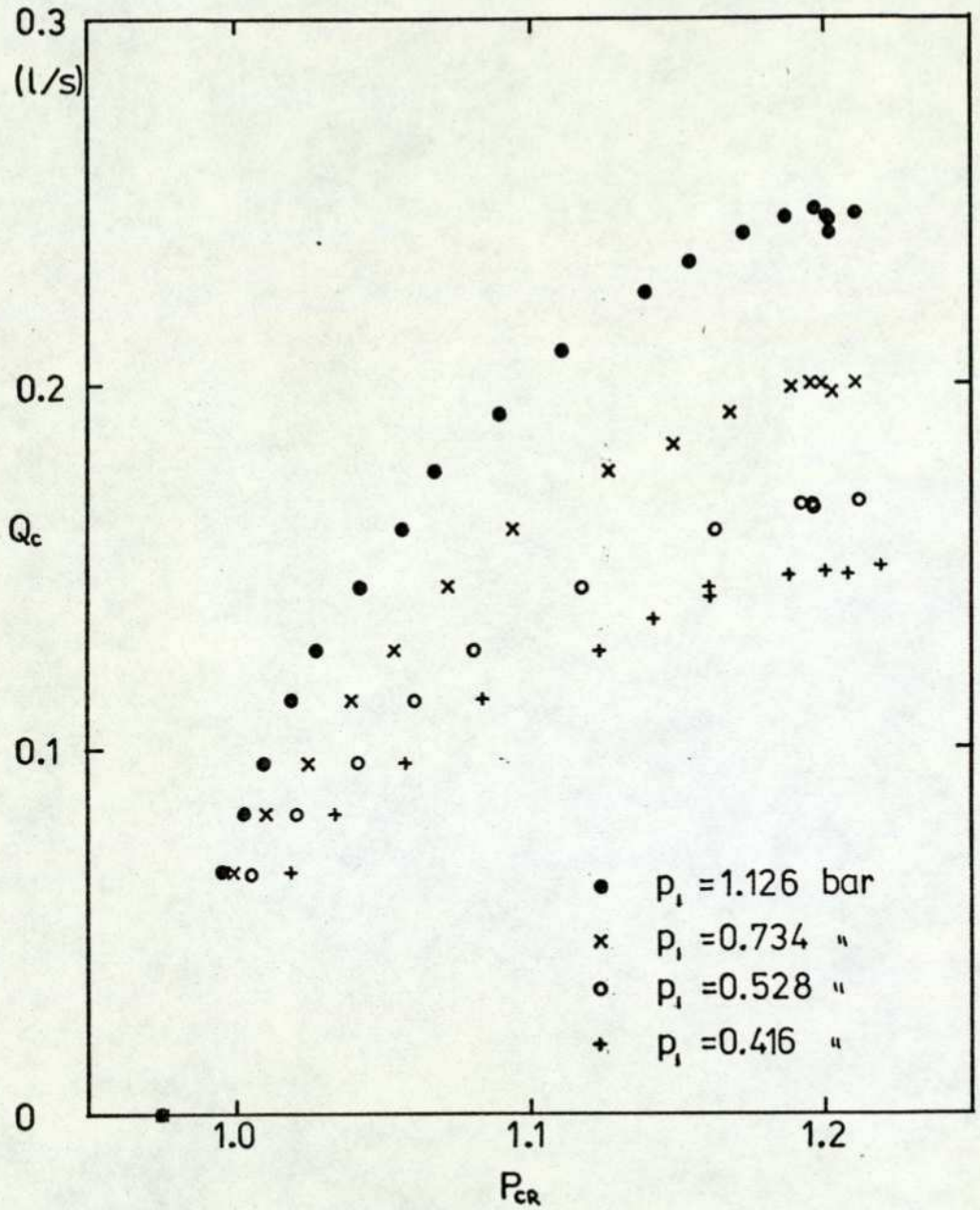

Control flow against control pressure ratio, geometry No 2

Figure 3-17

and 3-17 respectively. Very little, if any, control flow instability is noticeable and thus both configurations of the device appear to be predictable and easily controlled until very close to the cut-off point. Device No.2, the second configuration, appeared to be the better of the two devices. The original statement made by Al-Shamma is shown to be valid since a slight inflexion occurs close to the cut-off point. For the devices tested the effect was small and did not occur over that portion of the characteristic expected to be used.

3-4-3 Analysis of the Mixing Region Flow

See Figure 3-18 and consider station (1). The angular momentum flux about the nozzle axis 'O' can be given by:

$$d\dot{H}_I = d\dot{m} R v_c \quad ,$$

where $d\dot{m} = \rho v_c dA$ and $dA = l.ds$

$$\dot{H}_I = \rho l \int_{S_1}^{S_2} R v_c^2 ds \qquad -(3\text{-}3)$$

Assuming Vc is independent of the variable 's' and replacing the variable 's' by 'R' then:

$$\dot{H}_I = \rho l v_c^2 \int_{R_i}^{R_o} R\, dR = \frac{\rho l v_c^2}{2} (R_o^2 - R_i^2)$$

Consider station (2), the angular momentum flux crossing the station is:

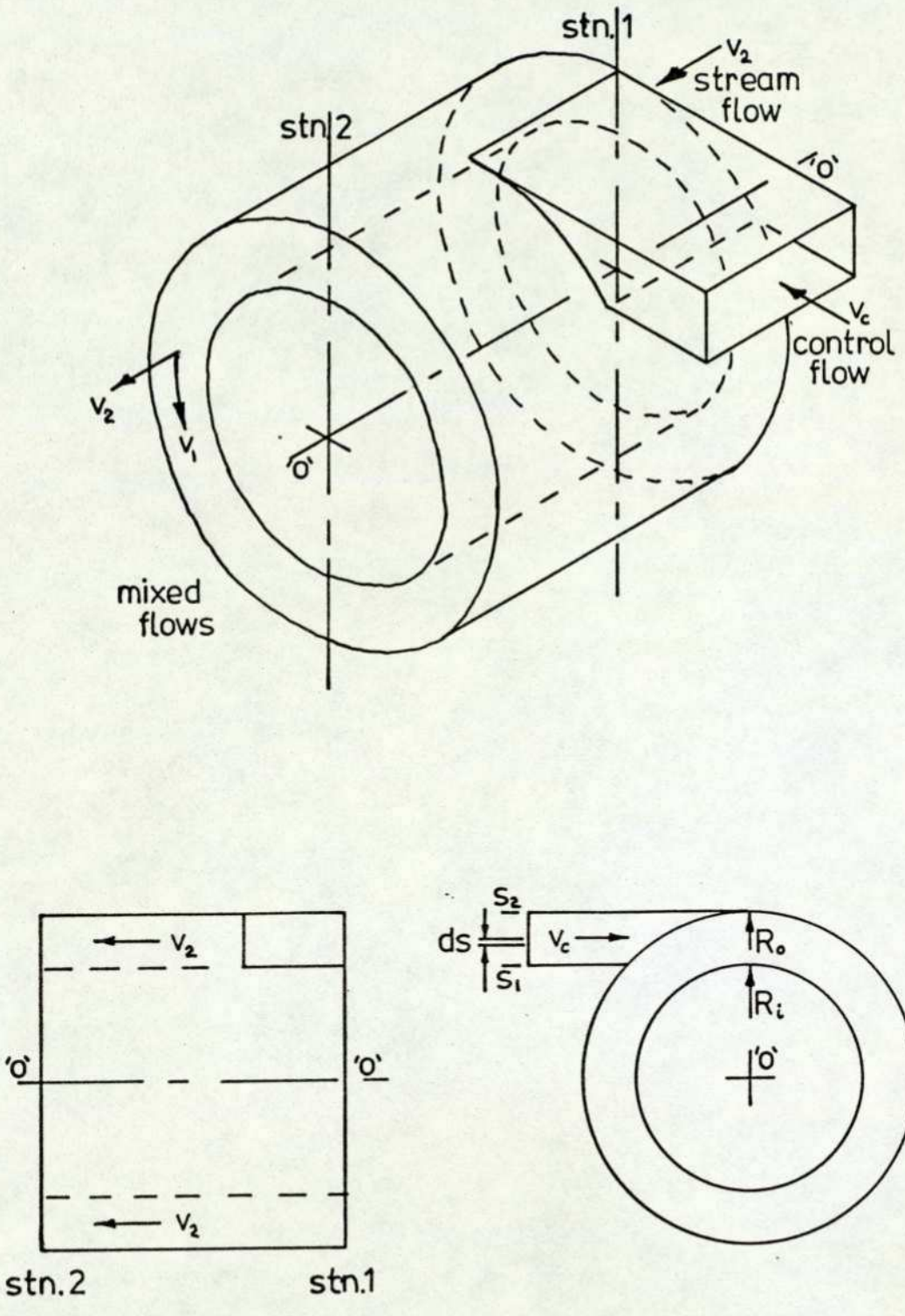

Control and stream flow mixing region.

Figure 3-18

$$\dot{H} = 2\pi\rho \int_{n_i}^{n_o} v_1 v_2 R^2 dn \qquad -(3\text{-}4)$$

where $d\dot{H} = d\dot{m} R v_1$; $d\dot{m} = \rho v_2 dA$; $dA = 2\pi R dn$

Assuming that the stream surfaces are parallel to the wall and that V_1 and V_2 are independent of the variable 'n', then the 'n' coordinate can be replaced by the cylindrical coordinate 'R'. Therefore:

$$\dot{H} = 2\pi\rho v_1 v_2 \int_{R_i}^{R_o} R^2 dR = \frac{2}{3}\pi\rho v_1 v_2 (R_o^3 - R_i^3)$$

Since the axial flow V_2 crossing station (1) has no angular momentum about the nozzle axis then:

$$\dot{H} = \dot{H}_I \quad , \text{ and}$$

$$v_1 = \frac{3}{4\pi} \cdot \frac{l}{v_2} \cdot \frac{v_c^2}{v_2} \cdot \frac{(R_o^2 - R_i^2)}{(R_o^3 - R_i^3)} \qquad -(3\text{-}5)$$

For the geometry of both devices tested the values of l, R_o and R_i are known and therefore:

$$v_1 = (0.04293) \frac{v_c^2}{v_2}$$

If at station (2) the distribution of swirling flow produces a free vortex then $Rv_1 = C$ and:

$$\dot{H} = 2\pi\rho v_2 \int_{R_i}^{R_o} \frac{c}{R} R^2 dR = \pi\rho v_2 c (R_o^2 - R_i^2)$$

Therefore: $$v_1 = \frac{l v_c^2}{2\pi R v_2} \qquad -(3\text{-}6)$$

Again, for the geometric configuration under test:

$$v_1 = \left(0.47746 \times 10^{-3}\right) \frac{v_c^2}{R v_2}$$

Thus, providing the stream and control flow velocities are known the tangential velocity of the mixed stream could be calculated. The tangential velocities given by equations (3-5) and (3-6) are the maximum possible for the conditions specified. In practice there is a loss in angular momentum flux due to fluid turbulence and inter-fluid shear gradients. Both Bichara and Orner (1969) and Wormley (1969) used a term 'jet recovery factor' to account for the angular momentum flux lost within the mixing region. The ideal tangential to radial velocity ratios used by Bichara and Orner were in the hundreds. In this investigation the tangential velocities at the mixing region were relatively low and if Bichara and Orner's graph were to be used (see Figure 3-4) the recovery factor was estimated to be between 0.98 and 0.95. For the initial theoretical work it was decided to assume no losses in the mixing region. The recovery factor was therefore set to unity.

3-4-4 Inviscid Analysis of Nozzle Fluid Flow

Appendix 7 explains the stream surface coordinate system used for the nozzle fluid flow analysis; the laminar flow Navier-Stokes equations are also derived. From Appendix 7 the inviscid, steady flow, vector equation of motion is:

$$\nabla\left[v^2 + gz\right] = \vec{v} \times \left(\nabla \times \vec{v}\right) - \nabla\left(\frac{p}{\rho}\right)$$

Following Vavra (1960) and defining the total pressure as:

$p_T = p + \rho\frac{v^2}{2} + \rho gz$, then the equation of motion became:

$$\nabla\left(\frac{p_T}{\rho}\right) = \vec{v} \times \left(\nabla \times \vec{v}\right)$$

Conforming to the conditions specified for the coordinate system in section (ii) of Appendix 7 then:

$$\vec{L}_2 \frac{1}{\rho}\frac{\partial p_T}{\partial m} + \vec{L}_3 \frac{1}{\rho}\frac{\partial p_T}{\partial n} = \vec{L}_1\left[-\frac{v_2}{R}\frac{\partial(Rv_1)}{\partial m}\right] + \vec{L}_2\left[\frac{v_1}{R}\frac{\partial(Rv_1)}{\partial m}\right]$$

$$+ \vec{L}_3\left[\frac{v_1}{R}\frac{\partial(Rv_1)}{\partial n} + v_2\left(\frac{\partial v_2}{\partial n} + v_2 k_m\right)\right]$$

and hence the scalar component equations became:

$$\frac{v_2}{R}\frac{\partial(Rv_1)}{\partial m} = 0 \qquad -(3\text{-}7)$$

$$\frac{1}{\rho}\frac{\partial p_T}{\partial m} = \frac{v_1}{R}\frac{\partial(Rv_1)}{\partial m} \qquad -(3\text{-}8)$$

$$\frac{1}{\rho}\frac{\partial p_T}{\partial n} = \frac{v_1}{R}\frac{\partial(Rv_1)}{\partial n} + v_2\left(\frac{\partial v_2}{\partial n} + v_2 k_m\right) \qquad -(3\text{-}9)$$

Providing that neither R nor V_2 becomes zero then from equation (3-7):

$\left(\partial(RV_1)/\partial m\right) = 0$ and therefore RV_1 was constant along a stream surface. Similarly from equation (3-8), providing R was greater than zero, the total pressure (p_T) was constant along a stream surface. Therefore since RV_1 and p_T were functions of 'n' only then the partial derivative notation could be replaced by the total derivative notation and equation (3-9) could be rewritten as:

$$\frac{\partial(V_2^2)}{\partial n} + 2k_m V_2^2 + \left(\frac{V_1}{R}\cdot\frac{d(RV_1)}{dn} - \frac{1}{\rho}\cdot\frac{dp_T}{dn}\right) = 0$$

The third term of the above equation was a function of 'n' only and was denoted by N(n). Therefore:

$$\frac{\partial(V_2^2)}{\partial n} + 2k_m V_2^2 + 2N(n) = 0 \qquad -(3\text{-}10)$$

It was noted that equation (3-10) was a first order linear partial differential equation in V_2^2 and could be solved by integrating along an 'n' curve. The solution of equation (3-10) was found to be (a detailed explanation being given in Appendix 10):

$$V_2^2(n) = \exp.\left[-\int_o^n 2k_m\, dn\right].\left[V_{2(i)}^2 - \int_o^n 2N.\exp.\left[\int_o^{u=n} 2k_m\, du\right] dn\right] \qquad -(3\text{-}11)$$

Before a value could be obtained for the stream velocity for the nozzle geometry under consideration the stream surface geometry had to be known, or assumed, and the velocities and pressure at a reference station had to be

specified. Figure 3-19 (a) illustrates a meridian section showing adjacent stream surfaces intersected by their orthogonal trajectories. Providing the geometric and fluid dynamic parameters were known at one station, along which the coordinate x_2 was a constant, then:

$$\left[\delta(Rv_l)\right]_{x_2=a} \triangleq \left[\frac{d(Rv_l)}{dn}\right]_{x_2=a} \cdot \delta n_{x_2=a}$$

$$\left[\delta p_T\right]_{x_2=a} \triangleq \left[\frac{dp_T}{dn}\right]_{x_2=a} \cdot \delta n_{x_2=a}$$

Defining station $x_2 = a$ as the reference station then:

$$\frac{d(Rv_l)}{dn} = \left[\frac{d(Rv_l)}{dn}\right]_{ref.} \cdot \left[\frac{\delta n_{ref.}}{\delta n}\right]$$

$$\frac{dp_T}{dn} = \left[\frac{dp_T}{dn}\right]_{ref.} \cdot \left[\frac{\delta n_{ref.}}{\delta n}\right]$$

The function N(n) could then be represented by:

$$N = \left[\frac{[Rv_l]_{ref.}}{R}\left[\frac{d(Rv_l)}{dn}\right]_{ref.} - \frac{1}{\rho}\left[\frac{dp_T}{dn}\right]_{ref.}\right] \cdot \left[\frac{\delta n_{ref.}}{\delta n}\right] \quad -(3\text{-}12)$$

The terms in equation (3-12) have the dimensions of acceleration which is also dimensionally equal to a 'specific energy gradient' (J/kgm). The terms can be thought of as constituting the specific energy change between stream surfaces due to fluid rotationality and total pressure gradients. Because of the inviscid nature of the initial equations, energy cannot diffuse through the fluid nor can it be dissipated. Hence whilst the energy gradients in equation (3-12) can change,

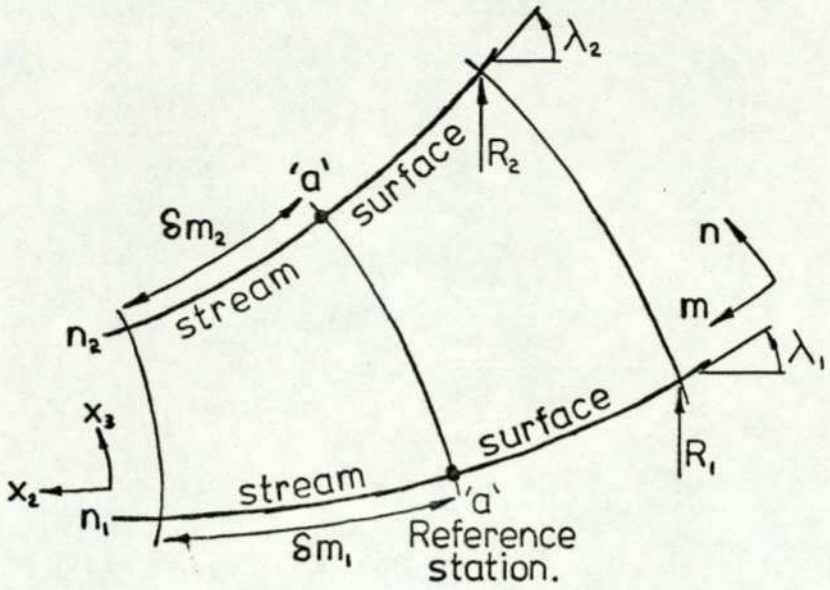

Fig. 3-19(a) Meridian section

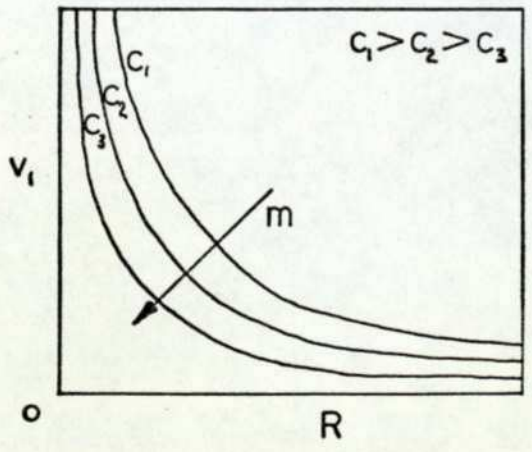

Fig. 3-19(b) Free vortex decay

Figure 3-19

the integral between any two stream surfaces must remain a constant. There is some difficulty in defining the function N(n) at the inner boundary where n = 0, since the term $\left(\delta n_{ref.}/\delta n\right)$ becomes indeterminate. For practical purposes this problem was resolved by obtaining the values of N(n) at other stream surfaces and then using the constancy of the integration between the stream surfaces to obtain the inner boundary value.

A computer programme was written to solve equation (3-11) for the two nozzle geometries mentioned in section (3-3-1) and illustrated in Figure 3-6. The swirling flow reference station values used were obtained from the mixing region analysis given in section (3-4-3). Two swirling flow conditions were specified for the reference station, irrotational flow (Rv_t = constant) and constant swirl velocity (v_t = constant).

For irrotational flow the reference station value of $\left(dp_T/dn\right)$ is:

$$\left[\frac{dp_T}{dn}\right]_{ref.} = \frac{d}{dn}\left[p + \frac{\rho}{2}\left(v_2^2 + v_t^2\right)\right]_{ref.} = -\frac{\rho c^2}{R^3}$$

$$\left[\frac{d(Rv_t)}{dn}\right]_{ref.} = 0 \quad ;$$

and for rotational flow where v_t = constant:

$$\left[\frac{dp_T}{dn}\right]_{ref.} = 0$$

$$\left[\frac{d(Rv_t)}{dn}\right]_{ref.} = \frac{d(KR)_{ref.}}{dn} = K \quad ;$$

since at the reference station dn ≡ dR .

Stations 1 m m. apart were specified along the nozzle inner boundary and a series of stream surfaces within the nozzle were assumed. The constancy of mass flow between any two stream surfaces was used to adjust the stream surface geometry until the velocity profile obtained from equation (3-11) and the stream surface geometry solutions converged. Figure 3-20 shows the programme flowchart. The numerical methods used within the computer programme were:

(a) The method of false position (regula falsi) to converge on the inner boundary stream velocity.

(b) Gausse-Laguerre interpolation and numerical integration to obtain the double integral and hence the stream velocity profile and also the flowrate between the stream surfaces. This method was used since the stream surfaces could be unequally spaced, thus giving function values at irregular intervals. This method of integration is very accurate but can only be used with confidence when the function values have a high degree of accuracy. Since all the reference station parameters, and all the downstream stations, were obtained from mathematical functions the necessary degree of accuracy could be maintained.

3-4-5 Nozzle Fluid Flow with Angular Momentum Flux Decay

Since the operation of the proposed vortex device depended upon the angular momentum flux of the fluid the only shear stresses considered were those opposing the swirling flow. This decision followed a number of other authors (Royle and Hasson (1967); Bichara and Orner (1969);

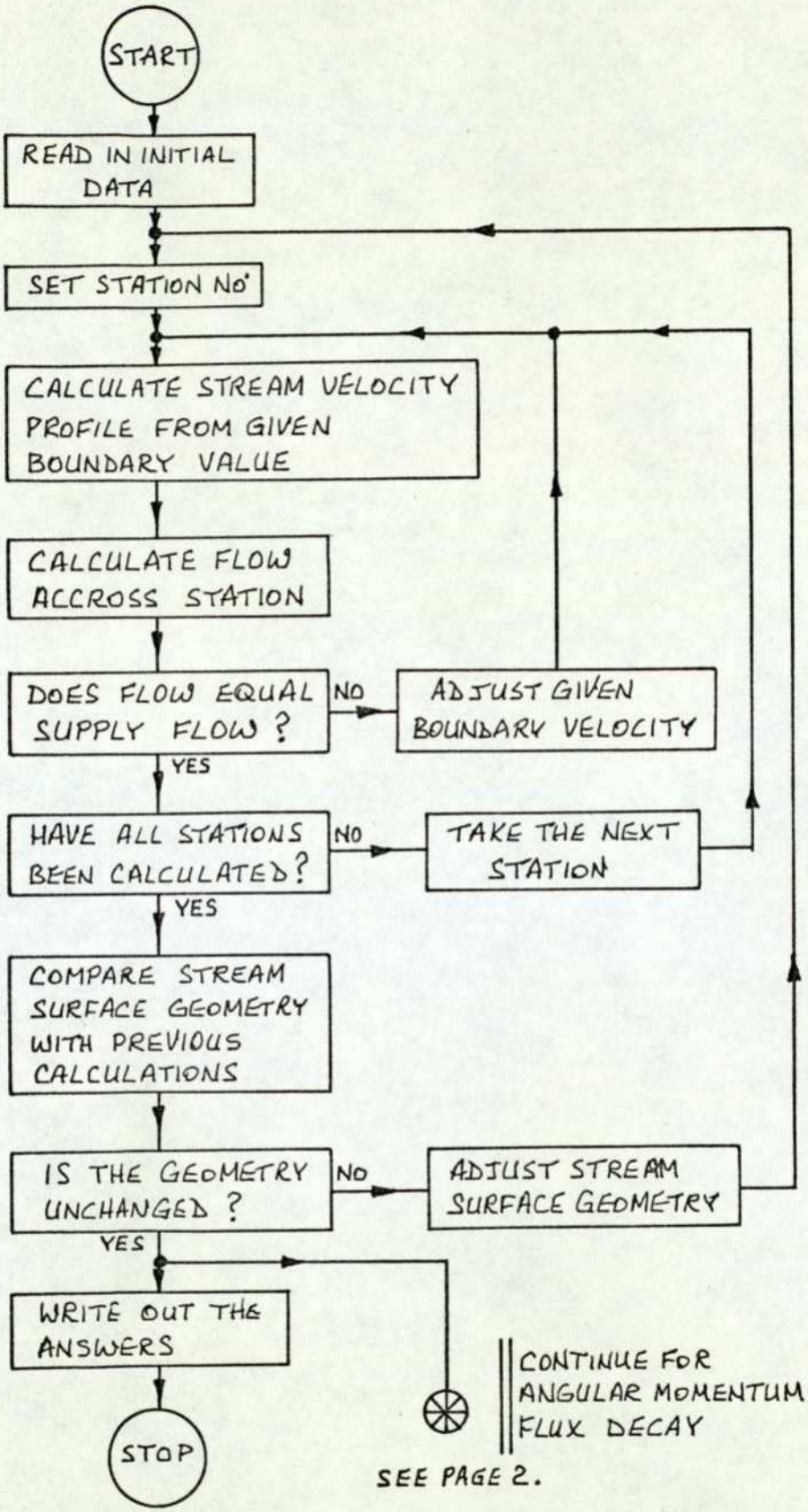

Figure 3-20, page 1

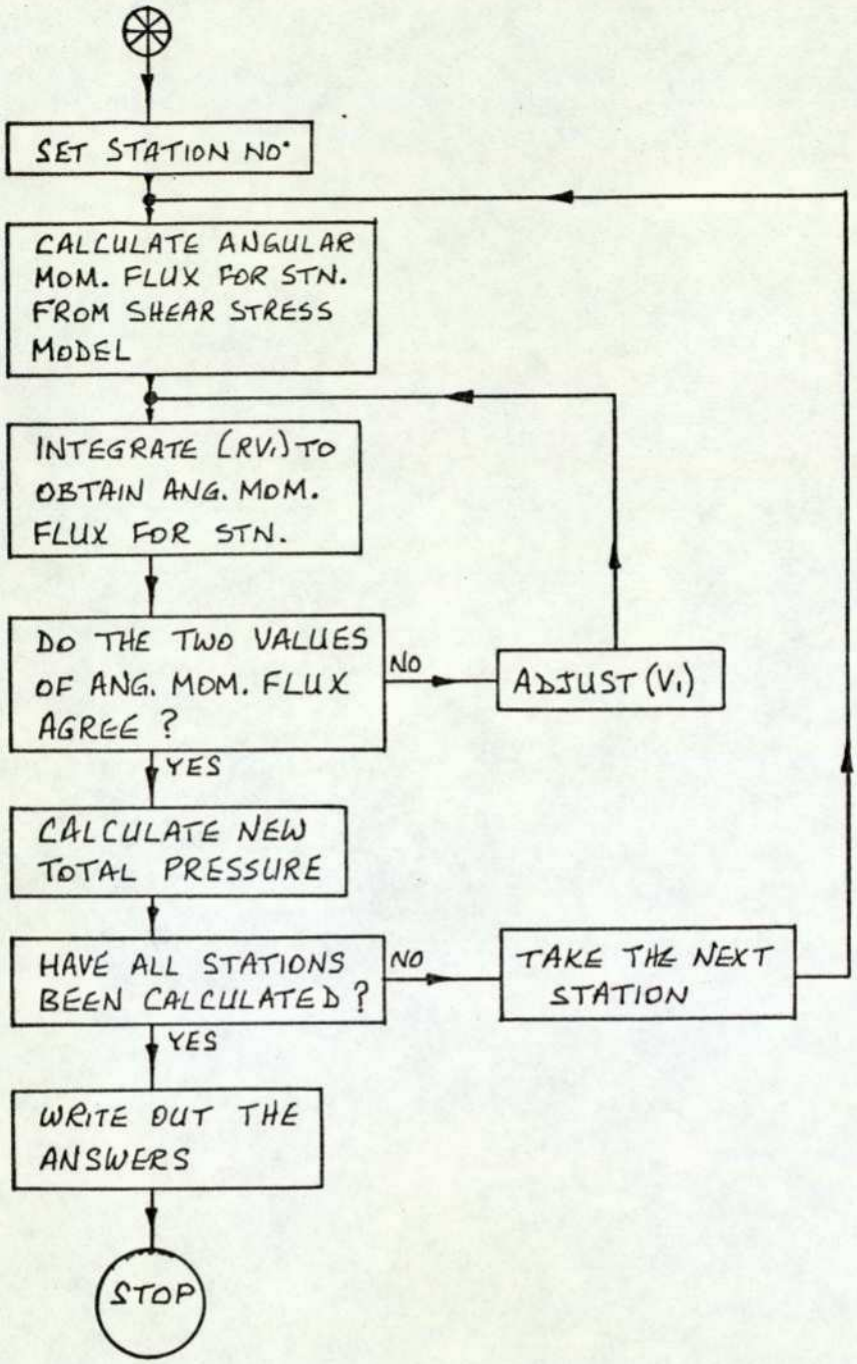

Computer algorithm for swirling flow.

Figure 3-20, page 2

Al-Shamma (1971)). Examination of the laminar flow stream surface equations given in Appendix 7 indicated that tangential shear stress terms occurred in only one equation. Rewriting the 'total pressure' equations:

$$\frac{v_2}{R}.\frac{\partial(Rv_1)}{\partial m} = \left[\theta \text{ direction shear stress terms}\right]$$

$$\frac{1}{\rho}.\frac{\partial p_r}{\partial m} = \frac{v_1}{R}.\frac{\partial(Rv_1)}{\partial m}$$

$$\frac{1}{\rho}.\frac{\partial p_r}{\partial n} = \frac{v_1}{R}.\frac{\partial(Rv_1)}{\partial n} + v_2\left(\frac{\partial v_2}{\partial n} + v_2 k_m\right)$$

The solution of the inviscid total pressure equations given in section (3-4-4) gave a series of stream surfaces with a specified geometry together with the stream and swirl velocities and pressure. If now a one-dimensional angular momentum flux decay were imposed upon the two-dimensional inviscid solution then, providing equation (3-10) remained unaltered, the stream surfaces would remain unaltered and could be used directly to provide an improved solution.

Consider, initially, swirling flow within a straight cylindrical pipe. The angular momentum flux about the pipe axis for fluid crossing any normal section of the pipe is:

$$\dot{H} = 2\pi\rho\int_0^{r_w} v_\theta v_r r^2\, dr$$

Newton's law applied between stations (1) and (2) gives:

$$\sum M_{1\text{-}2} = \Delta\dot{H}_{1\text{-}2}$$

Between two arbitrary stations a distance of 'dz' apart:

$$dM = -\left[\begin{array}{l}\text{wall shear stress} \\ \text{in the } \theta \text{ direction}\end{array}\right] \times \left[\begin{array}{l}\text{surface} \\ \text{area}\end{array}\right] \times \left[\begin{array}{l}\text{moment} \\ \text{arm}\end{array}\right]$$

$$= -\tau_{r\theta(w)} (2\pi r_w^2)\, dz$$

Therefore:

$$\frac{dM}{dz} = \frac{dH}{dz} = -(2\pi r_w^2)\, \tau_{r\theta(w)}$$

If now the wall shear stress $\tau_{r\theta(w)}$ is modelled by the equation:

$$\tau_{r\theta(w)} = f \rho \frac{V_{IM}^2}{2} \quad , \quad \text{then:}$$

$$\frac{d\dot{H}}{dz} = -(2\pi r_w^2) f \rho \frac{V_{IM}^2}{2} \quad , \quad \text{where the suffix 'M'}$$

denotes a mean value for the station.

Applying a similar analysis to the nozzle as that given for the swirling straight pipe flow, then examination of Figure 3-19 (a) shows that two elemental surfaces are involved. It can also be seen that the radius and the length of the coordinate increment 'δm' vary with 'n'.

Since, however, a one-dimensional decay pattern has been specified, then variations with 'n' will be ignored and a mean value for 'R' and 'δm' will be used. For this reason the analysis is approximate only, however the approximation was expected to be close. For clarity it should also be stated that since:

$$R_{(n)} = R_{(n_i)} + \int_{n_i}^{n} \cos\lambda \, dn \quad , \quad \text{then } \lambda \text{ will be}$$

assumed constant across the section (i.e. no curvature of the 'n' characteristics). Graphs of the stream surfaces show that the 'n' ordinate curvature is indeed small; a contributary factor being that the flow passage has an equal meridional depth.

Let the wall shear stress be denoted by:

$$\tau_{31(w)} = f\rho\frac{V_{1M}^2}{2} \qquad -(3\text{-}13)$$

Then:
$$\frac{d\dot{H}}{dm} = -2\pi\rho f R_M^2 V_{1M}^2 \qquad -(3\text{-}14)$$

Where:
$$\dot{H} = 2\pi\rho\int_{n_i}^{n_o} V_1 V_2 R^2\, dn \ ,$$

$$R_M = \frac{1}{2}(R_{n_o} + R_{n_i}) \ ,$$

$$V_{1M} = \frac{1}{(n_o - n_i)}\int_{n_i}^{n_o} V_1\, dn \ .$$

For any two stations δm apart, then:

$$\dot{H}_2 = \dot{H}_1 + \left(\frac{d\dot{H}}{dm}\right)_1 . \ \delta m \ ,$$

$$p_{T_2} = p_{T_1} + \left(\frac{\partial p_T}{\partial m}\right)_1 . \ \delta m \ ,$$

where:

$$\left(\frac{\partial p_T}{\partial m}\right)_I \triangleq \rho\left(\frac{V_{IM}}{R_M}\right)_I \left(\frac{\partial (RV_I)}{\partial m}\right)_I \quad , \quad \text{and}$$

$$\left(\frac{\partial (RV_I)}{\partial m}\right)_I \triangleq \frac{\delta (RV_I)}{\delta m}$$

For the inviscid stream surfaces to be valid every term in equation (3-11) must remain the same, therefore $\left(\partial p_T / \partial n\right)$ must remain a constant, as must $\left(V_I / R \cdot \partial (RV_I) / \partial n\right)$. However, since the circulation about the nozzle axis is now a function of 'm' then the application will be restricted to free vortex flows (i.e. $\partial (RV_I) / \partial n = 0$). Figure 3-19 (b) illustrates the angular momentum flux decay pattern. Note also that the partial derivative notation has been given for the gradients of total pressure and circulation since strictly they are now functions of the variables 'm' and 'n' even though the decay pattern imposed is one-dimensional.

A further point worth noting was that whilst the decay pattern imposed resulted in energy dissipation it did not include energy diffusion.

A section was added to the previous computer programme to impose a one-dimensional angular momentum flux decay upon the two-dimensional inviscid solution, (see Figure 3-20).

The calculation procedure was as follows:

(i) Obtain the two-dimensional inviscid solution

for the stream surface geometry, fluid pressure and orthogonal velocities.

(ii) Calculate the angular momentum flux and its gradient, the mean radius and the mean swirl velocity at the reference station.

(iii) Calculate the required angular momentum flux crossing the next station.

(iv) Adjust V_t at the next station until the angular momentum flux is correct.

(v) Calculate the total pressure gradient and then the new total pressure at the next station.

(vi) Repeat the process until all stations have been calculated.

A comparison between the various theoretical models and between the predicted and experimental results is given in section 3-5.

3-5 Discussion of the Swirling Flow Results

3-5-1 Comparison between Theory and Experiment

Streaming Flow - Pressure Distribution

The predicted static pressure distribution along the outer nozzle boundary under various streaming flow conditions, for both device configurations, are shown in Figures 3-21 and 3-22. The rapid acceleration imposed upon the fluid by the high values of stream surface curvature near the orifice of geometry No.1, (see Figure 3-21) are made manifest by the large pressure drop over the last six stations.

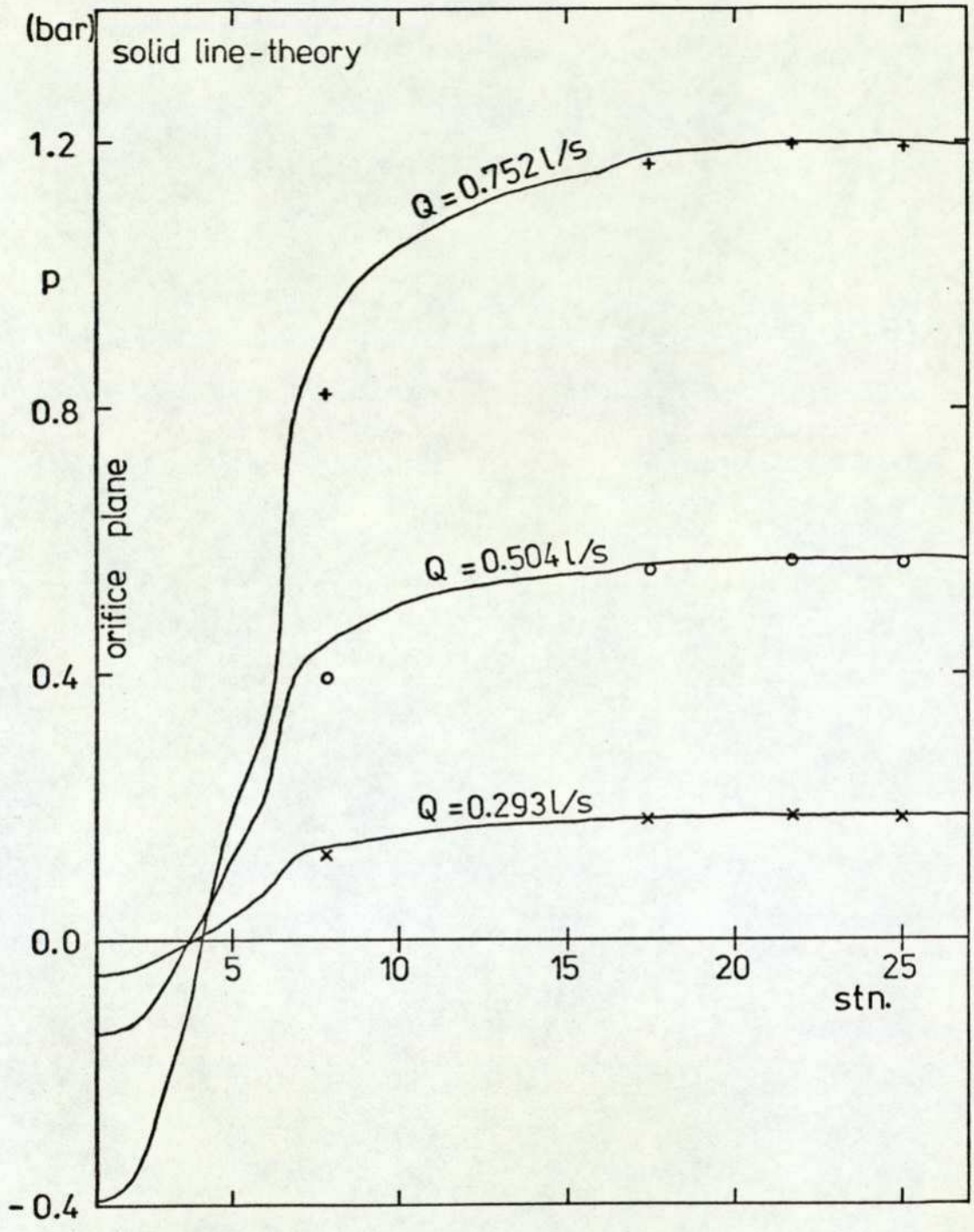

Stream Flow - geometry No. 1

Figure 3 - 21

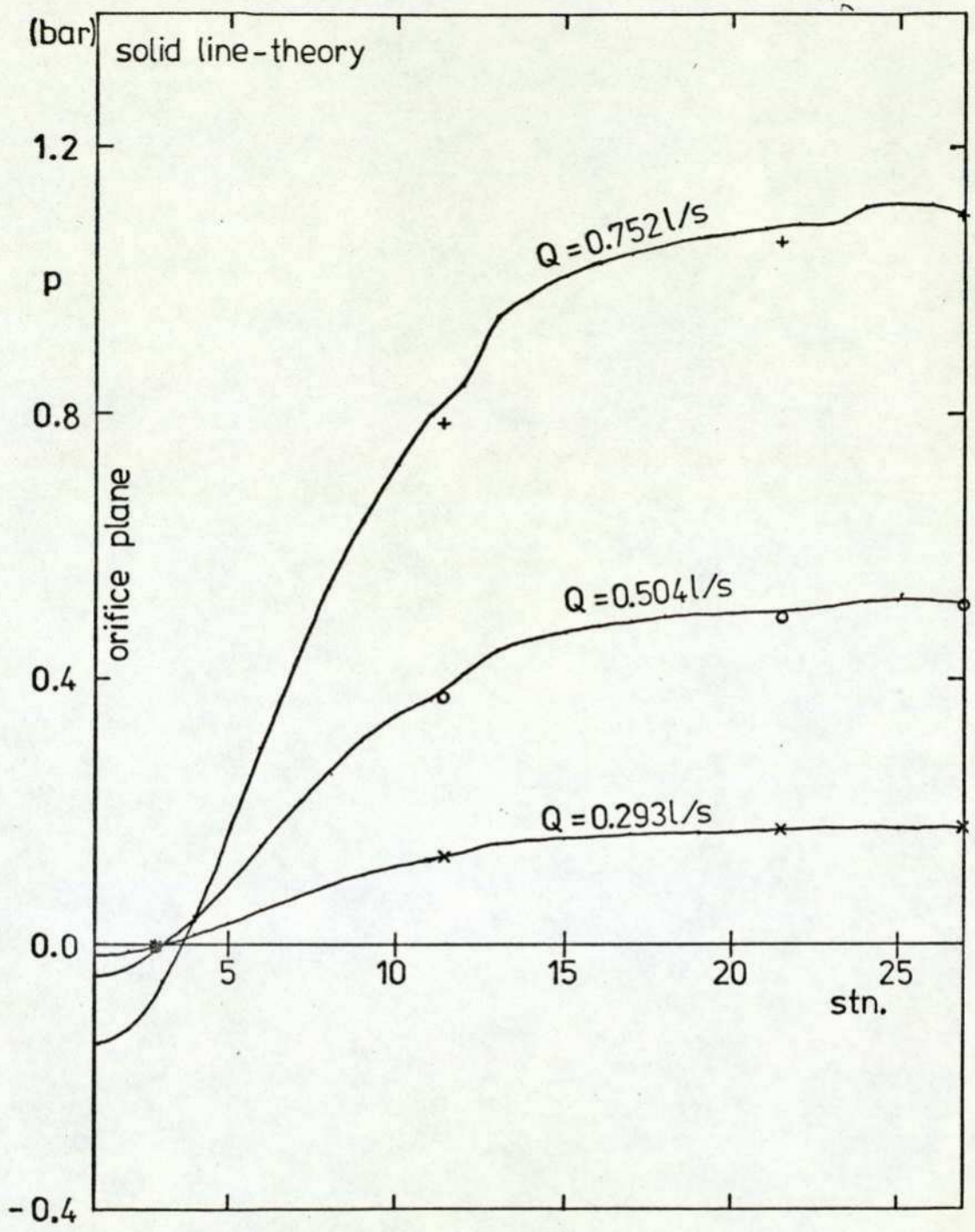

Stream Flow - geometry No. 2

Figure 3-22

Also noted was the predicted separation from the outer boundary illustrated by the negative pressures within the last three stations; no separation was noticed during testing. The experimental points obtained lie, encouragingly, within the predicted line and, after allowing for measurement inaccuracies, presumably indicate a loss of total pressure. The configuration of geometry No.2 led to a much more gradual pressure drop than occurred with device geometry No.1 and smaller negative pressures were predicted close to the orifice (again within the last three stations). The measurement point close to the orifice plane on geometry No.2 recorded small negative pressures and it was thought that a small degree of separation was occurring, although possibly not to the extent indicated by the theory. The theoretical and experimental points agree fairly well where experimental results are available for comparison.

Streaming Flow - Orifice Velocity Profile

The nozzle orifice plane stream flow velocity profiles for both geometries are shown in Figure 3-23. Unfortunately the experimental measurements taken with a hypodermic total head tube could not be made closer than 3 m m. downstream from the orifice. The shear stress relaxation effect on the liquid leaving the nozzle results in the jet velocity profile tending toward a constant value. A second error introduced into the experimental results was that the device centre body terminated $3\frac{1}{2}$ m m. within the nozzle rather than at the orifice plane; this resulted in

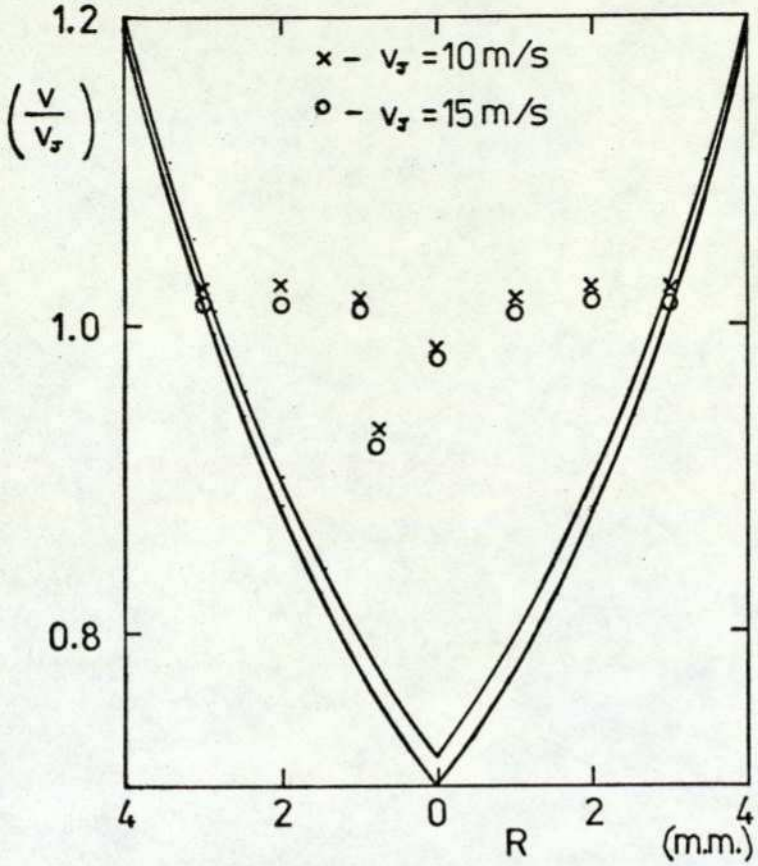

Geometry No. 1

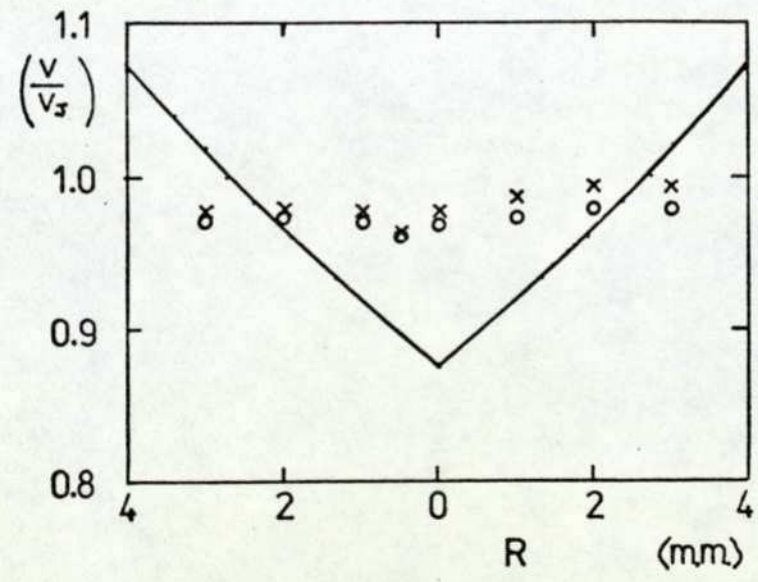

Geometry No. 2

Stream Flow - orifice velocity profile .

Figure 3-23

a further shear stress relaxation effect. The measurements taken confirm the form but not the magnitude of the predicted results. In spite of this the results were thought to be encouraging. As expected geometry No.1 showed a more pronounced cusp than geometry No.2, due to the nozzle curvature, and, since both cusps were displaced from the jet centre line, the results indicated that either the centre body was not central or that the tail of the central body was not cut off square.

Swirling Flow - Device Characteristics

The vortex device characteristics were shown in Figures 3-9 and 3-10. It can be seen that there is very little Reynolds number effect over the velocity range covered by the tests ($71.8 \times 10^3 \leq Re \leq 119.6 \times 10^3$, where $Re = (V_T d_T / \nu)$, $Q_c = 0$). At these high Reynolds numbers it is perhaps not surprising to find little Reynolds number influence; however, as has been mentioned previously, there is no generally accepted manner of specifying Reynolds number for swirling flows. Whilst for similar geometric configurations any specified Reynolds number would suffice for comparison, the actual number obtained may have little significance. The power turn down ratios of device geometries No.1 and No.2 were 2.26 and 2.50 respectively. These values are considerably lower than those obtained by Al-Shamma (1971) and McCloy and Stevenson (1972). The major geometric difference between the device tested and the devices of Al-Shamma and McCloy and Stevenson was the relatively large

annular area. A further slight difference was that the control flow inlet area was larger than the other devices mentioned and that little attention was devoted to the control flow inlet geometry. A direct result of the large annular area was that relatively little advantage was taken of the venturi effect and therefore higher control pressure ratios were required than would otherwise have been the case. An advantage conferred by the chosen geometry was the increased stability of the device since the non-linear term of the control flow characteristic was kept to a low value. Both devices were relatively stable but of the two configurations tested the second geometry gave the least bistability and had a lower pressure drop across the device for any given flow. Also the non-dimensional response of geometry No.2 was expected to be quite good since the flow through the device was almost unchanged until close to the stream flow cutoff point.

Swirling Flow - Pressure Distribution

Figures 3-24 and 3-25 show the predicted pressure distributions along the nozzle outer boundary for various degrees of swirling flow. The figures show that for both geometric configurations the major pressure changes are predicted to occur at the high swirl conditions, (high control pressure ratios). The experimental points show that the large pressure changes predicted did not occur in practice, although the largest pressure changes did

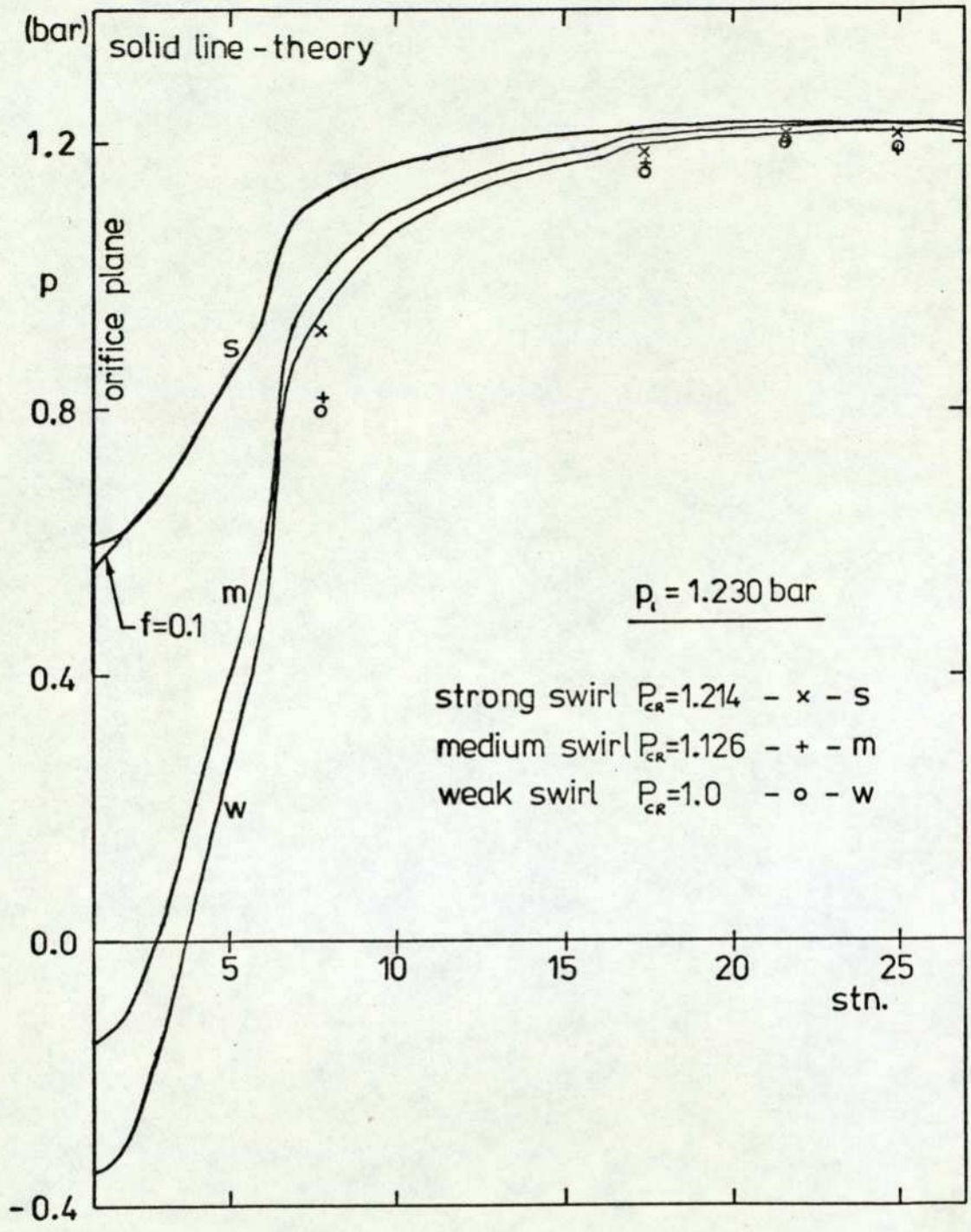

Swirling Flow - geometry No 1

Figure 3 - 24

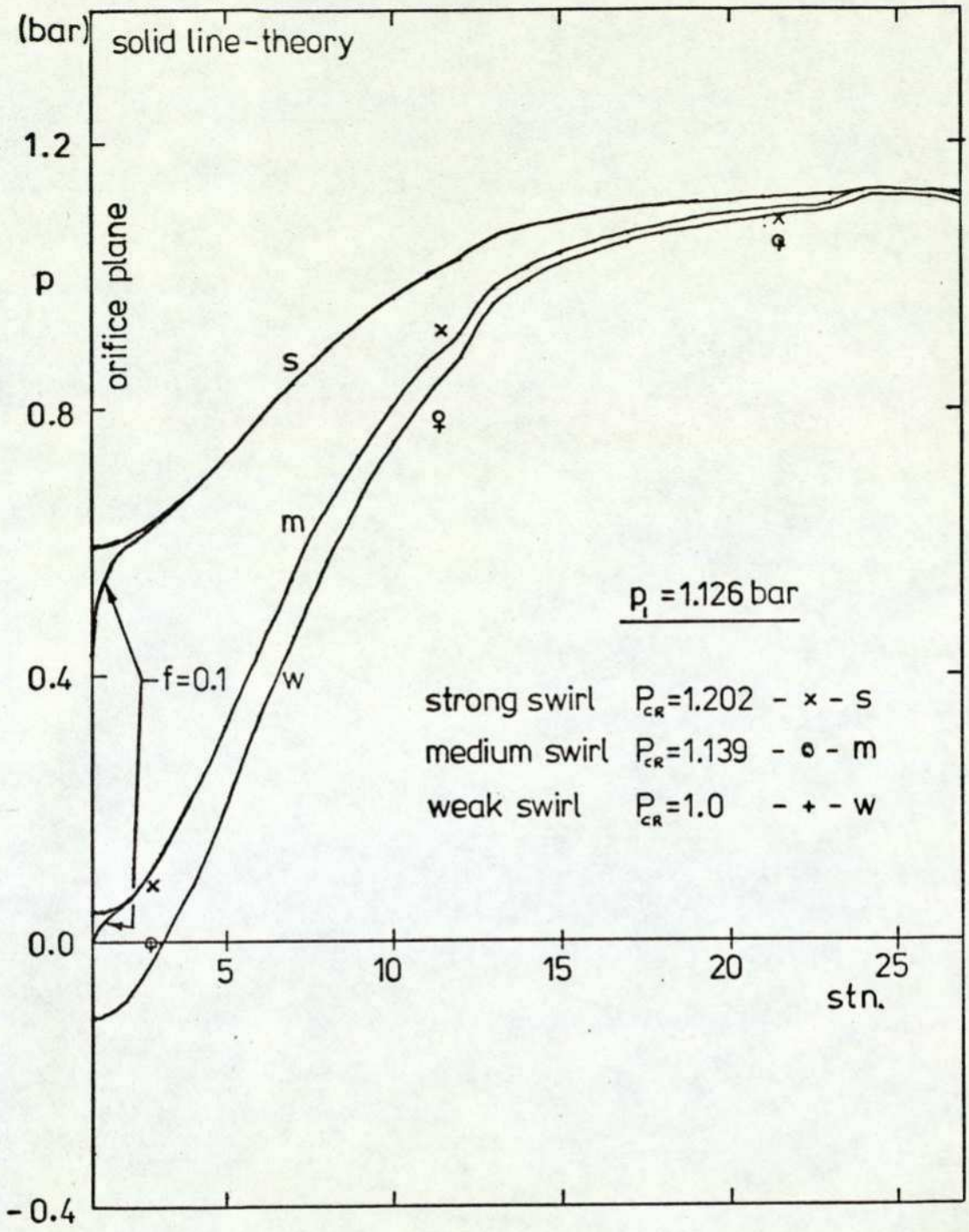

Swirling Flow - geometry No. 2

Figure 3-25

occur with high swirling flow values. The graphs also show that with a tangential shear stress model incorporated into the theory the effect on the pressure distribution was confined to a region close to the nozzle orifice; even then the effects were only noticeable at the higher swirling flow values. Geometry No.2 can be seen to be slightly more sensitive to the shear stress model. The experimental points lay even further inside the predicted lines than in the streaming flow graphs. For streaming flow it was thought that a loss of total pressure could contribute toward the error between theory and experiment. With swirling flow the cause could be due to either a loss of total pressure, greater than that calculated to be due to the tangential shear stress, or a swirl velocity distribution different to that assumed for the mixing flow analysis.

Figures 3-26 to 3-29 illustrate the changes in pressure at specific points within the nozzle with changes in the control pressure ratio (changes in the degree of swirling flow). These figures apply to geometry No.2 only and two sets of experimental points have been plotted for different static pressures at the stream flow entry to the device. It was thought that this would help to distinguish a general trend from an erroneous experimental reading. The two sets of experimental results compare well and indicate that a consistent flow pattern was experienced within the nozzle. The theoretical graph for measuring point three

(Figure 3-26) shows that as the stream flow through the supply annulus decreased the static pressure rose. This rise was more pronounced as the stream flow cutoff point was reached. This latter effect was due to the control flow characteristic mentioned previously, (see also section 3-4-2, Figure 3-15 and in particular the non-linear term in equation (3-2)). The addition of a control flow should result in the addition of a radial pressure gradient to the static pressure increase within the annulus due to the attenuated stream flow. The predicted pressures given by the theory for measuring point three were obtained from the reference station values where a zero radial static pressure gradient was assumed. The stream flow pressure values were obtained solely from Bernoulli's equation and it was interesting to note the discrepancy between theory and experiment even for the zero swirl case ($P_{cR} \triangleq 0.975$). Since, at this measurement point and under stream flow conditions, there was no stream surface curvature or swirling flow mixing effects, it was thought that the difference between the predicted and experimental values at this point ($P_{cR} \triangleq 0.975$) could be due to a loss in total pressure. Also, since this loss represented approximately 1½% of the original pressure, it was not thought to be an unreasonable figure. A major discrepancy between the predicted pressure and the experimental points was that the predicted pressure increased with an increase in the control pressure ratio. The experimental points showed, fairly consistently, that at low control pressure ratios (small control flow rates) the

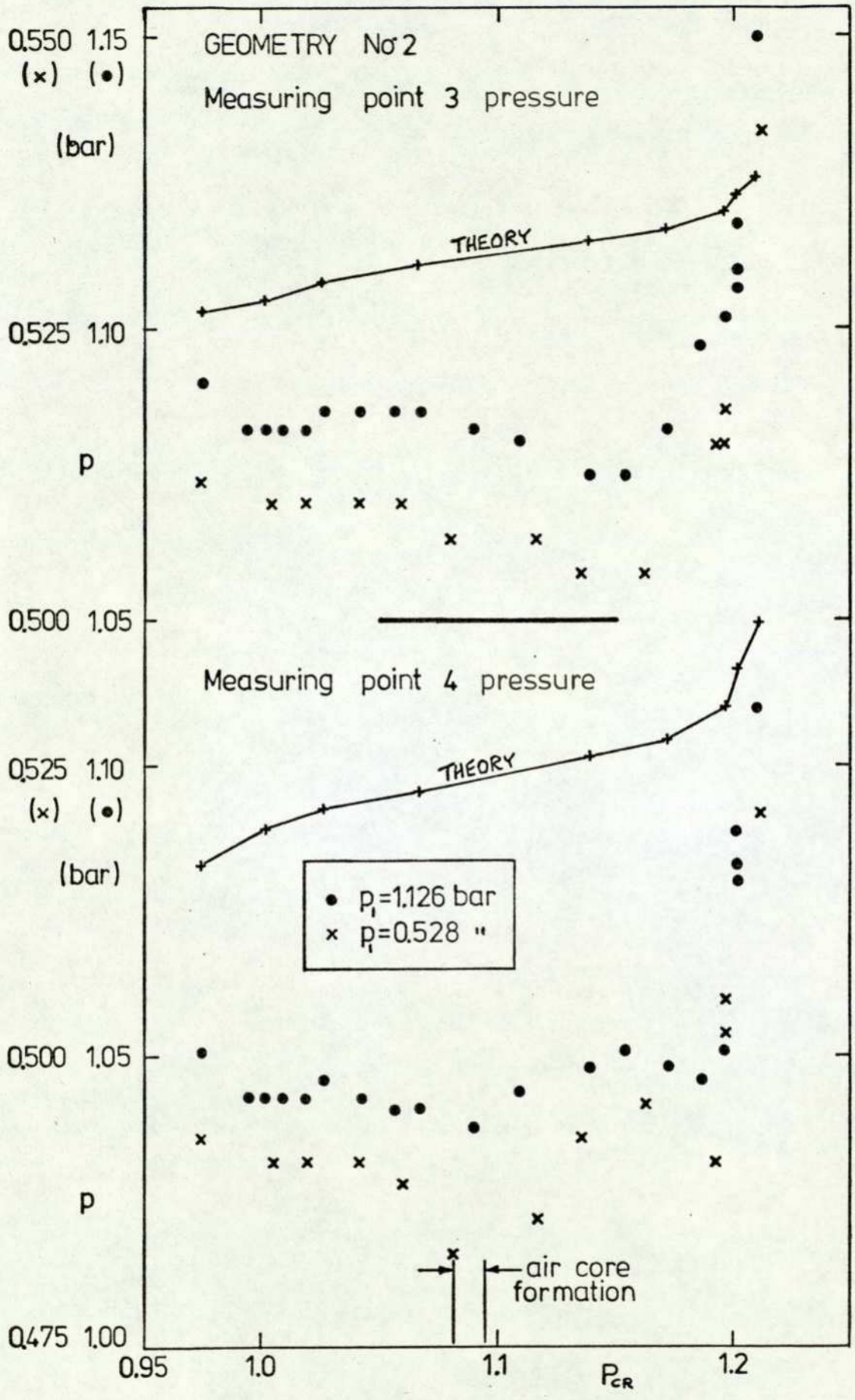
GEOMETRY Nº 2
Measuring point 3 pressure
THEORY
Measuring point 4 pressure
THEORY
• p_1=1.126 bar
× p_1=0.528 "
air core formation
0.550 1.15
(×) (•)
(bar)
0.525 1.10
p
0.500 1.05
0.525 1.10
(×) (•)
(bar)
0.500 1.05
p
0.475 1.00
0.95
1.0
1.1
1.2
P_{cR}

Figure 3 - 26

pressure at measuring points three, four and five, initially dropped below the stream flow value and then remained approximately constant until after an air cone was formed. For measuring point three further increases in the control pressure ratio resulted in a further slight fall in the pressure recorded until, close to the stream flow cutoff point, the pressure rose rapidly, finally exceeding the predicted value. The comparison of theory and experiment was poor from two points of view; the drop in pressure with the introduction of swirling flow and the relatively small pressure rise predicted at the stream flow cutoff point. The fact that the experimental pressure exceeded the predicted value at one point indicated that the swirl velocity distribution within the nozzle was not realised in practice at high control pressure ratios, (simple loss terms could only account for being within the predicted value).

The results from measuring point four were similar to measuring point three both in respect of predicted and experimental pressures (see Figure 3-26). Two differences were that the theory predicted a higher pressure at the cutoff point than was actually attained during the experiments and also that the experimental pressure points indicated a rise in the static pressure from the point of the air core formation. A further minor point was that close to the cutoff point a slight dip in the pressure trace was noticeable ($P_{CR} = 1.19$).

The comparison between theory and experiment for measuring point five was fairly good (see Figure 3-27). The accelerated swirling flow resulted in larger pressure changes being observed for both the theory and experiment. The air core formation was seen to affect the experimental pressure distribution quite markedly. Also it was noticeable that the theory predicted a marked change in the pressure trace at this point. The form of the predicted pressure trace from the air core formation onwards (increasing control pressure ratio) was very similar to the experiment. It was the low swirl (low control pressure ratio) region where the theory and experiments showed a marked disparity.

The comparison between theory and experiment for measuring point six showed a further disparity (see Figure 3-28). Because the theory assumed the nozzle boundary to be a stream surface, negative pressures could be obtained rather than flow separation from the boundary. If an error term had been taken from the calculated negative pressures then a new stream surface could have been calculated which would be separated from the nozzle boundary and along which the pressure would be zero. The experimental pressure points indicated that separation may have occurred up to the point of the air core formation. After the air core formation very little pressure rise was noticeable until close to the cutoff point when a rapid rise in pressure was noted. The theoretical rise in pressure

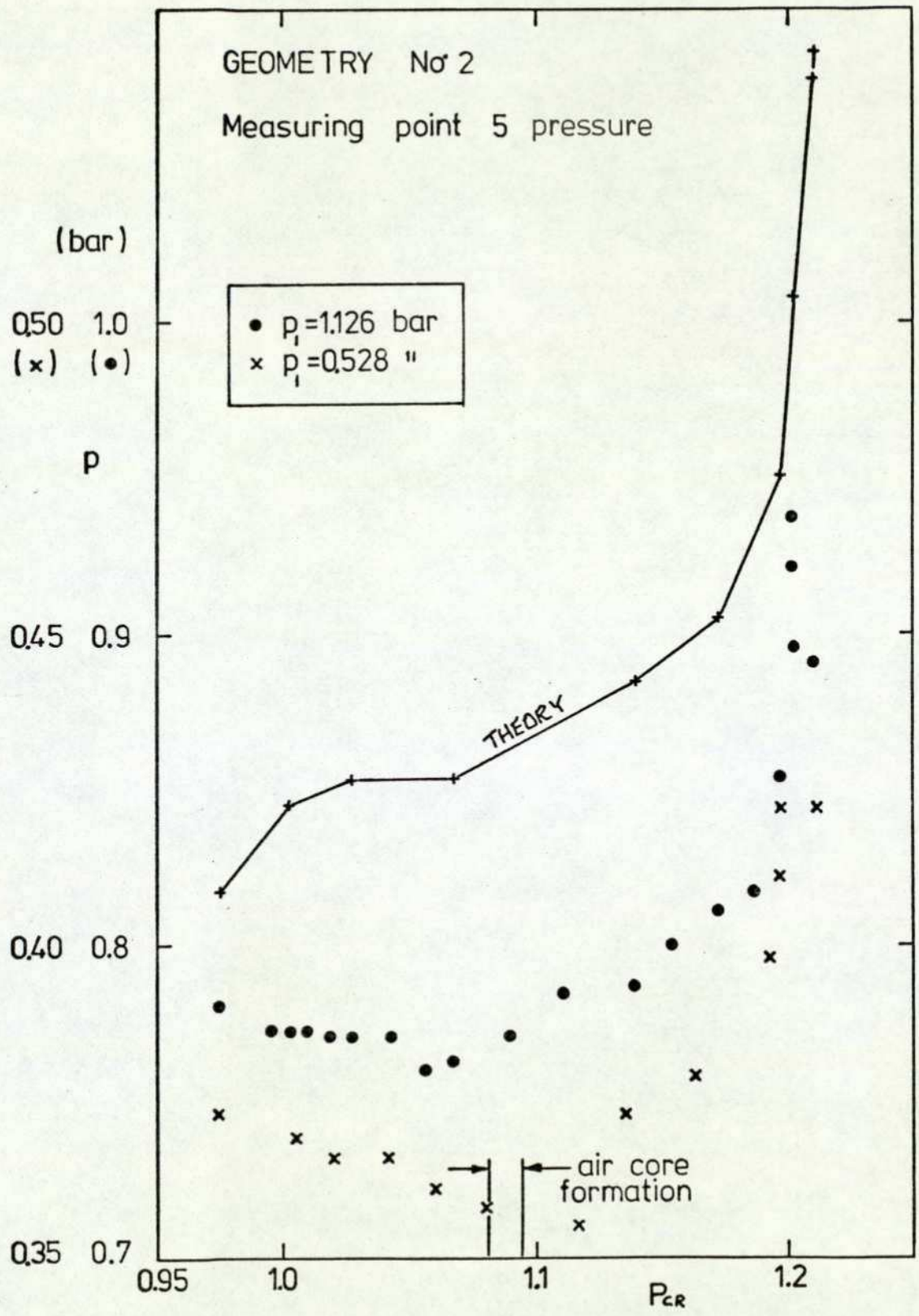
GEOMETRY No 2
Measuring point 5 pressure
(bar)
0.50 1.0
(×) (•)
p
0.45 0.9
0.40 0.8
0.35 0.7
• p_1=1.126 bar
× p_1=0.528 "
THEORY
air core formation
0.95
1.0
1.1
1.2
P_{cR}

Figure 3 - 27

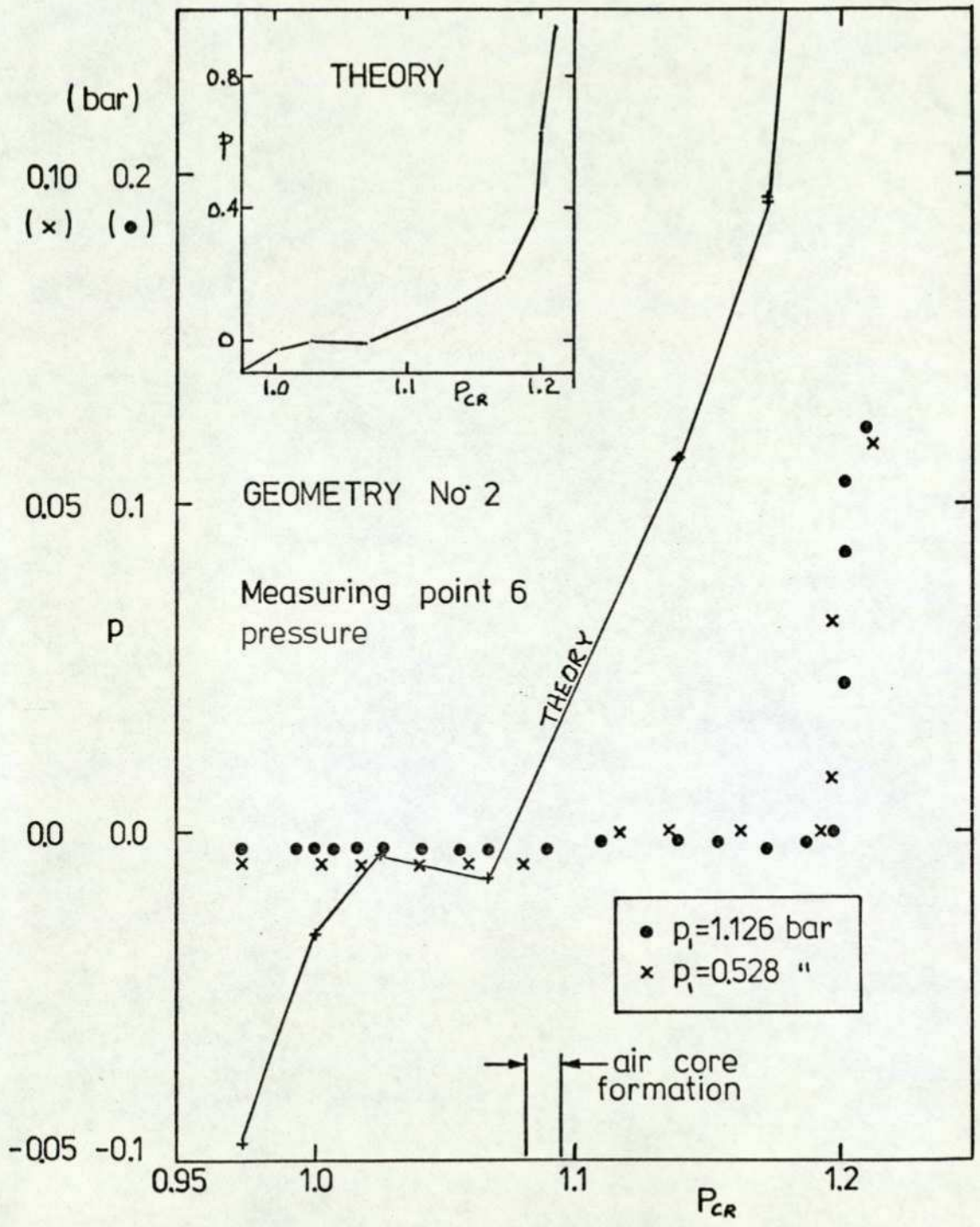

Station pressure against control pressure ratio

Figure 3 - 28

was much greater than that experienced in practice. A possible explanation for this lies not only with the tangential velocity distribution but also with the stream surface assumptions, mentioned previously, and the shear stress models, discussed later.

The predicted pressure distribution for measuring point seven was the only point where the various modifications to the theory showed any significant variations, (see Figure 3-29). The experimental pressures must be viewed with some caution since the pressure tapping was not normal to the flow stream. Any error due to this factor should have resulted in a lower than true reading. Also the error should have been fairly constant since the flow remained above 95% of its streaming flow value until after the formation of the air core. The zero swirl flow resulted in a positive pressure at the centre of the jet due to the stream curvature. The introduction of swirling flow resulted in a rapidly decreasing pressure in the centre of the jet. Apparently a slight negative pressure was experienced and it was into this region that, during the air core formation, the air was then drawn. The introduction of the air core resulted in a venting of the low pressure region and the pressure rose to approximately atmospheric pressure. The experimental pressures recorded appeared reasonable (negative guage pressures of less than 0.1 bar) and the results were thought to be reasonable. With streaming

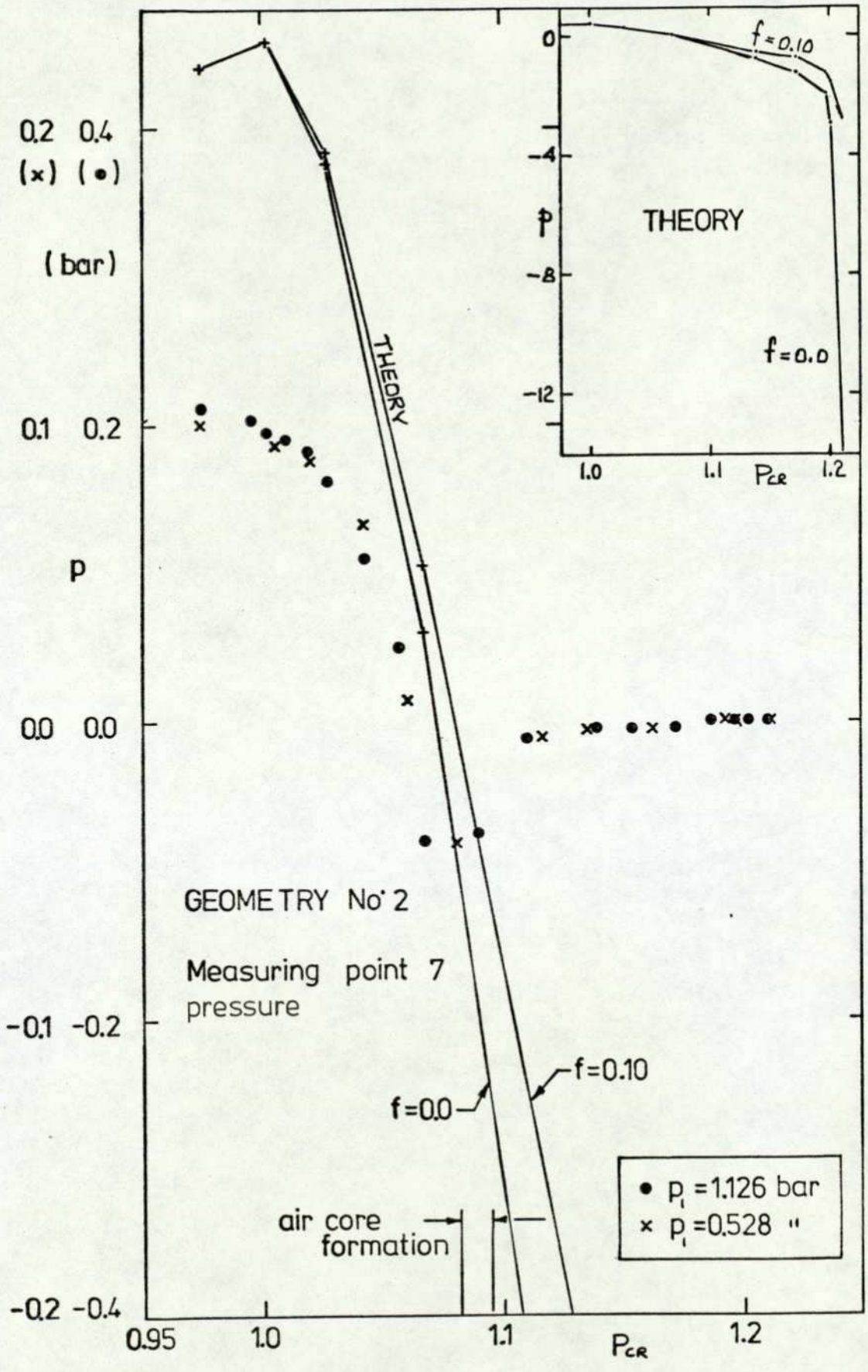
0.2 0.4
(x) (•)
(bar)
0.1 0.2
p
0.0 0.0
-0.1 -0.2
-0.2 -0.4
0.95
1.0
1.1
1.2
P_{CR}
THEORY
GEOMETRY No° 2
Measuring point 7
pressure
f=0.10
f=0.0
air core formation
• p_1 =1.126 bar
× p_1 =0.528 "
0
-4
-8
-12
p
THEORY
f=0.10
f=0.0
1.0
1.1
P_{CR}
1.2

Figure 3 - 29

flow the theory predicted higher pressures than were attained. Since only the tangential shear stress was modelled no loss terms were introduced for streaming flows, moreover, the different tangential velocity distributions did not affect the stream surface results to any significant extent. The theory did,however, predict the air core formation point fairly accurately, as it did with the previous two measuring points. Also it can be seen that close to the nozzle orifice, and in particular the centre of the jet where the tangential velocities were high, was the only region to show a noticeable difference between the various versions of the theory. Unfortunately the theory predicts very large pressure changes which are not realised but this again is due to the fixed boundary stream surface assumption.

Figures 3-30 to 3-32 illustrate the experimental readings for element geometry No.1. The results were very similar to geometry No.2, bearing in mind the different measurement points (see Figure 3-7), with one notable exception, measurement point seven (see Figure 3-32). When the air core was observed to form at the nozzle orifice of geometry No.1, it was noticeable that the pressure at the 'tail' of the centre body (measuring point seven), was significantly above atmospheric pressure. The large pressure gradient over the last six stations could result in the air core being unable to advance up the nozzle

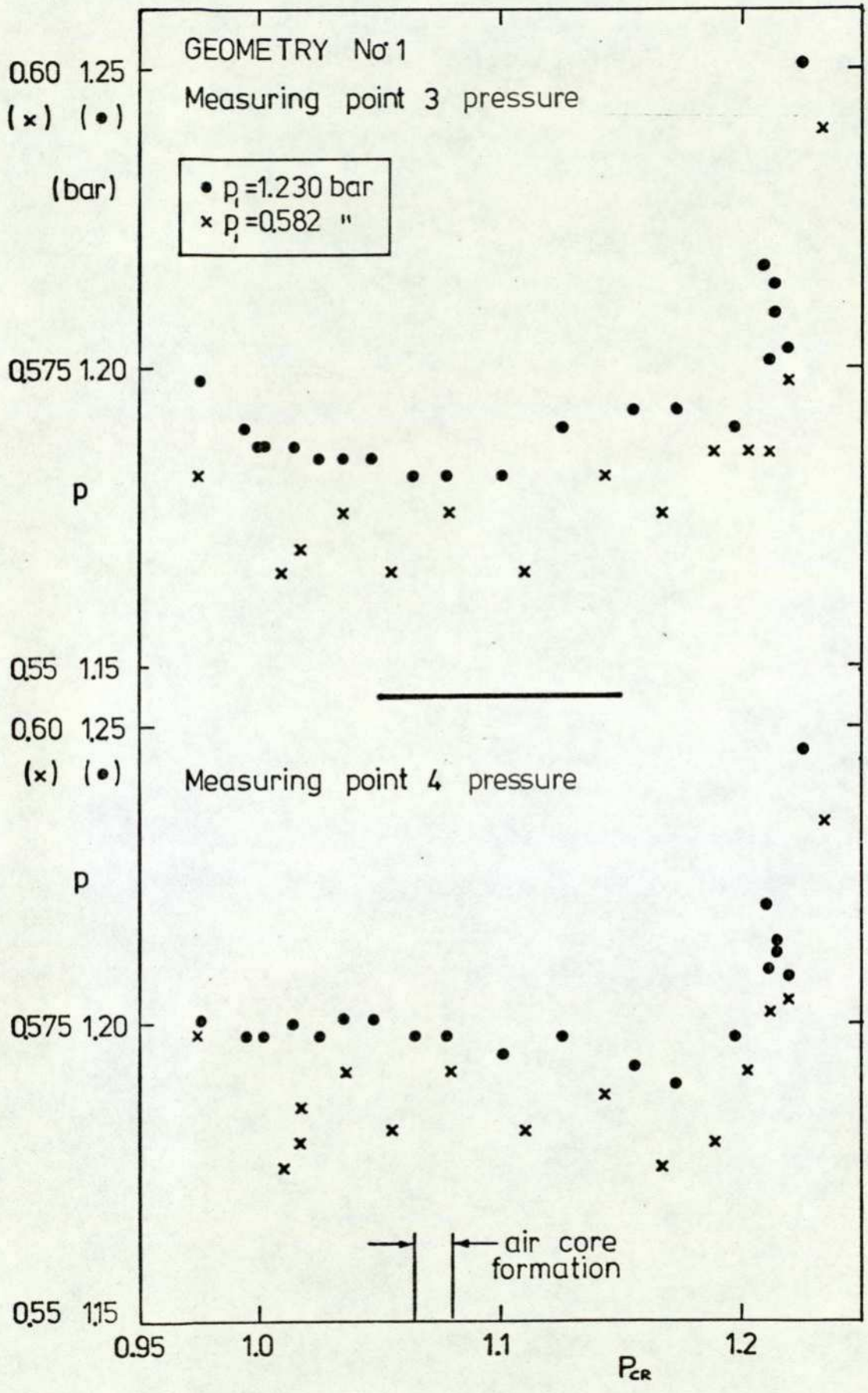
GEOMETRY No 1
Measuring point 3 pressure
• p_i =1.230 bar
× p_i =0.582 "
0.60 1.25
(×) (•)
(bar)
0.575 1.20
p
0.55 1.15
0.60 1.25
(×) (•)
Measuring point 4 pressure
p
0.575 1.20
air core formation
0.55 1.15
0.95
1.0
1.1
1.2
P_{CR}

Figure 3 - 30

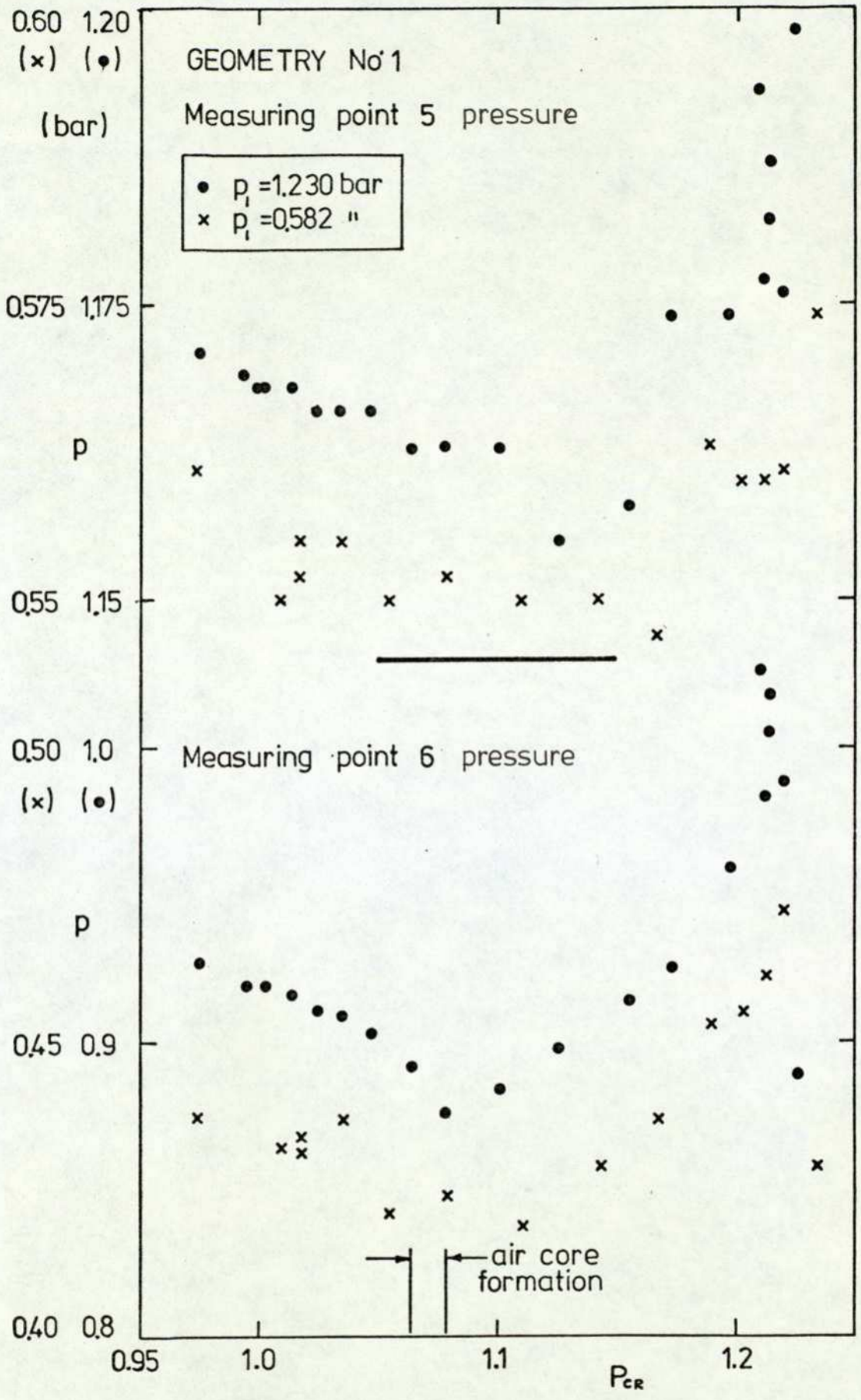
0.60 1.20
(×) (•)
(bar)
GEOMETRY No 1
Measuring point 5 pressure
• p_1 =1.230 bar
× p_1 =0.582 "
0.575 1.175
p
0.55 1.15
0.50 1.0
Measuring point 6 pressure
(×) (•)
p
0.45 0.9
air core
formation
0.40 0.8
0.95
1.0
1.1
1.2
P_{CR}

Figure 3-31

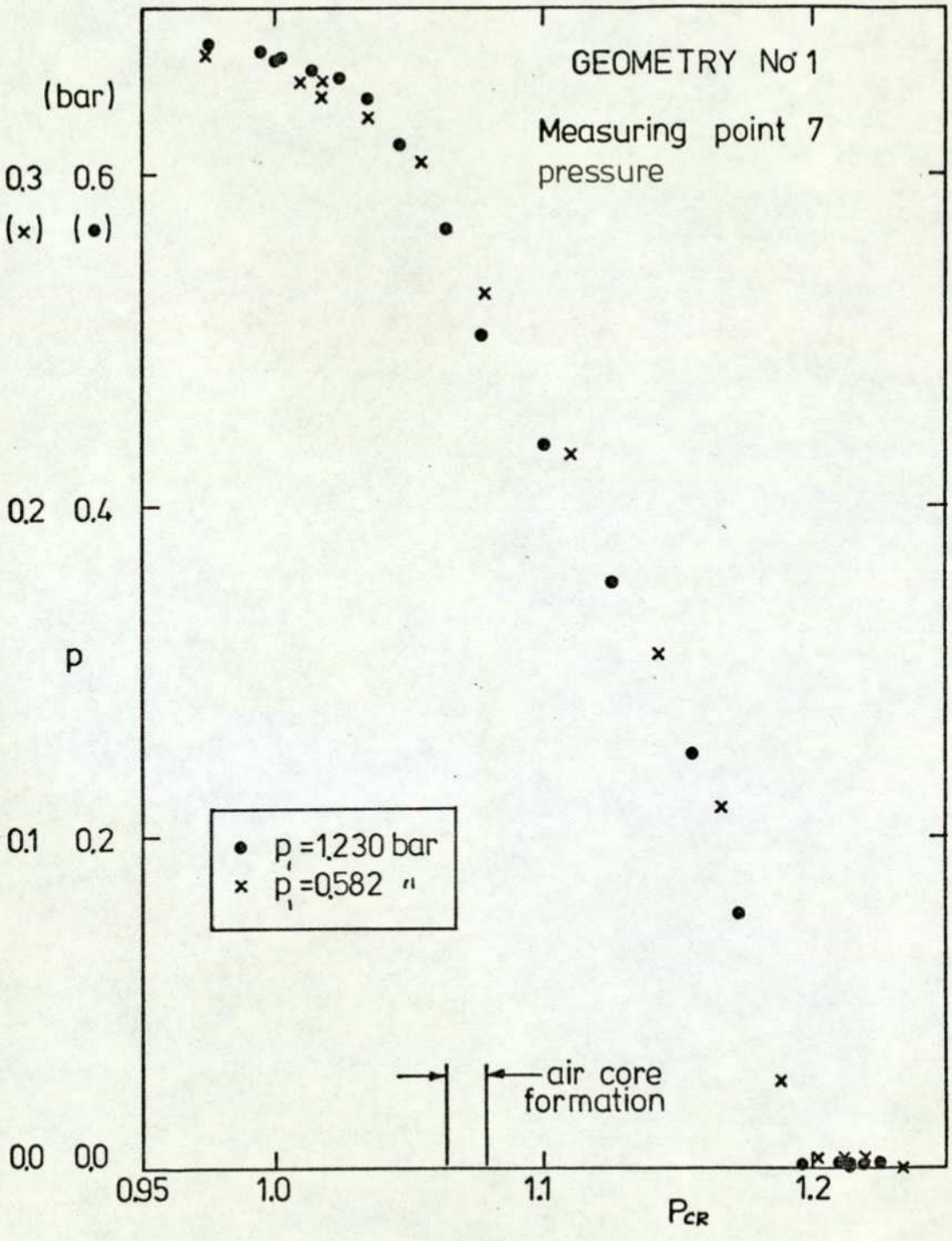

Station pressure against control pressure ratio

Figure 3-32

and attach to the centre body. This would make the air core and hence the entire device, more unstable about this operating point than geometry No.2 . With further increases in the control pressure ratio the pressure fell, until close to the cutoff point when atmospheric pressure was recorded. No negative pressures were recorded. It was postulated that negative pressures could only exist close to the nozzle orifice before a stable air core had formed. Once a stable air core had formed then the low pressure region could be vented immediately.

Swirling Flow - Orifice Plane Velocity Ratio

In section 3-3-2 it was mentioned that a thread was introduced into the liquid stream in an attempt to measure the velocity ratio at the orifice. The thread angle α was assumed to be related to the velocity components by the formula:

$$\alpha = \tan^{-1}\left[V_1/V_2 \right]_{ORIFICE}$$

Since both the stream and swirl velocities were functions of the radial position within the liquid stream an overall ratio for (V_1/V_2) had to be calculated for the orifice plane. This was accomplished indirectly by taking an increment of flow and obtaining the average value for α for the two enclosing stream surfaces. This value was then multiplied by the proportion the incremental flow made to the total flow and then added to values obtained from the other flow increments. The resulting figure was divided by the number of flow increments and hence a single value

of α obtained for the orifice plane. This was expressed mathematically as:

$$\alpha = \frac{1}{N} \sum_{1}^{N} \left[\left(\frac{\delta Q}{Q} \right) . x \right] \quad , \qquad \text{where}$$

$$x = \frac{1}{2} \left[\tan^{-1} \left(V_1 / V_2 \right)_{surface1} + \tan^{-1} \left(V_1 / V_2 \right)_{surface2} \right] .$$

The results of a single experiment are shown in Figure 3-33. The comparison between theory and experiment is fairly good; however, it is noticeable that the predicted values of α appear to be too large at control pressure ratios of between 1.0 and 1.05 and too low between 1.15 and 1.2. The final value predicted for α, at the cutoff point, was too high with the inviscid theory, approximately correct with the tangential shear stress friction coefficient set at 0.01 and too low with the friction coefficient set at 0.10.

The correlation between the measured values of the included angle of the jet (2β) and the velocity ratio at the orifice (α) is shown in Figure 3-34. It can be seen that whereas there is a reasonable correlation between 2β and α, almost invariably the tangential relationship of the orifice velocities underestimates the included jet angle. The rate of increase of the included jet angle was highest before a stable air core was formed, after the air core formation the rate of increase was approximately proportional to the measured orifice velocity ratio angle α.

The appearance of the liquid jet changed markedly with the introduction of swirling flow. With zero control

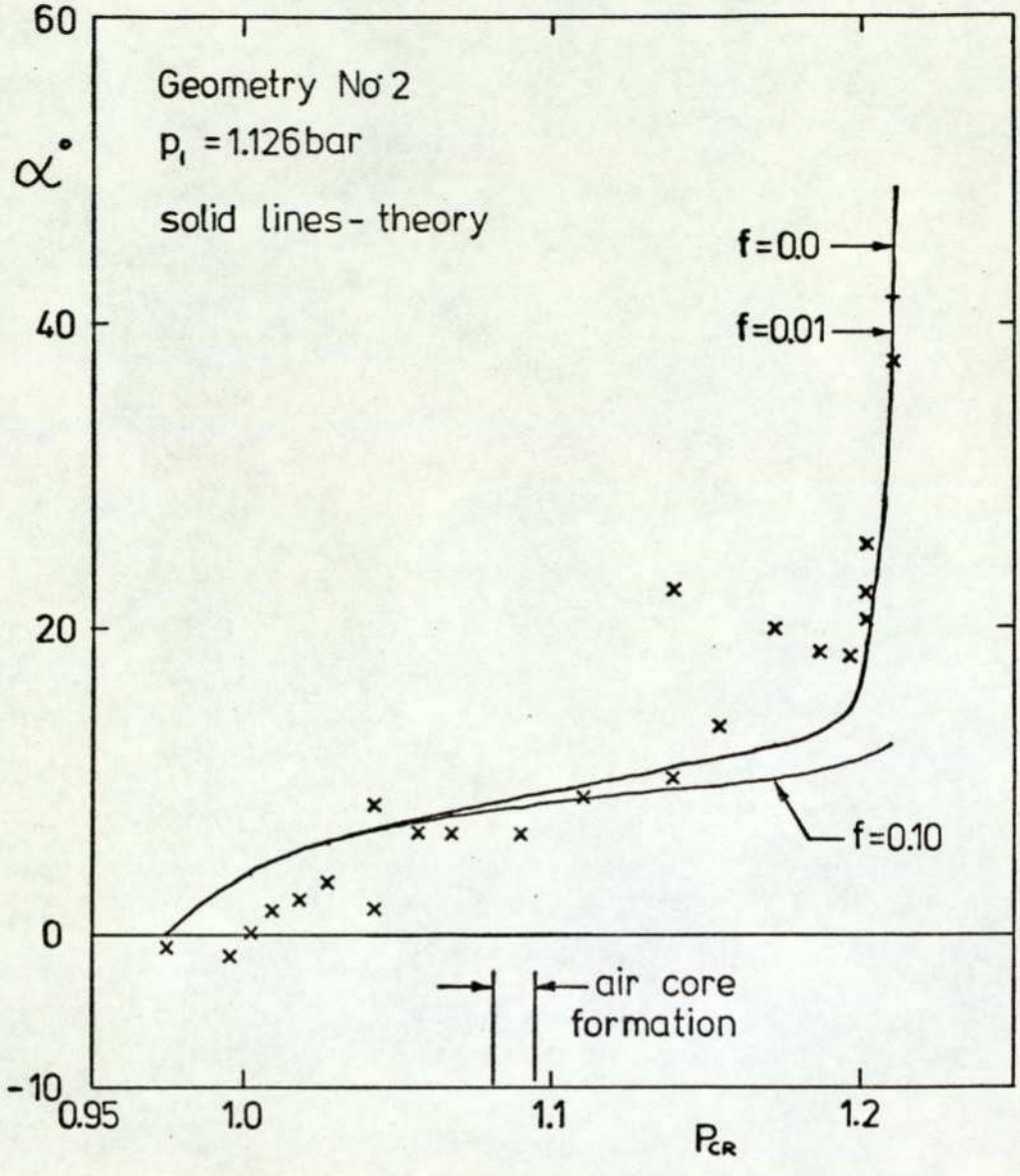

Tangent of orifice plane velocity ratio against control pressure ratio

Figure 3 - 33

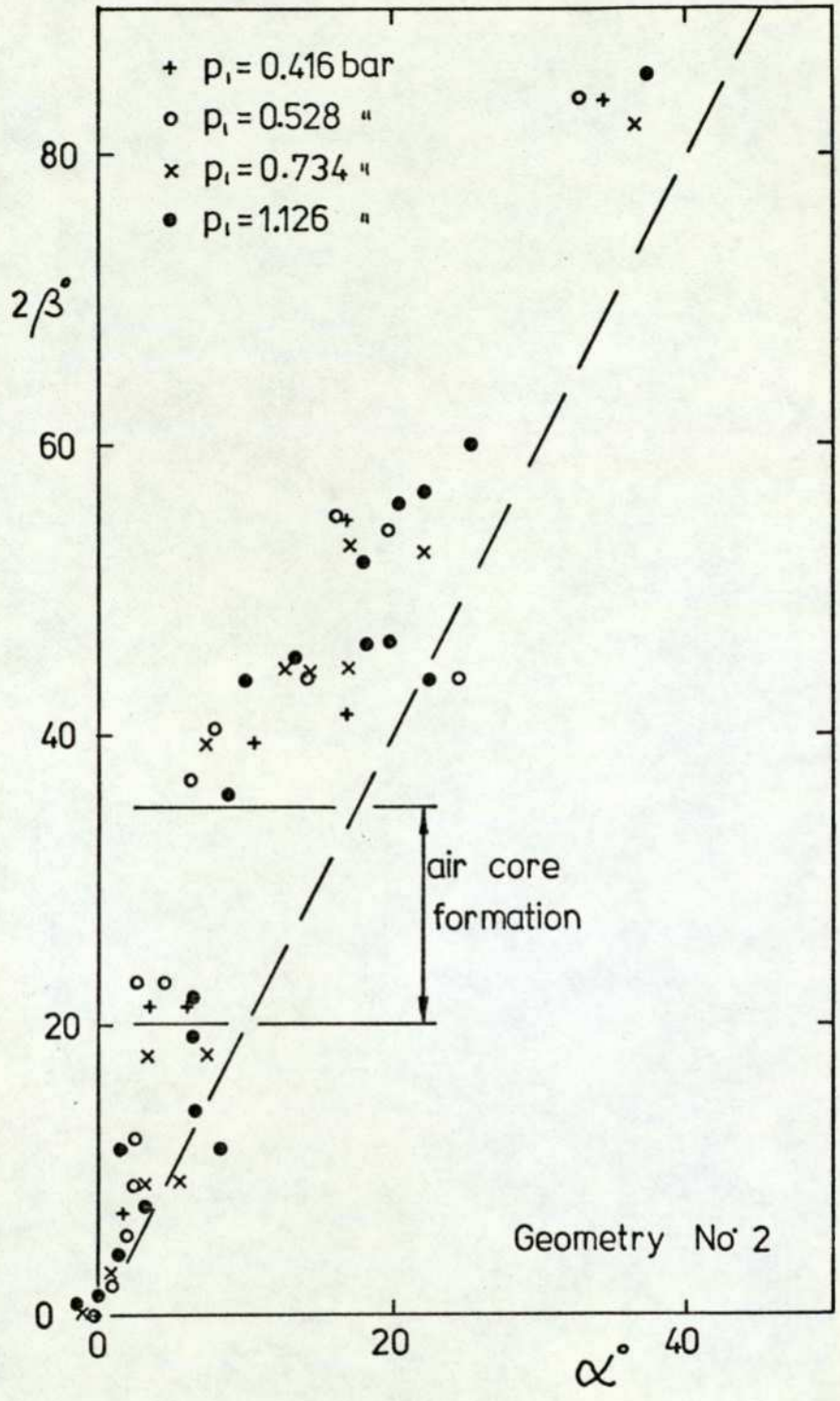

Correlation between included angle of jet and orifice plane velocity ratio angle

Figure 3-34

flow the liquid jet looked like a solid transparent rod, being smooth with no surface instabilities. The introduction of a very small control flow resulted in a disturbed liquid jet surface; Plate 11 illustrates this effect. Photographic Plate 12 illustrates the liquid jet with a control flow insufficient to form an air core, whilst Plate 13 shows the jet after the air core formation. Photographic Plate 14 illustrates the jet with a high control flow, (severe swirling flow close to the supply flow cutoff point). A further interesting aspect of the liquid jet's appearance was that with control flows sufficient to form a stable air core but not sufficient to cutoff the stream flow, the resulting conical sheet had four visible striations. It was thought that this indicated inhomogeneous mixing of the stream and control flows; it was only visible with device geometry No.2. The high nozzle curvature values close to the exit orifice and the resulting high fluid accelerations, may have obscured the effect on the liquid sheet from geometry No.1.

3-5-2 Observations on the Theory

Two inviscid versions of the stream surface theory were run, one allowing rotational flow and the other irrotational. A modification was incorporated into the irrotational flow model to allow for the decay of angular momentum flux along the nozzle.

All versions of the theory would predict points

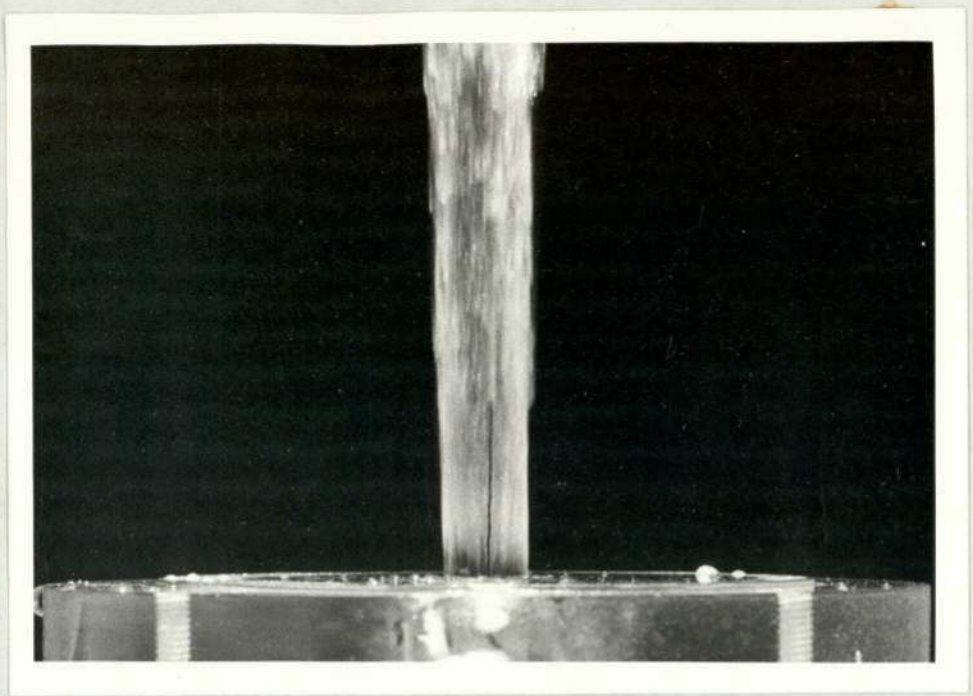

PLATE 11

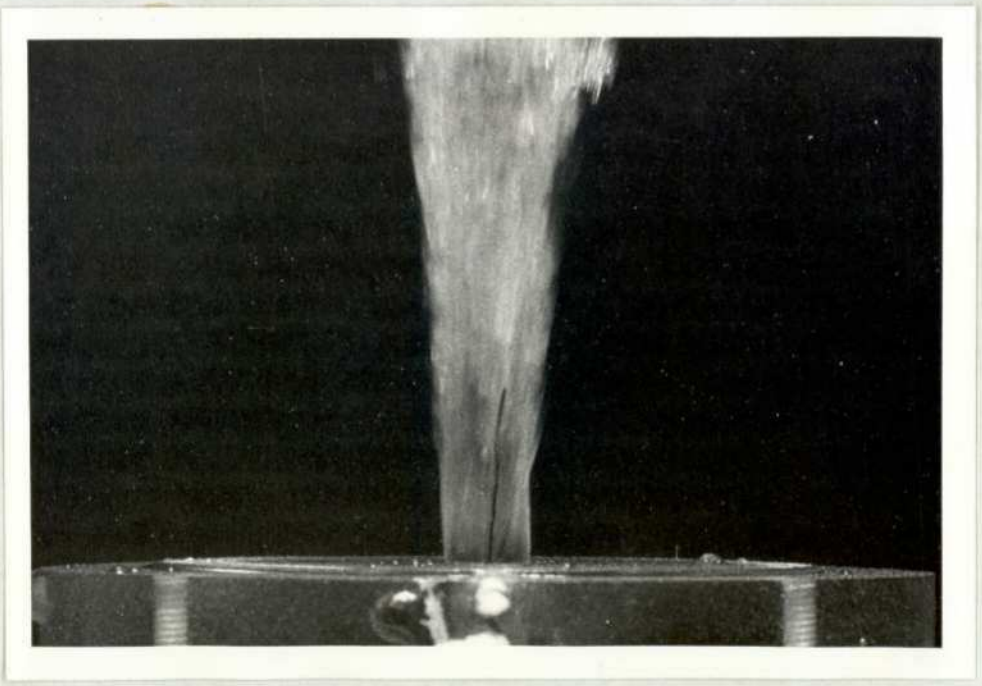

PLATE 12

Swirling liquid jet

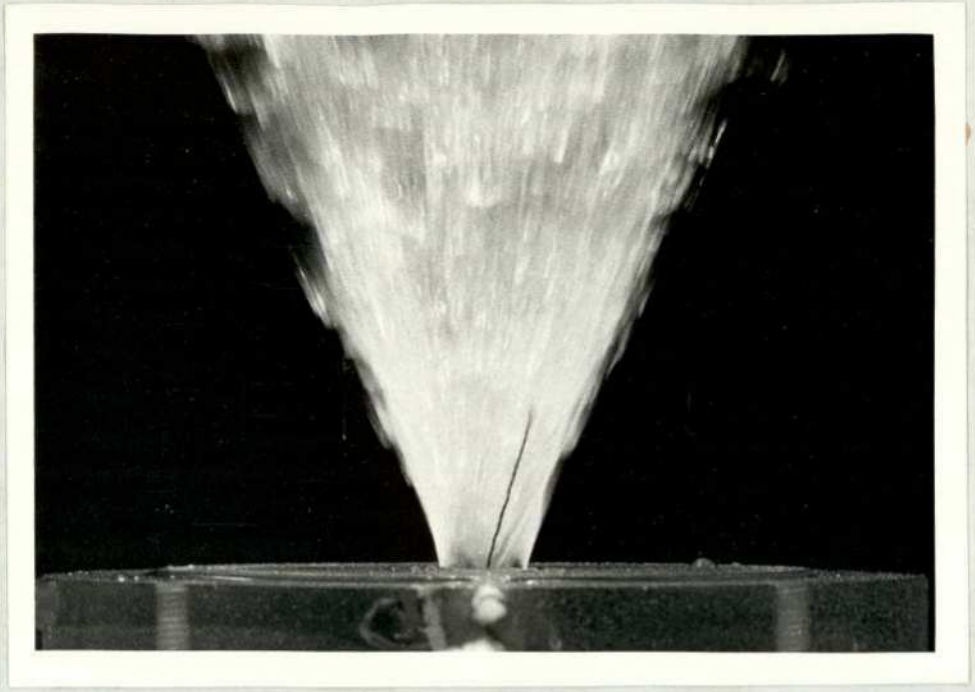

PLATE 13

PLATE 14

Swirling liquid jet

of flow stagnation and stream separation; however, as the computer programmes were written, the stream surfaces were not adjusted accordingly. With the theory in its present state a stagnation point would result in a zero square root. Usually stagnation occurs between two calculation stations and thus a negative square root would be required. In the present state of the theory the computer programme would be terminated. Flow separation was indicated by negative predicted pressures. In practice small negative pressures could exist but, as mentioned in chapters 1 and 3, aeration would usually occur well before the vapour pressure was reached.

The differences between the predicted values for the rotational and irrotational inviscid theories was so small as to be indistinguishable on the graphs plotted. Figure 3-35 illustrates the orifice plane parameters predicted by the different versions of the theory. The streaming flow velocity distribution has not been plotted since it was, for graphical purposes, identical for all versions of the theory.

The form of the tangential shear stress equation resulted in very little angular momentum flux loss with low and moderate swirl velocities and then very high losses close to the nozzle orifice, where the tangential velocity was high (see Figure 3-36). It was thought that with a reasonable angular momentum flux loss the diminution in total pressure was not of a sufficient magnitude . It would

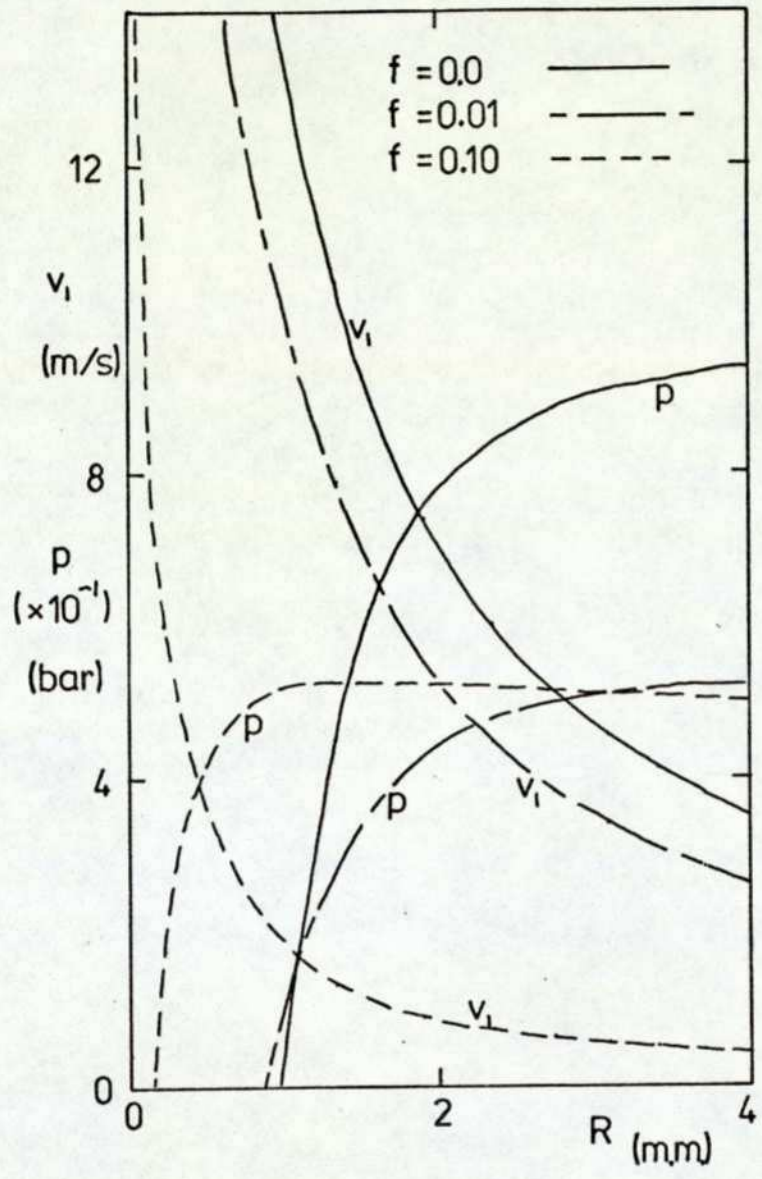

Orifice plane parameters (theory) -

Geometry No 2

Figure 3-35

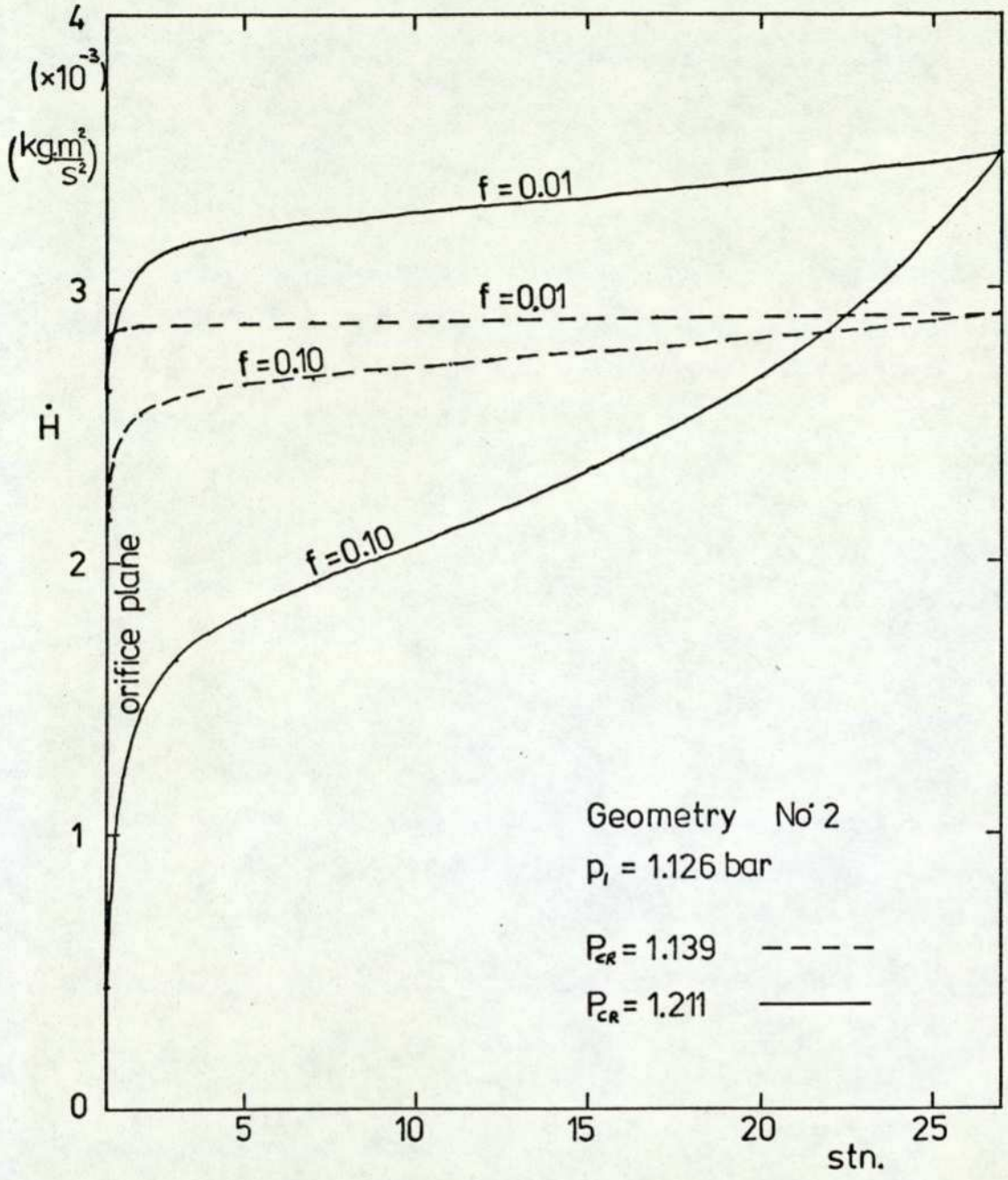

Angular momentum flux decay - theory

Figure 3 - 36

have been preferable to introduce a longitudinal shear stress term to reduce the static pressure predicted with streaming flow and then to add the losses due to the tangential shear stress necessary to produce the angular momentum flux losses. After examining the predicted results it was thought that the swirl velocity squared relationship for the tangential shear stress may have underestimated the losses at low swirl conditions and overestimated them at high swirl conditions. A tangential shear stress model directly proportional to the swirl velocity may result in improved prediction results.

3-6 Summary - Swirling Liquid Flow

A number of references have been examined and, where applicable, the results have been incorporated into the design of a new axial vortex element. The major new factor in the vortex element design was the configuration of the centre body and the stability of operation of the device was thought to be attributable to the centre body geometry.

A two dimensional inviscid analysis has been made of the fluid flow within the nozzle and a one dimensional decay pattern imposed upon the inviscid solution. The comparison between the predicted and experimental results was thought to be encouraging.

The vortex device was shown to operate in a satisfactory manner and it was thought that, providing the

transient response was adequate, the device would control the quite powerful liquid jets necessary for deflecting fairly large and heavy bodies.

4 THE TRANSIENT PERFORMANCE OF AN AXIAL VORTEX FLUID ELEMENT.

4-1 Preliminary Considerations

In chapter one, section (1-4-3), it was stated that one of the reasons for choosing an axial vortex element was that it was expected to have an adequate transient response. A switching rate of approximately thirty-five hertz was required. In this chapter an examination will be made into the switching processes of the axial vortex device and an estimate made of the switching time.

The transient characteristics of typical engineering systems are obtained and presented in a number of ways. The term 'transient response' is normally used when referring to the output characteristic resulting from a step input. Determining the transient response is difficult for all but the simplest systems and even then it may not yield all the desired information; namely, how to modify individual system parameters to obtain a specified response. The term 'frequency response' is usually used when examining the steady state output characteristics in relation to a sinusoidal input function.

The output characteristics obtained from the frequency response tests are usually presented graphically in the form of a Bode plot or, less often and usually for stability examination, a Nyquist plot. The explanation and usage of these methods is given in many standard books on control theory. It should also be stressed that these methods

are usually used to present the steady state output response.

When a system comprises a number of elements, each with its own transfer function, then the overall transfer function will be, (see Figure 4-1 (a)):

$$\frac{\theta_o}{\theta_i} = F_1(j\omega)F_2(j\omega)F_3(j\omega) = KG(j\omega).$$

Assuming that each element has a simple first order transfer function then the overall frequency response will be:

$$KG(j\omega) = (A_1A_2A_3)\, e^{j(\phi_1+\phi_2+\phi_3)}$$

where: A = amplitude ratio

ϕ = phase shift

It is, perhaps, stating the obvious, that if the amplitude ratio is plotted on a logarithmic scale (a common scale being decibels) then providing the system elements are of a linear first order form, the amplitude and phase shifts are additive.

It follows from the preceding paragraph that if a system has one or more elements with unknown transfer functions it becomes extremely difficult to obtain the transfer function of a particular element within the system. Providing the form of the various element characteristics are known then curve fitting methods can be used to fit predicted curves onto experimental data.

The systems previously considered have been idealised and modelled by linear differential equations.

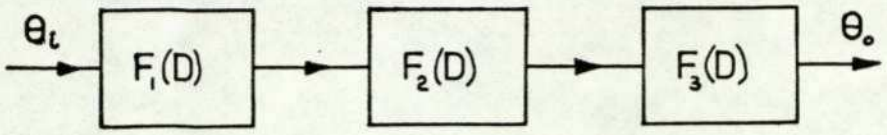

An open loop control system

FIG. 4-1 (a)

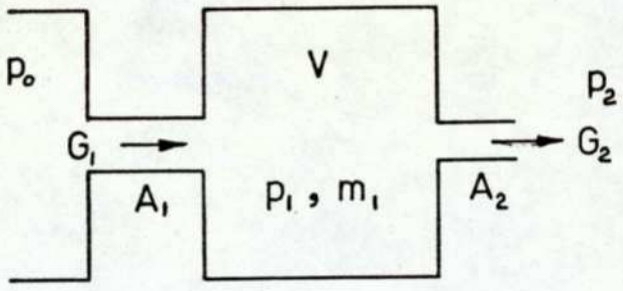

$$G_1' = a_o p_o' - a_1 p_1'$$
$$G_2' = b_1 p_1' - b_2 p_2'$$

$$p_1' \triangleq \frac{k}{(1+\tau D)} \qquad \text{where} \quad \tau = \frac{\rho V}{\gamma p_1 (a_1 + b_1)}$$

(from Neve , 1971)

FIG. 4-1 (b)

Figure 4-1

Some non-linear differential equations have been solved using graphical or computer techniques. However in practical systems there are time lags introduced in measuring and transmitting information. These time lags introduce serious difficulties into the analysis since the output is no longer a continuously varying function of the input. Morrison and Crossland (1970) mention that such lags have the effect of raising the order of the differential equation and that the conditions for stability are much more difficult to investigate and ensure.

Jacobs (1974) gave a much more elegant and rigorous explanation on this point. He stated that the minimum phase equations of Bode have a unique relationship between the phase angle and the amplitude of the frequency response function. A non-minimum phase equation has a phase shift, at any frequency, greater than a minimum phase equation having the same frequency response amplitude function. Also, Jacobs explained, a common non-minimum phase equation is that describing a time delay. Its transfer function e^{-sT} (where T is the time delay) however, cannot be expressed as a ratio of finite polynomials.

When fluid flows are initiated and terminated, effects additional to the steady flow parameters can manifest themselves. These transient effects are largely due to the inertia and compressibility of the fluid. Air, used for many transient and dynamic tests, has large compressibility effects but low inertia effects. The fluid

used for the transient testing of this device was water, which has large inertia effects but low compressibility effects, (except in tension when aeration and cavitation can occur).

A number of authors have sought to obtain a comprehensive analytical model for the transient behaviour of vortex flueric devices. As mentioned previously, one major difficulty, which becomes apparent when obtaining experimental results, is that it is difficult to isolate and test the vortex device alone. Almost invariably the equipment used to obtain and modulate the control and supply pressures and flows have unknown transient characteristics. What may then be obtained from the experimental tests is the combined transfer function of the entire system. Both Otsap (1968) and Al-Shamma (1971) recognised this difficulty. Al-Shamma stated that with the equipment he used he could not obtain the response time of the vortex device alone, whilst Otsap attributed much of the discrepancy between his predicted and experimental results to the fact that he could not obtain a step input function.

A number of references dealing with the transient analysis and testing of vortex devices will be examined in the next section; however, a qualitative description of the switching process will first be given.

Consider streaming flow conditions to be established within the nozzle. At the nozzle orifice plane a cylindrical liquid jet will issue into the surrounding air, finally to

break up into droplets, as described in Appendix 1. To initiate a control flow it is necessary to raise the pressure in the control flow supply annulus. Having raised the control pressure a flow from the control nozzles will gradually become established, rising with time to a steady state value. The stream and control flows mix and by a process of momentum transport and viscous diffusion, swirling flow becomes established close to the control and stream nozzles. Depending upon the vortex element geometry and the relative magnitude of the stream and control flows, the mixing process may occur over a considerable proportion of the vortex chamber. If a constant pressure drop were to be maintained across the vortex device, the introduction of a control flow would result in an attenuated stream flow. Continuity considerations result in swirling flow being propagated downstream until it becomes established throughout the nozzle. The swirling liquid upon issuing from the orifice into the surrounding air will, providing the radial pressure gradient is high enough, form into a conical liquid sheet.

If it is necessary to revert to stream flow then the pressure within the control flow supply annulus must be reduced. Because of the fluid inertia the control flow will not cease immediately; even if the supply to the control annulus is stopped immediately the flow will continue for a short period and a pressure dip below the steady state pressure will be noted. As the control flow ceases the

stream flow will revert to its original value and the swirling flow formerly established within the nozzle will be swept out by the stream flow.

4-2 The Transient Analysis of Vortex Fluid Elements

Some authors have, like Otsap (1968), performed a number of experiments and then fitted a transfer characteristic to the resulting experimental points. Otsap (1968) approximated the dynamic characteristics of his vortex device to a first order linear system having the transfer function $\left[K/(1 + \tau s) \right]$. He estimated that the time constant τ increased as the square root of the chamber volume.

Al-Shamma (1971), in his transient testing of an axial vortex device, found that a simple resistor/capacitor electrical circuit modelled the system comparatively well and gave good agreement with the measured values. Al-Shamma also mentioned two other points; he could not isolate the vortex device; the delay time for steady state conditions to prevail was substantially longer when the control flow was switched on than when it was switched off. This latter point will be returned to later.

Neve (1971) performed a considerable amount of transient work. He fitted a linear second order equation to his experimental results and, finding the agreement was poor, added a number of first order lead or lag terms to obtain better agreement. The final transfer function was

of the form:

$$\frac{1}{\left[\frac{s^2}{\omega_n^2}+\frac{2c}{\omega_n}s+1\right]} \cdot \frac{(1+\tau_1 s)(1+\tau_2 s)}{(1+\tau_3 s)}$$

Neve also obtained the transfer function for an isolated vortex chamber analytically. The problem was linearised, therefore restricting the solution to small pressure changes, and Neve further simplified the problem by eliminating the stream flow inlet, stating that changes in input pressure occur mainly in the control nozzle. A simple first order lag function was obtained (see Figure 4-1 (b)) and it is interesting to note that the time constant was directly proportional to the vortex chamber volume. One of Neve's particular concerns was the effect of the vortex chamber aspect ratio (length to diameter). He found that the optimum aspect ratio for dynamic performance was just under unity. He also noted that for the particular devices under test there was "- - - no marked difference between the times needed to set up or destroy a vortex." This contrasts with the remark made by Al-Shamma, although the vortex devices were of different types. Neve also demonstrated the similarity between the equations for fluid flow and those for electrical networks, drawing a parallel between inertia/inductance, pressure/voltage, compressibility/capacitance, flow/current and resistance.

Taplin and Seleno (1970) presented a very comprehensive dynamic equivalent electrical circuit for a

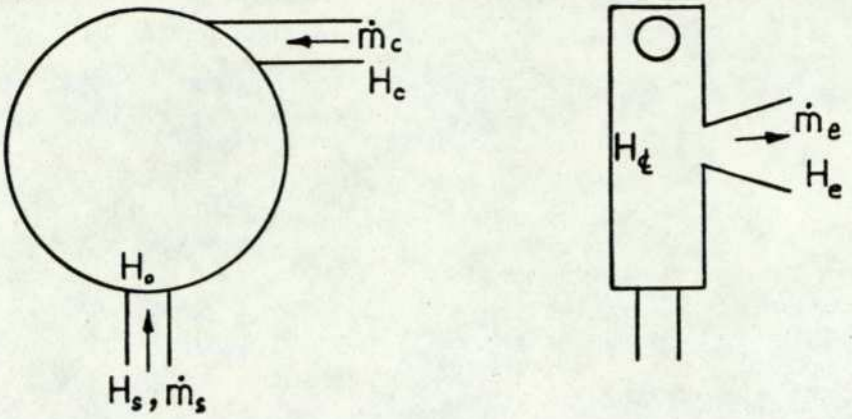

Configuration.

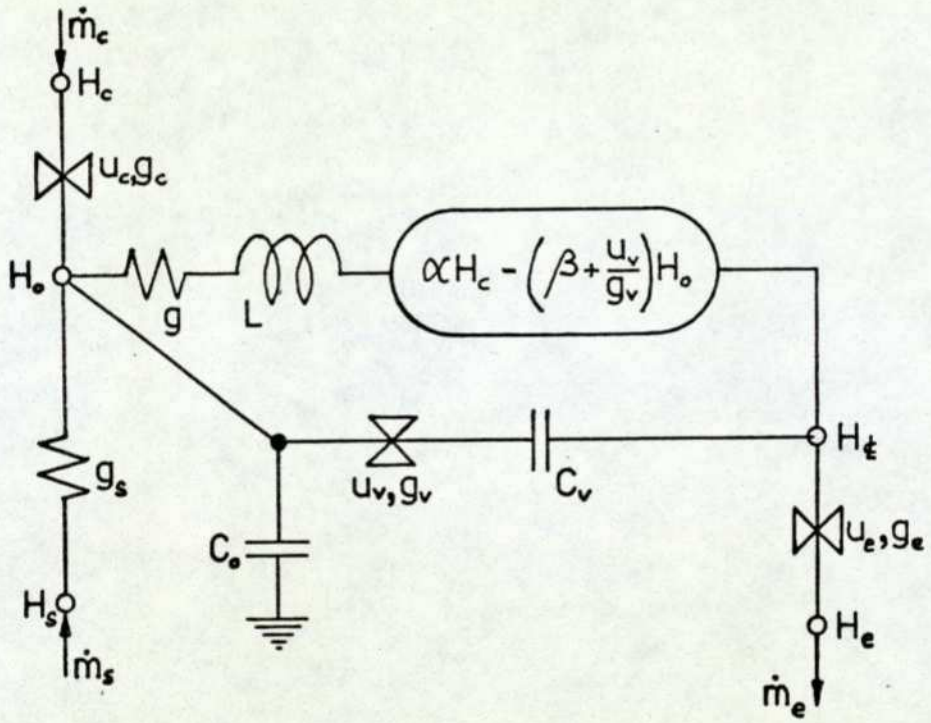

Vortex equivalent circuit (from Taplin & Seleno ; 1970)

Figure 4-2

vortex amplifier; their equivalent circuit is shown in Figure 4-2. It can be seen that there are two paths connecting the nodes H_o and H_ℓ ; one with an inductive term and one with capacitive terms. Each branch will have a specific time constant. If both time constants are equal a first order transfer function will result; however, if the branch time constants are unequal a second order term will be introduced. Taplin and Seleno used experimentally determined values for the required constants, but unfortunately almost all their quantitative data was presented in a non-dimensional form.

Taplin and Seleno's model was modified to meet the specific conditions of the vortex device under test. It was assumed that the stream flow inlet was perfectly regulated, then zero pressure change could occur at node H_s and this could be earthed. For the vortex device under test the exit pressure was also a constant (atmospheric pressure) and therefore the node point H_e was also earthed. The resulting simplified dynamic equivalent circuit is shown in Figure 4-3. A further simplification was considered. The stream flow inlet area was approximately five times greater than the exit orifice and the equivalent fluid flow path impedance was designed to be low. Therefore the admittance g_s should have been very much larger than g_e and it should introduce very little error to assume that the node H_o was pressure regulated.

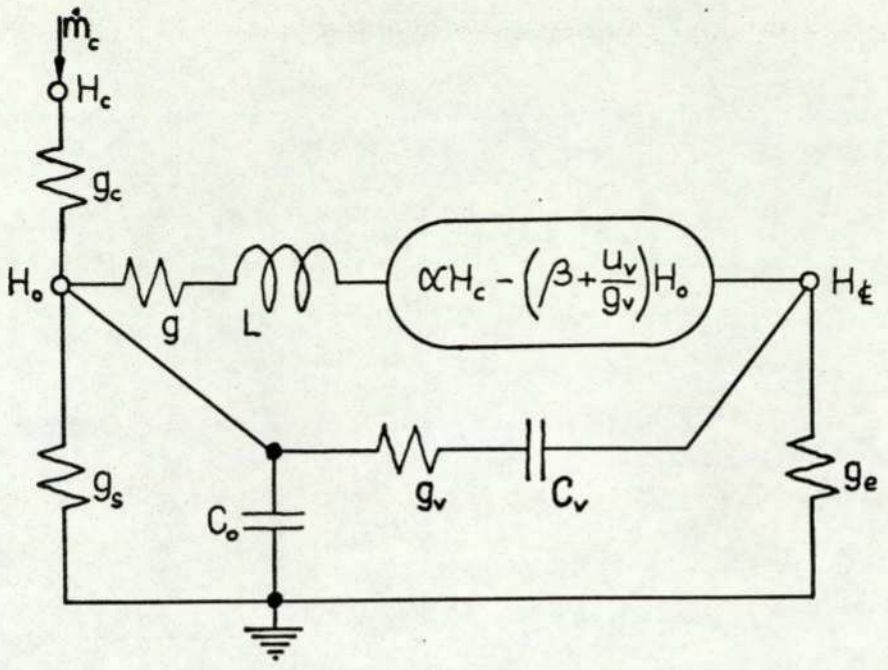

Vortex equivalent circuit - pressure regulated supply and exit .

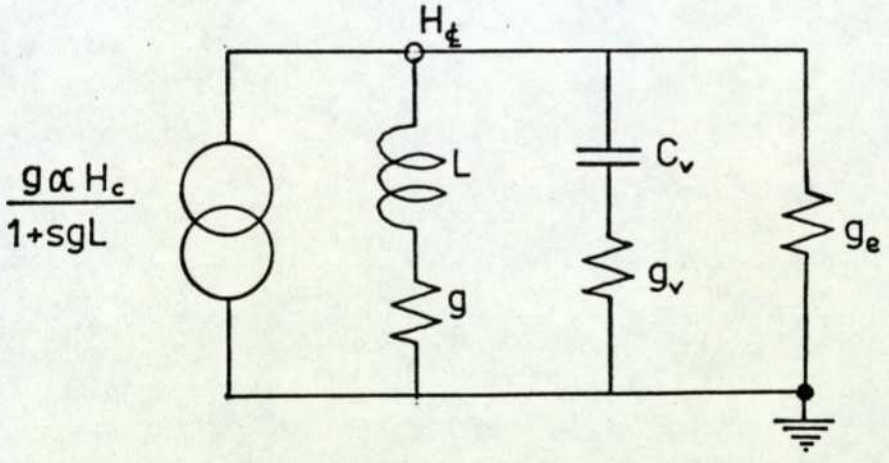

Vortex equivalent circuit - pressure regulated exit and infinite supply admittance .

Figure 4 - 3

The resulting equivalent circuit model is also shown in Figure 4-3.

From Figure 4-3 it can be seen that, in spite of the simplifications made, there are still two reactive elements in the circuit. It is likely, therefore, that second order terms will be present in the transfer function; however, when operating with liquids it was thought that the inertia (inductive) term would dominate the system.

4-3 Transient Testing - Experimental Procedure

The experimental configuration is shown in Figure 4-4. Both the control and stream flow inlet lines were pressure regulated to prevent the supply pump's flow characteristic having too much influence on the experimental results. After some testing it was decided to fit an electrical solenoid valve to switch the control flow on and off. The electrical signal to the solenoid valve was controlled by a signal generator via a reed switch unit (used to provide the valve current). A pressure transducer was installed in the control flow supply annulus to monitor the control pressure rise and a 'jet sensor' was positioned in line with the jet orifice but some distance downstream. The 'jet sensor' comprised a waterproofed pressure transducer, used to register the presence of the cylindrical jet by the pressure rise due to the liquid impact. When a control flow was initiated

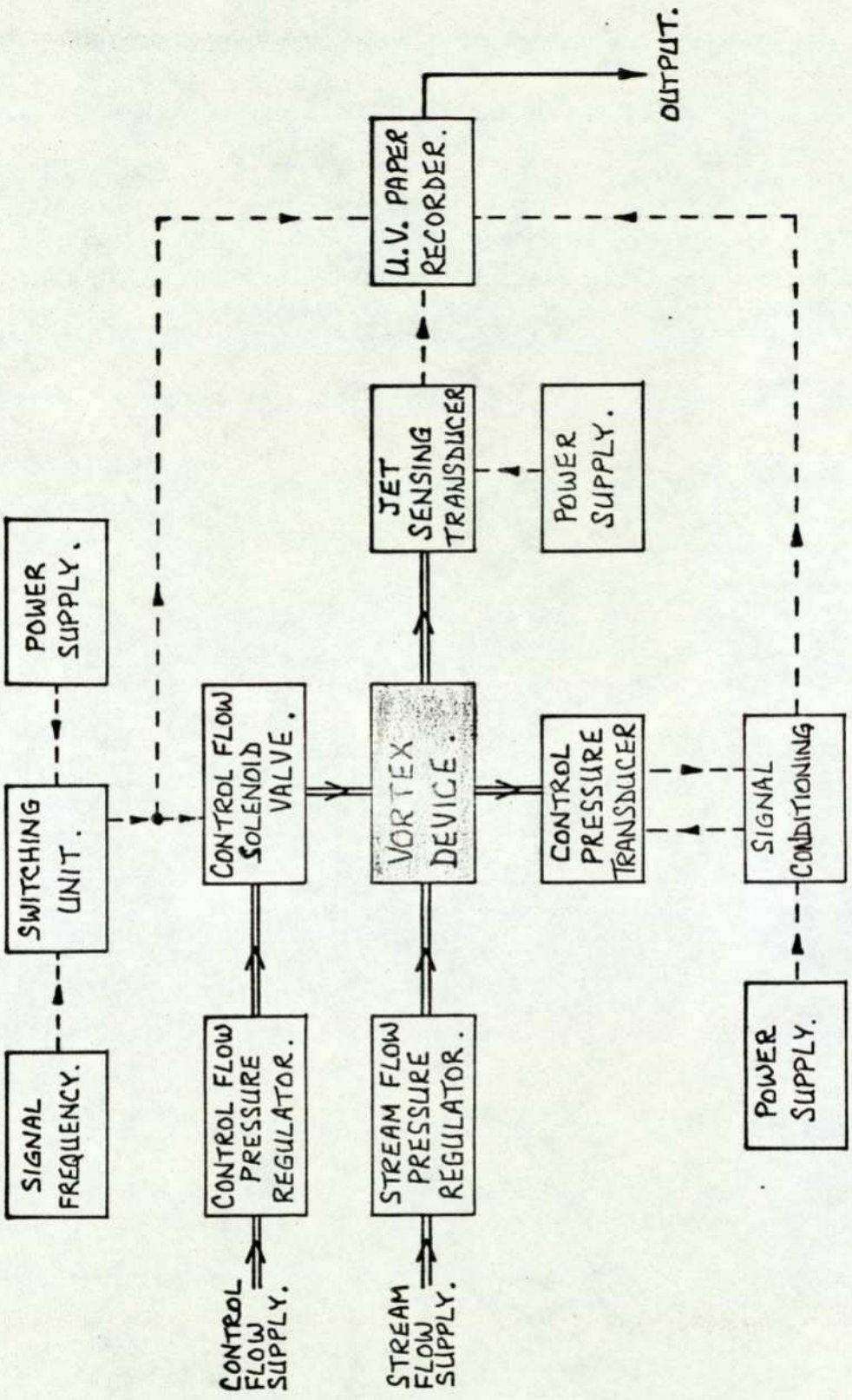

Transient response experimental flowchart .

Figure 4 - 4

the resulting conical liquid sheet avoided impacting on the 'sensor'. The downstream position of the jet sensor was chosen to approximate the position of a cylindrical body.

Signal lines from the control flow solenoid winding, the control annulus pressure transducer and the 'jet sensor' pressure transducer were taken to an ultra-violet paper recorder and an analogue record made of all the transient tests.

It was found that the manufacturers of both the pressure regulators and the solenoid valve were unable to provide the transfer functions of their respective devices. Even the limited information given by one manufacturer was found to be inaccurate and therefore the author was in the position, mentioned earlier in the chapter, of obtaining the overall characteristic of the system and being unable to isolate the vortex device. In spite of the limitations mentioned some very interesting and useful results were obtained. Details of the proprietary equipment used for the transient tests is given in Appendix 11.

The experimental procedure was to set the stream flow pressure regulator to the required static pressure with zero control flow. With the control flow solenoid valve open the control flow pressure regulator was altered until a stable air core was attached to the centre body of the vortex device. This procedure set the prevailing conditions of pressure and flow for the device. The signal

generator was set to give a square waveform at various frequencies and the transient response of the three monitored channels recorded on ultra-violet paper. A series of transient tests were run with various stream flow values and a number of control pressure ratios.

The transient results quoted in Table 4-1 were obtained by averaging from a number of cycles the time lags from a signal initiation to the initiation of a response and also the time taken from the initiation of a response to the time taken to reach 63.2% of the final steady state value (for a first order linear system this would have equalled the time constant). Figure 4-5 defines the times quoted in Table 4-1.

4-4 Discussion of the Transient Test Results

4-4-1 Observations on the Signal Traces

Figure 4-6 reproduces the output from an actual transient test. A number of points are clearly visible. The application and removal of the solenoid voltage (lower trace) is very rapid and closely approximates a true step input. Also visible, but not complete, is the high reverse voltage and current on removal of the solenoid signal voltage. This is typical of an inductive coil and, of course, means that the valve will not start to shut until the magnetic flux has collapsed; it can be seen that this takes at least 5 ms. The control flow supply annulus pressure (middle trace) starts to rise some time after the

TABLE 4 - 1

VORTEX ELEMENT GEOMETRY No.2

f (Hz)		t_1 (ms)	Δt_1 (ms)	t_2 (ms)	Δt_2 (ms)	St.no.
V_J = 10 m/s						
p_1 = 0.528 bar			p_2 = 0.665 bar			
Δp_1 = 0.064 bar			P_{CR} = 1.123			
1	ON	13.3	14.7	31.3	3.3	1.30
	OFF	26.7	8.0	31.3	2.0	1.30
5	ON	13.0	12.0	31.0	3.3	1.29
	OFF	28.0	8.0	30.7	2.7	1.28
10	ON	20.7	7.3	22.0	2.7	0.92
	OFF	30.0	6.7	26.0	2.7	1.08
V_J = 15 m/s						
p_1 = 1.123 bar			p_2 = 1.388 bar			
Δp_1 = 0.120 bar			P_{CR} = 1.117			
1	ON	10.0	13.3	22.7	5.3	1.58
	OFF	29.3	11.3	23.3	6.0	1.62
5	ON	11.3	12.0	22.7	4.0	1.58
	OFF	28.7	9.3	23.3	3.3	1.62
10	ON	18.0	10.7	12.0	6.0	0.83
	OFF	33.3	8.0	19.0	4.7	1.32
p_1 = 1.123 bar			p_2 = 1.467 bar			
Δp_1 = 0.144 bar			P_{CR} = 1.158			
1	ON	9.3	15.3	22.0	4.7	1.53
	OFF	30.7	14.0	28.0	4.0	1.95

f (Hz)		t_1 (ms)	Δt_1 (ms)	t_2 (ms)	Δt_2 (ms)	St.no.
p_1 = 1.123 bar			p_2 = 1.547 bar			
Δp_1 = 0.171 bar			P_{CR} = 1.196			
1	ON	8.0	18.0	20.7	5.3	1.44
	OFF	30.0	15.3	34.7	3.3	2.41
V_J = 9 m/s						
p_1 = 0.416 bar			p_2 = 0.526 bar			
Δp_1 = 0.051 bar			P_{CR} = 1.126			
1	ON	13.3	16.7	31.3	5.3	1.30
	OFF	28.7	8.7	32.7	2.7	1.36
V_J = 12 m/s						
p_1 = 0.734 bar			p_2 = 0.917 bar			
Δp_1 = 0.088 bar			P_{CR} = 1.116			
1	ON	10.0	14.0	28.7	4.0	1.58
	OFF	25.3	10.7	29.3	4.0	1.61

Transient test results

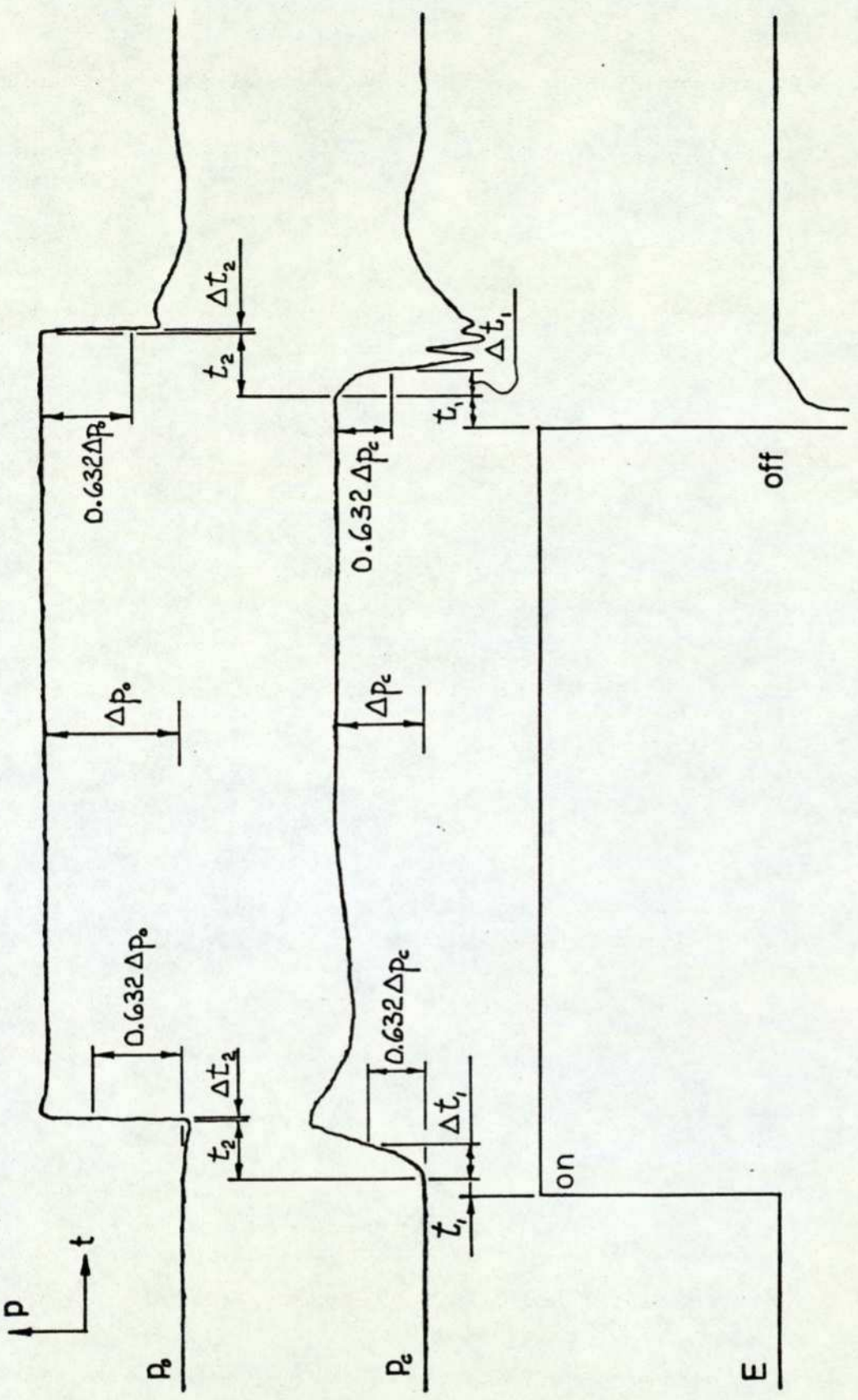

Definition of transient signal parameters .

Figure 4-5

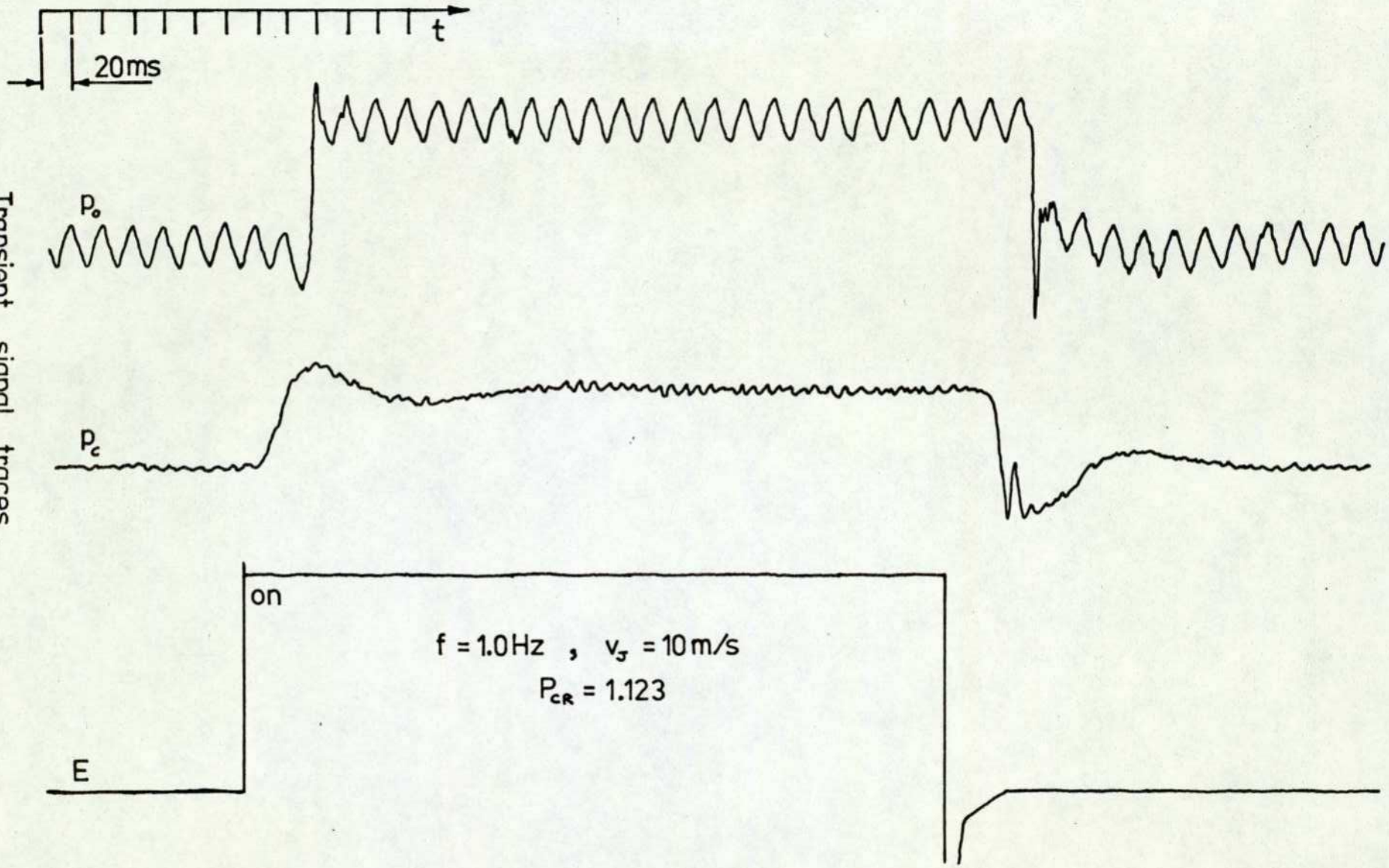

Figure 4-6 Transient signal traces.

valve signal voltage is applied, (see Table 4-1 for average figures), and this delay time is attributed to the solenoid valve. It was thought that the slight 'peaking' followed by a long shallow trough may be the response of the pressure regulator, rather than the solenoid valve or the vortex device. The time increment Δt_1 gives an indication of the rise time of the control annulus pressure.

The output of the 'jet sensor' pressure transducer is shown in the upper trace. Firstly it is rather obvious that some 50 Hz. noise is picked up by the 'jet sensor' signal line. The low signal to noise ratio of this transducer made the amplitude of the noise difficult to reduce (the maximum signal being approximately 20 mV). The signal was not filtered since the noise frequency was thought to be too close to the desired operating frequency of the device and the effect of filtering could affect the recorded response figures. The transducer could not be changed since a waterproofed device was required and few could be found to meet the experimental requirements. The upper trace does show, however, that the signal rise time is very rapid and that negligible overshoot occurs. The time delay between the start of the control annulus pressure rise and the start of the 'jet sensor' pressure rise was taken as the response time of the vortex device (termed t_2 in Table 4-1).

It was estimated that the measurements of the various time delays and signal rise times could be in error

by up to 2 ms. By averaging a number of cycles it was hoped that a representative figure would be obtained (see Table 4-1). Referring again to the control flow supply annulus pressure signal; it can be seen that when the control flow was switched on, there was a relatively smooth pressure rise with very little oscillation, whereas when the control flow was switched off there was a noticeable high frequency pressure oscillation. This aspect of the signal trace was attributed to the different behaviour of liquids to compressive and tensile stresses. With reference to section 4-1 it was stated that liquids have much lower compressibility effects than do gases. Whilst this is true, for the pressures used in these tests, the behaviour of the liquid under tensile stresses is different to that under compression. When the control flow is rapidly shut off the volume downstream of the solenoid valve experiences a rapid pressure drop due to the inertia of the moving fluid. These low pressures result in transient pressure wave transmission and reflection and in severe cases aeration or cavitation can occur behind the valve. Negative pressures apparently did not occur within the control flow annulus. In Figure 4-3 the compressibility effects are modelled by capacitor Co. To faithfully represent these differences in behaviour between switching on and switching off the control flow would require different values to be used for Co.

4-4-2 Observations on the Experimental Results

The average results given in Table 4-1 illustrate a number of points. It can be seen that the solenoid valve response times, defined as the times between the application or removal of the valve signal and a change in the control flow supply annulus pressure, sum to approximately forty milliseconds. These figures would imply that, to a first approximation, a switching rate of twentyfive hertz would result in no pressure signal reaching the vortex element. It can also be seen that as the control pressure ratio is increased the solenoid valve opens with increasing rapidity and takes increasingly longer to close, the sum being approximately constant. As the average jet velocity was increased the vortex element response time was reduced; however, the non-dimensional response time, measured in terms of Strouhal number, was increased, (where the Strouhal number was defined as the ratio of the actual response time to the transport time with zero control flow). Figure 4-7 not only illustrates the previous observations but also shows that with a control pressure ratio of approximately 1.12 there is very little difference in the element response time whether switching the vortex on or off. It can be seen from Figure 4-8 that as the control pressure ratio was increased from approximately 1.12 to 1.20 the time taken to switch the vortex on was reduced slightly whereas the time taken to switch the vortex off was increased considerably. Since the minimum overall response time was required the control pressure

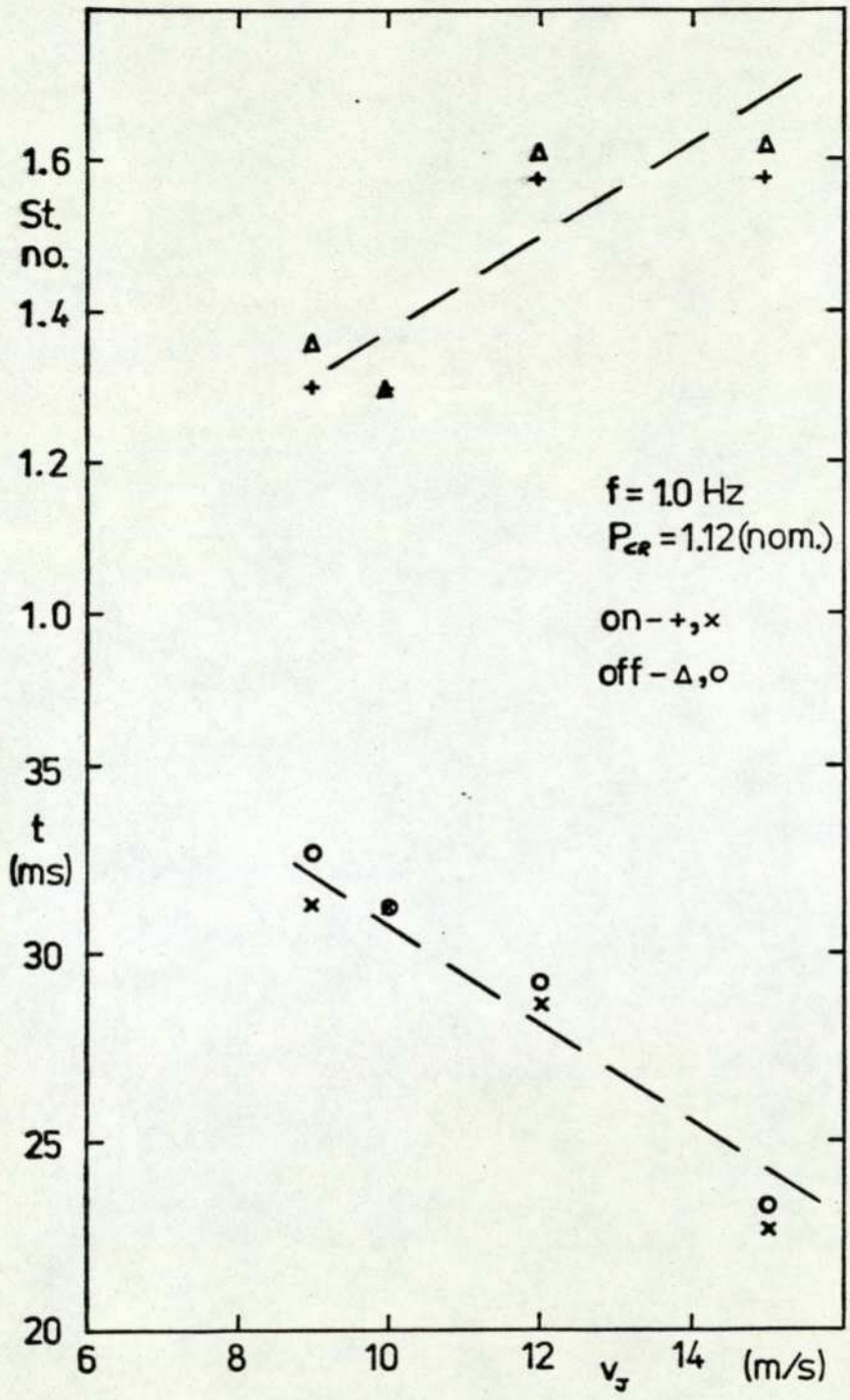

Switching time against jet velocity.

Figure 4-7

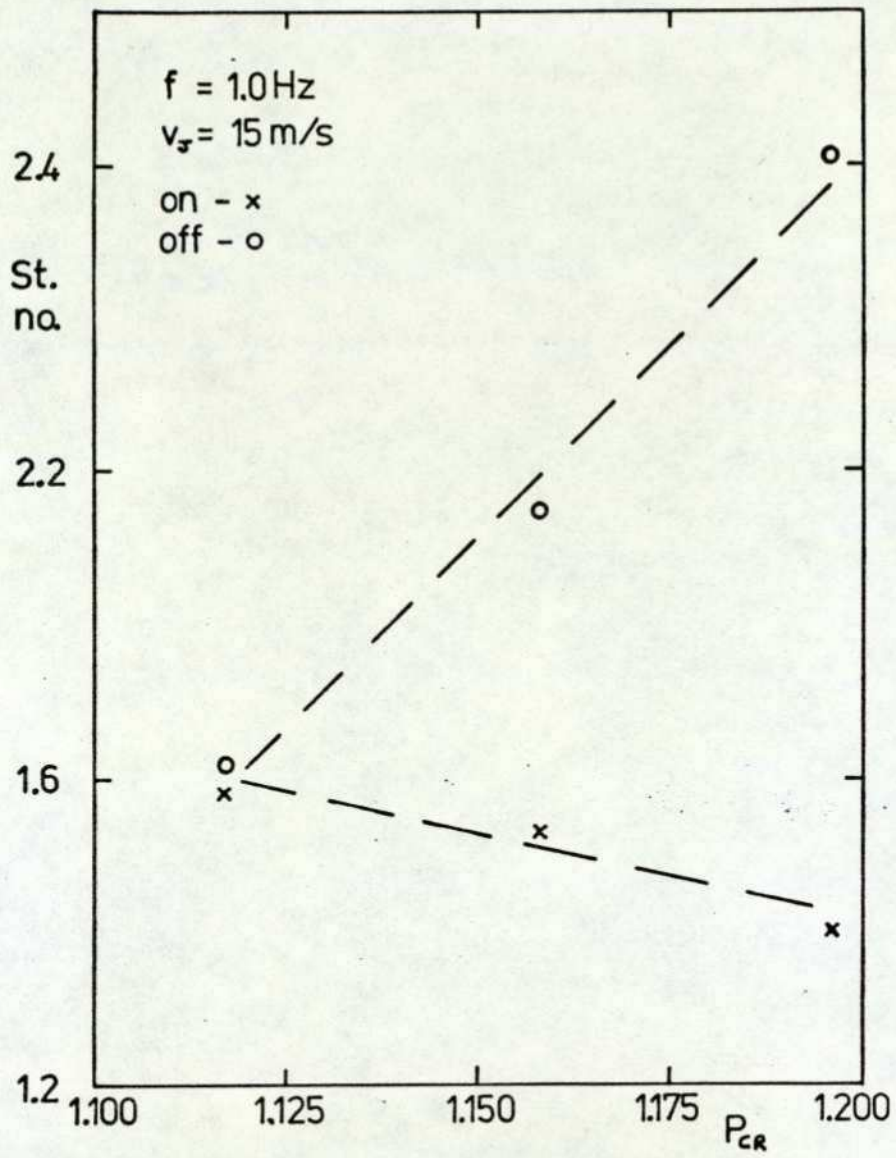

Switching time against control pressure ratio .

Figure 4 - 8

ratio should preferably be about 1.12.

The results given in Table 4-1 also show that as the frequency was increased from one to five hertz, the Strouhal number remained approximately constant; however, at ten hertz the Strouhal number dropped below unity. Examination of the tabulated experimental times shows that as the frequency was increased the time Δt_1 , indicating the rate of the control pressure rise at the supply annulus, was reduced. This was true whether the device was being switched on or off. It was thought that a form of resonance was occurring within the control flow supply system and the component that suspicion devolved upon was the pressure regulator, together with the supply pipe fluid volume. It can be seen that the previously mentioned signal overpressure on switch on and underpressure on switch off, are at ten hertz, fairly smoothly joined (see Figure 4-9). It was thought that the pressure wave transmission due to this resonance was the cause of the low value of Strouhal number obtained. If this were the case then the pressure waves would, in fact, modulate the control flow before the solenoid valve signal. Figure 4-9 illustrates a sample of the signal traces taken at ten hertz. If the control pressure trace (centre) is compared with that of Figure 4-6 it can be seen that, summing the times between the initiation of the solenoid control valve signal to the time taken for the overpressure peak, equals approximately fifty milliseconds; half the ten hertz cycle time. The same is true in the case

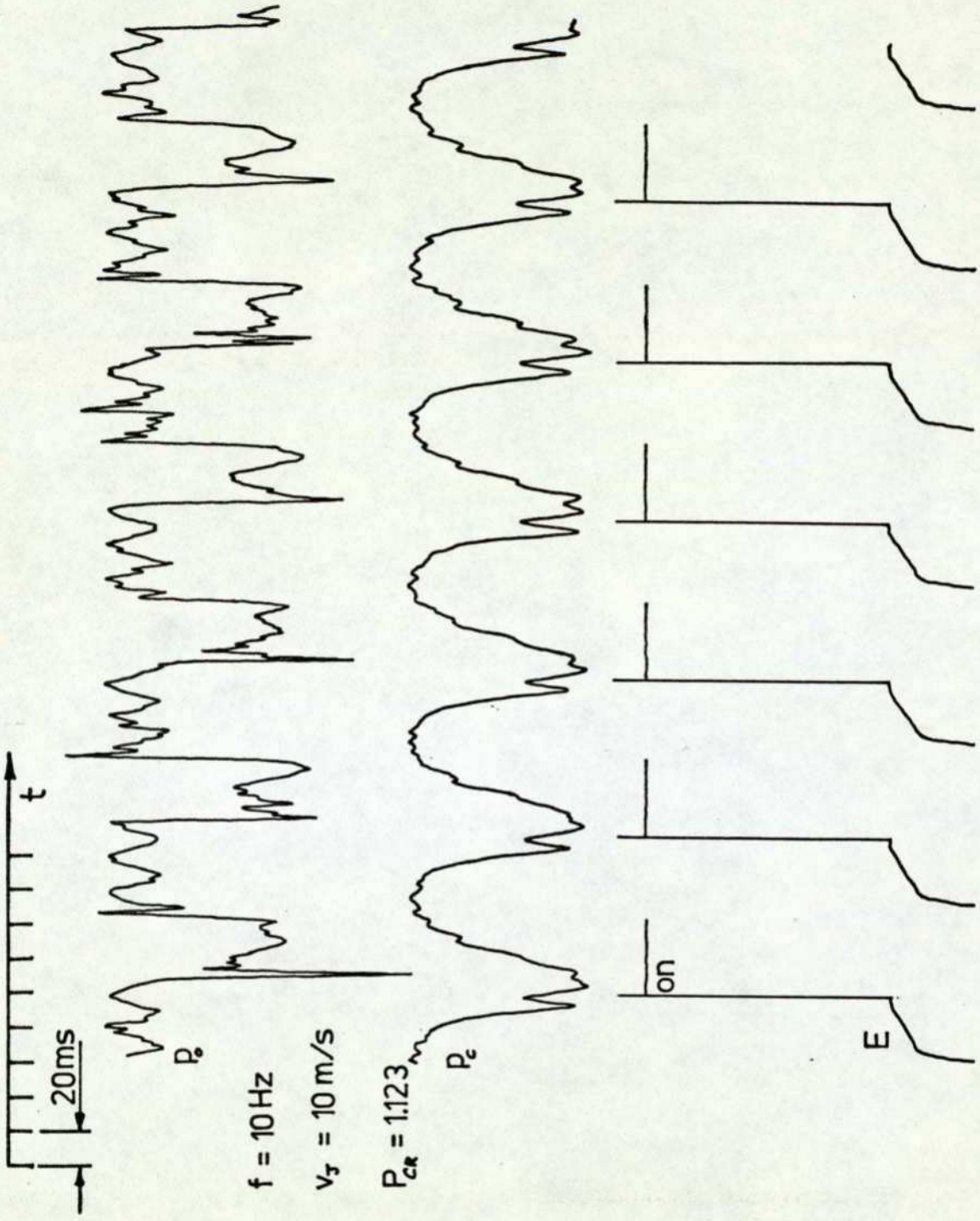

Transient signal traces at 10Hz .

Figure 4-9

of switching off the vortex signal.

The transient tests results compare fairly well with a qualitative assessment of the vortex element, apart from the last observation on signal resonance. From the steady state characteristics, illustrated in Figures 3-9 and 3-10, it can be seen that control pressure ratios of above 1.10 are required for a stable air core to be formed. Also with a control pressure ratio of 1.10 the flow through the device is almost the same as with no control flow. For this reason it was thought that the time taken to establish swirling flow within the nozzle should be very close to that required to establish streaming flow. If the control pressure ratio was raised above 1.10 then there would be a more marked disparity between streaming and swirling flow values and hence one could expect an increased divergence between the vortex element response time to an 'on' signal, to that for an 'off' signal. Since the vortex element was designed to have a low flow resistance to either streaming or swirling flow, all the flow passages being of a relatively large area, and since the device was operated on liquid, low Strouhal numbers were expected. The values achieved; however, were lower than expected and, as mentioned in Chapter 3, this had probably been achieved at the expense of the element's power turn down ratio.

It should also be noted that with zero control flow 66% of the transport time was accounted for by the

distance between the nozzle orifice plane and the 'jet sensor' transducer. After careful examination of the swirling sheet geometry, it was decided that the 'jet catcher' for the vortex element (see Figure 4-10) need be no longer than 40m m. Allowing for a clearance between the end of the device and any body of approximately 20 m m. then, assuming the Strouhal remained constant, the vortex element response time could be reduced by over 30%.

4-5 Summary - Transient Performance

A number of points were established as a result of the transient tests made on the axial vortex device.

Due to the influence of associated control equipment and the resulting unknown transfer functions, it became impossible to isolate the vortex device's transient characteristic from the overall system.

From the examination of Taplin and Seleno's (1970) work it was considered that a reasonable simulation of the vortex device could be possible. It was thought that the transfer function would be dominated by the inertia term and that compressibility and non-linear effects would add higher order terms of a much smaller magnitude.

The non-dimensional performance of the device was considered good. With a quite reasonable reduction in the jet transport time the device could meet the 35 Hz frequency specified in Chapter 1. If the jet velocity was further increased to 18 m/s and some attention was paid to the response of the control flow, it was thought that the

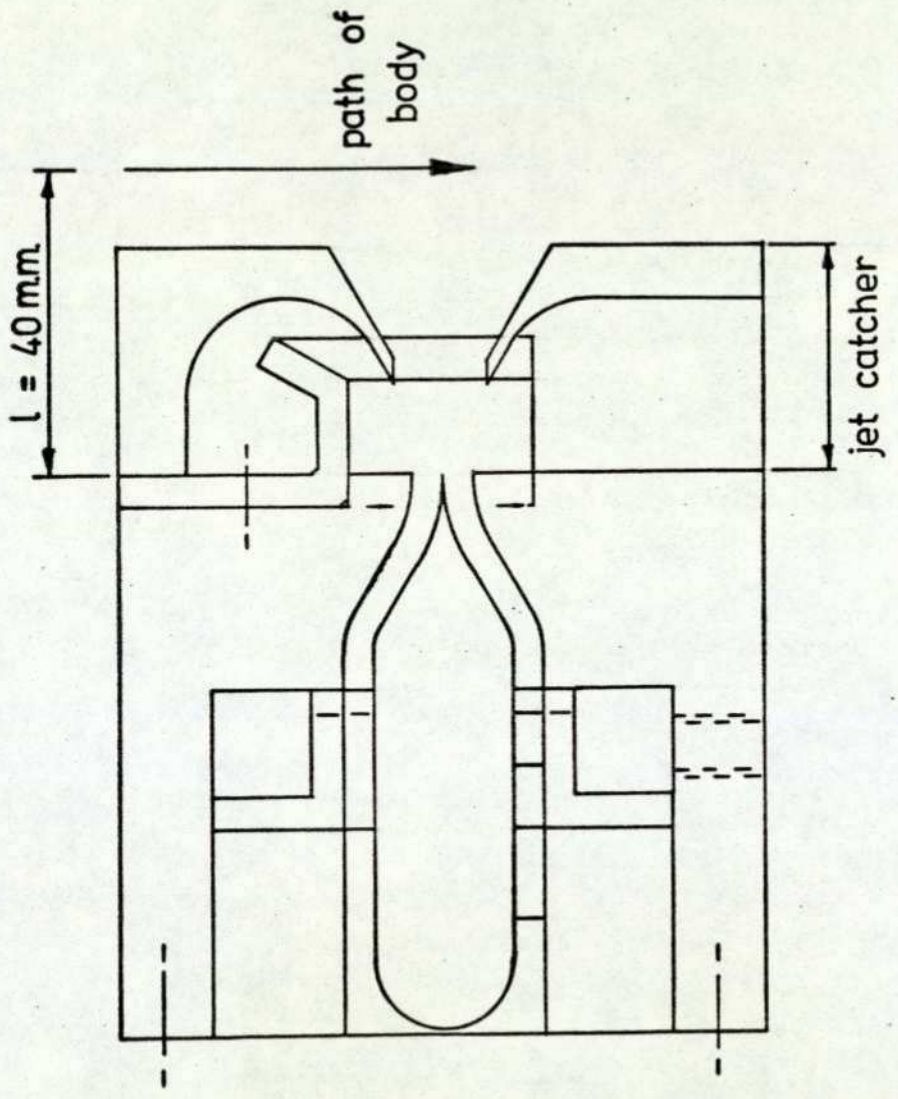

Axial vortex device with 'jet catcher'

Figure 4-10

proposed vortex device could operate well as a powerful and selective deflection device.

5 CONCLUSIONS ON PROJECT INVESTIGATION

Before itemising the conclusions drawn from the entire investigation it was thought that a reiteration of the objectives and problems mentioned in the introductory chapter would be advantageous.

To deflect and, as a result, sort heavy bodies requires a large deflecting force and hence a large jet momentum flux. Current sorting machines use multiple air jets which are noisy, inefficient, require high air pressures and concomitant expensive control valves. It was thought that a water jet could give the required high jet momentum flux at low jet velocities and, if controlled fluidically, might also be cheaper to install and run. Unfortunately no experimental or theoretical guidance was available on the parameters thought to influence the design of the sorting machine or of the effect of various degrees of swirling flow on the physical behaviour and appearance of the swirling liquid jet in air.

The results of the investigation and the conclusions drawn from it were as follows:

(i) Automatic sorting machine design parameters have been defined and a theoretical model of the dynamic interaction between a cylindrical body and a cylindrical liquid jet was formulated. The theoretical model was supported by an experimental programme and the results of the initial investigation compare favourably. With further experimental work it was thought likely that improvements

to the theory would result. No other results could be found on the dynamic movement of a body within a liquid jet to enable a comparison to be made with the results obtained.

(ii) With the assistance of previously published research papers on vortex fluid elements an axial vortex device was designed and built. A novel feature of the device was the centre body geometry. An experimental investigation to determine the operating characteristics of the vortex element showed it to be stable over a large operating range and to operate in a satisfactory manner. The power turn down ratio, however, was disappointing. In spite of the difficult nozzle geometry a two-dimensional theoretical model with a one-dimensional decay pattern was formulated. Previously only a one-dimensional analysis had been performed for an axial vortex element. The initial results from the two-dimensional analysis were thought to be encouraging and a number of useful parameters could be predicted. With the prospective improvements discussed in chapter six it was thought that the theory would enable a more accurate prediction to be made of the various fluid flow parameters, even under difficult flow conditions.

(iii) The experimental transient test results of the axial vortex device showed that the desired operating frequency was not met. The non-dimensional performance however was very fast and it was considered that with some quite realistic improvements the desired frequency could be

achieved.

The investigation achieved almost all of the goals set at its inception; moreover, the theoretical studies made should prove of considerable assistance to future investigations.

6 RECOMMENDATIONS FOR FURTHER WORK

6-1 Recommendations for Further Work on the Movement of a Body Under the Impact of a Cylindrical Liquid Jet

The recommendations for further work on this subject fall broadly into two areas: simple investigations which could give some additional knowledge relatively quickly and longer term research into the process of momentum transfer between the liquid jet and the body.

Short Term Investigations

(a) From the parabolic trajectory of the liquid jet a corrected impact angle of the jet on the body could be calculated together with a corrected drop height, (see Figure 2-9). The cross section of the jet as seen by the body would be elliptical with the ellipse, and angle of impact, changing with downstream distance. These factors could be calculated within the existing theoretical framework.

(b) Examination of the experimental film indicated that even when a small portion of the liquid jet was intercepted by the body the entire jet was deflected through some angle (see Plates 6 and 7). Also it was noted that the bodies did not penetrate the jet as rapidly as predicted (see Figures 2-13 and 2-15). The region of the theory thought to be most in error concerned the body's entry into the jet. One formulation that was thought to bias the jet deflection angle in the desired direction was to obtain the mean jet deflection angle as specified previously but then to apply

this angle to the entire jet.

(c) A jet momentum flux coefficient could be used to acccunt for the fluid losses within the jet impact region. A factor of 0.95 was tried during the initial investigation but the losses were obviously less than 5%. A factor of 0.98 may prove to give better correlation between theory and experiment.

(d) Removing the transparent guide walls used in the experimental investigation may give a more representative fluid flow. Guide wires may constrain the body sufficiently without containing the fluid flow to any great extent.

Long Term Investigations

Almost all the long term investigations envisaged centre on the impact region of the liquid jet on the body.

(a) Eventually it was thought that the three dimensional liquid flow away from the jet impact region would have to be investigated. The distribution of the function $F(\theta, \phi)$ shown by Taylor (1966) was similar in certain respects to a normal distribution, the angle θ controlling the spread parameter (see Figure 2-2). These are interesting aspects, since for a jet impacting normal to a flat surface the function $F(\theta, \phi)$ is a constant. In fact for any axisymmetric surface with the axis of symmetry coincident with the jet axis, the same constant function value would result. It was hoped that for certain common geometries, for example flat plates, cones, spheres

and cylinders, the flow distribution function could be obtained.

(b) If the flow distribution function could be obtained, then the theoretical forces imposed on the body could be calculated and compared with experimental values. The discrepancies should be due to momentum transfer losses. For the particular geometry investigated, a cylindrical jet impinging on a cylindrical body, momentum considerations result in a zero moment about the centre of mass. Any moment measured during an experiment would indicate the magnitude of the resultant shear forces on the body.

(c) To investigate the effects of body rotation would again result in a shear force investigation. It was thought that if the rotation was sufficient, it could significantly alter the pressure distribution within the jet impact region and thus alter the distribution of the fluid and the forces on the body.

It can be seen that the pressure distribution within the jet impact region controls the resulting flow distribution and hence the direct force and shear force distributions on the body.

6-2 Recommendations for Further Work on Proposed Axial Vortex Fluid Device

The recommendations for further work on this subject fall into the same two areas as in section (6-1), short term and long term research investigations.

Short Term Investigations

(a) In its present form the theory assumed the outer stream surfaces to be fixed and coincident with the nozzle boundary. It was considered that this was an unnecessary and restrictive limitation and that stream flow separation from the nozzle boundary could be permitted. It is proposed that the stream boundary should be defined as the nozzle boundary or the zero static pressure line. The computer programme could be rewritten such that the static pressure distribution would be calculated for each station before entering the section devoted to adjusting the stream surface geometry. Before adjusting the stream surface the pressure values for the station would be scanned. If any negative pressures were encountered the zero pressure position would be interpolated and this value would be used as the new fluid flow boundary. The remaining stream surfaces would be positioned and the solution continued as before. This improvement is being implemented on the existing computer programme.

(b) A phenomenon which terminates the existing method of solution is that of fluid stagnation and recirculation (when a negative square root may be demanded). One method of circumventing this problem would be to interrogate the function before obtaining the square root. If the function was found to be negative the results for that station could be diverted into a section where

the negative velocity could be obtained and hence the recirculation boundary point interpolated. The stream surface boundary could be redefined as the recirculation boundary. With a redefined boundary stream surface, control could be returned to the computer programme for a solution.

(c) It was thought that the accuracy of the predicted parameters would be improved if a stream flow shear stress could be incorporated into the theory. This could be accomplished in a similar manner to the angular momentum flux decay shear model. Thus:

$$\gamma_{32(w)} = f_s \rho . V_{2M}^2 / 2$$

The calculated one-dimensional total pressure loss due to the stream flow shear stress would then be added to the total pressure loss due to the tangential shear stress model.

(d) In the discussion section of chapter three it was mentioned that the tangential shear stress model may not be of a suitable form. It was decided to investigate a model based on the mean tangential velocity rather than the mean tangential velocity squared. To retain the non-dimensional character of the friction factor would require the addition of a second velocity term; it was decided to use the average stream velocity of the jet at the orifice.

Long Term Investigations

(a) There are two regions where the analysis of swirling liquid flow is extremely difficult. The first is the mixing region where the stream and control flows meet

and the second is the nozzle orifice region where the boundary conditions are abruptly changed. Attention was concentrated on the confined fluid flow within the mixing region since it was thought that this region would be more amenable to investigation and analysis. An experimental investigation into the mixing region could be most valuable. It was noted that on some of the device geometries tested by Al-Shamma (1971), the control nozzle inlets were not tangential to the stream flow. No advantage was claimed but it was considered that improved mixing could have resulted. In a paper by Al-Shamma 'et al' (1972) a number of precessing vortices were shown in the exit orifice. These vortices could have originated in the mixing region and be due to a particular geometric configuration.

A further reason for investigating this region is that the theoretical model requires details of the angular momentum flux lost during mixing. In particular, the tangential velocity distribution at the exit of the mixing region is of considerable importance because of the influence it has on the resulting flow within the nozzle.

(b) The existing computer programme was written to solve a linear partial differential equation for the stream flow profile. The profile obtained from the solution is valid along an 'n' characteristic (i.e. the coordinate x_2 = constant). The equation could be transformed into a non-linear total differential equation by introducing the stream function defined in Appendix 7.

Equation (3- 10) becomes:

$$\frac{d\psi}{dn}\cdot\frac{d^2\psi}{dn^2} + \left(\frac{d\psi}{dn}\right)^2\cdot\left(k_m - \frac{\cos\lambda}{R}\right) + R^2N = 0$$

The equation can be linearised in terms of $\left(d\psi/dn\right)$ but then has to be integrated twice.

Letting $\left(d\psi/dn\right) = y$ then equation (3- 10) becomes:

$$\frac{dy^2}{dn} + \left(2k_m - \frac{2}{R}\cos\lambda\right)y^2 + 2R^2N = 0$$

The advantage of a total differential equation is that the solution of the equation is not restricted to an 'n' characteristic curve. The equation can be solved at any point along the stream surface providing the incremental values of 'n' are known. Since the 'm' and 'n' characteristic curves are orthogonal and the 'm' surfaces must be known or assumed, then the increments of 'n' can be calculated.

LIST OF REFERENCES

ABRAMOVITCH, G. (1963) 'The Theory of Turbulent Jets'; M.I.T. Press, section 12-8.

AL-SHAMMA, K.A.A. (1971) 'Vortex Amplifiers for Flow Control'; Ph.D. Thesis, University of Sheffield, Dept. of Mech. Eng.

AL-SHAMMA, K.A.A. ROYLE, J.K. BOUCHER, R.F. and ASQUITH, R. (1972) 'Axial Vortex and Coanda Vortex Flow Controllers'; B.H.R.A. Fifth Cranfield Fluidics Conf., Uppsala, Sweden; Paper B2.

BAHRTON, S. (1970) 'A New Type of Fluidic Diverting Valve'; B.H.R.A. Fourth Cranfield Fluidics Conf., Coventry; Paper A4.

BICHARA, R.T. and ORNER, P.A. (1969) 'Analysis and Modelling of the Vortex Amplifier'; A.S.M.E. Trans., Jrnl. of Basic Eng. (Series D); V.91, p.755.

BINNIE, A.M. and HARRIS, D.P. (1949) 'The Application of Boundary-Layer Theory to Swirling Liquid Flow Through a Nozzle'; Quart. Jrnl. Mech. and Applied Math.; V.3, pt.1. p.89.

BINNIE, A.M. HOOKINGS, G.A. and KAMEL, M.Y.M. (1957) 'The Flow of Swirling Water Through a Convergent-Divergent Nozzle'; Jrnl. of Fluid Mech.; V.3, p.261.

BOUCHER, R.F. ASQUITH, R.W. and ROYLE, J.K. (1973) 'Vortex Flow Controllers: Design, Stability and Applications'; Institute of Measurement and Control, Symposium: Power Fluidics for Process Control; University of Surrey, Guildford.

BRIFFA, F.E.J. and DOMBROWSKI, N. (1966) 'Entrainment of Air into a Liquid Spray'; A.I.Ch.E. Jrnl.; V.12, No.4, p.708.

BROWN, F.T. (1964) 'A Combined Analytical and Experimental Approach to the Development of Fluid-Jet Amplifier'; A.S.M.E. Trans., Jrnl. of Basic Eng. (Series D); V.86, p.175.

CHADDA, Y.S. (1972) 'An Investigation of Fluid Mechanics Problems in the Pneumatic Deflection of Particles'; Ph.D. Thesis, The City University (London), Dept. of Mech. Eng.

COOKE, J.C. (1952) 'On Pohlhausen's Method with Application to a Swirl Problem of Taylor'; Jrnl. of Aeronautical Sci.; V.19, p.486.

COUSINS, A.R. (1970) 'The Resulting Density and Velocity Profiles of a Mixed Flow Turbulent Jet'; B.Sc. Project No.379, The City University (London), Dept. of Mech. Eng.

CRANE, C.M. and BURLEY, D.M. (1974) 'Numerical Studies for Viscous Swirling Flow Through Annular Diffusers, Part 2, Results'; Jrnl. of Eng. Math.; V.8, p.193.

DUDA, J.L. and VRENTAS, J.S. (1968) 'Laminar Liquid Jet Diffusion Studies'; A.I.Ch.E. Jrnl.; V.14, No.2 p.286.

DUFF, J. FOSTER, K. and MITCHELL, D.G. (1965) 'Some Experiments on the Vortex Valve'; First Int. Conf. on Fluid Logic and Amplification, Cranfield; Paper C1.

FISHER, M.J. and THOMSON, A. (1968) 'Some Measurements of Liquid Wall Attachment Diverter Valve Characteristics'; B.H.R.A. Third Cranfield Fluidics Conf., Turin, Italy; Paper B4.

FOSTER, K. (1970) 'A Bistable Fluid Amplifier Working on Oil'; Fluidistorkommitten Rapport FK70205; Sveriges Mekanförbund, Stockholm, Sweden.

FOSTER, K. and PARKER, G.A. (1970) 'Fluidics Components and Circuits'; Wiley-Interscience, New York.

GARMENDIA, L.A. (1975) 'An Experimental Study of the Combined Effects of an Electrostatic Field and Air Stream on Water Jet Break-up'; Ph.D. Thesis, The City University (London), Dept. of Mech. Eng.

GOLDSTEIN, S. (Ed.) (1938) 'Modern Developments in Fluid Dynamics'; Dover, (ARC Fluid Motion Panel).

GOSMAN, A.D. PUN, W.M. RUNCHAL, A.K. SPALDING, D.B. WOLFSHTEIN, M. (1969) 'Heat and Mass Transfer in Recirculating Flows'; Academic Press, New York; section 2-21.

GRANT, R.P. (1965) 'Newtonian Jet Stability'; Ph.D. Thesis, University of Rochester (New York), Dept. of Chem. Eng.

GRANT, R.P. and MIDDLEMAN, S. (1966) 'Newtonian Jet Stability'; A.I.Ch.E. Jrnl.; V.12, No.4, p.669.

HARVEY, J.F. and HERMANDORFER, A.W. (1943) [WADC Tech. Report 56-344; from PUTMAN 'et al' (1956)].

HASSON, D. (1956) 'A Study of the Formation and Disintegration of Liquid Sheets Produced by Spray Nozzles'; Ph.D. Thesis, University of London, Dept. of Chem. Eng.

HODGKINSON, T.G. (1950) 'Control by Surface Tension of a Conical Fluid Sheet Jet'; Porton Tech. Paper No.174; Chemical Defence Est., Porton Down, Salisbury.

HUGHES, W.F. and GAYLORD, E.W. (1964) 'Basic Equations of Engineering Science'; Schaum Outline Series, McGraw-Hill, New York.

JACOBS, O.L.R. (1974) 'Introduction to Control Theory'; Oxford University Press, Oxford; Ch.1, p.20.

JOHNSTON, J.P. (1960) 'On the Three-Dimensional Turbulent Boundary Layer Generated by Secondary Flow'; A.S.M.E. Trans., Jrnl. of Basic Eng. (Series D); V.82, p.233.

KELLEY, L.R. and BOOTHE, W.A. (1968) 'Hydraulic Fluidics'; A.S.M.E., Fluids Eng. Div.; Paper 68-WA/FE-26.

KING, M.K. ROTHFUS, R.R. and KERMODE, R.I. (1969) 'Static Pressure and Velocity Profiles in Swirling Incompressible Tube Flow'; A.I.Ch.E. Jrnl.; V.15, No.6, p.837.

LANCE, G.N. and PERRY, R.L. (1953) 'Waterbells'; Proc. Physical Soc., (B); V.66, p.1067.

LEVICH, V.G. (1962) 'Physiocochemical Hydrodynamics'; Prentice Hall; section 123 to 126.

McCLOY, D. and STEVENSON, I.J. (1972) 'Some Experiments with Oil Hydraulic Vortex Valves'; B.H.R.A. Fifth Cranfield Fluidics Conf., Uppsala, Sweden; Paper D6.

MIESSE, C.C. (1955)[Jet Propulsion, V.25, p.525; from GARMENDIA (1975)].

MODER, J.J. and OSWALT, J.H. (1959) 'An Investigation of Some Factors Affecting the Hand Quality Picking of Small Objects'; Jrnl. of Industrial Eng.; (May - June).

MORRISON, J.L.M. and CROSSLAND, B. (1970) 'An Introduction to the Mechanics of Machines'; Longman, London; Ch.6, p.399.

NEVE, R.S. (1965) 'A Short Review of Past Research into the Properties of Fluid Jet Amplifiers'; B.H.R.A., Report TN838.

NEVE, R.S. (1971) 'An Investigation of Factors Influencing the Static and Dynamic Performance of Fluid Vortex Amplifiers'; Ph.D. Thesis, The City University (London), Dept. of Mech. Eng.

NISSAN, A.H. and BRESAN, V.P. (1961) 'Swirling Flow in Cylinders'; A.I.Ch.E. Jrnl.; V.7, No.4, p.543.

NOVIKOV, I.I. (1948) 'Atomisation of Liquids by Centrifugal Nozzles'; The Engineers Digest, (March 1949); V.10, No.3, p.72.

OHTA, M. (1973) 'Diverter Valve (Air to Water Flow Converter)'; Institute of Measurement and Control, Symposium: Power Fluidics for Process Control; University of Surrey, Guildford.

OTSAP, B.A. (1968) 'The Vortex Pressure Amplifier Characteristics'; I.F.A.C. Symposium on Fluidics, London; Paper B3.

OZGU, M.R. and STENNING, A.H. (1971) 'Switching Dynamics of Bistable Fluidic Amplifiers with Low Setbacks'; A.S.M.E., Jrnl. of Dynamic Systems, Measurement and Control; Paper No.71-WA/Flcs-8.

PAI, SHIH-I. (1954) 'Fluid Dynamics of Jets'; Van-Nostrand; p.21.

PEARCE, I.D. and LICHTAROWICZ, A. (1971) 'Discharge Performance of Long Orifices with Cavitating Flow'; Second Fluid Power Symposium, University of Surrey, Guildford; Paper D2.

PEICHEV, V. (1972) 'Experimental Investigations on Water-Operating Bistable Fluidic Device Having Two Input'; Fourth International Fluidics Conf., Varna, Bulgaria; Paper B25.

PENNY, P.H.G. (1973) 'Liquid/Gas Digital Fluidic Elements Applied to Sorting Machines'; Research Memo. ML63, The City University (London), Dept. of Mech. Eng.

PUTMAN, A. 'et al' (1957) 'Injection and Combustion of Liquid Fuels'; Batelle Memorial Institute, WADC Tech. Report 56-344.

RAIMONDI, P. and TOOR, H.L. (1959) 'Interfacial Resistance in Gas Absorption'; A.I.Ch.E. Jrnl.; V.5, No.1, p.86.

RECHTEN, A.W. (1967) 'Flow Stability in Bistable Fluid Elements'; B.H.R.A. Second Cranfield Fluidics Conf., Cambridge University; Paper B6.

RIMMER, R. (1975) 'A Low Pressure Flow Distributor for Jet Engine Combustors'; B.H.R.A. Seventh Cranfield Fluidics Conf., Stuttgart, Germany; Paper E1.

ROSENZWEIG, M.L. LEWELLEN, W.S. and ROSS, D.H. (1964) 'Confined Vortex Flows with Boundary-Layer Interaction'; A.I.A.A. Jrnl.; V.2, No.12, p.2127.

ROYLE, J.K. and HASSAN, M.A. (1967) 'Characteristics of Vortex Devices'; B.H.R.A. Second Cranfield Fluidics Conf., Cambridge University; Paper D4.

RYOICHI, Y. (1968) 'Fluid Logic Device with Auxiliary Jet'; B.H.R.A. Third Cranfield Fluidics Conf., Turin, Italy; Paper F7.

SARPKAYA, T. (1965)[Proc. Fluid Amp. Symposium, Harry Diamond Labs.; V.2, p.185.; from OZGU and STENNING (1971)].

SCHAUB, W. (1965) 'Electronic Colour Sorting'; Industrial Electronics, (Oct.); p.462.

SCRIVEN, L.E. and PIGFORD, R.L. (1958) 'On Phase Equilibrium at the Gas-Liquid Interface During Absorption'; A.I.Ch.E. Jrnl.; V.4, No.4, p.439.

SCRIVEN, L.E. and PIGFORD, R.L. (1959) 'Fluid Dynamics and Diffusion Calculations for Laminar Liquid Jets'; A.I.Ch.E. Jrnl.; V.5, No.3, p.397.

SHINN, J.N. and BOOTHE, W.A. (1964) 'Connecting Elements into Circuits and Systems'; Control Engineering, (Sept.).

SIMSON, A.K. (1966) 'Gain Characteristics of Subsonic Pressure-Controlled, Proportional, Fluid Jet Amplifiers'; A.S.M.E. Trans., Jrnl. of Basic Eng. (Series D.); V.88, p.295; Paper No.64-WA/Aut-2.

SKOOG, A.I. (1972) 'Oil Hydraulic Fluidic Amplifiers'; B.H.R.A. Fifth Cranfield Fluidics Conf., Uppsala, Sweden; Paper D7.

SO, K.L. (1967) 'Vortex Phenomena in a Conical Diffuser'; A.I.A.A. Jrnl.; V.5, No.6, p.1072.

SOO, S.L. (1970) 'Core Velocity Distribution in Swirling Pipe Flow'; Zeit. Angew. Math.; V.21, No.1, p.125.

SYRED, N. ROYLE, J.K. and TIPPETTS, J.R. (1968) 'Optimization of High Gain Vortex Devices'; B.H.R.A. Third Cranfield Fluidics Conf., Turin, Italy; Paper J3.

TAFT, C.K. (1967) 'Hydraulic Fluidics'; S.A.E. Paper No. 670736.

TAPLIN, L.B. and SELENO, A.A. (1970) 'Dynamic Equivalent Circuit for a Vortex Amplifier'; B.H.R.A. Fourth Cranfield Fluidics Conf., Coventry; Paper B1.

TAYLOR, A.F. (1970) 'Vortex Devices in Aircraft Fluid Systems'; B.H.R.A. Fourth Cranfield Fluidics Conf., Coventry; Paper B2.

TAYLOR, G.I. (1948) 'The Mechanics of Swirl Atomisers'; International Cong. Applied Mech.; V.2, p.280

TAYLOR, G.I. (1949) 'The Boundary Layer in the Converging Nozzle of a Swirl Atomiser'; Quart. Jrnl. Mech. and Applied Math.; V.3, Pt.2 (1950), p.129.

TAYLOR, G.I. (1959) 'The Dynamics of Thin Sheets of Fluid'; (Parts 1,2 and 3); Proc. of the Royal Soc. (A); V.253.

TAYLOR, G.I. (1960) 'Formation of Thin Flat Sheets of Water'; Proc. of the Royal Soc. (A); V.259, p.1.

TAYLOR, G.I. (1966) 'Oblique Impact of a Jet on a Plane Surface'; Phil. Trans. of the Royal Soc. (A); V.260, p.96.

VAVRA, M.H. (1960) 'Aero-Thermodynamics and Flow in Turbomachines'; John Wiley and Sons, New York.

VITMAN, L.A. (1969) 'Problems of Heat Transfer and Hydraulics of Two-Phase Media'; Pergamon Press; (Ed. by S.S.KUTATELADZE, translated by O.M.BLUNN).

WATERS, C.J. (1969) 'The Interaction of Jets of Different Fluids in a Fluid Amplifier'; B.Sc. Project No.351, The City University (London), Dept. of Mech. Eng.

WEBER, C. (1931) [Zeit. Angew. Math. Mech., V.11, p.136; from GARMENDIA (1975)].

WEINBERG, S. (1952) 'Heat Transfer to Low Pressure Sprays of Water in a Steam Atmosphere'; Proc. Institution Mech. Engrs. (B); V.1B, p.240.

WIRASINGHE, N.E.A. (1975) 'Swirling and Non-Swirling Flow in Conical Diffusers'; Ph.D. Thesis, The City University (London), Dept. of Mech. Eng.

WOLFSOHN, D.L. (1970) 'The Atomisation of Viscous Liquids by Swirl Spray Pressure Nozzles'; Ph.D. Thesis, University of Leeds, Dept. of Chem. Eng.

WOODS, R.L. (1972) 'A Flueric Gas-to-Liquid Interface Amplifier'; A.S.M.E., Fluids Eng. Div.; Paper 72-WA/Flcs-11.

WORMLEY, D.N. (1969) 'An Analytical Model for the Incompressible Flow in Short Vortex Chambers'; A.S.M.E. Trans., Jrnl. of Basic Eng. (Series D); V.91, p.264.

WORMLEY, D.N. and RICHARDSON, H.H. (1968) [M.I.T. Tech. Report No.70167-1, Dept. of Mech. Eng.; from SKOOG (1972)].

WORMLEY, D.N. and RICHARDSON, H.H. (1970) 'A Design Basis for Vortex-Type Fluid Amplifiers Operating in the Incompressible Flow Regime'; A.S.M.E. Trans., Jrnl. of Basic Eng. (Series D); V.92, p.369.

YOUSSEF, T.E.A. (1966) 'Some Investigations on the Rotating Flow with a Recirculation Core in Straight Pipes'; A.S.M.E., Paper No.66-WA/FE-36.

APPENDIX 1

LIQUID JET BREAK-UP LENGTH

Liquid Jet Break-up Length

The break-up of a coherent liquid jet into droplets is a complicated phenomenon. The general consensus of opinion (Putnam 'et al', 1957; Levich, 1962; Garmendia, 1975) is that surface instabilities, which can be due to various causes, such as surface tension, nozzle vibration, fluid turbulence and jet velocity profile, grow on the jet surface until the jet disintegrates. The two types of jet surface instability mentioned in many research papers are axisymmetric or varicose deformations and long wave length, (in comparison with the jet radius), arbitrary or wave-like deformations, (see Figure A1 - 1).

Levich (1962) considered various types of instability on the jet surface and obtained different jet break-up lengths. His equations are complicated but under certain conditions simplify. It is the simplified equations that are used in this appendix.

For low flow velocities, neglecting viscosity and assuming axisymmetric deformations (Levich, 1962: p.634):

$$L \triangleq v_j t = 8.46\, v_j \left(\rho r_o^3/\sigma\right)^{1/2} \qquad -(A1\text{-}1)$$

Equation (A1-1) is valid providing:

$$\left(\sigma r_o/\rho v^2\right)^{1/2} >> 1 \qquad -(A1\text{-}2)$$

For low flow velocities, arbitrary deformations and including viscosity:

$$L = v_j \left[\frac{2 + 3v\left(2\rho/\sigma r_o\right)^{1/2}}{\left(\sigma/2\rho r_o^3\right)^{1/2}}\right] \qquad -(A1\text{-}3)$$

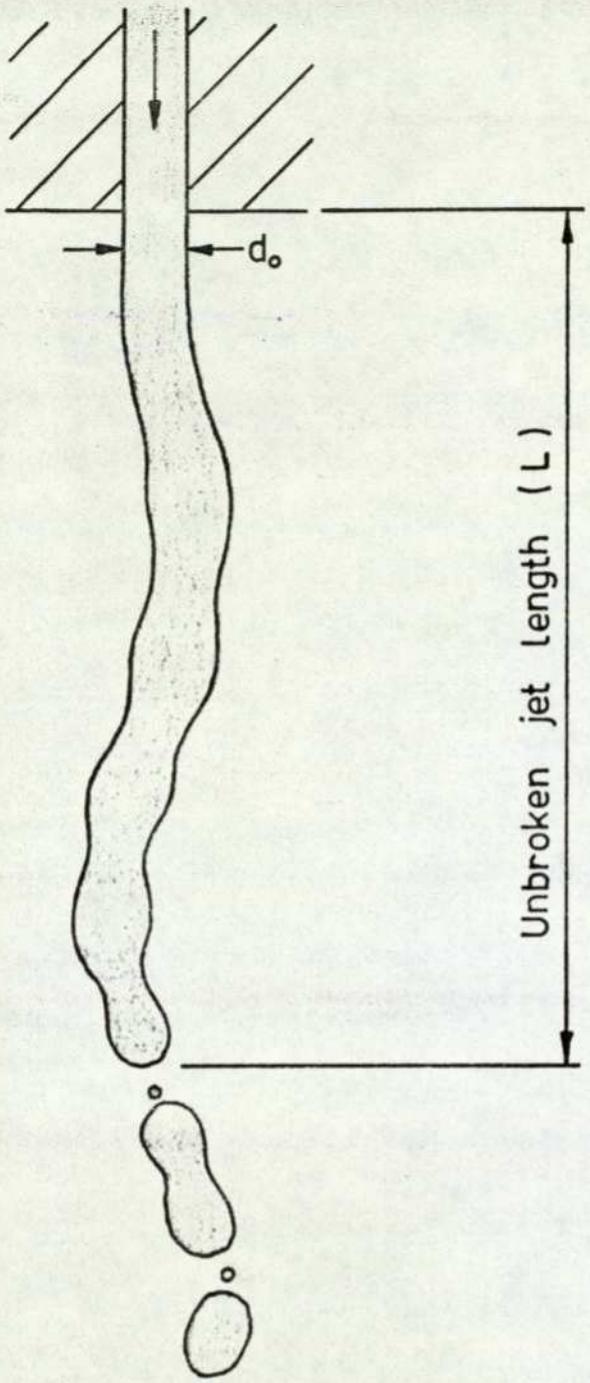

Liquid jet

Figure A1-1

Equation (A1-3) is valid providing the inequality (A1-2) is satisfied.

At high jet velocities:

$$L \triangleq (\rho/\rho_{gas})^{\frac{1}{2}} \cdot r_o \qquad -(A1\text{-}4)$$

Vitman (1969) took an equation of Weber's (1931) for the time at which the jet began to disintegrate and then correlated various experimental results to obtain a value of K in equation A1-5, (see Vitman, 1969: p.419):

$$t_o \frac{\sigma^2 \rho}{27\mu^3} = K\left[\left(\frac{2}{9}\cdot\frac{\sigma\rho r_o}{\mu^2}\right)^{\frac{3}{2}} + \frac{2}{9}\cdot\frac{\sigma\rho r_o}{\mu^2}\right] \qquad -(A1\text{-}5)$$

The equation (A1-5) only applies when $(\mu/\mu_{gas}) \gg 1$.
Vitman defined two critical times (t_{o1} and t_{o2}) and two critical velocities (V_{Jo1} and V_{Jo2}) to determine whether jet break-up was due to axisymmetric or wave-like oscillations. For the time to jet break-up due to axisymmetric deformations, (t_{o1}), Vitman recommended:

K = 10 , in equation (A1-5)

$$5 \times 10^{-3} \leq \left(\frac{\sigma\rho r_o}{\mu^2}\right) \leq 2 \times 10^{5}$$

For the time to break-up due to wave-like deformations:

K = 1.22 , in equation (A1-5)

$$1 \times 10^{2} \leq \left(\frac{\sigma\rho r_o}{\mu^2}\right) \leq 2 \times 10^{5}$$

The critical jet velocities (V_{Jo1} and V_{Jo2}) were obtained from:

$$\frac{V_{J0}/\mu}{\sigma}\cdot\left(\frac{\rho_{gas}}{\rho}\right)^{\frac{1}{2}} = A\left[\left(\frac{\sigma\rho r_o}{\mu^2}\right)\cdot\left(\frac{\mu}{\mu_{gas}}\right)^{m}\right]^{n} \qquad \text{—(A1-6)}$$

Vitman states that equation (A1-6) is valid for the parameter ranges:

$$0.33 \leq (\mu/\mu_{gas}) \leq 5.0 \times 10^{4}$$

$$1.0 \leq (\rho/\rho_{gas}) \leq 1.0 \times 10^{3}$$

$$1.0 \times 10^{-2} \leq (\sigma\rho r_o/\mu^2) \leq 2.0 \times 10^{5}$$

The exponent m was taken as 0.5.

From equation (A1-6) in conjunction with Figure A1-2:

The exponent n = -0.58 , except between the points 2 and 3 on Figure A1-2.

The constant A = 15, for the line 1-2-5, (see Figure A1-2).

A = 4 for the line 3-4 (see Figure A1-2).

Vitman then proposed the equation:

$$L = t v_J \qquad \text{—(A1-7)}$$

For liquid jets in air he gives the following expressions for the time to jet break-up. For axisymmetric deformations:

$$t = t_{o1} \qquad \text{—(A1-8)}, \quad \text{for} \quad v_J \leq v_{J01}$$

$$t = 0.23 t_{o1}\left(\frac{v_J}{v_{J01}} - 1\right)^{-0.6} \qquad \text{—(A1-9)}$$

for $v_J > 1.1\, v_{J01}$ and $t > t_{o2}$

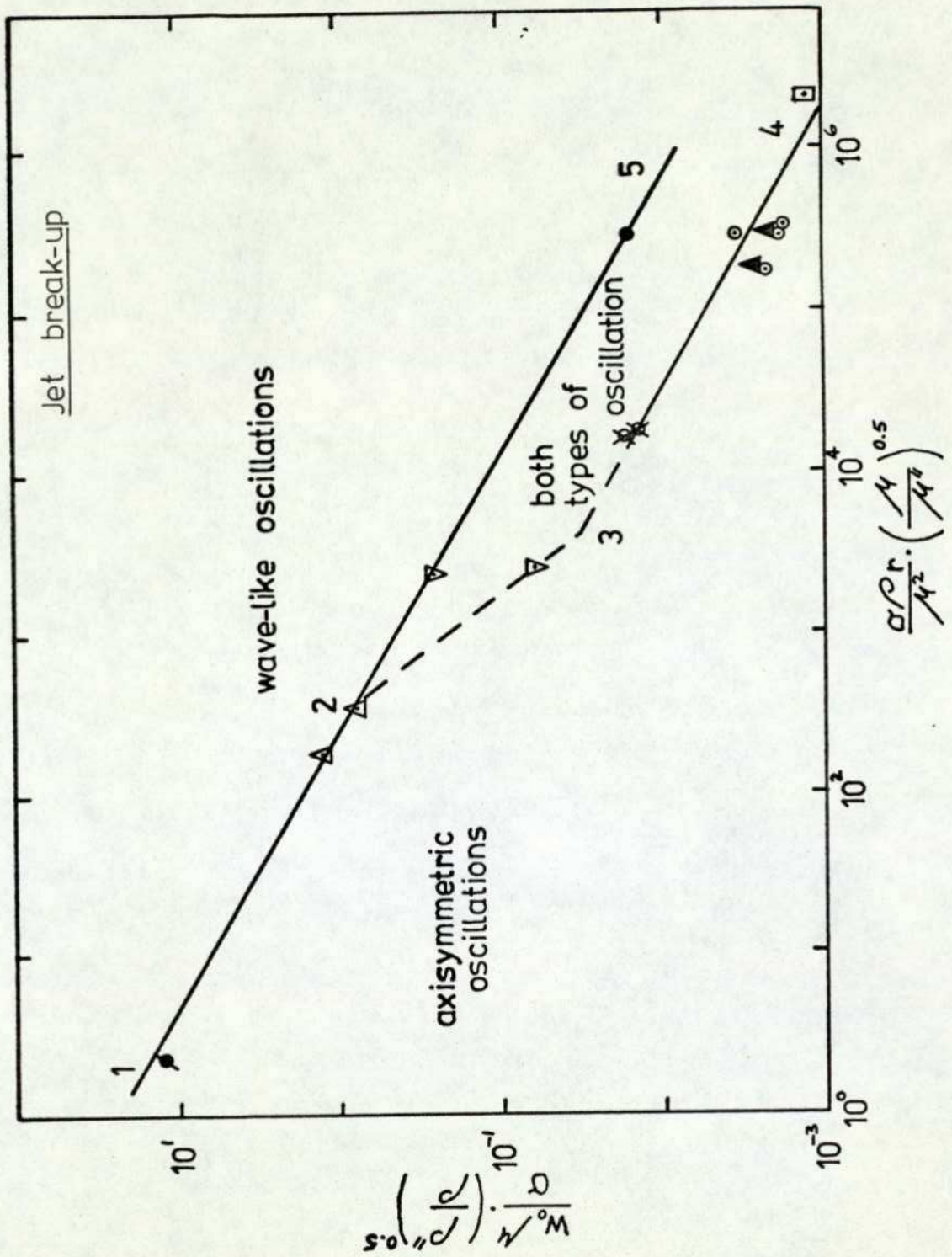

(from Vitman (1969)).

Figure A1–2

Symbols for Fig. A1-2.

- castor oil
- glycerine
- gas oil
- water

} in air. — A. Genlein (1936).

- water in air
- water in paraffin

} — Ya. Trotskii (1938).

- water in air. — L.F. Vereshchagin, A.A. Semerchan, S.S. Sekoyan (1959).
- water in air. — V.G. Dement'ev (1954).

For wave-like deformations:

$$t = t_{o2} \qquad \text{—(A1-10)}, \quad \text{for} \quad V_J \leq V_{J02}$$

$$t = 0.17 t_{o2} \left(\frac{V_J}{V_{J02}} - 1 \right)^{-1.0} \qquad \text{—(A1-11)}$$

for $V_J > 1.1 V_{J02}$

To obtain the jet break-up length the appropriate equation for time is substituted into equation (A1-7).

From Grant's (1965) thesis the simplified form of his rather complicated equation was used (Grant, 1965: p.181):

$$\frac{L}{d_o} = 8.51 \left(We^{\frac{1}{2}} \right)^{0.64} \qquad \text{—(A1-12)}$$

where $We = \rho d_o V_J^2 / \sigma$

Two sets of sample calculations were made for the jet nozzle size to be used and at the upper and lower jet velocity range expected.

$r_o = 4.0 \times 10^{-3}$ m. ; $\sigma = 0.073$ N/m.

$\rho = 999$ kg/m^3 ; $\rho_{gas} = 1.205$ kg/m^3

$\mu = 1.002 \times 10^{-3}$ Ns/m^2 ; $\mu_{gas} = 1.81 \times 10^{-5}$ Ns/m^2

Taking $V_J = 10$ m/s. Levich's equations give:

Axisymmetric oscillations (equation (A1-1)):

$$L \triangleq 8.46 \times 10 \left[\frac{999 \left(4 \times 10^{-3} \right)^3}{0.073} \right]^{\frac{1}{2}} = 0.25 \text{ m.}$$

Arbitrary oscillations:

$$L = 10\left[\frac{2 + 3\left(\frac{1.002\times10^{-3}}{999}\right)\left(\frac{2\times999}{0.073\times4\times10^{-3}}\right)^{1/2}}{\left(\frac{0.073}{2\times999\times(4\times10^{-3})^{3}}\right)^{1/2}}\right]$$

$$= 0.843 \text{ m.}$$

Equations (A1-1) and (A1-3) are valid since in equality (A1-2) is satisfied, as shown:

$$\left[\frac{0.073\times4\times10^{-3}}{999\left(\frac{1.002\times10^{-3}}{999}\right)^{2}}\right]^{1/2} = 540$$

At high jet velocities, (equation (A1-4)):

$$L \triangleq \left(\frac{999}{1.205}\right)^{1/2}\times4\times10^{-3} = 0.115 \text{ m.}$$

For $V_J = 20 m/s$ equations (A1-1) and (A1-3) change to:

$$L \triangleq 0.148 \text{ m.} \qquad (A1\text{-}1)$$

$$L \triangleq 1.686 \text{ m.} \qquad (A1\text{-}3)$$

Before Vitman's equations (A1-5) and (A1-6) were applied the parameters were checked:

$$(\mu/\mu_{gas}) = 55.4$$

$$(\rho/\rho_{gas}) = 829$$

$$\left(\frac{\sigma\rho r_o}{\mu^2}\right) = 2.92\times10^{5}$$

The parameter $(\sigma\rho r_o/\mu^2)$ exceeds the recommended maximum value but examination of Figure A1-2 indicates that all the data points shown for water jets injected into air the

parameter equals or exceeds the maximum value recommended. Therefore the calculations were continued but close agreement was not expected. The critical times for axisymmetric and arbitrary oscillations were respectively, (equation (A1-5)):

$$t_{o1} = \frac{10 \times 27 (1.002 \times 10^{-3})^3}{(0.073)^2 \times 999} \left[\left(\frac{2}{9} \times 2.92 \times 10^5 \right)^{3/2} + \left(\frac{2}{9} \times 2.92 \times 10^5 \right) \right]$$

$$= 0.841 \text{ s.}$$

$$t_{o2} = \frac{1.22 \times 27 (1.002 \times 10^{-3})^3}{(0.073)^2 \times 999} \left[\left(\frac{2}{9} \times 2.92 \times 10^5 \right)^{3/2} + \left(\frac{2}{9} \times 2.92 \times 10^5 \right) \right]$$

$$= 0.1026 \text{ s.}$$

And from equation (A1-6) the critical velocities are:

$$V_{so1} = \frac{A \times 0.073}{1.002 \times 10^{-3} (1/829)^{1/2}} \left[2.92 \times 10^5 \times (55.4)^{1/2} \right]^n$$

$$= 4 \times 2095 \left(21.75 \times 10^5 \right)^{-0.58}$$

$$= 1.773 \text{ m/s.}$$

$$V_{so2} = 15 \times 2095 \left(21.75 \times 10^5 \right)^{-0.58}$$

$$= 6.65 \text{ m/s.}$$

Since for the jet velocities of 10 and 20 m/s. both exceed V_{J02} , then the appropriate time equation is (A1-11). This was substituted into equation (A1-7) and the jet break-up lengths obtained:

V_J = 10 m/s.

$$L = 10 \times 0.17 \times 0.1026 \left(\frac{10}{6.65} - 1 \right)^{-1.0}$$

$$= 0.3475 \text{ m.}$$

V_J = 20 m/s.

$$L = 20 \times 0.17 \times 0.1026 \left(\frac{20}{6.65} - 1 \right)^{-1.0}$$

$$= 0.1738 \text{ m.}$$

Equation (A1-12) from Grant's thesis gives:

V_J = 10 m/s.

$$L = 8 \times 10^{-3} \times 8.51 \left[\left(\frac{999 \times 8 \times 10^{-3} \times 10.0^2}{0.073} \right)^{\frac{1}{2}} \right]^{0.64}$$

$$= 1.329 \text{ m.}$$

V_J = 20 m/s.

$$L = 2.074 \text{ m.}$$

APPENDIX 2

THE PHYSICAL PROPERTIES OF THE JET FLUID

The Physical Properties of the Jet Fluid

Fluid: London tap water.

Properties: (An average of five samples, September 1974).

Temp.(°C)	18	20	22	Tolerance	Measurement method
DENSITY (gm/cm^3)	0.999	0.999	0.998	± 0.001	Density balance
SURFACE TENSION (dynes/cm)	74.6	73.6	73.2	± 2%	Stalagometer
DYNAMIC VISCOSITY (Ns/m^2)	1.09×10^{-3}	1.03×10^{-3}	1.01×10^{-3}	± 1%	'U' tube viscometer

DISTILLED WATER

SURFACE TENSION (dynes/cm)		72.75		± 2%	Stalagometer
DYNAMIC VISCOSITY (Ns/m^2)		1.002×10^{-3}		± 1%	'U' tube viscometer

CHEMICAL ANALYSIS: (Courtesy of the Metropolitan Water Board. An average of 357 samples, September 1974).

Ammoniacal Nitrogen	0.039	mg/l.
Albuminoid Nitrogen	0.080	mg/l.
Nitrate Nitrogen	7.4	mg/l.
$CaCO_3$	276.0	mg/l.
Magnesium	5.7	mg/l.
Chloride as Cl.	41.0	mg/l.
Phosphate as PO_4	3.0	mg/l.
Silicate as SiO_2	9.0	mg/l.
Sulphate as SO_4	62.0	mg/l.
Fluoride as F	0.15	mg/l.
Surface active material as Manoxol O.T.	0.02	mg/l.
pH	7.8	

APPENDIX 3

TOTAL HEAD TUBE CALIBRATION EXPERIMENT

Total Head Tube Calibration Experiment

The hypodermic total head tube was to be used to measure the velocity of a liquid jet.

For the total head tube it was assumed that:

$$\Delta p = \rho v_J^2 / 2$$

and therefore if the electrical output of the transducer was directly proportional to the pressure difference then:

$$v_J \propto (2E/\rho)^{1/2}$$

The electrical output from the transducer was measured by two different methods. For the body deflection experiments an oscilloscope was used and for the jet velocity profile measurements of the vortex element a digital voltmeter was used. In both cases the calibration experiment used a liquid jet with a flat topped velocity profile.

For a specific electrical output from the transducer, measured by an oscilloscope, a volume of liquid was collected, weighed and the collection time noted. Thus since the area of the orifice was known, the mean jet velocity could be calculated and calibrated against the measured transducer signal.

Transducer: Bell and Howell

Type: 4 - 366 - 0105 - 03M0; Serial No. L 41468.

Oscilloscope: Tektronix

Type: 564; Serial No. 100724 (Time base:Type 3B3, Serial No. 100130. Dual trace differential amplifier: Type 3A3, Serial No.001596).

Stabilized power supply: Farnell

Type: L30A ; Serial No.000729

	OSCILLOSCOPE READING	EXPERIMENT	
E (mv)	$\left(\frac{2E}{\rho}\right)^{\frac{1}{2}} \times 10^{-2}$ $(mV/kg.m^3)^{\frac{1}{2}}$	Q $(m^3/s) \times 10^{-4}$	V_J (m/s)
1	4.47	2.454	4.081
2	6.3	3.333	5.543
4	8.94	4.873	8.104
6	10.95	5.739	9.545
8	12.65	6.580	10.942
10	14.14	7.404	12.312
14	16.73	8.863	14.738
18	18.97	10.174	16.920
22	20.98	10.908	18.140

For more accurate velocity profile measurements a digital voltmeter was used. In this case the flow was measured by noting a Rotameter scale reading together with the transducer voltage displayed on a digital voltmeter. The Rotameter had previously been calibrated (see Appendix 8).

Digital Voltmeter: Solatron

Type: LM. 1420.2 Serial No. 151210

Flow measurement: Rotameter

Type: Metric 65 P , (Korannite float).

DIGITAL VOLTMETER READINGS		ROTAMETER SCALE READING		
E (mV)	$\left(\frac{2E}{\rho}\right)^{\frac{1}{2}}$		Q (l/s)	V_J (m/s)
0.6	3.46	1	0.1833	3.06
1.03	4.54	2	0.2381	3.97
1.56	5.59	3	0.2933	4.89
2.18	6.60	4	0.3454	5.76
2.89	7.60	5	0.3988	6.65
3.74	8.65	6	0.4513	7.52
4.70	9.70	7	0.5040	8.40
5.82	10.79	8	0.5642	9.40
7.14	11.95	9	0.6221	10.37
8.55	13.08	10	0.6875	11.46
10.10	14.21	11	0.7517	12.53
11.82	15.38	12	0.8029	13.38
13.71	16.56	13	0.8802	14.67
15.77	17.76	14	0.9330	15.55
18.02	18.98	15	0.9936	16.56

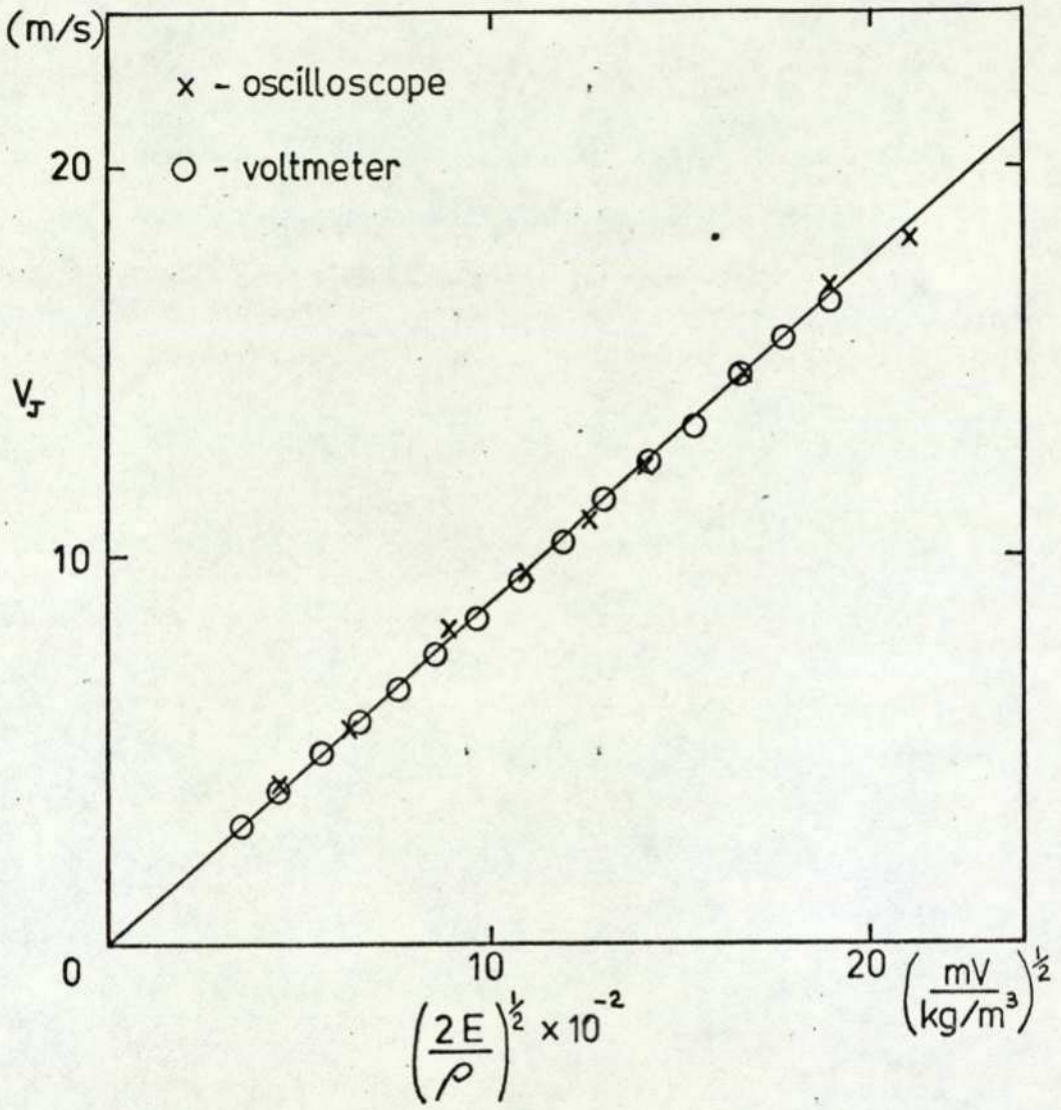

Total head tube calibration

Figure A 3-1

Hypodermic total head tube

PLATE 15

APPENDIX 4

PROPRIETARY EQUIPMENT LIST - CYLINDRICAL BODY DEFLECTION EXPERIMENTS

Proprietary Equipment List - Cylindrical Body Deflection Experiments

High Speed Camera: Hy-Cam

Camera speed: 400 or 500 frames/second, timing marks on the film edge from a Hy-Cam Timing Light Generator.

Lens aperture: f5.6

Lightmeter: Hy-Cam

Film: Ilford Mk.V , Type 782 (16 m.m.)

Developing chemicals: 'Exprol' and 'Amfix'

(from May and Baker, Dagenham).

For a list of the equipment used to measure the liquid jet's velocity, see Appemdix 3.

APPENDIX 5

CYLINDRICAL BODY DEFLECTION EXPERIMENTS

- SOURCE DATA

Cylindrical Body Deflection

Experiments - Source Data

Jet velocity	Body Diameter	Drop height	Mass	Displacements Horizontal	Vertical	Rotary	Time
Vj	dp	h	mp	x	y	θ°	t
(m/s)	(m)	(m)	(kg)	(m m)	(m m)		(ms)
9	0.1	0.175	0.1320	0	0	0	0
				0.3	16.5	1.2	10
				3.7	35.5	1.8	20
				10.2	54.6	2.9	30
				19.0	74.8	4.9	40
				29.4	97.5	5.9	50
				40.3	120.3	8.1	60
				51.3	144.1	9.4	70
				62.3	169.5	10.9	80
			0.2316	0	0	0	0
				0.2	11.9	- 3.0	7.5
				2.5	24.1	- 7.5	17.5
				5.5	39.2	-12.7	27.5
				10.7	51.6	-17.8	37.5
				17.2	65.4	-24.8	47.5
				26.1	80.1	-32.4	57.5
				34.7	93.4	-41.2	67.5
				43.4	106.8	-51.0	77.5
				53.2	119.2	-61.7	87.5
				61.4	133.0	-72.5	97.5

Vj (m/s)	dp (m)	h (m)	mp (kg)	x (m m)	y (m m)	θ°	t (ms)
		0.095	0.1320	0	0	0	0
				- 0.1	7.7	0.2	6
				1.9	21.3	1.6	16
				5.5	34.3	3.5	26
				11.5	48.3	6.2	36
				20.2	63.1	10.0	46
				32.1	79.6	12.6	56
				45.2	98.4	16.3	66
				57.5	117.7	19.2	76
				70.0	137.3	21.8	86
9	0.1	0.095	0.2316	0	0	0	0
				0	7.7	0.1	2
				0.3	14.8	-0.2	12
				1.5	29.4	0.1	22
				4.7	42.6	0.7	32
				9.1	55.9	3.6	42
				14.9	71.1	6.3	52
				20.7	85.2	9.7	62
				28.1	102.8	12.1	72
				34.1	118.1	15.5	82
				41.3	135.7	18.1	92
	0.05	0.20	0.0581	0	0	0	0
				0.5	10.7	-0.8	5
				2.8	27.1	1.3	10
				6.7	30.1	0.3	15

Vj (m/s)	dp (m)	h (m)	mp (kg)	x (m m)	y (m m)	θ°	t (ms)
				10.4	42.0	1.3	20
				15.0	52.4	1.6	25
				24.3	73.7	1.6	35
				34.0	95.7	0.1	45
		0.120		0	0	0	0
				0.1	6.7	1.5	6
				1.5	13.9	6.3	12
				4.1	20.5	11.3	18
				6.6	25.4	20.3	24
				10.4	30.9	31.2	30
				14.6	35.5	40.7	36
				20.4	42.3	48.7	42
				28.4	49.1	58.6	48
				37.3	57.0	70.5	56
				50.8	69.3	84.5	66
				62.6	82.7	99.2	76
12	0.1	0.175	0.1320	0	0	0	0
				0.8	16.7	-0.5	10
				4.6	34.2	1.8	20
				13.5	48.4	0.2	30
				26.3	65.7	-0.4	40
				42.3	84.0	-2.2	50
				61.1	102.8	-4.4	60
				79.1	122.7	-7.4	70
				97.9	143.1	-10.8	80

Vj (m/s)	dp (m)	h (m)	mp (kg)	x (m m)	y (m m)	θ°	t (ms)
12.0	0.1	0.175	0.2316	0	0	0	0
				-0.2	5.2	0.8	5
				-0.2	15.2	3.0	15
				1.0	25.5	4.9	25
				4.1	33.4	7.7	35
				8.3	42.3	11.9	45
				16.0	51.4	15.7	55
				26.8	60.6	20.5	65
				39.2	71.6	24.6	75
				54.2	82.7	28.6	85
				72.0	97.2	31.6	95
				87.6	111.0	35.2	105
				105.3	126.2	39.1	115
				121.5	142.0	41.7	125
		0.095	0.1320	0	0	0	0
				0.1	6.8	0.1	6
				2.7	18.8	2.8	16
				8.7	30.7	6.1	26
				19.0	40.5	9.6	36
				33.8	51.9	13.9	46
				53.6	65.1	17.1	56
				75.9	77.7	18.6	66
				101.3	92.7	19.6	76
				126.7	109.6	20.7	86
				153.1	127.5	20.7	96
				179.6	146.9	21.6	106

Vj (m/s)	dp (m)	h (m)	mp (kg)	x (m m)	y (m m)	θ°	t (ms)
			0.2316	0	0	0	0
				0	4.3	0.6	4
				-0.1	15.1	3.3	14
				2.5	26.1	5.6	24
				6.7	36.9	8.7	34
				13.6	47.7	12.9	44
				23.6	60.4	16.3	54
				35.8	74.6	19.8	64
				48.8	88.9	24.1	74
				63.9	105.3	27.2	84
				77.8	121.7	29.9	94
				92.7	138.8	32.6	104
12	0.05	0.20	0.0581	0	0	0	0
				0.5	9.4	0.3	5
				4.2	20.5	-0.7	10
				9.6	30.4	1.3	15
				16.8	41.8	2.3	20
				24.3	52.2	3.6	25
				39.1	72.1	3.5	35
				54.0	96.0	4.5	45
		0.120		0	0	0	0
				0.8	8.6	-0.5	6
				6.9	21.3	0.4	14
				17.7	33.5	-0.1	22
				32.5	47.3	0.4	30

Vj (m/s)	dp (m)	h (m)	mp (kg)	x (m m)	y (m m)	θ°	t (ms)
				49.0	60.0	-1.1	38
				65.0	75.1	-1.6	46
				85.3	93.0	-2.7	56
15	0.1	0.175	0.1320	0	0	0	0
				0	4.2	0.1	2.5
				3.1	22.4	1.1	12.5
				12.1	36.9	3.2	22.5
				28.3	53.4	6.6	32.5
				51.3	71.2	10.4	42.5
				80.1	90.6	14.0	52.5
				109.5	112.1	17.3	62.5
				138.9	134.8	19.9	72.5
				168.5	159.7	22.4	82.5
			0.2316	0	0	0	0
				0.5	7.9	-1.6	5
				3.1	21.2	-6.3	15
				9.1	32.2	-11.5	25
				20.0	41.5	-16.4	35
				35.6	50.8	-21.6	45
				54.3	60.2	-26.5	55
				75.4	70.8	-29.6	65
				98.7	82.8	-32.6	75
				124.1	96.2	-36.5	85
				149.9	110.3	-39.5	95
				176.5	125.2	-43.1	105
				203.0	140.0	-47.7	115

Vj (m/s)	dp (m)	h (m)	mp (kg)	x (m m)	y (m m)	θ°	t (ms)
15	0.1	0.175	0.2316	0	0	0	0
				1.5	18.4	0.4	10
				7.2	36.8	0.1	20
				15.1	53.7	0.1	30
				28.7	73.2	0.1	40
				44.9	93.6	0.1	50
				61.2	114.8	-1.5	60
				78.5	137.4	-3.1	70
				95.3	160.0	-5.5	80
			0.5282	0	0	0	0
				0	4.5	0	2.5
				0.8	23.3	0.6	12.5
				3.2	43.2	1.1	22.5
				7.4	62.3	1.3	32.5
				14.0	84.4	2.2	42.5
				21.9	107.1	1.6	52.5
				28.8	128.8	1.6	62.5
				36.2	153.1	1.2	72.5
		0.095	0.1320	0	0	0	0
				0.8	10.9	1.7	10
				5.1	19.6	7.2	20
				14.3	27.9	15.4	30
				27.9	35.9	26.0	40
				49.2	44.0	36.0	50
				75.3	49.5	45.8	60
				108.2	56.3	52.6	70

Vj (m/s)	dp (m)	h (m)	mp (kg)	x (m m)	y (m m)	θ°	t (ms)
				146.4	64.7	60.4	80
				190.2	75.1	67.0	90
			0.2316	0	0	0	0
				0.5	11.1	0.8	10
				3.3	22.7	2.7	20
				8.7	32.7	4.2	30
				17.9	42.9	6.3	40
				31.2	53.5	8.0	50
				48.7	64.9	9.5	60
				69.9	77.1	10.7	70
				93.1	91.3	12.1	80
				117.0	107.5	12.1	90
				142.2	123.4	12.1	100
				167.0	140.5	13.4	110
15	0.05	0.20	0.0581	0	0	0	0
				0.6	7.5	-8.0	5
				4.2	14.2	-13.4	10
				10.7	22.7	-19.7	15
				20.2	30.4	-26.1	20
				27.4	38.2	-33.6	25
				48.4	47.2	-41.7	30
				63.7	55.2	-48.7	35
				94.9	69.7	-63.4	45
				127.4	85.0	-77.2	55
			0.1381	0	0	0	0
				0.2	4.9	0.1	2.5

Vj (m/s)	dp (m)	h (m)	mp (kg)	x (m m)	y (m m)	θ°	t (ms)
				0.8	15.0	-0.3	7.5
				3.2	24.7	-0.6	12.5
				7.6	35.9	-0.1	17.5
				12.0	46.7	-0.1	22.5
				17.7	57.0	0.2	27.5
				23.5	68.3	0.2	32.5
				33.9	90.7	1.2	42.5
				45.1	113.9	2.0	52.5
		0.120	0.0581	0	0	0	0
				0.1	2.8	0.1	2
				3.5	14.1	7.5	10
				13.7	24.0	15.3	18
				31.2	33.9	23.9	26
				55.2	45.3	32.3	34
				82.3	57.1	38.3	42
				115.0	72.2	47.6	52
				148.8	90.2	57.3	62
18	0.1	0.175	0.2316	0	0	0	0
				0.1	8.5	0.6	5
				3.4	24.0	-0.2	15
				11.7	39.2	0.2	25
				26.8	54.5	0.6	35
				49.2	70.9	-1.8	45
				74.5	89.8	-2.3	55
				102.1	109.8	-5.3	65

Vj (m/s)	dp (m)	h (m)	mp (kg)	x (m m)	y (m m)	θ°	t (ms)
				129.4	130.0	-7.9	75
				156.7	151.0	-11.1	85
18	0.1	0.175	0.5282	0	0	0	0
				0.3	9.9	0	5
				1.9	27.6	0.5	15
				5.8	46.2	1.6	25
				13.6	65.3	2.3	35
				23.8	86.5	1.9	45
				35.2	108.5	1.6	55
				46.4	131.9	1.5	65
				57.8	155.5	0.1	75
		0.095	0.1320	0	0	0	0
				-0.1	6.1	0.7	6
				2.5	15.2	4.9	16
				10.5	21.7	14.6	26
				24.2	25.9	25.9	36
				45.9	28.7	38.9	46
				75.0	31.0	53.3	56
				109.9	30.1	67.1	66
				150.3	28.7	81.1	76
				196.1	27.2	95.7	86
				0	0	0	0
				0.2	2.1	0.4	2
				1.1	12.5	3.7	12
				6.9	21.5	10.2	22

Vj (m/s)	dp (m)	h (m)	mp (kg)	x (m m)	y (m m)	θ°	t (ms)
				19.3	29.7	20.6	32
				40.5	35.0	31.5	42
				69.3	38.9	43.0	52
				107.4	43.1	56.4	62
				151.9	47.3	69.6	72
			0.2316	0	0	0	0
				0	2.3	-0.1	2
				1.1	13.9	-0.9	12
				4.9	24.1	-0.6	22
				13.3	33.7	0.5	32
				27.5	42.5	0.5	42
				47.7	50.8	0.5	52
				72.9	59.6	1.3	62
				104.1	70.8	0.7	72
				139.1	84.0	2.7	82
				176.4	98.2	0.6	92
18	0.1	0.095	0.2316	214.9	113.4	0.1	102
				252.9	130.3	-0.5	112
				290.7	146.7	1.6	122
			0.5282	0	0	0	0
				0	2.5	0.1	2
				0.8	15.6	-0.8	12
				2.3	29.5	-0.8	22
				7.5	42.8	0.4	32
				15.4	56.3	1.2	42
				24.6	71.8	0.9	52

Vj (m/s)	dp (m)	h (m)	mp (kg)	x (m m)	y (m m)	θ°	t (ms)
				37.6	87.8	0.5	62
				51.5	106.1	0.1	72
				66.0	125.3	-1.3	82
				79.6	145.3	-2.3	92
	0.05	0.20	0.1381	0	0	0	0
				0	8.8	2.0	5
				2.3	18.6	2.5	10
				6.7	26.3	7.6	15
				12.3	35.5	12.0	20
				19.7	44.0	14.4	25
				28.6	53.2	17.2	30
				37.9	62.5	19.7	35
				55.6	81.2	23.7	45
				73.7	100.5	30.7	55
				0	0	0	0
				0.8	14.3	0.9	7.5
				3.8	24.9	1.7	12.5
				9.4	34.7	1.7	17.5
				16.5	44.9	1.7	22.5
				24.5	54.8	1.7	27.5
				31.9	65.0	2.5	32.5
				47.1	87.3	1.9	42.5
				62.1	110.6	0.8	52.5
			0.3823	0	0	0	0
				0.2	10.4	0.6	5
				1.4	19.7	-0.6	10

Vj (m/s)	dp (m)	h (m)	mp (kg)	x (m m)	y (m m)	θ°	t (ms)
				3.5	30.6	-1.2	15
				7.3	40.6	-1.1	20
				10.0	51.8	-1.0	25
18	0.05	0.20	0.3823	13.3	63.8	-2.0	30
				20.6	85.5	-2.7	40
				28.0	108.8	-3.6	50
		0.120	0.0581	0	0	0	0
				6.1	5.8	0	4
				6.4	17.2	1.5	12
				23.0	29.0	7.0	20
				51.4	39.6	9.4	28
				86.2	51.8	10.7	36
				122.2	61.6	12.5	44
				167.6	75.8	14.5	54
				214.2	90.9	16.4	64
			0.1381	0	0	0	0
				-0.2	6.2	-0.1	4
				2.6	18.5	0.7	12
				10.0	29.9	-2.3	20
				22.0	40.0	-0.9	28
				37.0	51.7	-0.9	36
				54.6	63.6	-3.5	44
				76.0	79.0	-3.5	54
				96.9	95.0	-5.0	64

Tolerance on measurements:

Translation ± 0.5 m m.

Rotation ± 1.0°

BODY				EXPERIMENT			CALCULATED		
Jet velocity	Diameter	Drop height	Mass	Defln. time	Jet contact time	Max. defln. within jet	Defln. time	Jet contact time	Max. defln. within jet
Vj (m/s)	dp (m)	h (m)	mp (kg)	td (ms)	tc (ms)	$\hat{x}$ (m m.)	td (ms)	tc (ms)	$\hat{x}$ (m m.)
9	0.1	0.175	0.1320	69.2	54.9	34.9	71.9	56.4	32.3
			0.2316	84.5	77.4	43.4	103.7	54.1	17.5
		0.095	0.1320	70.0	71.4	51.8	71.3	75.0	55.3
			0.2316	105.9	75.8	30.5	95.9	69.7	28.3
	0.05	0.20	0.0581	36.0	27.9	17.6	34.3	30.6	20.3
		0.120		45.4	57.9	39.4	34.8	40.8	35.2
12	0.1	0.175	0.1320	54.1	63.3	66.7	53.3	61.7	67.8
			0.2316	82.3	110.0	96.5	70.1	56.4	33.6
		0.095	0.1320	54.3	85.5	125.0	57.1	90.9	141.9
			0.2316	74.8	86.2	66.8	69.9	75.2	58.1
	0.05	0.20	0.0581	25.5	28.3	29.2	26.2	34.1	44.1
		0.120		26.0	37.3	47.3	28.1	52.7	102.9
15	0.1	0.175	0.1320	42.0	61.2	105.1	45.3	73.3	147.0
			0.2316	53.0	97.5	156.6	55.2	60.2	59.5
				53.2	57.2	60.5	55.2	60.2	59.5
			0.5282	89.7	53.2	22.3	88.4	54.7	22.2
		0.095	0.1320	50.5	-	-	49.8	-	-
			0.2316	60.5	90.4	118.0	58.9	85.9	118.4

			EXPERIMENT				CALCULATED		
Vj (m/s)	dp (m)	h (m)	mp (kg)	td (ms)	tc (ms)	$\hat{x}$ (m m.)	td (ms)	tc (ms)	$\hat{x}$ (m m.)
15	0.05	0.20	0.0581	23.2	37.4	71.0	22.4	43.3	109.2
			0.1381	33.8	28.3	18.6	31.0	31.2	25.6
		0.120	0.0581	23.2	43.4	85.7	25.0	-	-
18	0.1	0.175	0.2316	45.5	64.5	101.0	47.7	66.6	104.8
			0.5282	68.2	55.0	35.2	69.6	56.4	33.9
		0.095	0.1320	47.3	-	-	45.6	-	-
				45.3	-	-	45.6	-	-
			0.2316	53.0	99.0	202.0	52.3	119.3	328.5
			0.5282	71.0	73.4	53.3	69.4	75.0	59.0
	0.05	0.20	0.1381	27.9	33.1	34.1	26.5	33.6	42.8
				27.9	29.5	27.5	26.5	33.6	42.8
			0.3823	46.0	28.0	11.9	45.0	29.3	12.1
		0.120	0.0581	20.7	41.7	112.0	22.8	-	-
			0.1381	28.7	39.8	45.2	28.0	50.7	98.4

APPENDIX 6

SURFACE TENSION EFFECTS OF SWIRLING LIQUID SHEETS IN AIR

Surface Tension Effects of Swirling Liquid Sheets in Air.

An analysis of a swirling liquid jet in air was performed by Hodgkinson (1950) and the analysis that follows is broadly similar; however Hodgkinson neglected the surface tension terms resulting from the sheet curvature in the meridian plane. Both Lance and Perry (1953) and Taylor (1959) gave the correct equations of motion for stream flow over a conical obstruction and Taylor demonstrated that the influence of gravity was small.

Hasson (1956) disagreed with Hodgkinson (1950) and Novikov (1948), among others, and disputed the experimental results of Weinberg (1952). Hasson maintained that the liquid sheet velocity was constant and that the energy equation used by Hodgkinson was not valid. Taylor also used a constant sheet velocity, although he mentioned the effect of air drag, but a contribution by Howarth in the same paper calculated the effect of the air boundary layers on the liquid sheet velocity.

In spite of these possible limitations the energy equation was retained within the analysis. It was thought that other phenomena not considered, for example heat and mass transfer between the liquid sheet and surrounding air, may have a considerable effect (Weinberg, 1952). The analysis was thought to be useful as it stood and further experimental work will, no doubt, verify or disprove the predictions.

The liquid sheet configuration is shown in Figure A6 - 1 and an elemental volume of fluid is shown in Figure A6 - 2. It was assumed that the fluid was incompressible, the liquid sheet

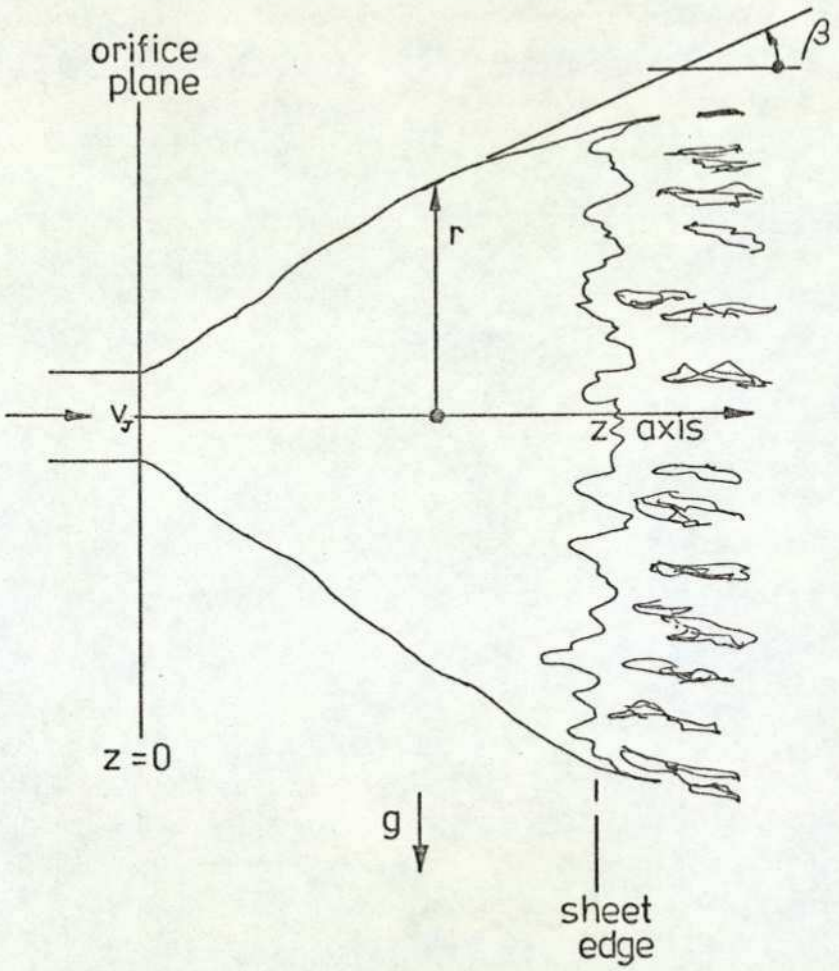

Swirling liquid sheet issuing from an orifice .

Figure A6-1

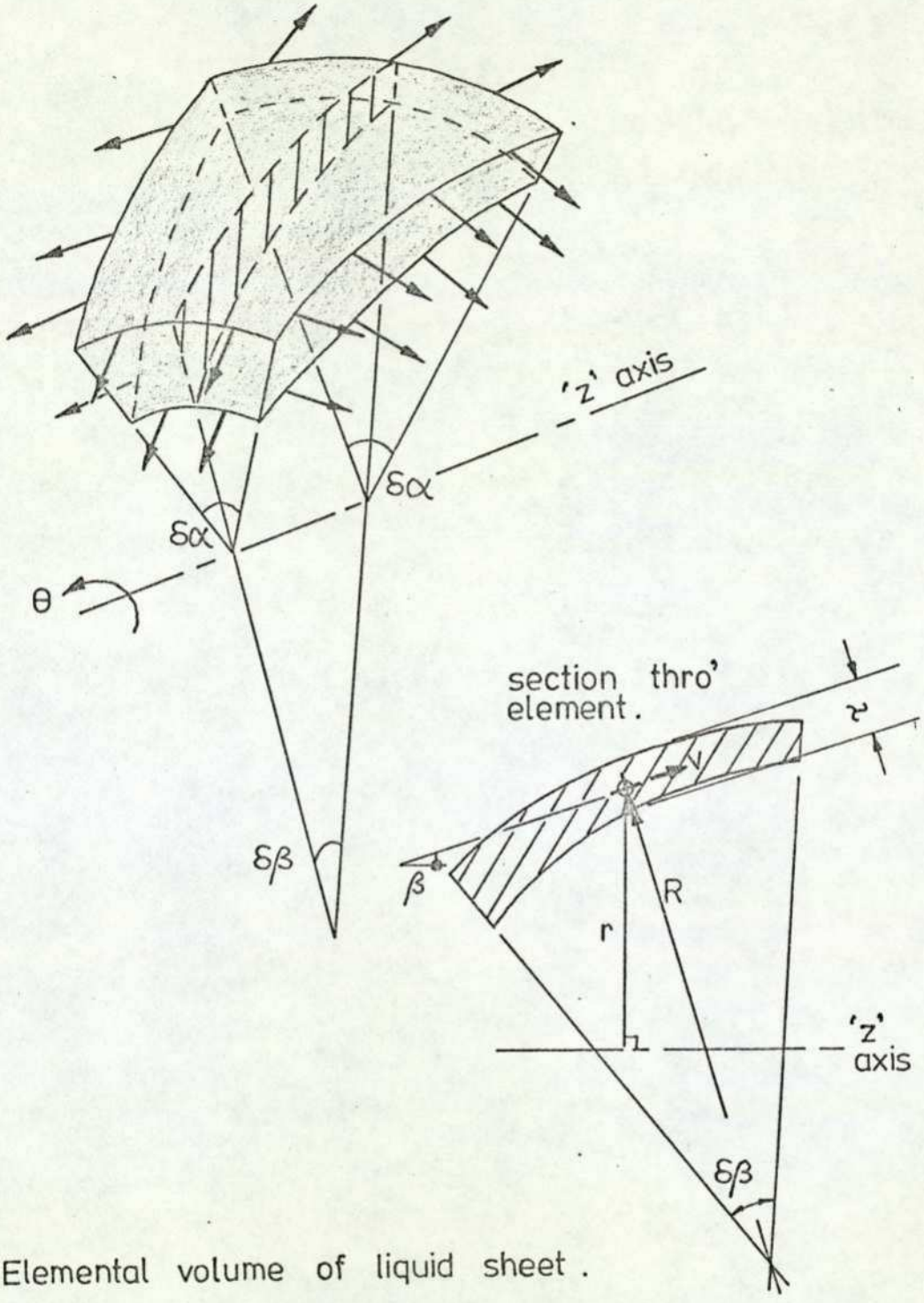

Elemental volume of liquid sheet.

Figure A6-2

thickness was very much less than the sheet radius and that there was a negligible static pressure difference across the sheet. Viscous, gravitational heat and mass transfer effects were neglected. The governing equations were :

(i) The radial equation of motion

$$-2\sigma\cos\beta\left(r\,\mathrm{SEC}\beta\,\delta\alpha\,\delta\beta + R\,\delta\alpha\,\delta\beta\right) = \left(\rho\tau R r\,\mathrm{SEC}\beta\,\delta\alpha\,\delta\beta\right) a_r$$

$$-2\sigma\left[\frac{\cos\beta}{R} + \frac{\cos^2\beta}{r}\right] = \rho\tau\left[\frac{d}{dt}(v\sin\beta) - \frac{V_\theta^2}{r}\right]$$

$$-2\sigma\left[\frac{\cos\beta}{R} + \frac{\cos^2\beta}{r}\right] = \rho\tau\left[v\cos\beta\frac{d\beta}{dt} + \sin\beta\frac{dv}{dt} - \frac{V_\theta^2}{r}\right] \quad -(A6\text{-}1)$$

(ii) Conservation of energy (only kinetic and surface energy terms are considered) :

$$\left[\frac{V^2}{2} + \frac{V_\theta^2}{2}\right]\rho R\,\delta\beta\, r\,\mathrm{SEC}\beta\,\delta\alpha\,\tau + 2\sigma R\,\delta\beta\,\mathrm{SEC}\beta\,\delta\alpha = \mathrm{CONSTANT}$$

$$\rho\left[\frac{V^2}{2} + \frac{V_\theta^2}{2}\right] + \frac{2\sigma}{\tau} = \mathrm{CONSTANT} \quad -(A6\text{-}2)$$

(iii) Conservation of mass :

$$r_o\tau_o V_o = r\tau V = \mathrm{CONSTANT} \quad -(A6\text{-}3)$$

(iv) Conservation of angular momentum :

$$r_o V_{\theta o} = r V_\theta = \mathrm{CONSTANT} \quad -(A6\text{-}4)$$

Differentiating equations A6 - 2 and A6 - 3 with respect to time and substituting for $\left(d\gamma/dt\right)$ in equation A6 - 2 then:

$$V\frac{dV}{dt} + V_\theta\frac{dV_\theta}{dt} + \frac{2\sigma}{\rho r_o \gamma_o V_o}\left[r\frac{dV}{dt} + V^2 SIN\beta\right] = 0 \qquad -(A6-5)$$

Differentiating equation A6 - 4 with respect to time and substituting into A6 - 5 gives, after some rearrangement:

$$\frac{dV}{dt} = -V SIN\beta\left[\frac{K_1 V - K_2/r^3}{V + K_1 r}\right] \qquad -(A6-6)$$

where $K_1 = 2\sigma/\rho r_o \gamma_o V_o$, and $K_2 = (r_o V_{\theta o})^2$

Since $V = \Omega R$ then,

$$\frac{1}{R} = -\frac{1}{V}\cdot\frac{d\beta}{dt} \qquad -(A6-7) \text{ , where } \Omega = -\frac{d\beta}{dt}$$

Substituting for R, γ and V_θ from equations A6 - 7, A6 - 3 and A6 - 4 into equation A6 - 1 and rearranging, gives:

$$\frac{d\beta}{dt} = -\frac{\left[\frac{\cos^2\beta}{r} + \frac{1}{K_1 r V}\left(SIN\beta\frac{dV}{dt} - \frac{K_2}{r^3}\right)\right]}{\cos\beta\left[\frac{1}{K_1 r} - \frac{1}{V}\right]} \qquad -(A6-8)$$

Substituting for V_θ from equation A6 - 4 into equation A6 - 2 and rearranging, then:

$$V^2 - K_4^2 + K_2\left(\frac{1}{r^2} - \frac{1}{K_3^2}\right) + 2K_1\left(rV - K_3K_4\right) = 0 \quad -(A6-9)$$

where $K_3 = r_o$ and $K_4 = V_o$

The three equations A6 - 6, A6 - 8 and A6 - 9 contain four unknowns, V, β, r and t, and were solved numerically using increments of time as a base. Since β was not required explicitly the substitution $U = \sin\beta$ was made and the three equations solved in the order given below using an I.B.M. computer subroutine for initial value differential equations. The numerical integration procedure followed by the I.B.M. routine used a modified Runge-Kutta process.

$$V^2 + K_2\left(\frac{1}{r^2} - \frac{1}{K_3^2}\right) + 2K_1\left(rV - K_3K_4\right) - K_4^2 = 0$$

$$\frac{dV}{dt} = UV\,\frac{\left[K_2/r^3 - K_1V\right]}{\left(V + K_1r\right)} \quad -(A6-10)$$

$$\frac{du}{dt} = \frac{K_1V\left(U^2-1\right) - U\,dV/dt + K_2/r^3}{\left(V + K_1r\right)} \quad -(A6-11)$$

The three equations above predict the liquid sheet velocity, radius and sine of the sheet semi-angle against time. They do not prdeict where the sheet is likely to break up and assume a constantly expanding, rapidly thinning, but continuous liquid sheet. In a continuation of his work on the dynamics of thin liquid sheets Taylor (1959) studied the effects of waves on liquid sheets and their final disintegration. The conclusions drawn by Taylor pertinent to this work were that the break up of a liquid sheet edge fixed in space was determined by the sheet velocity and the velocity of an 'antisymmetrical wave'. For a liquid sheet of uniform thickness a stationary edge would occur when the sheet velocity equalled the velocity of an 'antisymmetrical wave'. The velocity of 'antisymmetrical waves' was given as:

$$V_{WAVE} = \left(2\sigma/\rho\tau\right)^{1/2}$$

For a radially expanding turbulent liquid sheet the Weber number could not exceed unity, where the Weber number was defined as:

$We = 2\sigma/\rho V^2\bar{\tau}$ and $\bar{\tau}$ = mean sheet thickness.

Fluid viscosity and turbulence would reduce the Weber number below unity and the criteria for the sheet edge was given as: $0.25 \leq We \leq 0.4$

The liquid sheets used in this work were expected to expand radially and therefore an edge was defined as occurring when the Weber number equalled one third.

Figures A6 - 3 and A6 - 4 show the variation in sheet curvature with various swirl and stream velocities. The parameter ($\sin \beta$) has been plotted since it was thought that this parameter most clearly showed curvature changes.

Under zero swirl flow conditions, equation (A6- 10) indicates that $\left(dv/dt\right)$ must always be negative, for normal orifice outlet conditions. The denominator of equation (A6 - 11) will be positive since the Weber number must always be less than unity.

The effect of increasing the swirl velocity is to make $\left(dv/dt\right)$ less negative and if $\left(K_2/r^3\right)$ is greater than $\left(K_1 V\right)$ then $\left(dv/dt\right)$ can become positive. A similar effect occurs with the numerator in equation (A6 - 11). Both the second and third terms in equation (A6 - 11) become increasingly positive and eventually $\left(du/dt\right)$ may become positive and the liquid sheet semiangle is predicted to increase. Solutions to the equations become increasingly difficult to obtain as the swirl velocity increases. The solution to equation (A6 - 9) can oscillate and the I.B.M. subroutine be unable to hold the answers within the permitted error band. If the swirl velocities are further increased the instability can be overcome and the predicted values for the conical sheet semiangle can exceed unity.

The work was thought to be useful and showed that curvature effects should be negligible at the anticipated liquid sheet velocities. Also it appeared likely that a stable conical liquid sheet should be obtained with swirl velocities considerably

Initial conditions:

$\beta_o = 30^\circ$; $r_o = 4$ m.m. ; $\gamma_o = 1.5$ m.m. ; $v_{\theta o} = 0.0$ m/s.

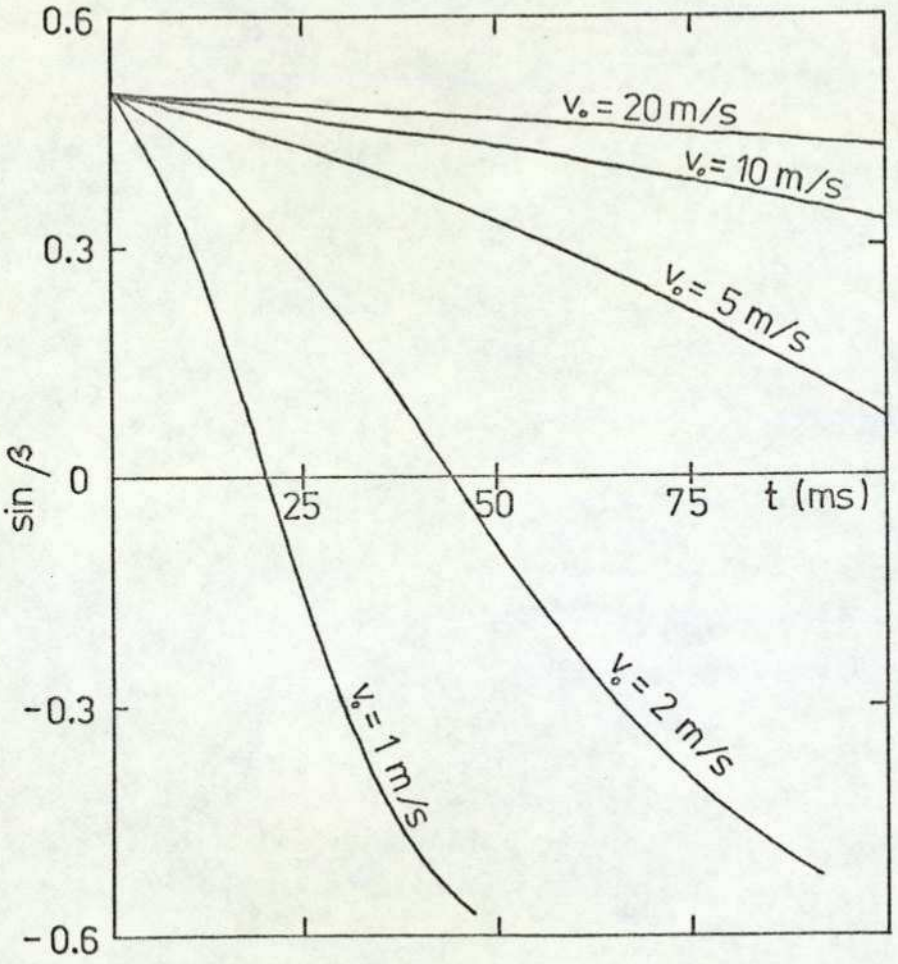

Sine of liquid sheet semi-angle against time

Figure A6-3

Initial conditions:

$\beta_o = 30°$; $r_o = 4$ m.m. ; $\tau_o = 1.5$ m.m. ; $v_o = 1.0$ m/s.

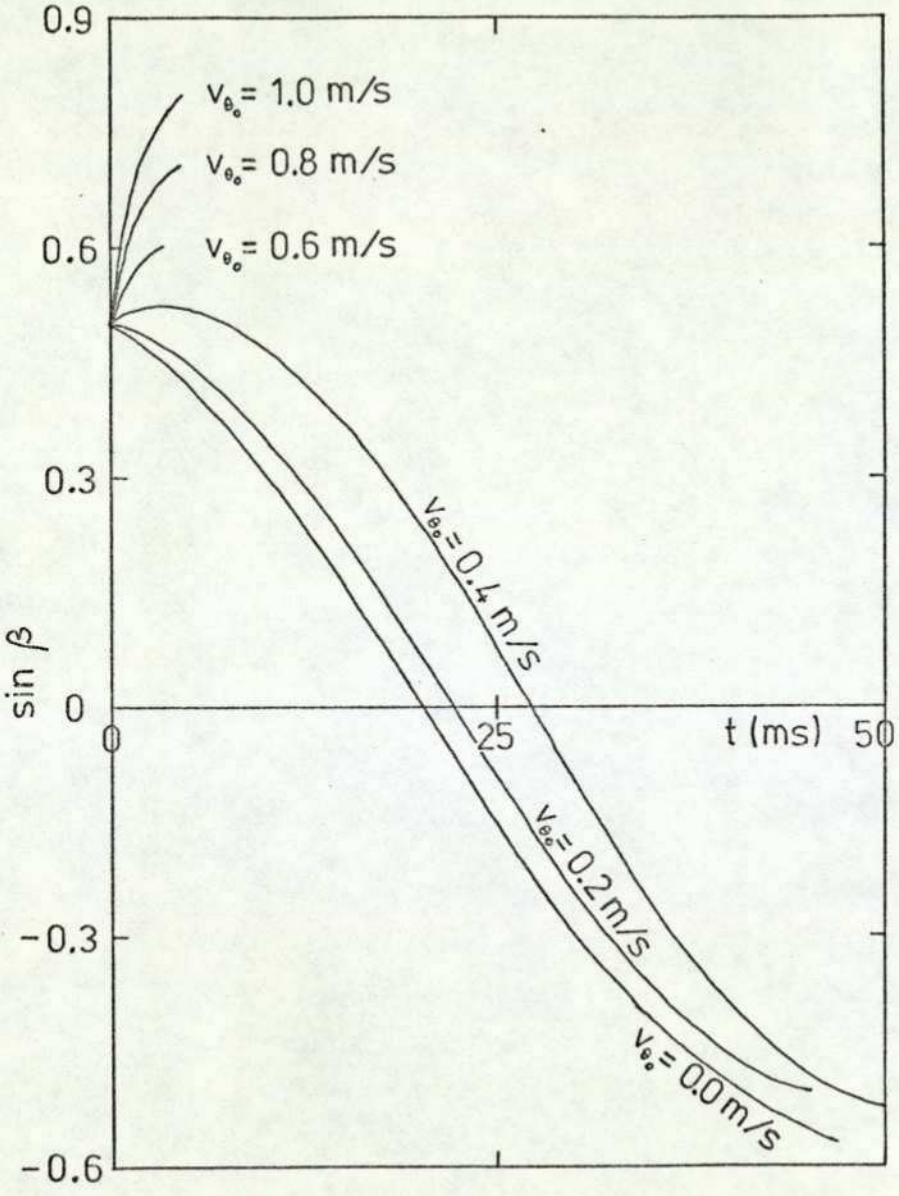

Sine of liquid sheet semi-angle against time

Figure A6-4

lower than the liquid sheet stream velocity. The work was not continued since the most difficult region for analysis, the nozzle orifice region, still had to have the initial conditions arbitrarily specified; also a number of assumptions made were thought to be doubtful. In view of the small contribution likely to be made by any improvement in the theory the subject was terminated.

APPENDIX 7

THE EQUATIONS OF FLUID FLOW

A7 - (i) The Equations of Fluid Flow.

The vector equation of motion for fluid flow, in an inertial coordinate system, is :

$$\frac{\partial \vec{v}}{\partial t} + \nabla\left[\frac{\vec{v}}{2} + gz\right] = \vec{v} \times (\nabla \times \vec{v}) - \nabla\left[\frac{p}{\rho}\right] + \vec{f}$$

where $\vec{f}$ = frictional force per unit mass exerted on the fluid. For constant viscosity, incompressible, laminar flows :

$$\vec{f} = \nu \nabla^2 \vec{v}$$

The continuity equation for incompressible flows is :

$$\nabla \cdot \vec{v} = 0$$

A7 - (ii) The Coordinate System used for Analysis.

The coordinate system used for the analysis of fluid flow within the nozzle is an axisymmetric, orthogonal, curvilinear system. The coordinate system is shown in Figure A7-1 and an elemental volume of fluid, with the stresses exerted upon it, is shown in Figure A7-2.

The unit vectors $\vec{\iota}_1$, $\vec{\iota}_2$, $\vec{\iota}_3$ are tangent to the coordinate curves X_1, X_2, X_3 respectively. The coordinate surfaces of one particular family (X_1 or X_2 or X_3) are not necessarily parallel to each other. For example the distance between the surfaces X_3 = constant and $X_3 + dX_3$ = constant are not necessarily equal although the increment of the coordinate X_3 is the same everywhere. Care must be taken to distinguish between the actual distance between the two coordinate surfaces and the change in the coordinate X_3 . This is done by using variable parameters, known as metric coefficients h_1, h_2, h_3 .

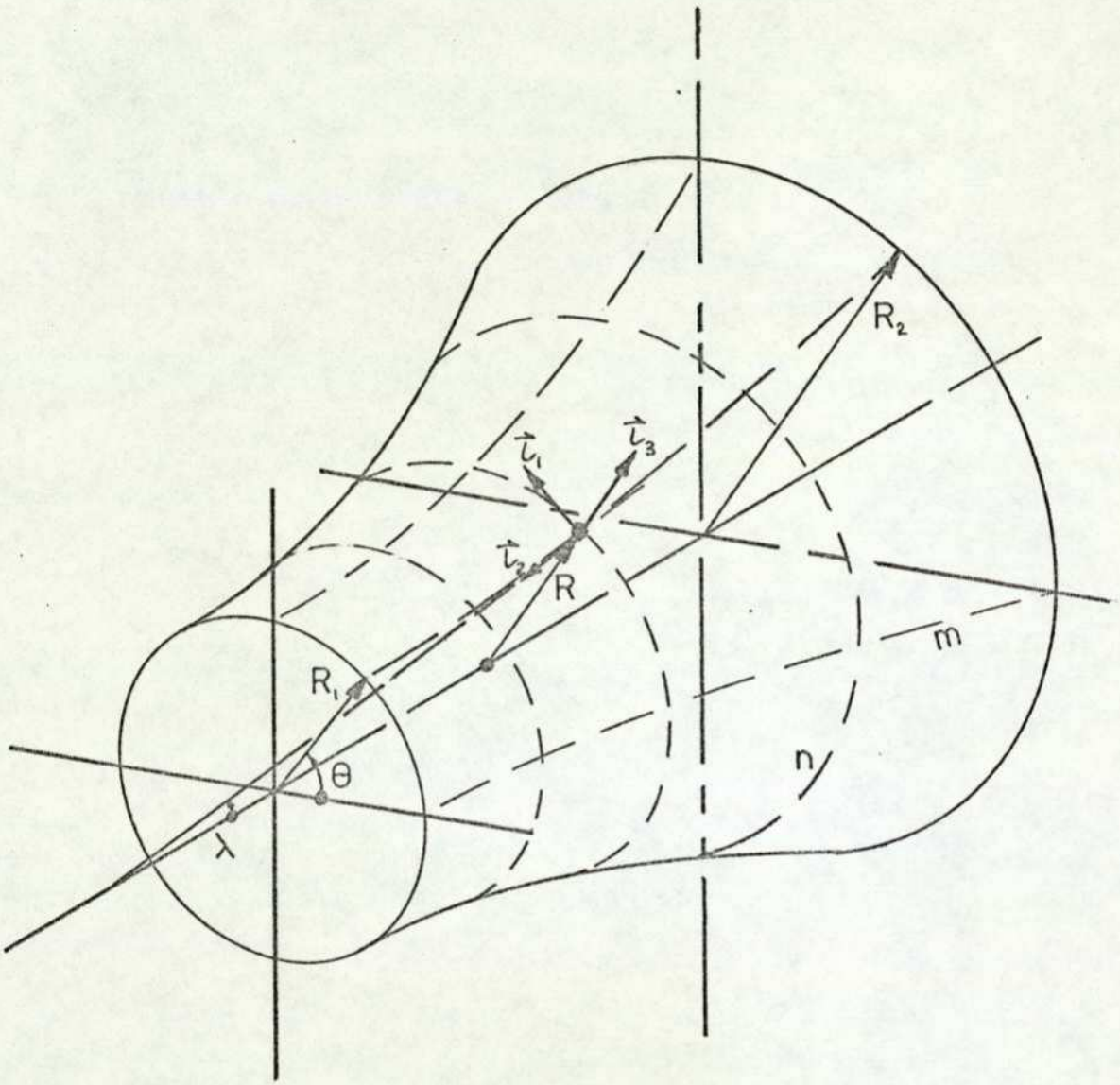

Axisymmetric stream surface coordinate system

Figure A7-1

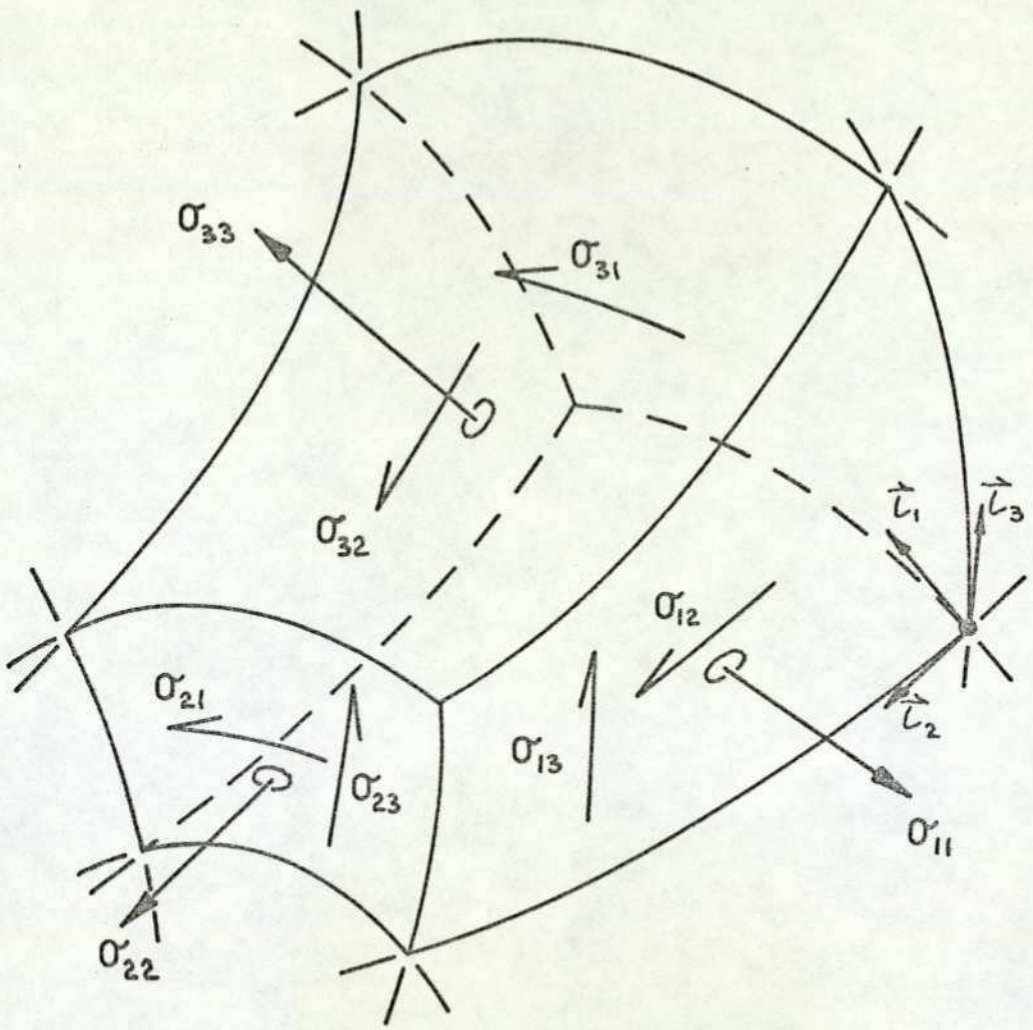

Elemental volume of fluid showing stress notation

Figure A7-2

For any particular coordinate system there exist definite functional relationships between the variable parameters h_1, h_2, h_3 and the coordinates x_1, x_2, x_3.

The system used in this analysis is an axisymmetric, orthogonal coordinate system with the distances along the coordinates x_1, x_2, x_3 increased by θ, m, n respectively. The orthogonality condition gives a right handed unit vector system such that:

$$\vec{i}_1 \times \vec{i}_2 = \vec{i}_3$$

The surface $x_1 = \theta$ = constant, is a meridian plane passing through the axis of rotation. The coordinate surface x_2 = constant is obtained by rotating an 'n' curve about the axis of symmetry. The surface x_3 = constant is obtained by rotating an 'm' curve, a stream surface, around the axis.

The assumptions made in deriving the equations were:

(i) Steady flow.

(ii) Incompressible constant viscosity flow (ρ = constant, μ = constant).

(iii) Axisymmetric flow. (Therefore any derivative with respect to θ is zero).

(iv) The velocities v_1, v_2, v_3 are positive in the directions of increasing values of θ, m and n respectively and since the 'm' curves are stream surfaces (there is no flow across a stream surface) then v_3 and all its derivatives are zero.

In this thesis the coordinate system described above will be termed an 'axisymmetric stream surface' coordinate system.

For this particular coordinate system Vavra (1960) gives the metric coefficients and their derivatives as:

$$h_1 = R \quad ; \quad h_2 = \frac{dm}{dx} \quad ; \quad h_3 = \frac{dn}{dx}$$

$$x_1 = \theta \; ; \quad dx_1 = d\theta$$

$$\frac{\partial h_1}{\partial x_1} = 0 \quad ; \quad \frac{\partial h_2}{\partial x_1} = 0 \quad ; \quad \frac{\partial h_3}{\partial x_1} = 0$$

$$\frac{\partial h_1}{\partial x_2} = h_2 \frac{\partial R}{\partial m} \quad ; \qquad \frac{\partial h_3}{\partial x_2} = h_2 h_3 k_m$$

$$\frac{\partial h_1}{\partial x_3} = h_3 \frac{\partial R}{\partial n} \quad ; \quad \frac{\partial h_2}{\partial x_3} = h_2 h_2 k_m$$

These results have been checked against the work of Gosman 'et al' (1969: section 2.21)

Two other axisymmetric coordinate systems commonly used are the cylindrical and spherical systems.

A7 - (iii) Laminar, viscous equations of fluid flow in axisymmetric stream surface coordinates.

With the conditions stated in the previous section and neglecting body forces, the curvilinear equations of fluid motion given by Hughes and Gaylord (1964) reduce to:

$$\rho\left[\frac{v_2}{h_2}\cdot\frac{\partial v_1}{\partial x_1} + \frac{v_1 v_2}{h_1 h_2}\cdot\frac{\partial h_1}{\partial x_2}\right] = \frac{1}{h_1 h_2 h_3}\left[\frac{\partial}{\partial x_2}(h_1 h_2 \sigma_{21}) + \frac{\partial}{\partial x_3}(h_1 h_2 \sigma_{31})\right] + \frac{\sigma_{12}}{h_1 h_2}\cdot\frac{\partial h_1}{\partial x_2} + \frac{\sigma_{31}}{h_1 h_2}\cdot\frac{\partial h_1}{\partial x_3} \cdot$$

$$\rho\left[\frac{v_2}{h_2}\frac{\partial v_2}{\partial x_2} - \frac{v_1^2}{h_1 h_2}\cdot\frac{\partial h_1}{\partial x_2}\right] = \frac{1}{h_1 h_2 h_3}\left[\frac{\partial}{\partial x_2}(h_3 h_1 \sigma_{22}) + \frac{\partial}{\partial x_3}(h_1 h_2 \sigma_{32})\right] + \frac{\sigma_{23}}{h_2 h_3}\cdot\frac{\partial h_2}{\partial x_3} - \frac{\sigma_{33}}{h_2 h_3}\cdot\frac{\partial h_3}{\partial x_2} - \frac{\sigma_{11}}{h_2 h_1}\cdot\frac{\partial h_1}{\partial x_2} .$$

$$\rho\left[-\frac{v_1^2}{h_1 h_3}\cdot\frac{\partial h_1}{\partial x} - \frac{v_2^2}{h_2 h_3}\cdot\frac{\partial h_2}{\partial x_3}\right] = \frac{1}{h_1 h_2 h_3}\left[\frac{\partial}{\partial x_2}(h_3 h_1 \sigma_{23}) + \frac{\partial}{\partial x_3}(h_1 h_2 \sigma_{33})\right] + \frac{\sigma_{23}}{h_3 h_2}\cdot\frac{\partial h_3}{\partial x_2} - \frac{\sigma_{11}}{h_3 h_1}\cdot\frac{\partial h_1}{\partial x_3} - \frac{\sigma_{22}}{h_3 h_2}\cdot\frac{\partial h_2}{\partial x_3} .$$

where:

$$\sigma_{11} = -p + 2\mu\frac{v_2}{h_1 h_2}\cdot\frac{\partial h_1}{\partial x_2}$$

$$\sigma_{22} = -p + 2\mu\frac{1}{h_2}\cdot\frac{\partial v_2}{\partial x_2}$$

$$\sigma_{33} = -p + 2\mu\frac{v_2}{h_2 h_3}\cdot\frac{\partial h_3}{\partial x_2}$$

$$\sigma_{12} = \sigma_{21} = \mu\frac{h_1}{h_2}\cdot\frac{\partial}{\partial x_2}\left(\frac{v_1}{h_1}\right)$$

$$\sigma_{13} = \sigma_{31} = \mu\frac{h_1}{h_3}\cdot\frac{\partial}{\partial x_3}\left(\frac{v_1}{h_1}\right)$$

$$\sigma_{23} = \sigma_{32} = \mu\frac{h_2}{h_3}\cdot\frac{\partial}{\partial x_3}\left(\frac{v_2}{h_2}\right)$$

After performing the differentiation and substituting for the metric coefficients and their derivatives, the equations of motion become:

$$\rho\left[V_2\left(\frac{\partial V_1}{\partial m} + \frac{V_1}{R}\cdot\frac{\partial R}{\partial m}\right)\right] = \frac{1}{R}\left[\frac{\partial}{\partial m}(R\sigma_{21}) + Rk_n\sigma_{21} + \frac{\partial}{\partial n}(R\sigma_{31}) + Rk_m\sigma_{31}\right] + \frac{\sigma_{12}}{R}\cdot\frac{\partial R}{\partial m} + \frac{\sigma_{31}}{R}\cdot\frac{\partial R}{\partial n}\,.$$

$$\rho\left[V_2\cdot\frac{\partial V_2}{\partial m} - \frac{V_1^2}{R}\cdot\frac{\partial R}{\partial m}\right] = \frac{1}{R}\left[\frac{\partial}{\partial m}(R\sigma_{22}) + \sigma_{22}Rk_n + \frac{\partial}{\partial n}(R\sigma_{32}) + \sigma_{32}Rk_m\right] + \sigma_{23}k_m - \sigma_{33}k_n - \frac{\sigma_{11}}{R}\cdot\frac{\partial R}{\partial m}\,.$$

$$\rho\left[-\frac{V_1^2}{R}\cdot\frac{\partial R}{\partial n} - V_2^2k_m\right] = \frac{1}{R}\left[\frac{\partial}{\partial m}(R\sigma_{23}) + \sigma_{23}Rk_n + \frac{\partial}{\partial n}(R\sigma_{33}) + \sigma_{33}Rk_m\right] + \sigma_{23}k_n - \frac{\sigma_{11}}{R}\cdot\frac{\partial R}{\partial n} - \sigma_{22}k_m\,.$$

where for laminar flow:

$$\sigma_{11} = -p + 2\mu\frac{V_2}{R}\cdot\frac{\partial R}{\partial m}$$

$$\sigma_{22} = -p + 2\mu\frac{\partial V_2}{\partial m}$$

$$\sigma_{33} = -p + 2\mu V_2 k_n$$

$$\sigma_{12} = \sigma_{21} = \mu R\frac{\partial}{\partial m}\left(\frac{V_1}{R}\right)$$

$$\sigma_{13} = \sigma_{31} = \mu R\frac{\partial}{\partial n}\left(\frac{V_1}{R}\right)$$

$$\sigma_{23} = \sigma_{32} = \mu\left(\frac{\partial V_2}{\partial n} - V_2k_m\right)$$

Substituting the velocity gradient terms for the shear stresses, the equations of motion become (after some rearrangement):

$$V_2\left(\frac{\partial V_1}{\partial m} + \frac{V_1}{R}.\frac{\partial R}{\partial m}\right) = \nu\left[\frac{\partial^2 V_1}{\partial m^2} + \frac{\partial V_1}{\partial m}\left(\frac{1}{R}.\frac{\partial R}{\partial m} + k_n\right) + \frac{\partial^2 V_1}{\partial n^2}\right.$$

$$+ \frac{\partial V_1}{\partial n}\left(\frac{1}{R}.\frac{\partial R}{\partial n} + k_m\right) - \frac{V_1}{R}\left(\frac{\partial^2 R}{\partial m^2} + \frac{\partial R}{\partial m}\left(\frac{1}{R}.\frac{\partial R}{\partial m} + k_n\right) +\right.$$

$$\left.\left.\frac{\partial^2 R}{\partial n^2} + \frac{\partial R}{\partial n}\left(\frac{1}{R}.\frac{\partial R}{\partial n} + k_m\right)\right)\right].$$

$$V_2\,\frac{\partial V_2}{\partial m} - \frac{V_1^2}{R}.\frac{\partial R}{\partial m} = -\frac{1}{\rho}.\frac{\partial P}{\partial m} + \nu\left[2\frac{\partial^2 V_2}{\partial m^2} + 2\frac{\partial V_2}{\partial m}\right.$$

$$\left(\frac{1}{R}.\frac{\partial R}{\partial m} + k_n\right) + \frac{\partial^2 V_2}{\partial n^2} + \frac{\partial V_2}{\partial n}\left(\frac{1}{R}.\frac{\partial R}{\partial n} + k_m\right) - V_2\left(\frac{\partial k_m}{\partial n}\right.$$

$$\left.\left. + k_m\left(\frac{1}{R}.\frac{\partial R}{\partial n} + 2k_m\right) + \frac{2}{R^2}\left(\frac{\partial R}{\partial m}\right)^2 + 2k_n^2\right)\right].$$

$$-V_2^2 k_m - \frac{V_1^2}{R}.\frac{\partial R}{\partial n} = -\frac{1}{\rho}.\frac{\partial P}{\partial n} + \nu\left[\frac{\partial}{\partial m}\left(\frac{\partial V_2}{\partial n}\right) -\right.$$

$$3k_m.\frac{\partial V_2}{\partial m} + \frac{\partial V_2}{\partial n}\left(\frac{1}{R}.\frac{\partial R}{\partial m} + 4k_n\right) + V_2\left(2\frac{\partial k_n}{\partial n} - \frac{\partial k_m}{\partial m} +\right.$$

$$\left.\left.\frac{1}{R}\left(2k_n.\frac{\partial R}{\partial n} - k_m.\frac{\partial R}{\partial m} - \frac{2}{R}.\frac{\partial R}{\partial m}.\frac{\partial R}{\partial n}\right)\right)\right].$$

With the conditions given in the second section the continuity equation becomes:

$$\nabla \cdot \vec{v} = \frac{1}{h_1 h_2 h_3} \cdot \frac{\partial}{\partial x_2}(h_1 h_3 v_2) = 0 \ .$$

Upon substituting the functions for the metric coefficients and their derivatives:

$$\frac{\partial v_2}{\partial m} + v_2\left(\frac{1}{R}\cdot\frac{\partial R}{\partial m} + k_n\right) = 0 \ .$$

Two further substitutions can be made, if desired. These are:

$$\frac{\partial R}{\partial m} = \sin\lambda \quad ; \qquad \frac{\partial R}{\partial n} = \cos\lambda \quad ;$$

where the angle λ is shown in FigureA7 - 1.

The continuity condition can be satisfied by the introduction of a stream function. Goldstein (1938) gave the equations for axisymmetric general orthogonal coordinates as:

$$h_1 v_2 = \frac{1}{h_3}\cdot\frac{\partial \psi}{\partial x_3} \quad ; \qquad h_1 v_3 = -\frac{1}{h_2}\cdot\frac{\partial \psi}{\partial x_2} \quad ;$$

(where the symbols have been manipulated into those used previously).

Substituting for the metric coefficients gives:

$$v_2 = \frac{1}{R}\cdot\frac{\partial \psi}{\partial n} \qquad v_3 = -\frac{1}{R}\cdot\frac{\partial \psi}{\partial m} = 0$$

However, since the 'm' curves are stream surfaces,

$$v_3 = 0 \ , \quad \partial\psi/\partial m = 0 \quad \text{and} \quad \psi$$

is a constant along any 'm' curve; therefore ψ is a function of 'n' only and the partial derivative notation can be removed

from the stream function equation for V_2 .

A7 - (iv) Cylindrical Coordinates

The metric coefficients for orthogonal axisymmetric cylindrical coordinates are:

$$h_1 = h_\theta = r \quad ; \quad h_2 = h_z = 1 \quad ; \quad h_3 = h_r = 1$$

Neglecting body forces, the steady flow laminar, viscous incompressible flow equations become:

$$V_r \cdot \frac{\partial V_r}{\partial r} + V_z \cdot \frac{\partial V_r}{\partial z} - \frac{V_\theta^2}{r} = -\frac{1}{\rho} \cdot \frac{\partial p}{\partial r} + \nu \left[\frac{1}{r} \cdot \frac{\partial}{\partial r} \left(r \cdot \frac{\partial V_r}{\partial r} \right) + \frac{\partial^2 V_r}{\partial z^2} - \frac{V_r}{r^2} \right] .$$

$$V_r \cdot \frac{\partial V_\theta}{\partial r} + V_z \cdot \frac{\partial V_\theta}{\partial z} + \frac{V_r V_\theta}{r} = \nu \left[\frac{1}{r} \cdot \frac{\partial}{\partial r} \left(r \cdot \frac{\partial V_\theta}{\partial r} \right) + \frac{\partial^2 V_\theta}{\partial z^2} - \frac{V_\theta}{r^2} \right] .$$

$$V_r \cdot \frac{\partial V_z}{\partial r} + V_z \cdot \frac{\partial V_z}{\partial z} = -\frac{1}{\rho} \cdot \frac{\partial p}{\partial z} + \nu \left[\frac{1}{r} \frac{\partial}{\partial r} \left(r \frac{\partial V_z}{\partial z} \right) + \frac{\partial^2 V_z}{\partial z^2} \right] .$$

The continuity equation becomes:

$$\frac{\partial V_r}{\partial r} + \frac{V_r}{r} + \frac{\partial V_z}{\partial z} = 0$$

A7 - (v) Spherical Coordinates

The metric coefficients are:

$$h_1 = h_\phi = R \sin\theta \qquad h_2 = h_\theta = R \qquad h_3 = h_R = 1$$

The axis of symmetry is with respect to the ϕ coordinate (i.e. $\partial F/\partial\phi = 0$). The flow conditions are identical to those in section A7 - (iv).

$$V_R \frac{\partial V_R}{\partial R} + \frac{V_\theta}{R}\frac{\partial V_R}{\partial\theta} - \frac{V_\theta^2}{R} - \frac{V_\phi^2}{R} = -\frac{1}{\rho}\frac{\partial p}{\partial R} + \nu\left[\frac{1}{R}\frac{\partial^2(RV_R)}{\partial R^2} + \frac{1}{R^2}\frac{\partial^2 V_R}{\partial\theta^2} + \frac{\cot\theta}{R^2}\frac{\partial V_R}{\partial\theta} - \frac{2}{R^2}\frac{\partial V_\theta}{\partial\theta} - \frac{2V_R}{R^2} - \frac{2\cot\theta}{R^2}V_\theta\right].$$

$$V_R \frac{\partial V_\theta}{\partial R} + \frac{V_\theta}{R}\frac{\partial V_\theta}{\partial\theta} + \frac{V_R V_\theta}{R} - \frac{V_\phi^2 \cot\theta}{R} = -\frac{1}{\rho R}\frac{\partial p}{\partial\theta} + \nu\left[\frac{1}{R}\frac{\partial^2(RV_\theta)}{\partial R^2} + \frac{1}{R^2}\frac{\partial^2 V_\theta}{\partial\theta^2} + \frac{\cot\theta}{R^2}\frac{\partial V_\theta}{\partial\theta} + \frac{2}{R^2}\frac{\partial V_R}{\partial\theta} - \frac{V_\theta}{R^2\sin^2\theta}\right].$$

$$V_R \frac{\partial V_\phi}{\partial R} + \frac{V_\theta}{R}\frac{\partial V_\phi}{\partial\theta} + \frac{V_R V_\phi}{R} + \frac{V_\theta V_\phi \cot\theta}{R} = \nu\left[\frac{1}{R}\frac{\partial^2(RV_\phi)}{\partial R^2} + \frac{1}{R^2}\frac{\partial^2 V_\phi}{\partial\theta^2} + \frac{\cot\theta}{R^2}\frac{\partial V_\phi}{\partial\theta} - \frac{V_\phi}{R^2\sin^2\theta}\right].$$

The continuity equation is:

$$\frac{\partial V_R}{\partial R} + \frac{2V_R}{R} + \frac{1}{R}\frac{\partial V_\theta}{\partial\theta} + \frac{V_\theta}{R}\cot\theta = 0 .$$

APPENDIX 8

'ROTAMETER' CALIBRATION EXPERIMENTS

'Rotameter' Calibration Experiments.

Rotameter Limited quoted the flow rates of the two models used as follows:

Fluid : Water

Metric 35 XG, (series 1000) - stainless steel float
3.0 to 30.0 l/min.
Korannite (ceramic) float
1.4 to 14 l/min.

Metric 65P - stainless steel float
20 to 200 l/min.
Korannite(ceramic) float
10 to 100 l/min.

Both instruments were calibrated by plumbing them into a water supply, opening a gate valve until the desired Rotameter scale reading was reached and timing the collection of a volume of water. The water was weighed and the flow rate calculated. If the collection time fell below thirty seconds the time quoted is the average of three collections.

Rotameter model: Metric 35 x G, stainless steel float.

Scale reading	Collection time (sec)	Weight of water (lbf)	Flow rate (l/s)
1	285.0	41.50	0.0661
2	214.0	38.50	0.0816
3	200.0	32.35	0.0961
4	180.0	44.75	0.1128
6	145.2	46.25	0.1445
8	118.1	45.75	0.1757
10	93.0	42.75	0.2085
12	91.0	48.25	0.2405
14	78.6	48.00	0.2770
16	70.4	48.00	0.3093
18	61.8	46.50	0.3413
20	57.2	48.00	0.3806
22	53.2	48.75	0.4157
24	48.0	47.25	0.4465
26	45.7	49.25	0.4888

Rotameter model: Metric 65P, Korannite ceramic float.

1	120.0	48.50	0.1833
2	90.0	47.25	0.2381
3	75.0	48.50	0.2933
4	65.0	49.50	0.3454
5	60.0	52.75	0.3988

Scale reading	Collection time (sec)	Weight of water (lbf)	Flow rate (l/s)
6	50.0	49.75	0.4513
7	45.0	50.00	0.5040
8	40.0	49.75	0.5642
9	35.0	48.00	0.6221
10	32.0	48.50	0.6875
11	28.0	46.40	0.7517
12	25.0	44.25	0.8029
13	23.0	44.63	0.8802
14	22.0	45.25	0.9330
15	21.0	46.00	0.9936
16	19.0	45.38	1.0834
17	18.0	45.00	1.1340
18	16.0	42.50	1.2049
19	16.0	44.88	1.2723
20	15.0	44.38	1.3420
21	14.0	43.75	1.4175
22	12.5	41.50	1.5059
23	12.0	40.78	1.5415
24	12.0	43.00	1.6254
25	12.0	44.15	1.6688

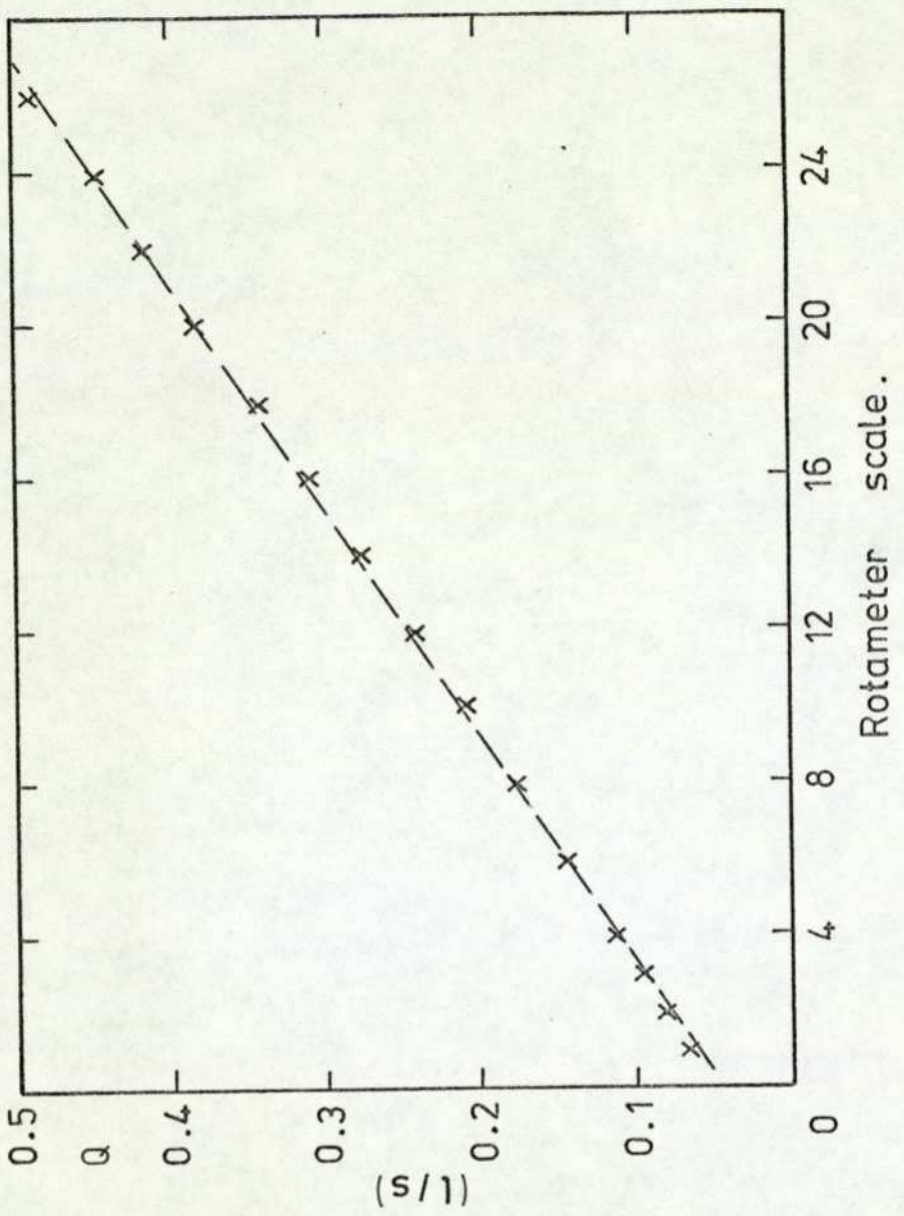

Rotameter model : METRIC 35 XG

Float : Stainless Steel

Fluid : Water

Figure A8-1

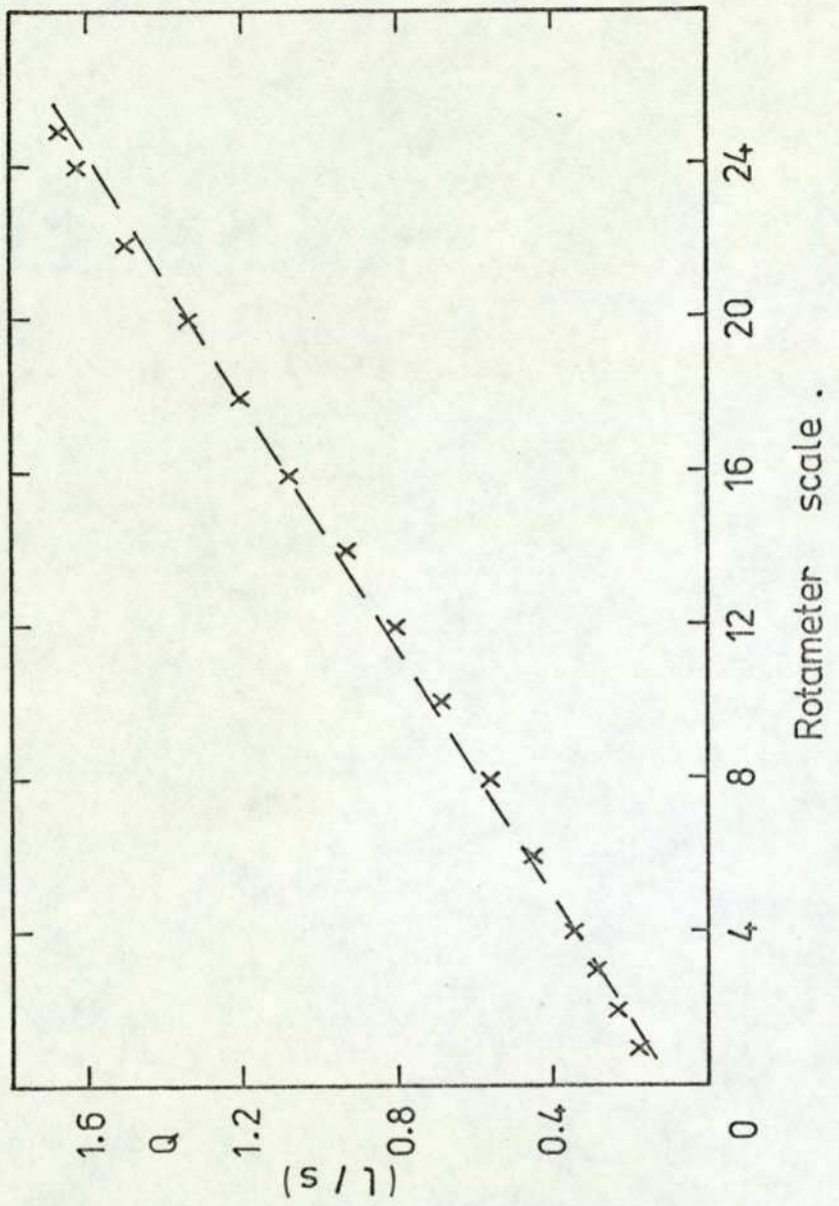

Rotameter model : METRIC 65 P

Float : Korannite (ceramic)

Fluid : Water

Figure A8-2

APPENDIX 9

AXIAL VORTEX DEVICE - EXPERIMENTAL RESULTS

A9 - (i) Location of Pressure Tapping Points.

Measurement tolerance : ± 0.3 m m.

Tapping size: 1 m m. diameter holes

All measurements taken from the orifice plane and measured in m m.

See also Figure 3 - 7.

GEOMETRY No.1

	Axial distance	Station no.
p1	82.0	
p2	Control flow supply annulus	
p3	21.8	24.96
p4	18.2	21.65
p5	12.7	17.44
p6	4.4	7.85
p7	3.4	4.45

GEOMETRY No.2

p1	82.0	
p2	Control flow supply annulus	
p3	26.3	29.40
p4	16.8	21.53
p5	8.0	11.43
p6	1.3	2.83
p7	3.5	4.55

A9 - (ii) Liquid Jet Velocity Profile

Flow conditions: streaming flow

Measurement station: 3 m m. downstream of the orifice plane.

See Appendix 3 for total head probe calibration.

GEOMETRY No.1

Probe position (rel. to jet edge) (m m.)	Probe signal (mV)	Jet velocity (m/s)	
Q_s = 0.5040 l/s (V_J = 10 m/s)			
0	6.61	10.14	
1	6.80	10.28	
2	6.83	10.31	
3	6.72	10.22	
4	6.28	9.89	
5	6.70	10.21	
6	6.82	10.30	
7	6.78	10.27	
8	6.62	10.15	
3.24	5.63	9.36	Minimum reading
Q_s = 0.7517 l/s (V_J = 15 m/s)			
0	14.18	14.85	
1	14.81	15.18	
2	14.83	15.19	
3	14.69	15.12	
4	13.83	14.67	
5	14.64	15.09	
6	14.87	15.21	

GEOMETRY No.1

Probe position (rel. to jet edge) (m m.)	Probe signal (mV)	Jet velocity (m/s)	
7	14.79	15.17	
8	14.30	14.91	
3.20	12.23	13.79	Minimum reading

GEOMETRY No.2

Q_s = 0.5040 l/s (V_J = 10 m/s)

0	5.50	9.25	
1	6.18	9.81	
2	6.20	9.83	
3	6.18	9.81	
4	6.18	9.81	
5	6.32	9.91	
6	6.41	9.98	
7	6.38	9.97	
8	6.29	9.90	
3.5	6.01	9.67	Minimum reading

Q_s = 0.7517 l/s (V_J = 15 m/s)

0	12.63	14.01	
1	13.59	14.54	
2	13.64	14.57	
3	13.60	14.54	
4	13.49	14.49	
5	13.63	14.56	
6	13.80	14.65	

GEOMETRY No.2

Probe position (rel. to jet edge) (m m.)	Probe signal (mV)	Jet velocity (m/s)	
7	13.79	14.65	
8	13.45	14.46	
3.5	13.30	14.39	minimum reading

A9 - (iii) Swirling Flow Experimental Results

GEOMETRY No.1

	Qs (l/s)	Qc (l/s)	p2	p3	p4	p5	p6	p7	2β°
			←		(bar)			→	
	p1 = 0.462 bar								
	0.451	0.0	0.448	0.448	0.448	0.443	0.309	0.264	0
	0.382	0.066	0.467	0.446	0.446	0.438	0.302	0.261	4.2
	0.363	0.082	0.472	0.446	0.449	0.441	0.302	0.259	7.0
	0.353	0.096	0.483	0.443	0.448	0.438	0.302	0.240	12.2
*	0.340	0.113	0.494	0.443	0.448	0.438	0.294	0.216	17.8
	0.317	0.127	0.509	0.443	0.448	0.438	0.286	0.168	25.6
	0.300	0.135	0.520	0.446	0.446	0.435	0.297	0.147	35.3
	0.278	0.144	0.528	0.446	0.443	0.433	0.297	0.117	37.4
	0.253	0.151	0.538	0.446	0.443	0.433	0.305	0.067	41.1
	0.238	0.153	0.547	0.448	0.443	0.443	0.315	0.040	40.9
	0.205	0.158	0.549	0.448	0.445	0.437	0.317	0.0	49.1
	0.187	0.160	0.558	0.448	0.451	0.443	0.325	0.0	52.2
	0.183	0.161	0.560	0.451	0.454	0.443	0.323	0.0	53.6
	0.0	0.166	0.568	0.472	0.467	0.451	0.296	0.003	94.7

GEOMETRY No.1

Qs (l/s)	Qc (l/s)	p2	p3	p4	p5	p6	p7	2β°
		←		(bar)			→	
p1 = 0.582 bar								
0.504	0.0	0.566	0.566	0.574	0.561	0.387	0.336	0
0.443	0.066	0.587	0.558	0.563	0.550	0.382	0.328	3.2
0.426	0.082	0.592	0.560	0.568	0.552	0.381	0.328	8.7
0.426	0.082	0.592	0.560	0.565	0.555	0.384	0.323	-
0.406	0.096	0.602	0.563	0.571	0.555	0.387	0.318	9.7
0.390	0.114	0.613	0.558	0.566	0.550	0.371	0.304	14.1
* 0.374	0.127	0.627	0.563	0.571	0.552	0.374	0.264	18.9
0.347	0.147	0.646	0.558	0.566	0.550	0.369	0.216	32.4
0.310	0.160	0.664	0.566	0.569	0.550	0.379	0.155	37.2
0.293	0.167	0.678	0.563	0.563	0.547	0.387	0.109	37.3
0.258	0.176	0.691	0.568	0.565	0.563	0.403	0.027	45.1
0.238	0.177	0.699	0.568	0.571	0.560	0.405	0.003	(47.4 / 48.3)
0.205	0.179	0.704	0.568	0.576	0.560	0.411	0.003	51.0
0.183	0.182	0.709	0.574	0.577	0.561	0.422	0.003	(57.3 / 59.6)
0.0	0.187	0.717	0.595	0.592	0.574	0.379	0.0	90.0
p1 = 0.814 bar								
0.595	0.0	0.792	0.790	0.790	0.777	0.542	0.592	0
0.523	0.066	0.811	0.787	0.790	0.774	0.536	0.454	4.0
0.510	0.082	0.818	0.784	0.787	0.771	0.531	0.451	4.6
0.494	0.096	0.829	0.784	0.789	0.771	0.531	0.443	7.7
0.480	0.113	0.840	0.779	0.790	0.766	0.526	0.446	8.6
0.462	0.127	0.851	0.782	0.793	0.769	0.529	0.424	10.2
* 0.451	0.144	0.867	0.782	0.793	0.771	0.523	0.384	16.2

Qs (l/s)	Qc (l/s)	p2	p3	p4	p5	p6	p7	2β°
		←		(bar)			→	
p1 = 0.814 bar								
0.435	0.160	0.886	0.779	0.790	0.768	0.507	0.320	23.4
0.399	0.176	0.906	0.779	0.790	0.766	0.515	0.270	27.0
0.350	0.192	0.931	0.787	0.787	0.763	0.528	0.187	36.2
0.293	0.209	0.966	0.787	0.784	0.774	0.555	0.008	42.5
0.293	0.209	0.971	0.787	0.787	0.779	0.560	0.008	-
0.261	0.211	0.976	0.787	0.795	0.782	0.571	0.0	49.0
0.238	0.214	0.984	0.792	0.797	0.779	0.573	0.003	53.6
0.204	0.215	0.987	0.792	0.797	0.779	0.589	0.003	55.9
0.183	0.214	0.984	0.795	0.795	0.779	0.603	0.003	60.6
0.0	0.218	0.998	0.827	0.824	0.792	0.523	0.003	91.4
p1 = 1.230 bar								
0.752	0.0	1.200	1.198	1.201	1.171	0.827	0.678	0
0.678	0.066	1.222	1.190	1.198	1.169	0.819	0.675	1.3
0.660	0.082	1.230	1.187	1.198	1.168	0.819	0.670	4.4
0.647	0.096	1.235	1.187	1.198	1.168	0.819	0.670	6.0
0.627	0.113	1.248	1.187	1.200	1.168	0.816	0.664	8.4
0.608	0.127	1.261	1.185	1.198	1.166	0.811	0.659	10.4
0.595	0.144	1.274	1.185	1.201	1.166	0.809	0.646	14.0
0.580	0.160	1.288	1.185	1.201	1.166	0.803	0.619	18.2
* 0.564	0.176	1.310	1.182	1.198	1.163	0.792	0.568	21.2
0.540	0.192	1.326	1.182	1.198	1.163	0.776	0.504	(21.9 / 24.6)
0.504	0.209	1.355	1.182	1.195	1.163	0.784	0.438	33.9
0.470	0.225	1.385	1.190	1.198	1.155	0.798	0.355	42.9
0.436	0.241	1.421	1.193	1.193	1.158	0.814	0.251	42.1

Qs (l/s)	Qc (l/s)	p2	p3	p4	p5	p6	p7	2β°
		←		(bar)			→	
p1 = 1.230 bar								
0.403	0.250	1.443	1.193	1.190	1.174	0.82 5	0.155	46.3
0.328	0.258	1.472	1.190	1.198	1.174	0.859	0.003	52.4
0.277	0.263	1.491	1.201	1.209	1.177	0.883	0.0	68.8
0.261	0.265	1.500	1.203	1.208	1.176	0.888	0.003	60.7
0.238	0.264	1.493	1.209	1.212	1.182	0.905	0.0	62.8
0.204	0.261	1.493	1.214	1.214	1.187	0.918	0.003	64.3
0.183	0.258	1.489	1.217	1.220	1.193	0.926	0.003	63.3
0.0	0.267	1.508	1.251	1.246	1.198	0.789	0.003	96.4

Qs (l/s)	p1	p2	p3	p4	p5	p6	p7	2β°
	←			(bar)			→	
Qc = 0.0								
0.293	0.192	1.184	0.184	0.185	0.182	0.130	0.106	0.0
0.345	0.274	0.265	0.264	0.265	0.261	0.189	0.161	
0.399	0.360	0.350	0.346	0.351	0.343	0.229	0.203	
0.451	0.470	0.455	0.452	0.453	0.444	0.320	0.271	
0.504	0.584	0.566	0.568	0.571	0.555	0.394	0.331	
0.564	0.728	0.704	0.706	0.711	0.694	0.502	0.431	
0.622	0.873	0.847	0.845	0.850	0.832	0.590	0.486	
0.687	1.033	1.003	1.003	1.008	0.984	0.701	0.597	
0.752	1.225	1.191	1.190	1.197	1.166	0.820	0.674	
0.803	1.447	1.411	1.406	1.415	1.375	0.968	0.796	

Qc (l/s)	p1	p2	p3	p4	p5	p6	p7	2β°
	←			(bar)			→	
Qs = 0.0								
0.082	0.101	0.127	0.101	0.101	0.096	0.069	-.003	86.3
0.113	0.204	0.252	0.207	0.207	0.195	0.136	-.003	89.3
0.144	0.343	0.425	0.350	0.349	0.332	0.228	-.003	81.7

Qc (l/s)	p1	p2	p3	p4	p5	p6	p7	2β°
	←			(bar)			→	
Qs = 0.0								
0.176	0.516	0.636	0.526	0.525	0.500	0.338	-.003	97.8
0.209	0.731	0.899	0.744	0.741	0.708	0.474	-.003	93.0
0.241	0.998	1.224	1.015	1.012	0.967	0.641	-.005	90.6
0.277	1.298	1.592	1.319	1.316	1.259	0.836	-.011	97.0
0.292	1.489	1.822	1.510	1.502	1.451	0.974	-.016	
0.309	1.601	1.957	1.628	1.625	1.556	1.025	-.011	
0.341	1.820	2.224	1.852	1.849	1.769	1.164	-.019	

GEOMETRY No.2

Qs (l/s)	Qc (l/s)	p2	p3	p4	p5	p6	p7	2β°
		←		(bar)			→	
p1 = 0.416 bar								
0.451	0.0	0.406	0.406	0.390	0.297	-.003	0.080	0.0
0.374	0.066	0.424	0.403	0.387	0.291	-.003	0.075	2.9
0.360	0.082	0.430	0.403	0.387	0.291	-.003	0.059	7.2
0.347	0.096	0.440	0.400	0.384	0.283	-.003	0.021	12.0
* 0.328	0.113	0.451	0.400	0.381	0.283	-.003	-.056	21.4
0.304	0.127	0.467	0.400	0.384	0.288	-.003	-.003	36.4
0.280	0.135	0.475	0.398	0.385	0.291	-.003	-.003	39.6
0.262	0.141	0.483	0.398	0.385	0.299	0.0	-.003	40.4
0.258	0.144	0.483	0.400	0.387	0.296	-.003	0.0	41.4
0.238	0.147	0.494	0.403	0.384	0.299	0.0	-.003	46.0
0.205	0.148	0.499	0.403	0.384	0.310	0.0	-.003	54.8
0.183	0.147	0.502	0.408	0.395	0.325	0.011	-.003	51.5
0.0	0.149	0.507	0.427	0.411	0.331	0.048	0.0	83.7

	Qs (l/s)	Qc (l/s)	p2	p3	p4	p5	p6	p7	2β°
			←		(bar)			→	
	p1 = 0.528 bar								
	0.504	0.0	0.515	0.512	0.493	0.373	-.005	0.101	0.0
	0.443	0.066	0.531	0.510	0.491	0.369	-.005	0.093	2.1
	0.426	0.082	0.539	0.510	0.491	0.366	-.005	0.088	5.6
	0.406	0.096	0.550	0.510	0.491	0.366	-.005	0.067	9.1
	0.390	0.113	0.560	0.510	0.489	0.361	-.005	0.008	12.3
*	0.367	0.127	0.571	0.507	0.483	0.358	-.005	-.040	23.0
	0.353	0.144	0.590	0.507	0.486	0.355	0.0	-.005	37.0
	0.323	0.151	0.600	0.504	0.493	0.373	0.0	-.003	40.5
	0.297	0.160	0.614	0.504	0.496	0.379	0.0	-.003	43.9
	0.238	0.167	0.630	0.515	0.491	0.398	0.0	0.0	51.8
	0.205	0.167	0.632	0.515	0.502	0.411	0.008	0.0	55.2
	0.183	0.166	0.632	0.518	0.505	0.422	0.032	0.0	54.1
	0.0	0.168	0.640	0.542	0.521	0.422	0.059	0.0	83.8
	p1 = 0.734 bar								
	0.595	0.0	0.715	0.715	0.688	0.518	0.0	0.139	0.0
	0.536	0.066	0.734	0.710	0.683	0.510	0.0	0.131	1.6
	0.510	0.082	0.742	0.707	0.680	0.507	0.0	0.128	3.0
	0.494	0.096	0.752	0.704	0.675	0.501	0.0	0.120	5.2
	0.480	0.113	0.763	0.710	0.681	0.499	0.0	0.091	9.3
	0.462	0.127	0.774	0.710	0.681	0.499	0.0	0.035	13.0
	0.451	0.144	0.787	0.710	0.681	0.499	0.0	-.067	17.9
*	0.420	0.160	0.803	0.710	0.681	0.510	0.0	-.008	29.5
	0.390	0.176	0.827	0.696	0.680	0.507	0.0	-.003	39.5
	0.372	0.183	0.843	0.702	0.688	0.513	0.0	-.003	41.9

Qs (l/s)	Qc (l/s)	p2	p3	p4	p5	p6	p7	2β°
		←		(bar)			→	
p1 = 0.734 bar								
0.346	0.192	0.857	0.704	0.683	0.525	0.0	-.003	44.3
0.345	0.192	0.857	0.704	0.683	0.528	0.0	-.003	42.2
0.317	0.199	0.873	0.715	0.680	0.534	-.003	0.0	44.7
0.293	0.200	0.878	0.718	0.681	0.542	-.003	0.0	50.3
0.261	0.200	0.881	0.720	0.691	0.563	-.003	-.003	53.1
0.238	0.198	0.883	0.720	0.701	0.581	0.027	0.0	52.4
0.204	0.198	0.883	0.720	0.704	0.589	0.051	0.0	52.6
0.183	0.197	0.883	0.720	0.701	0.600	0.061	0.0	57.9
0.0	0.200	0.889	0.744	0.717	0.576	0.083	0.0	81.9
p1 = 1.126 bar								
0.752	0.0	1.099	1.091	1.051	0.781	-.005	0.213	0.0
0.678	0.066	1.121	1.083	1.043	0.773	-.005	0.205	0.9
0.660	0.082	1.129	1.083	1.043	0.773	-.005	0.197	1.6
0.642	0.096	1.137	1.083	1.043	0.773	-.005	0.192	4.3
0.622	0.113	1.147	1.083	1.043	0.771	-.005	0.184	7.0
0.608	0.127	1.158	1.086	1.046	0.771	-.005	0.163	7.7
0.592	0.144	1.174	1.086	1.043	0.771	-.005	0.112	11.7
0.576	0.160	1.190	1.086	1.041	0.760	-.005	0.051	14.2
0.562	0.176	1.203	1.086	1.041	0.763	-.005	-.080	19.4

Qs (l/s)	Qc (l/s)	p2	p3	p4	p5	p6	p7	2β°
		←		(bar)			→	
p1 = 1.126 bar								
* 0.535	0.192	1.227	1.086	1.038	0.771	-.005	-.075	22.0
0.504	0.209	1.251	1.081	1.044	0.785	-.003	-.011	36.0
0.470	0.225	1.283	1.075	1.048	0.787	-.003	-.005	43.8
0.451	0.233	1.299	1.075	1.051	0.800	-.003	-.005	45.6
0.426	0.241	1.321	1.083	1.048	0.811	-.005	-.005	46.7
0.399	0.246	1.337	1.097	1.046	0.817	-.003	0.0	46.4
0.345	0.248	1.348	1.102	1.051	0.854	0.0	0.0	52.0
0.293	0.246	1.353	1.107	1.080	0.896	0.045	0.0	56.1
0.238	0.245	1.353	1.110	1.083	0.921	0.085	0.0	56.9
0.183	0.241	1.353	1.118	1.089	0.937	0.107	0.0	60.0
0.0	0.247	1.364	1.150	1.110	0.891	0.123	0.0	85.5

Qs (l/s)	p1	p2	p3	p4	p5	p6	p7	2β°
	←			(bar)			→	
Qc = 0.0								
0.183	0.069	0.067	0.069	0.066	0.045	-.005	0.019	0.0
0.238	0.117	0.115	0.120	0.112	0.088	0.0	0.021	
0.293	0.179	0.173	0.176	0.171	0.133	0.0	0.040	
0.345	0.243	0.237	0.237	0.229	0.173	0.0	0.051	
0.399	0.326	0.310	0.315	0.304	0.227	0.0	0.067	
0.451	0.419	0.411	0.406	0.393	0.297	-.005	0.077	
0.504	0.528	0.515	0.512	0.493	0.373	-.005	0.101	
0.564	0.656	0.640	0.635	0.614	0.451	-.005	0.125	
0.622	0.795	0.776	0.771	0.744	0.558	-.005	0.147	
0.687	0.953	0.931	0.923	0.894	0.659	-.005	0.179	

Qs (l/s)	p1	p2	p3	p4	p5	p6	p7	2β°
	←			(bar)			→	
Qc = 0.0								
0.752	1.134	1.107	1.099	1.059	0.784	-.005	0.208	0.0
0.803	1.321	1.289	1.278	1.235	0.910	-.005	0.243	↓
0.880	1.532	1.497	1.484	1.431	1.060	-.005	0.280	

Qc (l/s)	p1	p2	p3	p4	p5	p6	p7	2β°
	←			(bar)			→	
0.066	0.075	0.093	0.077	0.072	0.061	0.011	0.0	77.8
0.082	0.117	0.147	0.123	0.112	0.099	0.013	0.0	80.9
0.096	0.168	0.208	0.208	0.195	0.168	0.021	0.0	80.1
0.113	0.227	0.278	0.232	0.219	0.181	0.027	0.0	82.1
0.127	0.296	0.363	0.304	0.288	0.237	0.035	0.0	80.4
0.144	0.379	0.462	0.390	0.374	0.305	0.043	0.0	83.5
0.160	0.467	0.568	0.480	0.461	0.373	0.051	0.0	80.0
0.176	0.566	0.688	0.579	0.555	0.451	0.059	0.0	79.0
0.192	0.675	0.817	0.686	0.659	0.531	0.075	0.0	83.9
0.209	0.798	0.966	0.814	0.785	0.630	0.088	0.0	83.0
0.225	0.934	1.131	0.953	0.918	0.740	0.104	0.0	85.7
0.241	1.075	1.299	1.097	1.057	0.846	0.120	0.0	85.3
0.258	1.209	1.468	1.233	1.190	0.947	0.133	0.0	83.1
0.277	1.366	1.652	1.390	1.342	1.072	0.149	0.0	84.3
0.292	1.516	1.830	1.540	1.492	1.188	0.165	0.0	85.5

Note: * Denotes visible indication of air core formation.

GEOMETRY No.2

Thread Angle Experimental Results

Qs (l/s)	Qc (l/s)	α°	Qs (l/s)	Qc (l/s)	α°
pl = 0.416 bar			pl = 0.528 bar		
0.451	0.0	-0.1	0.504	0.0	-0.1
0.360	0.082	1.7	0.443	0.066	1.1
0.328	0.113	(3.6) (6.1)	0.426	0.082	2.0
0.280	0.135	10.7	0.406	0.096	2.5
0.258	0.144	17.0	0.390	0.113	2.7
0.205	0.148	17.0	0.367	0.127	(4.5) (2.7)
0.0	0.149	34.6	0.353	0.144	6.3
			0.323	0.151	8.0
pl = 1.126 bar			0.297	0.160	(14.2) (24.5)
0.752	0.0	-0.9	0.238	0.167	17.4
0.678	0.066	-1.5	0.205	0.167	16.2
0.660	0.082	0.0	0.183	0.166	19.8
0.642	0.096	1.6	0.0	0.168	32.8
0.622	0.113	2.2	pl = 0.734 bar		
0.608	0.127	3.3	0.595	0.0	-1.4
0.592	0.144	(1.7) (8.4)	0.510	0.082	0.8
0.576	0.160	6.7	0.480	0.113	(3.2) (5.6)
0.562	0.176	6.6	0.451	0.114	(3.4) (7.3)
0.535	0.192	6.6	0.390	0.176	7.3
0.504	0.209	8.9	0.346	0.192	14.6
0.470	0.225	(10.1) (22.6)	0.317	0.199	(12.7) (17.0)
0.451	0.233	13.6	0.261	0.200	17.2

Q_s (l/s)	Q_c (l/s)	α°	Q_s (l/s)	Q_c (l/s)	α°
0.426	0.241	19.9	0.204	0.198	22.2
0.399	0.246	18.3	0.0	0.200	36.6
0.345	0.248	18.2			
0.293	0.246	20.5			
0.238	0.245	22.3			
0.183	0.241	25.5			
0.0	0.247	37.5			

APPENDIX 10

THE SOLUTION OF EQUATION (3-10)

The Solution of Equation 3-10

Given equation (3-10):

$$\frac{\partial(V_2^2)}{\partial n} + 2k_m V_2^2 + 2N(n) = 0 \qquad -(3\text{-}10)$$

If the equation is rewritten in the form:

$$A(n, V_2^2)\, d(V_2^2) + B(n, V_2^2)\, dn = 0 \ ,$$

then the above equation is exact if:

$$\frac{\partial B}{\partial(V_2^2)} = \frac{\partial A}{\partial n}$$

This condition is not satisfied but the equation has an integrating factor (α) which, since $(\partial A/\partial n) = 0$, is a function of 'n' only.

Therefore:
$$\frac{1}{\alpha}\cdot\frac{d\alpha}{dn} = \frac{1}{A}\left[\frac{\partial B}{\partial(V_2^2)} - \frac{\partial A}{\partial n}\right]$$

$$\int \frac{d\alpha}{\alpha} = \int \left[\frac{1}{A}\cdot\frac{\partial B}{\partial(V_2^2)}\right] . dn = \int 2k_m . dn$$

$$\ln . \alpha = \int 2k_m . dn$$

$$\alpha = \exp . \left[\int 2k_m . dn\right]$$

Thus along an 'n' curve equation (3-10) becomes:

$$\alpha \frac{d(V_2^2)}{dn} + \alpha(2k_m V_2^2) = -\alpha 2N$$

Since: $\frac{1}{\alpha}\cdot\frac{d\alpha}{dn} = 2k_m$, then: $\frac{d\alpha}{dn} = \alpha 2k_m$,

and along an 'n' curve equation (3-10) becomes:

$$\alpha \frac{d(V_2^2)}{dn} + V_2^2 \frac{d\alpha}{dn} = -\alpha 2N$$

$$\frac{d(\alpha V_2^2)}{dn} = -\alpha 2N$$

Integrating: $$\alpha V_2^2 = \int -\alpha 2N . dn + C$$

Therefore: $$V_2^2 = \frac{1}{\alpha}\left[\int -2\alpha N . dn + C\right]$$

For the application under consideration at the inner boundary $n = 0$ and the integral becomes zero, since examination of the functions α and N indicates that they cannot become infinite. At the inner boundary a stream velocity can exist because of the inviscid condition. Therefore $C = V_{2(n=0)}^2 = V_{2(i)}^2$ and the complete solution to equation (3-10), along an 'n' curve, becomes:

$$V_{2(n)}^2 = \exp.\left[-\int_o^n 2k_m . dn\right].\left[V_{2(i)}^2 - \int_o^n 2N . \exp.\left[\int_o^{u=n} 2k_m . du\right] dn\right] \quad -(3\text{-}11)$$

, where U is a dummy variable.

APPENDIX 11

TRANSIENT TESTS - EXPERIMENTAL EQUIPMENT LIST

Transient Tests - Experimental Equipment List

Reference to Figure 4-5 in the main body of the report may prove helpful in interpreting the following data.

The two fluid supply routes to the vortex element were pressure regulated by water regulators manufactured by C.A.NORGREN LTD. Type 11 - 009 - 994 (1" BSP) regulated the streaming flow while type 11 - 009 - 994 ($\frac{3}{4}$" BSP) regulated the control flow.

The control flow solenoid valve was of a direct acting type MB202/0/6 with a D.C. coil, manufactured by JOUCOMATIC CONTROLS LTD. The electrical power activating the solenoid valve was provided by a D.C. power pack (WIER ELECTRONICS LTD.) and routed through a reed switch unit built by [redacted] of The City University. The reed switch control frequency came from a function generator, type TWG 501 manufactured by FEEDBACK LTD. A tapping was made into the solenoid coil's electrical supply line and, after passing through a suitable impedance, connected to a U.V. galvanometer.

The static pressure within the control flow supply annulus was monitored by an inductive differential pressure transducer (HONEYWELL CONTROLS LTD., type 1028) with one side open to atmosphere. The transducer was excited by an oscillator - demodulator (HONEYWELL CONTROLS LTD. type OD31) and powered by a HONEYWELL CONTROLS LTD. unit, type PU 21. The pressure transducer signal output

from the oscillator-demodulator unit was connected to another U.V. galvanometer, after being passed through a suitable impedance.

The 'jet sensor' comprised a resistance strain guage pressure transducer (BELL AND HOWELL LTD., type 4 - 366 - 0105 - 03M0) excited by a 10 volt D.C. signal (FARNELL LTD., stabilised power supply type L30A). Because of the low signal level obtained from this transducer the output was placed directly onto a U.V. galvanometer. The ultra-violet paper records made of the galvanometer readings during the transient tests were produced by a SOUTHERN INSTRUMENTS LTD., ten channel U.V. recorder, type M1300.